Inaugural dissertation

for

obtaining the doctoral degree

of the

Combined Faculty of Mathematics, Engineering and Natural Sciences

of the

Ruprecht - Karls - University

Heidelberg

Presented by

M.Sc. Lisa Rösch

Born in Heiden, Switzerland

Oral Examination: 02.02.2023

ERBB and P-glycoprotein inhibitors break resistance in relapsed neuroblastoma through P-glycoprotein

Referees: Prof. Dr. Peter Angel

Prof. Dr. Olaf Witt

Acknowledgments

There are many people without who I would not have been able to complete my PhD. I am very grateful to each and every one of you for your support and your contribution to the success of the project!

I would like to thank Prof. Dr. Olaf Witt for creating and supporting the collaborative scientific environment in the department and for making our work there possible. You always keep our focus on the translational potential of our projects.

A great thank you to PD Dr. Ina Oehme for your wonderful support in all aspects of my project and for your patience in guiding me through the ups and downs of my PhD. You always helped me see the positive aspects of my project. I could not have done this without your input and motivation. An especially big thank you for your tremendous support in the last year of my PhD!

I would like to thank the members of my TAC committee for all your ideas and input how to best advance the project: Prof. Dr. Peter Angel, who also kindly agreed to be the first examiner of my thesis; Prof. Dr. Matthias Fischer for valuable input; and Dr. David T.W. Jones for sharing expertise and data.

Thank you Prof. Dr. Walter Haefeli and Dr. Christiane Opitz for agreeing to act as examiners in my thesis examination committee.

A lot of my work would not have been possible without our collaborators: Prof. Dr. Martin Michaelis provided us with the resistant cell lines I used throughout my project and also with invaluable insights and advice. Prof. Dr. Anette Kopp-Schneider and Dr. Manuela Hummel gave excellent support with the gene expression analysis. Thank you all!

To all members of B310, past and present: Till M., Sina, Heike, Johannes, Jagoda, Emily, Sara, Sonja, Simay, Marta, Michael, Fiona, Katharina, Rabia, Till S., Charlotte, Coco, Alexandra, Aileen, Clarissa, Marko, Flo, Jonas, Romain, Ginny, Anna, Daniela, Nora, Juliane, Diren, Johanna, Simon, Leo, Carina, Isabel, Dani, Yannick, Natja and Nicola. You filled my time as a PhD student with life, I know I could not have come this far without your advice, discussions, conversations, jokes and laughter. Heike always had an open ear and great suggestions for all problems. Johannes was the person to go to for any and all discussions concerning the lab or any odd topic under the sun. Jagoda, Juliane and Emily helped me so much in getting settled in the lab in the first months of my PhD. Sonja, Simay and Marta thank you for our wonderful, supportive and fun community as AG Ina PhDs. Coco, it was so much fun to work with you on your project and to show you the ways of the lab – and I certainly feel that I learned as much as I taught! Our coffee gang, in its varying compositions, but always punctual at the opening of HotSpot – and during the Corona lock downs even online! – you helped me get going every day and made getting up in the mornings so much easier! And of course Alex, you helped me so much, with your wonderful work when I couldn't finish the last experiments myself, but also and especially by simply being a friend throughout my PhD years – thank you!

My friends at the DKFZ and beyond, who always supported and entertained me: Julia, my Corona buddy. Manu, Katja, Siv and Jean from the University Choir and my old friends Milli and Lulu.

And finally I would like to thank my family, especially my parents and my sister. Your support and your belief in me kept me going! Last but not least the two most important people in my life: Romain and Zoé. I never would have dreamed when I started my PhD that I would find you two along the way. Thank you for making every day of my life special and joyful!

Summary

Neuroblastoma is a pediatric tumor of the sympathetic nervous system that most commonly affects infants and young children. It is a disease with very variable outcomes, which range from spontaneous regression to aggressive disease. Particularly problematic are high-risk cases after relapse, with only 10% of patients surviving for longer than five years and chemotherapy resistance making treatment difficult. In this thesis, I examined differences between primary and relapsed patient gene expression data and between chemotherapy-sensitive and chemotherapy-resistant neuroblastoma cell lines to find a vulnerability that can be targeted to overcome chemotherapy resistance and lead to cell death. I further investigated which type of cell death was induced.

My analysis of gene expression data from primary and relapsed neuroblastoma patients suggested that the ERBB family of receptor tyrosine kinases, particularly ERBB4, plays a role in relapsed high-risk neuroblastomas. The ERBB family is crucial in development and is well known for its link to cancer. Furthermore, I functionally examined the resistance breaking effect of 15 clinically relevant drugs on a neuroblastoma cell line that was treated to be resistant to the standard-of-care chemotherapeutic vincristine (VCR). Tariquidar, an inhibitor of P-glycoprotein (P-gp), and afatinib, a FDA approved inhibitor of the ERBB family, were the two most efficient drugs in breaking resistance in this screen. P-gp/*ABCB1* is a transmembrane transporter that very efficiently eliminates drugs and other xenobiotics from the cell and has long been recognized for its contribution to chemotherapy resistance.
Analysing gene expression datasets of more than 50 different neuroblastoma cell lines (primary and relapsed) and more than 160 neuroblastoma patient samples from the pediatric precision medicine platform INFORM (Individualized Therapy For Relapsed Malignancies in Childhood) confirmed a crucial role of P-gp in neuroblastoma resistance at relapse. The ERBB family appeared to play a minor part. I mechanistically investigated chemotherapy resistance through four pairs of vincristine-sensitive/resistant neuroblastoma sublines - each pair with the same genetic background - and two additional high-risk neuroblastoma cell lines. I effectively overcame resistance by the addition of the pan-ERBB family inhibitors afatinib and lapatinib, as well as the P-gp inhibitors tariquidar and verapamil, to VCR treatment, which synergistically reduced viability. Functional analyses of the ERBB downstream pathways, as well as *ERBB4* knock-down, showed the resistance breaking effect of afatinib to be unrelated to ERBB signaling and suggested an off-target effect on P-gp. *ABCB1* knock-down and analysis of transporter function confirmed that resistance was mediated through P-gp.

My analysis of programmed cell death, in particular apoptosis and ferroptosis, in neuroblastoma cell lines showed that apoptosis was consistently induced, while ferroptosis contributed to cell death in the IMR-32 cell line. The combination treatments of VCR with afatinib or tariquidar in VCR-sensitive and VCR-resistant cell lines led to cell death by apoptosis.

In summary, this study showed that P-gp is an important player in chemotherapy resistance in high-risk, relapsed neuroblastoma. ERBB4, although upregulated in individual cases or cell lines, did not contribute to resistance, and the sensitizing effect of the ERBB family inhibitor afatinib was due to an off-target effect on P-gp. I further showed that both apoptosis and ferroptosis are induced in neuroblastoma cell lines, with apoptosis being the dominant mechanism of cell death when chemotherapy resistance was broken.

Zusammenfassung

Das Neuroblastom ist ein pädiatrischer Tumor des sympathischen Nervensystems, der am häufigsten Säuglinge und Kleinkinder betrifft. Es ist eine Krankheit mit sehr unterschiedlichen Auswirkungen, die von spontaner Regression bis zu aggressiver Krankheit reichen. Besonders problematisch sind Hochrisikofälle nach Rückfällen, bei denen nur 10 % der Patienten länger als fünf Jahre überleben und Chemotherapieresistenzen die Behandlung erschweren. In dieser Doktorarbeit untersuchte ich Unterschiede zwischen Genexpressionsdaten von primären und rezidivierten Patienten sowie zwischen Chemotherapie sensitiven und resistenten Neuroblastom Zelllinien, um eine Angriffspunkt zu finden, der gezielt zur Überwindung der Chemotherapieresistenz und zum Zelltod führen kann. Zudem untersuchte ich, welche Art von Zelltod dadurch ausgelöst wurde.

Meine Analyse der Genexpressionsdaten von Patienten mit primärem und rezidiviertem Neuroblastom wies darauf hin, dass die ERBB-Familie von Rezeptortyrosinkinasen, insbesondere ERBB4, eine Rolle im rezidiviertem Hochrisiko-Neuroblastom spielt. Die ERBB-Familie spielt in der Entwicklung eine entscheidende Rolle und ist für ihre Verbindung zu Krebs bekannt. In einem zweiten Ansatz untersuchte ich funktionell die resistenzbrechende Wirkung von 15 Medikamenten auf eine Neuroblastomzelllinie, die gegen das Chemotherapeutikum Vincristin (VCR) resistent gemacht worden waren. Tariquidar, ein Inhibitor des P-glycoproteins (P-gp), und Afatinib, ein Inhibitor der ERBB-Familie, brachen in diesem Screen am effizientesten die Chemotherapieresistenz. P-gp/*ABCB1* ist ein Transporter der Zellmembran, der Medikamente sehr effizient aus der Zelle heraustransportiert und seit langem für seinen Beitrag zur Chemotherapieresistenz bekannt ist.
Die weitere Untersuchung, welchen Beitrag ERBB4 zur Resistenz leistet, zeigte, dass ERBB4 nicht generell hochreguliert ist, jedoch einzelne Patienten und Zelllinien die Expression von ERBB4 bei einem Rückfall oder bei der Entwicklung von Resistenz erhöhten. Die Behandlung mit Afatinib sensibilisierte resistente Neuroblastom-Zelllinien für VCR und führte zu einer synergistischen Verringerung der Viabilität. Funktionsanalysen der ERBB Signalwege sowie ein ERBB4 Knockdown zeigten jedoch, dass dieser resistenzbrechende Effekt nicht mit den ERBB Signalwegen zusammenhängt, und deuten auf einen Off-Target-Effekt von Afatinib auf P-gp hin.
P-gp war bei rezidivierten Neuroblastompatienten oder resistenten Zelllinien konsistenter hochreguliert als ERBB4. Tariquidar Behandlung der VCR-resistenten Neuroblastomzellen, erhöhte die Sensitivität zu VCR und verringerte synergistisch die Viabilität. Der ABCB1 Knockdown und die Analyse der Transporterfunktion bestätigten, dass die Resistenz durch P-gp vermittelt wurde.
Meine Analyse der programmierten Zelltodmechanismen Apoptose und Ferroptose in Neuroblastomzelllinien zeigte, dass Apoptose durchgehend induziert wurde, während Ferroptose zum Zelltod in der Zelllinie IMR-32 beitrug. Die Kombinationsbehandlungen von VCR mit Afatinib oder Tariquidar in den VCR-sensitiven und -resistenten Zelllinien führten zum Zelltod durch Apoptose.

Zusammenfassend zeigte diese Studie, dass P-gp eine wichtige Rolle bei der Chemotherapieresistenz von rezidivierten Hochrisiko-Neuroblastomen spielt. Obwohl ERBB4 in Einzelfällen hochreguliert war, trug es nicht zur Resistenz bei, und die sensibilisierende Wirkung des ERBB Inhibitors Afatinib war auf

einen Off-Target-Effekt auf P-gp zurückzuführen. Ich habe ferner gezeigt, dass sowohl Apoptose als auch Ferroptose in Neuroblastomzelllinien induziert werden, wobei Apoptose der dominierende Mechanismus des Zelltods war, wenn die Chemotherapieresistenz gebrochen wurde.

Abbreviations

4ICD	Cleaved, soluble intracellular domain of ERBB4
ABC	ATP Binding Cassette
ABCB1	ATP Binding Cassette Subfamily B Member 1
Afa	Afatinib
ALK	Anaplastic lymphoma kinase
ALT	Alternative lengthening of telomeres
APAF1	Apoptotic protease-activating factor 1
APC	Allophycocyanin
AUC	Area under the curve
BCA	Bicinchoninic acid
BCL-2	B-cell lymphoma 2
BCRP	Breast cancer resistance protein
BF	Bright field
BID	BH3-interacting domain death agonist
CTG	CellTiter-Glo
CuOOH	Cumene hydroperoxide
CYP	Cytochrome P450
DIPG	Diffuse intrinsic pontine gliomas
DISC	Death inducing signaling complex
DMSO	Dimethylsulfoxid
DPBS	Dulbecco's Phosphate Buffered Saline
ECL	Enhanced chemiluminescence
ECM	Extracellular matrix
EFS	Event free survival
EGFR	Epidermal growth factor receptor
ERBB	Erythroblastic leukemia viral oncogene homolog
FC	Fold change
FCS	Fetal calf serum
FDA	U.S. Food and Drug Administration
GAPDH	Glyceraldehyde-3-phosphate dehydrogenase
GPX4	Glutathione peroxidase 4
HB-EGF	Heparin-binding EGF-like growth factor
HER2	Human epidermal growth factor receptor 2
HGG	High grade glioma
HRP	Horse radish peroxidase
IAP	Inhibitor of apoptosis protein
IDRF	Image defined risk factors
IHC	Immunohistochemistry
INFORM	Individualized Therapy for Relapsed Malignancies in Childhood
INRG	International Neuroblastoma Risk Group Staging System
INSS	International Neuroblastoma Staging System

JAK	Janus kinase
JM	Juxtamembrane
KD	Knock down
Lapa	Lapatinib
LOX	Lipoxygenases
MAPK	Mitogen-activated protein kinase
MCA	Multiplex Cell Line Authentication
McCT	Multiplex Cell Contamination Test
MDR	Multi drug resistance
MDR-1	Multi drug resistance protein 1
MOMP	Mitochondrial outer membrane permeabilization
MRP-1	Multi drug resistance associated-protein-1
NRG	Neuregulin
NSCLC	Non-small-cell lung cancer
OS	Overall survival
P-gp	P-glycoprotein
PAGE	Polyacrylamide gel electrophoresis
PARP	Poly(ADP-ribose) polymerase
cl-PARP	Cleaved PARP
fl-PARP	Full length PARP
PCR	Polymerase chain reaction
PF-EPN-A	Anaplastic ependymoma group A found in the posterior fossa
PFP	Percentage of false prediction
PI3K	Phosphoinositide 3-kinase
PUFA	Polyunsaturated fatty acid
RMS	Rhabdomyosarcoma
ROS	Reactive oxygen species
rpm	Rounds per minute
SDS	Sodium dodecyl sulfate
SMAC	Second mitochondria-derived activator of caspase
SN	Supernatant
STAT	Signal transducer and activator of transcription
TACE	Tumor necrosis factor-α-converting enzyme
Tar	Tariquidar
tBID	Truncated BID
TfR	Transferrin receptor-1
VCR	Vincristine
Verap	Verapamil

Table of contents

List of Figures

List of Tables

1. Introduction

1.1. Neuroblastoma

Neuroblastoma is a pediatric tumor of the sympathetic nervous system. In Germany, 1 in 6000 children under the age of 18 are affected by this disease, the vast majority under the age of five.[1] Neuroblastoma is initiated in utero and derived from neural crest cells and is therefore referred to as an embryonal tumor.[2]
During normal development of the adrenal medulla, neural crest cells migrate and expand, regulated by the protooncogene MYCN. Decreased levels of MYCN are necessary for the maturation and differentiation of the sympathetic neurons.[3,4] During this differentiation early Schwann cell precursor cells develop into late Schwann cell precursors and a population of bridge cells, which further differentiates into sympathetic neuroblasts and chromaffin cells.[5] Different clinical phenotypes of neuroblastoma can be associated with different temporal states along this developmental axis of sympathetic neurons, with high-risk disease being more closely associated to early stages (Schwann cell precursor cells, bridge cells and cycling neuroblasts), while low-risk neuroblastomas more closely resemble the more differentiated late neuroblasts.[5]
Grade of differentiation is indeed one important factor, which is used to assess the risk associated with neuroblastoma cases in the clinic. Other risk factors are age at diagnosis, stage, *MYCN* amplification, histological category of the tumor, aberrations in chromosome 11q and tumor ploidity.[6]

1.1.1. Neuroblastoma staging systems and risk groups

Two main staging systems exist for neuroblastoma: the International Neuroblastoma Staging System (INSS)[7] and the International Neuroblastoma Risk Group Staging System (INRG)[8]. The two systems overlap to some degree, the main difference being that INSS includes to what extent a tumor was excised by surgery, while the INRG uses image defined risk factors (IDRF) and allows a tumor to be staged pre-surgery.

The INSS stages neuroblastomas according to spread and resectability.[7] Stage 1 includes localized tumors that were removed by complete gross excision. Any remaining lymph nodes must be tumor free. Stage 2 is further divided into stage 2A and 2B. Stage 2A tumors are localized with tumor free remaining lymph nodes, but only incomplete gross excision was possible. Stage 2B tumors are localized with complete or incomplete gross excision and remaining tumor burden in ipsilateral lymph nodes. Stage 3 neuroblastomas are defined as unresectable, unilateral tumors infiltrating across the midline, unilateral tumors with tumor cell positive contralateral lymph nodes or midline tumors with bilateral extension by tumor infiltration of lymph nodes. Stage 4 in the INSS are tumors with distant metastasis, excepting the special case of stage 4s, which is defined as localized stage 1 or 2 primary tumors with metastasis only to skin, liver and bone marrow in children under 12 months of age. Children with stage 4s neuroblastomas have a very good survival probability. It is often observed that these tumors spontaneously regress with minimal treatment.[6,9]

In the INRG staging system the occurrence of IDRF play an important role. Examples for IDRF include tumor extension within two body compartments (e.g. neck and chest), the tumor encasing important blood vessels or infiltration of adjacent organs or structures.[8]
Stage L1 in the INRG system is defined as localized tumors confined to one body compartment without IDRF. Stage L2 tumors are locoregional with one or more IDRF. Stage M tumors include distant metastases, excepting stage MS, which is defined as metastasis only in skin, liver and bone marrow in children under 18 months of age. Stage M and MS are equivalent to stage 4 and 4s in the INSS.

The INRG uses several risk factors - stage, age at diagnosis, histological category, grade of tumor differentiation, *MYCN* status, aberrations of chromosome 11q and tumor cell ploidity - to define four pretreatment risk groups: very low-risk, low-risk, intermediate-risk and high-risk neuroblastoma.[6] The risk groups are defined by the estimated 5 year event free survival (EFS) of the patients, with a 5 year EFS of > 85% for the very low-risk group, 75-85% for the low-risk group, 50-75% for the intermediate-risk group and < 50% for high-risk neuroblastomas.
Very low-risk neuroblastoma includes all patients in the histological categories ganglioneuroma or intermixed ganglioneuroblastoma in stage L1 or L2, as well as any other histological category in stage L1 and without *MYCN* amplification, and stage MS without *MYCN* amplification or 11q aberration.
Low-risk cases are stage L2 without *MYCN* amplification or 11q aberration in patients < 18 months of age or in patients > 18 months of age with a differentiating tumor. Hyperdiploid, metastatic neuroblastomas without *MYCN* amplification or 11q aberration in patients < 18 months of age are also considered low-risk.
Intermediate-risk neuroblastoma includes cases in stage L2 with 11q aberration in patients < 18 months of age or in patients > 18 months of age with a differentiating tumor. Any poorly differentiated stage L2 tumor in patients > 18 months of age is also considered intermediate -risk, irrespective of 11q status. Finally, metastatic, diploid tumors in patients < 18 months are also considered intermediate-risk. All tumors in the intermediate-risk group have to be non-*MYCN* amplified.
The high-risk group includes all tumors with *MYCN* amplification, as well as metastatic, non-*MYCN* amplified tumors in patients > 18 months, and stage MS, non-*MYCN* amplified tumors with 11q aberrations.

Treatment options for neuroblastoma depend greatly on the respective risk groups. In very low and low-risk neuroblastoma minimal therapy is given, as these tumors often spontaneously regress and have an overall survival (OS) > 90%.[6,9,10] Intermediate-risk neuroblastomas are treated by surgery, followed by chemotherapy. Radiation is only recommended in individual cases with residual disease.[10] High-risk neuroblastoma patients on the other hand receive intensive, multimodal treatments, including surgery, chemotherapy, stem cell transplantation and radiotherapy.[6,10] While OS of high-risk neuroblastoma patients has increased since the 1990s, 5 year OS is still < 60%, with high rates of progressing and relapsed disease.[11]

1.1.2. Molecular risk factors of neuroblastoma

1.1.2.1. MYCN amplification

MYCN is a well-known protooncogene, which is necessary during normal embryonic development. In the sympathoadrenal development, MYCN regulates the ventral migration and necessary expansion of neural crest cells.[3] MYCN expression decreases during differentiation.[3,4] In normal cells, supraphysiological MYCN levels lead to cell death through the p53 pathway, which makes survival under *MYCN* amplification a selection pressure for developing tumors.[12] When this is successfully overcome, *MYCN* amplification is a major risk factor for many tumor entities, including neuroblastoma. Indeed, *MYCN* amplification alone is sufficient to class a neuroblastoma case as high-risk disease[6] and is present in 37% of these cases.[13] *MYCN* amplified neuroblastomas are most similar to neuroblasts at a very early point in their development, which is associated with adverse outcome.[5] High MYCN levels cause dedifferentiation, activation of proliferation and induce telomere maintenance through TERT.[5,14]

1.1.2.2. Other molecular risk factors

Neuroblastoma is most often a sporadic disease, with only 1-2% of familial cases.[15] In these rare cases mutations of *PHOX2B* and *ALK* (anaplastic lymphoma kinase) play a role in neuroblastoma development.[15,16]

PHOX2B plays an important part in neural crest development and differentiation.[2] Mutations are present in 6.4% of familial neuroblastoma cases and promote non-physiological proliferation of neural precursor cells.[17]

ALK is a tyrosine receptor kinase and mutations or amplifications play a role both in familial and sporadic cases of neuroblastoma leading to ligand independent, constitutive signaling.[15,18] Mutations at the subclonal level also play a role in the development of resistance.[19] Downstream signaling of ALK include among others the phosphoinositide 3-kinase (PI3K)/AKT, the Janus kinase (JAK)/signal transducer and activator of transcription (STAT) pathway and the mitogen activated protein kinase (MAPK) pathway.[20] Interestingly for neuroblastoma, *MYCN* expression is activated by ALK and they act together to drive tumor development.[21–23]

Telomere maintenance is a critical component in enabling unlimited replicative potential, one of the hallmarks of cancer.[24] Telomere maintenance is achieved through several mechanisms in neuroblastoma and its importance for the identification of high-risk cases has been emphasized in recent years.

Rearrangements of the *TERT* locus, which encodes the catalytic subunit of telomerase, are detected in in 26% of high-risk neuroblastoma cases.[13] There are a large number of different rearrangements, but all lead to the same outcome: *TERT* overexpression and telomere maintenance.[13,14] *TERT* overexpression is also a consequence of *MYCN* amplification.[14]

Telomere maintenance can also be achieved through an inactivating mutation of *ATRX*, which encodes a chromatin remodeling protein. This mechanism is termed alternative lengthening of telomeres (ALT).[25,26] In neuroblastoma 11% of high-risk cases have inactivating *ATRX* mutations, the likelihood for

which increase with age of the patient.[13,25] Interestingly, *TERT* rearrangement, *MYCN* amplification and *ATRX* mutations are almost always mutually exclusive in neuroblastoma, but all lead to the same end result: a very poor prognosis for the patient due to telomere maintenance.[13,14] A new risk classification based on telomerase activity or ALT activation has therefore been proposed for neuroblastoma: tumors without telomerase/ALT activity are considered low-risk, as the likelihood for tumor differentiation or regression is high; tumors with telomerase/ALT activity are considered high-risk or even very high-risk, depending on the concurrence with RAS or p53 alterations.[27]

1.1.2.3. Mesenchymal and adrenergic neuroblastoma

Not only genetic factors, but also epigenetic regulation is important in neuroblastoma. Two states of neuroblastoma, adrenergic and mesenchymal, can exist within the same tumor and are controlled by super-enhancer associated transcription factor networks.[28] Adrenergic neuroblastomas exhibit a more differentiated phenotype and are more lineage committed, while mesenchymal neuroblastomas are more undifferentiated and chemoresistant.[28] A strong mesenchymal signature is also associated with relapsed tumors, indicating a selective pressure of chemotherapy on the adrenergic lineage.[28,29] While cell lines often exhibit either adrenergic or mesenchymal features, they can convert from one state to the other, either spontaneously or through experimental intervention.[29,30] In tumors there is a continuum between the adrenergic and mesenchymal states, indicating intratumoral heterogeneity.[29]

1.1.3. Relapse in neuroblastoma

Relapse, particularly of high-risk neuroblastoma, remains a clinical challenge in spite of intensive therapy, with 50% of patients who achieved clinical remission later suffering a relapse.[11] Median post-relapse OS has improved from 3 months to 8.4 months since the 1990s, however, still only 12% of patients survive for longer than 5 years after relapsing.[31] The majority of these curable patients have *MYCN* non-amplified tumors, were initially diagnosed at < 18 months of age and suffered their relapse > 36 months after first diagnosis, while patients who relapse between 6-18 months after diagnosis have the worst outcome.[32] Often patients suffer several recurrences of their tumors, with disease free intervals decreasing with each relapse.[33] New treatment strategies and targets are therefore needed for this particularly vulnerable group of neuroblastoma patients.

1.2. Chemotherapy resistance mechanisms in cancer

Some tumors are inherently resistant to treatment, others develop resistance mechanisms over time. All resistant tumors, whether at primary diagnosis or after progression or relapse, are a devastating clinical problem, with up to 90% of cancer deaths being related to resistance.[34]

Resistance mechanisms can have their origin within the cancer cell. They are then most often caused by genetic or epigenetic alterations that lead to changes in expression and/or activity of relevant genes and proteins. Genetic changes include mutations (e.g. *TP53* mutations in a wide range of tumors)[35], gene amplification (e.g. *MYCN* amplification)[13] or aneuploidity[36]. Epigenetic changes, such as

alterations in histone modifications or in the methylation of genes (e.g. hypermethylation of *TERT* in stage M neuroblastomas)[37], are also an effective and relevant cause for resistance.[34,37–39]
Intratumor heterogeneity further complicates matters and fosters acquired resistance. Heterogeneity evolves over time and space in a branched manner, leading to a remarkable 70% of mutations or lesions not being found in every tumor region.[40] Consequently, treatment response can be non-uniform, both within one tumor area and particularly between the primary site of a tumor and metastatic regions.[41,42] Selection pressure from these differing environments or from drug treatments lead to the survival and enrichment of resistant clones and subsequent relapse.
Besides changes within the cancer cells, changes in the microenvironment, e.g. increased presence of growth factors or a persistent inflammation, can also lead to therapy resistance.[43–45] Cell-adhesive interactions further promote the microenvironment as a niche capable of protecting tumor cells and promoting alternative survival pathways.[41,46,47]

How chemotherapy resistance is mediated can differ between entities and patients, but also depends on the treatment the tumor is resistant to. Classical chemotherapeutics like cisplatin or doxorubicin interfere with the structure of DNA or otherwise cause DNA damage, thus targeting all fast dividing cells. These compounds are often weakened by an increase of the DNA repair mechanisms.[34] Overexpression of the DNA repair machinery, e.g. the endonuclease XPF or DNA excision repair protein ERCC1, have been implicated in resistance against classical chemotherapeutics.[48,49]
Targeted treatments, which inhibit a specific pathway relevant for a particular entity or patient, develop resistance in others ways. A very direct influence is an alteration in the target protein, e.g. a mutation that prevents the specific inhibitor from binding, or overexpression or amplification of the target, increasing protein levels to a point where achievable inhibitor concentrations are no longer sufficient to reach inhibition.[41] Examples include mutations in the *BCR-ABL* fusion in imatinib resistance,[50] or amplification of *EGFR* in response to specific EGFR inhibition.[51]
Alternatively, the targeted pathway can be reactivated, either up- or downstream of the original target. This effect is well described for the MAPK pathway, where *BRAF* upregulation was observed after MEK inhibition,[52] or activating *MEK* mutations in BRAF inhibition.[53] Another example is an activating mutation in *PI3K* or loss of PI3K inhibiting protein PTEN following ERBB2 inhibition.[54,55]
Activation of a parallel signaling pathway can also play a role in evading targeted treatment. This mostly involves interplays between the PI3K/AKT and the MAPK pathways, which are often both activated by the same receptors and growths factors.[56,57] This close crosstalk mediates resistance in both directions, with resistance to mTORC1 inhibition being mediated through MAPK activation, as well as MEK inhibitor resistance being mediated through the PI3K/AKT pathway.[58–61]

More general mechanisms, which can influence many compounds irrespective of their target, include evasion of apoptosis or a reduction of the concentration of the active compound in the target cells.
Evasion of apoptosis can occur at different points of the apoptotic process and is particularly important, as it mediates resistance not only to drugs but also to other therapeutic approaches like radiotherapy.[62] Intrinsic apoptosis is controlled by a balance between pro- and anti-apoptotic members of the BCL-2 (B-cell lymphoma 2) family of proteins (compare 1.4.1 Apoptosis, p. 10). Upregulation of the anti-apoptotic members (e.g. BCL-2 and BCL-xL in paclitaxel resistance in

melanoma)[63] or downregulation of the pro-apoptotic members (e.g. BIM in bortezomib resistant breast cancer)[64] lead to a shift away from apoptotic cell death and toward resistance. At the post-mitochondrial level apoptotic signaling can be stopped by decreased expression or activity of APAF, inhibiting the formation of the apoptosome,[62,65,66] or by increased expression or activity of the inhibitor of apoptosis (IAP) family of proteins (particularly XIAP), stopping the initiation of the caspase activation cascade.[67-69]

Reducing the concentration of active drug affecting the tumor cell leads to resistance very efficiently. This can be achieved through changes in the xenobiotic metabolism. Enzymes involved in xenobiotics metabolism are divided into phase I and phase II enzymes and aim at detoxifying xenobiotics.[70] Phase I enzymes of the cytochrome P450 (CYP) family make their target molecules more polar, mainly through oxidation. In some cases this is a necessary step in drug activation, as some drugs, e.g. cyclophosphamide, ifosfamide and tamoxifen, are administered in an inactive form and need to be metabolized by CYPs in intestine, liver, kidney or the tumor itself to yield the active drug.[62,71] Other compounds, including taxanes, vinca alkaloids and some kinase inhibitors, are deactivated by the CYP family.[62,72,73] Mutations, changes in expression or activity of these phase I enzymes can therefore greatly influence drug efficacy. Phase II enzymes, e.g. glutathione-S-transferases, uridine diphospho-glucuronosyltransferases, gamma-glutamyl transferases or thiopurine methyltransferases, are conjugating enzymes transferring different molecular groups to xenobiotics, making them inactive.[34,74] High levels of expression or activity of these enzymes therefore decrease the concentration of active drug in the cell and can contribute to multi drug resistance (MDR).

Last but not least, MDR is often mediated by increased drug transport from the cell. Enhanced efflux leads to decreased accumulation of drugs and accordingly to reduced drug efficacy. This is mediated by transmembrane transporters of the ABC (ATP binding cassette) family of transmembrane transporters.[34,75] The ABC family consists of over 40 members across seven subfamilies (ABCA-ABCG), however only a subset is considered relevant in multi drug resistance.[75] Most prominent are *ABCC1*/MRP-1 (multi drug resistance-associated protein-1), *ABCG2*/BCRP (breast cancer resistance protein) and last but not least *ABCB1*/P-gp (P-glycoprotein).[34]

1.2.1. P-glycoprotein/*ABCB1*

P-gp, gene name ATP-binding cassette subfamily B member 1 (*ABCB1*) and also known as multidrug resistance protein 1 (MDR-1), was the first member of the ABC family to be discovered and is the most studied. Its name is derived from the observation that this glycoprotein modulates drug permeability in cells.[76] The physiological function of P-gp is to protect the body from harmful substances, including toxins, xenobiotics and drugs.[77] Accordingly, P-gp levels are high in the intestine, the liver and the kidneys, where it transports its substrates into the intestinal lumen, bile and urine for excretion.[78] Particularly vulnerable compartments like brain, fetus or testis, are additionally protected by high P-gp levels in the blood-brain barrier, placenta and testis-blood barrier.[79–81]

Like all members of the ABC family, P-gp consists of four domains: two cytoplasmic nucleotide binding domains, which bind ATP, and two transmembrane domains, which recognize and bind the substrates.[82] P-gp requires two ATPs to transport a target molecule across the plasma membrane, making transport against a concentration gradient possible.[83] It recognizes a broad range of substances. Their only common feature is the necessity to be amphipathic.[75] Substrates range from conventional chemotherapeutics (e.g. vinca alkaloids or anthracyclines[77]), over targeted cancer therapeutics (e.g. kinase inhibitors such as afatinib[84] and trametinib[85]) and antibiotics[75] to tool compounds that are used to study P-gp function (e.g. dyes like calcein-AM[86], rhodamine 123[87] or Hoechst 33342[75]).

The large number of cancer therapeutics, which are transported by P-gp, make it an important player in the development of MDR in cancer. P-gp is expressed in many different entities, including lung cancer,[88] breast cancer,[89] ovarian cancer,[90,91] bladder cancer,[92] brain tumors[93] and leukemias.[94,95] Although it is not consistently expressed in all patients, it is almost always expressed either at higher levels or in a higher percentage of patients after chemotherapeutic treatment, emphasizing the contribution of P-gp to acquired chemotherapy resistance.
P-gp interaction with cancer therapeutics is not limited to their transport. Some kinase inhibitors have been shown to inhibit P-gp activity,[96–98] and inhibition of the MAPK pathway leads to P-gp degradation,[91] showing the complexity of the resistance mechanisms involved in MDR.

1.3. The ERBB family

The ERBB (Erythroblastic leukemia viral oncogene homolog) family consist of four receptor tyrosine kinases: ERBB1, better known as epidermal growth factor receptor (EGFR); ERBB2, also known as human epidermal growth factor receptor 2 (HER2); ERBB3 and ERBB4. The ERBB receptors are mainly located at the plasma membrane, where they play an integral part in transmitting growth and survival signals from growth factors into the cell.[99]

The ERBB family proteins consist of three main domains: the extracellular domain, which mediates ligand binding and dimerization; a single transmembrane domain; and the intracellular domain, which contains the catalytic domain with several phosphorylation sites and binding sites for downstream signaling proteins.[100] Only EGFR and ERBB4 are fully functioning receptors. ERBB2 cannot be activated by ligands, as the structure of its extracellular domain blocks the ligand binding pocket, but also making the dimerization loop permanently accessible.[100] ERBB3 was long considered an inactive pseudokinase due to critical amino acid substitutions in the catalytic domain, however, the detection of limited kinase activity showed that ERBB3 is only kinase impaired.[101] Both ERBB2 and ERBB3 require another member of the ERBB family for competent signaling.

The different ERBB family members can be activated by several ligands. EGFR can bind epidermal growth factor, transforming growth factor α, amphiregulin, epigen, betacellulin, epiregulin and heparin-binding EGF-like growth factor (HB-EGF). ERBB3 is activated by neuregulin-1 (NRG-1) and NRG-2. ERBB4 binds betacellulin, epiregulin, HB-EGF and NRG1-4.[102,103] Upon ligand binding a shift in

the extracellular domain allows the formation of a dimerization loop.[100] Dimerization is required for continued downstream signaling and dimer pairs of the ERBB family consist of both homo- and heterodimers. As only EGFR and ERBB4 have fully functioning extracellular and intracellular domains, only EGFR/EGFR and ERBB4/ERBB4 homodimers are functional. Heterodimers can consists of any two ERBB family members, but most commonly include ERBB2.[104] In particular the ERBB2/ERBB3 heterodimer is very potent in signaling and plays an important role in neural and cardiac development, but also in carcinogenesis.[100,105,106]

Downstream signaling of the ERBB family can go several ways and partly depends on the family members involved. The PI3K/AKT pathway is strongly activated through heterodimers including ERBB3.[102,107–109] ERBB2 does not directly activate PI3K, while EGFR and ERBB4 are capable of it, but the activation is more efficient with an ERBB3 containing heterodimer.[102,110,111] The PI3K/AKT pathway leads to cell survival by activating the pro-survival protein mTOR, as well as inhibiting the pro-apoptotic BAD.[112,113]
The pro-proliferative MAPK signaling pathway is activated by the whole ERBB family, but especially strongly by ERBB2.[102] The adaptor proteins GRB2 or SHC bind the ERBB receptors and transmit the signal to the MAPK pathway, activating kinases and transcription factors leading to cell division.[103,114]
EGFR and ERBB4 are also capable of binding and activating the non-receptor tyrosine kinase SRC.[114-117] SRC promotes cell survival and proliferation through interactions with the PI3K/AKT and MAPK signaling pathways, but also facilitates invasion and migration through interactions with the cytoskeleton and cell adhesion components.[117] The importance of ERBB4 mediated SRC signaling in pediatric cancer has recently been shown for medulloblastoma.[118]

Dysregulated ERBB signaling plays an important role in many tumor entities. Activating *EGFR* mutations drive non-small-cell lung carcinoma (NSCLC),[119–121] making these tumors highly susceptible to EGFR inhibitors.[122–124] *ERBB2* amplification plays a major role in breast cancer,[99,125] while *ERBB2* mutations have been detected in lung adenocarcinomas, gastric, bladder and endometrial cancers.[102] *ERBB2* amplification or mutations often coincide with elevated ERBB3 levels, e.g. in breast, gastric, prostate, bladder and colorectal cancers.[108,126–128]

1.3.1. ERBB4

ERBB4, the last of the ERBB family to be discovered,[129] has some specific characteristics that the other three receptors lack. ERBB4 is the only member of the ERBB family for which different splice variants are known. The cytosolic splice site either includes (Cyt1) or excludes (Cyt2) exon 26 in the intracellular domain of ERBB4.[104,130,131] The juxtamembrane (JM) splice site gives rise to the JMa isoform, which contains exon 16 of the *ERBB4* gene, or the JMb isoform, which contains exon 15b.[104,132] This leads to four main isoforms: ERBB4-JMa-Cyt1, ERBB4-JMa-Cyt2, ERBB4-JMb-Cyt1 and ERBB4-JMb-Cyt2.[104,133]
Very rarely two more JM variants exist: JMc, which contains neither exon 15b nor exon 16, and JMd, which contains both.[133,134] These rare variants are exclusively found in developing or neoplastic tissues, e.g. the fetal cerebellum, medulloblastoma, pilocytic astrocytoma and ovarian cancer.[134–136] A study

exploring the different JM isoforms in a panel of four neuroblastoma cell lines found the JMa variant to be most strongly expressed, followed by JMd, while JMb and JMc were hardly expressed.[137]

Functionally the splice variants differ in two main aspects: (1) Exon 26 of *ERBB4* contains a WW domain, which is necessary for the binding of, among others, PI3K and ubiquitin ligases.[130,138,139] Therefore, the Cyt2 isoforms of ERBB4 are unable to activate the PI3K/AKT pathway and have an impaired degradation process. (2) Exon 16, but not exon 15b, of the *ERBB4* gene contains the cleavage site for the tumor necrosis factor-α-converting enzyme (TACE), which can consequently only cut ERBB4 proteins containing the JMa isoform.[140] This cleavage by TACE is necessary for further cleavage by γ-secretase, which releases the intracellular domain of ERBB4 (4ICD) as a soluble protein into the cytosol.[141,142]
Once 4ICD is released into the cytosol it can influence cellular signaling in different ways. 4ICD can enter the nucleus, where it acts as a co-activator or co-repressor,[133] e.g. of YAP1,[143] STAT5A,[144,145] ETO2[146] or AP-2,[147] leading to a variety of outcomes. 4ICD also exerts epigenetic control as increased levels of trimethylation at the lysine 9 residue of histone 3 can be linked to 4ICD levels and kinase activity in the nucleus.[148] 4ICD can also act in the cytosol, e.g. by acting as a chaperone for the nuclear entry of STAT5A,[144] or by promoting apoptosis by acting similar to BH3-only proteins.[149]

Like the other ERBB family members, ERBB4 plays a crucial role in development. It is required for normal cardiac development, but also for many aspects of neurodevelopment.[5,104,150] Later in life, ERBB4 is required for the differentiation of mammary glands in late pregnancy and for cardiac homeostasis.[150–152] Its levels remain high in the brain and nervous system, mammary tissue, larger arteries, heart, kidney, testis and thyroid.[104] ERBB4 has also been linked to anti-inflammatory and anti-fibrotic processes and to schizophrenia.[153–155] Unlike ERBB1-3, ERBB4 often plays a role in differentiation processes, rather than acting purely as a pro-proliferative growth signal.[5,104,151,152]

In cancer, the role of ERBB4 is more difficult to pin down than that of the other ERBB family members. Loss of *ERBB4* copy number can be found in several tumor entities, such as lung, esophageal, cervical and bladder carcinomas.[104] In pancreatic tumors *ERBB4* expression correlates with a favorable tumor stage[156] and in hepatocellular cancer ERBB4 is downregulated in patients, while knock out of *ERBB4* in mice led to more severe tumors.[157] All this indicates that ERBB4 might actually act in an anti-oncogenic manner in these tumors. On the other hand, *ERBB4* mutations were identified as the driver of some melanomas,[158] and the importance of the ERBB4/SRC signaling axis in medulloblastoma has also been described.[118] Possible reasons for these discrepancies lie in the different functions of the ERBB4 isoforms, but different ligands - leading to the phosphorylation of different tyrosine residues and recruitment of different downstream proteins - or disease type and stage might also play a role.[103,104]

1.4. Cell death mechanisms

Regulated cell death is an integral part of normal physiology and tissue homeostasis. Cells that are dysfunctional, damaged, or simply no longer necessary, are efficiently cleared away and replaced by new, healthy cells.[159] Dysregulation of cell death mechanisms can have devastating consequences,

ranging from cancer to neurodegenerative or autoimmune diseases. Since the first description of apoptosis as a regulated cell death mechanism in 1972,[160] more than ten different mechanisms have been discovered and described, which are defined by their genetics, biochemistry and functionality.[161] In this thesis I concentrated on two cell death mechanisms that play a role in neuroblastoma: apoptosis and ferroptosis.[162–169]

1.4.1. Apoptosis

Apoptosis was the first regulated cell death mechanism described and is the one studied in most detail and contexts.[160] Apoptosis was initially described by morphological features, such as nuclear condensation and membrane blebbing. More recently, the involvement of caspases has become the defining functional feature. Depending on the cell death initiating event, which determines the subsequent signaling pathway leading to caspase activation, two types of apoptosis are distinguished: intrinsic and extrinsic apoptosis.

Intrinsic apoptosis is initiated, among others, by growth factor withdrawal, DNA damage, endoplasmic reticulum stress, overload of reactive oxygen species (ROS) or replication stress.[161,170,171] These cellular disturbances disrupt a fine balance between members of the BCL-2 family, which control the initiation of intrinsic apoptosis.[172] The BCL-2 family consists of three subgroups: anti-apoptotic proteins (e.g. BCL-2, BCL-xL, MCL-1), pro-apoptotic BH3-only proteins (e.g. BIM, BID, PUMA, BAD) and effector proteins (BAK and BAX).
The effector proteins BAK and BAX form pores in the mitochondrial outer membrane, leading to mitochondrial outer membrane permeabilization (MOMP), the critical step in intrinsic apoptosis.[173,174] While BAK is continuously present at the mitochondrial membrane, BAX cycles between the mitochondrial membrane and the cytosol.[161,175,176] Supporting this retranslocation of BAX is one mechanism by which the anti-apoptotic proteins inhibit pore formation.[175] The pro-apoptotic BH3-only proteins act either as sensitizers (e.g. BIK, BMF, BAD) by inhibiting the anti-apoptotic proteins or as direct activators of BAK and BAX (e.g. BID, BIM, PUMA). Disruption of the balance between anti-apoptotic and pro-apoptotic members of the BCL-2 family leads to MOMP and the release of apoptotic factors, including cytochrome c and SMAC (second mitochondria-derived activator of caspase), from the mitochondria into the cytosol.[173]
Once released into the cytosol, cytochrome c binds apoptotic protease-activating factor 1 (APAF1) and pre-caspase-9, which leads to cleavage of pre-caspase-9 into the active protease.[177] Caspase-9 continues the initiation of the caspase activation cascade by cleaving and activating the executioner caspases-3 and -7.[68] The release of SMAC into the cytosol promotes apoptosis by inhibiting XIAP, which can block the caspase cascade by inhibiting caspase activity.[68,69,178]

Extrinsic apoptosis is initiated through the extracellular microenvironment and is driven by receptors. These are either dependence receptors, where caspase-9 or caspase-3 activation follows loss of the ligand, or death receptors, where apoptosis follows after ligand binding.[161,179–181] When such a cell death inducing ligand binds a death receptor, the death inducing signaling complex (DISC) is formed at the cytosolic side of the cell membrane. The DISC is a multiprotein complex containing several adapter

proteins and pre-caspases-8 or -10, which are subsequently cleaved to their active forms.[182–184] Caspase-8 starts the caspase activation cascade by cleaving and thus activating caspases-3 and -7. Additionally, capsase-8 cleaves BH3-interacting domain death agonist (BID), resulting in the active pro-apoptotic truncated BID (tBID) and linking the extrinsic to the intrinsic apoptosis pathway.[185,186] This mechanism is particularly important in cells expressing the caspase inhibiting protein XIAP, which blocks caspases-3 and -7. By initiating the intrinsic apoptosis pathway via tBID, MOMP is triggered and SMAC is released into the cytosol, inhibiting XIAP and making the progression of apoptosis possible.[178,187,188]

Caspases are the central executive mechanism of apoptosis. They are categorized into three groups: Group I, consisting of caspases-1, -4 and -5, are mainly involved in inflammation. Group II are the effector caspases-3 and -7, and also includes caspase-6. Group III are the initiator caspases-8, -9 and -10.[68] Once caspases-3 and -7 are activated, they cleave a large number of substrates, including - but not limited to - proteins involved in miRNA processing, the endocytotic pathway and DNA repair,[189,190] which ultimately leads to cell death. Typical apoptotic cell death includes membrane blebbing, externalization of phosphatidylserine to the outside of the plasma membrane, nuclear fragmentation and chromatin condensation.[161] It ends by the formation of apoptotic bodies, which are taken up by macrophages *in vivo* or disintegrate in secondary necrosis *in vitro*.[191,192]

1.4.2. Ferroptosis

Ferroptosis is a relatively newly described mechanism of cell death.[193] It is characterized by the oxidation of intracellular lipids and a dependency on intracellular iron. Dixon and Stockwell defined three hallmarks, all of which are necessary for ferroptotic cell death to occur[194]:

The first hallmark of ferroptosis is the oxidation of phospholipids containing polyunsaturated fatty acids (PUFAs), e.g. arachidonic or adrenic acid.[195] Unlike saturated fatty acids, PUFAs are very susceptible to oxidation,[196–198] which can occur with enzymatic help, e.g. by lipoxygenases (LOXs),[198,199] but also in a non-enzymatic manner via Fenton reactions at the lysosomes.[200–202] In both cases iron is involved, either as the di-iron centers of the LOXs or as part of the Fenton reaction.[203,204]

Availability of redox-active iron is therefore the second hallmark of ferroptosis. Iron is taken up into the cell by transferrin via transferrin receptor-1 (TfR) and released in the acidic environment of lysosomes.[200] Both iron chelators and blocking iron uptake efficiently inhibits ferroptosis.[200,205–207]

The third and final hallmark of ferroptosis is loss of lipid peroxide repair. Under physiological circumstances, PUFA oxidation is tightly controlled. The selenoenzyme glutathione peroxidase 4 (GPX4) specializes in reducing oxidized PUFAs.[208] GPX4 inactivation is often sufficient to induce ferroptosis.[199,209–211] Due to GPX4 dependency on glutathione, ferroptosis can also be induced by a disruption of the glutathione metabolism, e.g. by decreasing intracellular cysteine levels through inhibition of the cystine/glutamate antiporter system X_c^-.[193,210,212] While GPX4 plays the most important part in reducing PUFAs, other molecules like vitamin E or coenzyme Q10 also play a role.[194,213] Pharmacologically, lipophilic antioxidants such as ferrostatin-1 or liproxstatin-1 very efficiently inhibit ferroptosis.[193,199,211,214]

Unlike apoptosis, ferroptosis does not require a complex machinery of transcriptional upregulation or posttranscriptional control of proteins, but is rather the result of a metabolic imbalance within the cell.[193,194,205,215] It results in a necrotic phenotype with mitochondrial alterations such as shrinkage, disappearance of cristae and ruptured mitochondrial membranes.[161,215] Still, the sensitivity of cells to ferroptotic stimuli can vary greatly and is dependent on transport, storage and metabolism of iron, on the levels of cystine, cysteine, glutamine and glutathione, and on the availability of PUFAs to be oxidized.[194,205]

2. Aims

New diagnostic tools and therapeutic options have increased the survival chance of pediatric oncology patients in the last decades. However, chemotherapy resistance, particularly after relapse, remains a clinical challenge. Wang *et al.* coined the term of the one-two punch model, which stipulates that the initial treatment of a tumor causes changes within the tumor cells. While these changes on the one hand lead to resistance, they might on the other hand also cause a novel vulnerability within the tumor, which can be targeted to break resistance to the initial compound.[216]

Following this line of thought, I first aimed to identify such novel vulnerabilities in relapsed pediatric tumors to overcome resistance. For this, I used two different approaches: (1) by comparing gene expression data from relapsed patients included in the Individualized Therapy for Relapsed Malignancies in Childhood (INFORM) study to data from patients at primary diagnosis, using an unbiased approach allowing the analysis of a wide range of genes and several pediatric tumor entities; (2) by functionally identifying compounds that could actively break chemotherapy resistance in neuroblastoma cell lines in combination with the chemotherapeutic vincristine (VCR).

The second aim of my thesis was the validation of the identified targets in neuroblastoma, using further gene expression datasets derived from patient and cell line samples, as well as cell line models for functional studies. For those, my focus lay on validating inhibitors against my identified targets, which induced efficient cell death in combination with VCR, and on functionally showing their on-target effects.

Finally, I performed cell death analysis to identify which type of cell death - apoptosis or ferroptosis, both known to be of importance in neuroblastoma - was induced by the combination of VCR with the identified inhibitors. I aimed to identify if inhibition of the novel vulnerability would favor one cell death mechanism over the other.

3. Material & Methods

3.1. Material

3.1.1. Cell lines and cell culture

3.1.1.1. Cell lines

Table 1: Cell lines. NA = Not applicable

Cell line	**Tissue of origin**	**Characteristic**	**Patient received chemotherapy prior to cell line establishment**	**Supplier**
CHP-134 (RRID: CVCL_1124)	Left adrenal gland[217]	*MYCN* amplified[218]	Yes[217]	F. Westermann, DKFZ, Heidelberg, Germany
IMR-32 (RRID: CVCL_0346)	Abdomen[219]	*MYCN* amplified[218]; partially *ALK* amplified[220]	No[219]	DSMZ, Darmstadt, Germany
Kelly (RRID: CVCL_2092)		*MYCN* amplified; activating *ALK* mutation[221]	Unknown	DSMZ, Darmstadt, Germany
LA-N-5 (RRID: CVCL_0389)	Bone marrow (metastasis)[218]	*MYCN* amplified; activating *ALK* mutation[220]	No[222]	F. Westermann, DKFZ, Heidelberg, Germany
MHH-NB-11 ctrl (RRID: CVCL_1412)		*MYCN* amplified[223]	Yes[223]	M. Michaelis, University of Kent, UK
MHH-NB-11 rVCR		VCR resistant sub-clone of MHH-NB-11	Yes[223]	M. Michaelis, University of Kent, UK
NB-1 (RRID: CVCL_1440)	Cervical lymph node (metastasis)[224]	*MYCN* amplified;[225] *ALK* amplified[220]	Unknown	RIKEN Cell Bank, Japan
NB8 / NB-S-124	Bone marrow[226]	*MYCN* amplified[226]	Unknown	F. Westermann, DKFZ, Heidelberg, Germany
NB-S-124 ctrl	See above	Equivalent to NB8/NB-S-124	Unknown	M. Michaelis, University of Kent, UK
NB-S-124 rVCR	See above	VCR resistant sub-clone of NB-S-124	Unknown	M. Michaelis, University of Kent, UK
NGP ctrl (RRID: CVCL_2141)	Lung (metastasis)[218]	*MYCN* amplified[218,227]	Yes[228]	M. Michaelis, University of Kent, UK

Cell line	Tissue of origin	Characteristic	Patient received chemotherapy prior to cell line establishment	Supplier
NGP rVCR	See above	VCR resistant sub-clone of NGP	Yes[228]	M. Michaelis, University of Kent, UK
SIMA (RRID: CVCL_1695)	Adrenal gland[229]	*MYCN* amplified[229]	Yes[229]	F. Westermann, DKFZ, Heidelberg, Germany
SK-N-BE(1) (RRID: CVCL_9898)	Bone marrow (metastasis)[230]	Same patient as SK-N-BE(2); *MYCN* amplified[218]	No[230]	COG, Philadelphia, USA
SK-N-BE(2) (RRID: CVCL_0528)	Bone marrow (metastasis)[230]	Same patient as SK-N-BE(1); *MYCN* amplified;[218] non-functional *TP53*[164] and *NF1*[231]	Yes[230]	DSMZ, Darmstadt, Germany
SK-N-BE(2)-C (RRID: CVCL_0529)	See above	Sub-clone of SK-N-BE(2)	Yes	ECACC, Salisbury, UK
SK-N-BE(2)-C ctrl	See above	Equivalent to SK-N-BE(2)-C	Yes	M. Michaelis, University of Kent, UK
SK-N-BE(2)-C rVCR	See above	VCR resistant sub-clone of SK-N-BE(2)-C ctrl	Yes	M. Michaelis, University of Kent, UK
SMS-KAN (RRID: CVCL_7131)	Pelvis[232]	Same patient as SMS-KANR; *MYCN* amplified[218]	No[232]	COG, Philadelphia, USA
SMS-KANR (RRID: CVCL_7132)	Bone marrow (metastasis)[232]	Same patient as SMS-KAN; *MYCN* amplified[218]	Yes[232]	COG, Philadelphia, USA

3.1.1.2. Cell culture media and solutions

Table 2: Cell culture media, supplements & dissociation reagent

Medium / Supplement	Cat. No.	Supplier
DMEM	41965-062	Gibco, ThermoFisher Scientific Inc., Waltham, MA, USA
RPMI-1640	21875-091	Gibco, ThermoFisher Scientific Inc., Waltham, MA, USA
IMDM	21980-032	Gibco, ThermoFisher Scientific Inc., Waltham, MA, USA
Neurobasal A	10888-022	Gibco, ThermoFisher Scientific Inc., Waltham, MA, USA
Phenol red-free RPMI-1640	11835-030	Gibco, ThermoFisher Scientific Inc., Waltham, MA, USA
OptiMEM	31985-047	Gibco, ThermoFisher Scientific Inc., Waltham, MA, USA
Fetal calf serum (FCS)	F7524	Sigma-Aldrich, Munich, Germany
Non-Essential Amino Acids Solution (100X)	11140035	Gibco, ThermoFisher Scientific Inc., Waltham, MA, USA
B27	17504-044	Gibco, ThermoFisher Scientific Inc., Waltham, MA, USA
EGF	C-60170	PromoCell, Heidelberg, Germany

Medium / Supplement	Cat. No.	Supplier
FGFb	C-60240	PromoCell, Heidelberg, Germany
Heparin	H3149-100KU	Sigma-Aldrich, Munich, Germany
L-Glutamin, 200 mM	G7513	Merck, Darmstadt, Germany
Trypsin –EDTA (0.05%)	25300096	Gibco, ThermoFisher Scientific Inc., Waltham, MA, USA
Dulbecco's phosphate buffered saline (DPBS)	D8537	Sigma-Aldrich, Munich, Germany

Table 3: Composition of versene (1 mM EDTA in DPBS, pH 7). Versene was autoclaved and sterile filtered prior to use.

DBPS	500 ml
0.5 M EDTA in H_2O	1 ml

3.1.2. Treatment reagents and drugs

Table 4: Treatment reagents and drugs

Substance	Cat. No.	Supplier
Afatinib	S1011	Selleckchem, Houston, TX, USA
anti-ERBB4 antibody	MA513016	Invitrogen (Thermo Fisher Scientific Inc., Waltham, MA, USA).
BKM120	11587	Cayman Chemicals, Ann Arbor, MI, USA
Bortezomib	CT-BZ001	ChemieTek, Indianapolis, IN, USA
Ceritinib	S7083	Selleckchem, Houston, TX, USA
Copanlisib	S2802	Selleckchem, Houston, TX, USA
Cumene Hydroperoxide (CuOOH)	820502	Merck KGaA, Darmstadt, Germany
Dactinomycin	A4262	Merck KGaA, Darmstadt, Germany
Dasatinib	D-3307	LC Laboratories, Woburn, MA, USA
Decitabine	S1200	Selleckchem, Houston, TX, USA
Dimethylsulfoxid (DMSO)	D8418	Merck KGaA, Darmstadt, Germany
Everolimus	E-4040	LC Laboratories, Woburn, MA, USA
Hydroxychloroquin	C6628	Merck KGaA, Darmstadt, Germany
Lapatinib	S2111	Selleckchem, Houston, TX, USA
Larotrectinib	HY-12866	MedChemExpress, Monmouth Junction, NJ, USA
Neuregulin-1 (NRG-1)	396-HB-050	R&D Systems, Minneapolis, MN, USA
Olaparib	O-9201	LC Laboratories, Woburn, MA, USA
Panobinostat	13280	Cayman Chemicals, Ann Arbor, MI, USA
Staurosporine (STS)	HY-15141	MedChemExpress, Monmouth Junction, NJ, USA
Tariquidar	S8028	Selleckchem, Houston, TX, USA
Trametinib	CT-GSK112	ChemieTek, Indianapolis, IN, USA
Venetoclax	CT-A199-2	ChemieTek, Indianapolis, IN, USA
Verapamil	V4629	Merck KGaA, Darmstadt, Germany
Vincristine (VCR)	S2141	Selleckchem, Houston, TX, USA
Z-VAD-FMK	4800-520	MBL International, Woburn, MA, USA

3.1.3. Antibodies

Table 5: Primary antibodies for Western Blot

Antibody – type	Dilution	Cat. No.	Supplier
rabbit anti-α/β-Tubulin – polyclonal	1:1000	2148	Cell Signaling Technology, Danvers, MA, USA
mouse anti-Actin – monoclonal (AC-15)	1:50.000	A5441	Sigma-Aldrich, Munich, Germany
rabbit anti-AKT – polyclonal	1:1000	9272	Cell Signaling Technology, Danvers, MA, USA
rabbit anti-p-AKT (S473) – polyclonal	1:1000	9271	Cell Signaling Technology, Danvers, MA, USA
rabbit anti-BID – polyclonal	1:1000	2002	Cell Signaling Technology, Danvers, MA, USA
rabbit anti-ErbB4 – monoclonal (111B2)	1:1000	4795	Cell Signaling Technology, Danvers, MA, USA
rabbit anti-ERK – monoclonal (137F5)	1:1000	4695	Cell Signaling Technology, Danvers, MA, USA
rabbit anti-p-ERK (T202/Y204) – monoclonal (D13.14.4E)	1:1000	4370	Cell Signaling Technology, Danvers, MA, USA
mouse anti-GAPDH – monoclonal (6C5)	1:40.000	MAB374	Merck, Darmstadt, Germany
mouse anti-PARP – monoclonal (4C10-5)	1:1000	556494	BD Biosciences, Heidelberg, Grmany
rabbit anti-P-glycoprotein – monoclonal (E1Y7S)	1:1000	13978	Cell Signaling Technology, Danvers, MA, USA
rabbit anti-p-SRC (Y419) – polyclonal	1:200	AF2685	R&D Systems, Minneapolis, MN, USA
rabbit anti-SRC – monoclonal (32G6)	1:1000	2123	Cell Signaling Technology, Danvers, MA, USA
mouse anti-Transferrin Receptor – monoclonal (H68.4)	1:1000	13-6800	ThermoFisher Scientific, Braunschweig, Germany

Table 6: Secondary antibodies for Western Blot

Antibody – type	Dilution	Cat. No.	Supplier
donkey anti-rabbit IgG HRP – polyclonal	1:60.000	31.458	ThermoFisher Scientific, Braunschweig, Germany
goat anti-mouse IgG HRP – polyclonal	1:70.000	115-035-003	Diaova, Hamburg, Germany

Table 7: Antibodies for immunofluorescent microscopy

Antibody – type	Dilution	Cat. No.	Supplier
rabbit anti-ErbB4 – monoclonal (111B2)	1:100	4795	Cell Signaling Technology, Danvers, MA, USA
mouse anti-P-glycoprotein – monoclonal (MRK16)	1:250	Ab00143-1.1	Absolut Antibody Ltd, Redcar, UK
donkey anti-rabbit IgG Alexa Fluor 508 – polyclonal	1:500	A10042	ThermoFisher Scientific Inc., Waltham, MA, USA
goat anti-mouse IgG Alexa Fluor 488 – polyclonal	1:1000	4408S	Molecular Probes, ThermoFisher Scientific Inc., Waltham, MA, USA

Table 8: Antibodies for surface P-gp measurement

Antibody – type	Dilution	Cat. No.	Supplier
mouse anti-P-glycoprotein – monoclonal (MRK16)	1:100	Ab00143-1.1	Absolut Antibody Ltd, Redcar, UK
goat anti-mouse IgG APC – polyclonal	1:500	115-136-068	DIANOVA, Hamburg, Germany

3.1.4. siRNA

Table 9: siRNAs used for knock downs. The three ERBB4 siRNAs were pooled.

siRNA	Cat. No.	Supplier
ERBB4 siRNAs #4	SI00074214	QIAGEN, Hilden, Germany
ERBB4 siRNAs #5	SI02223893	QIAGEN, Hilden, Germany
ERBB4 siRNAs #10	SI04435067	QIAGEN, Hilden, Germany
smartPool ABCB1 siRNA	L-003868-00-0005	Dharmacon, Lafayette, CO, USA
control siRNA #1	AM4635	Ambion, Austin, TX, USA
control siRNA #5	AM4642	Ambion, Austin, TX, USA

3.1.5. Primers

Table 10: Primer used for realtime-PCR. for = forward, rev = reverse.

Primer	Sequence	Supplier
EGFR for	5'-GGAGAACTGCCAGAAACTGACC-3'	Sigma-Aldrich, Munich, Germany
EGFR rev	5'-GCCTGCAGCACACTGGTTG-3'	Sigma-Aldrich, Munich, Germany
ERBB2 for	5'-GGGAAGAATGGGGTCGTCAAA-3'	Sigma-Aldrich, Munich, Germany
ERBB2 rev	5'-CTCCTCCCTGGGGTGTCAAGT-3'	Sigma-Aldrich, Munich, Germany
ERBB3 for	5'-GGTGATGGGGAACCTTGAGAT-3'	Sigma-Aldrich, Munich, Germany
ERBB3 rev	5'-CTGTCACTTCTCGAATCCACTG-3'	Sigma-Aldrich, Munich, Germany
ERBB4 for	5'-GCCTGTCCTTGCTTATCCTCAA-3'	Sigma-Aldrich, Munich, Germany
ERBB4 rev	5'-CCTGCGCTGATTTCCTTCA-3'	Sigma-Aldrich, Munich, Germany
HPRT for	5'-TGACACTGGCAAAACAATGCA-3'	Sigma-Aldrich, Munich, Germany
HPRT rev	5'-GGTCCTTTTCACCAGCAAGCT-3'	Sigma-Aldrich, Munich, Germany
ABCB1 for	5'-GGGATGGTCAGTGTTGATGGA-3'	Sigma-Aldrich, Munich, Germany
ABCB1 rev	5'-GCTATCGTGGTGGCAAACAATA-3'	Sigma-Aldrich, Munich, Germany
SDHA for	5'-TGGGAACAAGAGGGCATCTG-3'	Sigma-Aldrich, Munich, Germany
SDHA rev	5'-CCACCACTGCATCAAATTCATG-3'	Sigma-Aldrich, Munich, Germany

3.1.6. Buffers and solutions

3.1.6.1. Western Blot Solutions

3.1.6.1.1. Cell lysis buffers for protein lysates

Table 11: SDS lysis buffer for protein lysates

Ingredient	Volume	Final concentration
0.5 M Tris/HCl pH 6.8 (stacking gel buffer)	12.4 ml	62.5 mM
20% SDS (w/v) in H_2O	10 ml	2% SDS (w/v)
87% Glycerol	11.5 ml	10% (v/v)
ddH_2O	ad 100 ml	
0.1 M DTT (added immediately before use)	10 µl / 1 ml buffer	1 mM

Table 12: 2x NP-40 buffer

Ingredient	Amount	Final concentration
1 M Trizma Base/HCl, pH 8	5 ml	100 mM
1 M NaCl	15 ml	300 mM
NP-40	1 ml	2% (v/v)
ddH_2O	ad 50 ml	

Table 13: 1x NP-40 buffer

Ingredient	Volume / 100 µl buffer	Final concentration
2x NP-40 buffer (Table 12)	50 µl	50 mM Tris/HCl, 150 mM NaCl, 1% NP-40
10x PhosSTOP	10 µl	1x
10x Protease Inhibitor Cocktail	10 µl	1x
ddH_2O	30 µl	

For the preparation of 10x phosphatase and 10x protease inhibitor stocks, 1 tablet of PhosSTOP or cOmplete Protease inhibitor, respectively, were solved in 1 ml ddH_2O and stored at -20°C.

Table 14: 4x Laemmli buffer. Prior to use 5% (v/v) β-Mercaptoethanol (14.3 M) were added.

Ingredient	Amount	Final concentration
0.5 M Tris/HCl pH 6.8 (stacking gel buffer)	10 ml	62.5 mM Tris/HCl
Glycerol	8 ml	20% (v/v)
20% SDS (w/v)	8 ml	4% (w/v)
Bromophenol blue	2 mg	0.005%
ddH_2O	ad 40 ml	

3.1.6.1.2. Gels for SDS PAGE

Table 15: Stacking gel buffer

Ingredient	Amount	Final concentration
Trizma Base	6.06 g	0.5 M
HCl	added dropwise	to pH 6.8
ddH_2O	ad 100 ml	

Table 16: Running gel buffer

Ingredient	Amount	Final concentration
Trizma Base	18.15 g	1.5 M
HCl	added dropwise	to pH 8.8
ddH_2O	ad 100 ml	

Table 17: Running gel composition

Ingredient	Volume for 8% gel	Volume for 10% gel
H_2O	8.09 ml	7.34 ml
Running gel buffer (1.5 M Tris/HCl, pH 8.8)	3.75 ml	3.75 ml
Acrylamide/Bis solution (40% w/v)	3 ml	3.75 ml
20% SDS in H_2O	75 µl	75 µl
10% APS	75 µl	75 µl
TEMED	25 µl	25 µl
Total volume (2 gels)	15 ml	15 ml

Table 18: Stacking gel composition

Ingredient	Volume
H_2O	3.20 ml
Stacking gel buffer (0.5 M Tris/HCl, pH 6.8)	1.25 ml
Acrylamide/Bis solution (40% w/v)	0.5 ml
20% SDS in H_2O	25 µl
10% APS	25 µl
TEMED	15 µl
Total volume (2 gels)	5 ml

3.1.6.1.3. Running and Transfer buffer

Table 19: 10x Running buffer

Ingredient	Amount	Final concentration
Trizma Base	30.3 g	250 mM
Glycine	144.4 g	1.92 M
SDS	10 g	1%
ddH_2O	ad 1000 ml	

Table 20: 1x Running buffer

Ingredient	Volume	Final concentration
10x Running buffer	100 ml	25 mM Trizma Base, 192 mM Glycine, 0.1% SDS
ddH_2O	ad 1000 ml	

Table 21: 10x Transferbuffer

Ingredient	Amount	Final concentration
Trizma Base	58 g	480 mM
Glycine	29.3 g	390 mM
ddH_2O	ad 1000 ml	

Table 22: 1x Transferbuffer. Stored at 4°C.

Ingredient	Volume	Final concentration
10x Transferbuffer	50 ml	48 mM Trizma Base, 39 mM Glycine
Methanol	100 ml	20%
ddH_2O	ad 500 ml	

3.1.6.1.4. TBS and TBS-T

Table 23: 10x TBS

Ingredient	Amount	Final concentration
Trizma Base	120 g	200 mM
NaCl	400 g	1.37 M
HCl	added dropwise	until pH 7.5
ddH_2O	ad 5000 ml	

Table 24: TBS-T

Ingredient	Volume	Final concentration
10x TBS, pH 7.5	100 ml	20 mM Trizma Base, 137 mM NaCL
Tween-20	1 ml	0.1% (v/v)
ddH_2O	ad 1000 ml	

3.1.6.1.5. Staining solutions

Table 25: Coomassie Brilliant Blue staining solution for SDS gels. Filtered before use and stored protected from light.

Ingredient	Amount	Final concentration
Brilliant Blue G	500 mg	0.05% (w/v)
Isopropanol	250 ml	25% (v/v)
Acetic acid	100 ml	10% (v/v)
ddH_2O	ad 1000 ml	

Table 26: Ponceau staining for membranes. Stored protected from light.

Ingredient	Amount	Final concentration
Ponceau S Solution	5 ml	10% (v/v)
ddH_2O	45 ml	

3.1.6.1.6. Blocking buffer and antibody dilution buffers

Table 27: Standard blocking buffer. Aliquoted at 50 ml and stored at -20°C.

Ingredient	Amount	Final concentration
Nonfat dry milk	200 g	20% (w/v)
FCS (non-inactivated)	200 ml	20% (v/v)
BSA (bovine serum albumin)	30 g	3% (w/v)
NGS (normal goat serum)	10 ml	1% (v/v)
Tween-20	2 ml	0.2% (v/v)
1x TBS	ad 1000 ml	

Table 28: 2% Milk/TBS-T. Stored at 4°C.

Ingredient	Amount	Final concentration
Nonfat dry milk	2 g	2% (w/v)
1x TBS-T	ad 100 ml	

Table 29: 5% BSA/TBS-T. Stored at 4°C.

Ingredient	Amount	Final concentration
BSA (bovine serum albumin)	5 g	5% (w/v)
1x TBS-T	ad 100 ml	

3.1.6.1.7. Stock solutions for WB

Table 30: APS and DTT

Ingredient	Concentration	Note
Ammoniumpersulfate (APS)	10% (w/v) in ddH_2O	stored at -20°C
Dithiothreitol (DTT)	1 M in ddH_2O	stored at -20°C

Table 31: 20% SDS

Ingredient	Amount	Final concentration
SDS	10 g	20% (w/v)
ddH_2O	ad 50 ml	

Table 32: 1 M Tris/HCl, pH 8

Ingredient	Amount	Final concentration
Trizma Base	12.1 g	1 M
HCl	added dropwise	to pH 8
ddH_2O	ad 100 ml	

Table 33: 1 M NaCl

Ingredient	Amount	Final concentration
NaCl	5.8 g	1 M
ddH_2O	ad 100 ml	

3.1.6.1.8. 0.5 M EDTA, pH 8

Table 34: 0.5 M EDTA, pH 8

Ingredient	Amount	Final concentration
EDTA	18.617 g	0.5 M
5 M NaOH	added dropwise	to pH 8
ddH_2O	ad 100 ml	

3.1.6.2. Immunofluorescence microscopy solutions

Table 35: Permeabilization solution

Ingredient	Amount	Final concentration
TritonX100	50 µl	0.1% (v/v)
DBPS	ad 50 ml	

Table 36: Blocking solution for immunofluorescent microcopy

Ingredient	Amount	Final concentration
0.1% TritonX100	25 ml	0.05% (v/v)
BSA	1.5 g	3% (w/v)
DBPS	ad 50 ml	

3.1.6.3. Crystal violet stain

Table 37: Crystal violet stain. Stored protected from light.

Ingredient	Amount	Final concentration
Crystal violet	5 g	1% (w/v)
Ethanol	350 ml	70% (v/v)
ddH_2O	ad 500 ml	

3.1.7. Chemicals and reagents

Table 38: Chemicals and reagents

Article	Cat. Number	Supplier
2-Propanol	13404	VWR Chemicals, Radnor, PA, USA
Acrylamide/Bis solution, 40 % (w/v)	10681.01	Serva Electrophoresis, Heidelberg, Germany
Albumin Standard	23209	Thermo Fisher Scientific Inc., Waltham, MA, USA
APS	A3678	Merck KGaA, Darmstadt, Germany
Beta-mercaptoethanol	39563	SERVA, Heidelberg, Germany
BODIPY 581/591 Lipid Peroxidation Sensor stain	D3861	ThermoFisher Scientific Inc., Waltham, MA, USA
Bovine Serum Albumin	A7906	Merck KGaA, Darmstadt, Germany
Brilliant Blue G	B6529	Merck KGaA, Darmstadt, Germany
Bromphenol blue	A23331.0005	AppliChem, Darmstadt, Germany
Calcein-AM	65-0853-39	ThermoFisher Scientific Inc., Waltham, MA, USA

Article	Cat. Number	Supplier
Caspase Assay 2x Reaction buffer	JM 1068-20	MBL, Woburn, MA, USA
Caspase Assay Cell Lysis buffer	BV-1067-100	Axxora, Enzo Life Sciences GmbH, Lörrach, Germany
Caspase-3 substrate: Ac-DEVD-AFC	556574	BD Pharmingen™, BD Biosciences, Heidelberg, Germany
Caspase-8 substrate: Ac-IETD-AFC	556552	BD Pharmingen™, BD Biosciences, Heidelberg, Germany
cOmplete protease inhibitor cocktail	11697498001	Roche Diagnostics GmbH, Mannheim, Germany
Crystal violet	C6158	Merck KGaA, Darmstadt, Germany
DTT	A1101	AppliChem, Darmstadt, Germany
EDTA	1034	GERBU Biotechnik GmBH, Heidelberg, Germany
Ethanol, absolute	20.821.321	VWR Chemicals, Radnor, PA, USA
Glycerol	15523	Honeywell Riedel-de-Haen, Seelze, Germany
Glycine	13073	GERBU Biotechnik GmBH, Heidelberg, Germany
HCl	13-1683	Merck KGaA, Darmstadt, Germany
HiPerFect	301704	Gibco, Thermo Fisher Scientific Inc., Waltham, MA, USA
Hoechst33342	H3570	Thermo Fisher Scientific Inc., Waltham, MA, USA
Methanol	12693	VWR Chemicals, Radnor, PA, USA
Milk powder	T145.2	Carl Roth, Karlsruhe, Germany
NaCl	BP358-1	Thermo Fisher Scientific Inc., Waltham, MA, USA
NaOH	30620	Merck KGaA, Darmstadt, Germany
OptiMEM	31985-047	Gibco, Thermo Fisher Scientific Inc., Waltham, MA, USA
Paraformaldehyde	43368	Thermo Fisher Scientific Inc., Waltham, MA, USA
Phenol red-free RPMI	11835030	Gibco, Thermo Fisher Scientific Inc., Waltham, MA, USA
PhosSTOP EASYPack	4906845001	Roche Diagnostics GmbH, Mannheim, Germany
Ponceau S solution	A2935.0500	AppliChem, Darmstadt, Germany
Precision Plus Protein™ Kaleidoscope™ Prestained Protein Standard	1610375	Bio-Rad, Munich, Germany
Rnase free Dnase	79254	QIAGEN, Hilden, Germany
Sodium dodecyl sulfate (SDS) pellets	2326.1	Carl Roth, Karlsruhe, Germany
TEMED	2367.3	Th. Geyer, Renningen, Germany
Trisma Base	T1503	Merck KGaA, Darmstadt, Germany
TritonX100	A4975.0500	AppliChem, Darmstadt, Germany
Trypan Blue solution for microscopy	93595	Merck KGaA, Darmstadt, Germany
Tween 20	500-018-3	MP Biomedicals, Santa Ana, CA, USA
Vi-Cell Reagent Coulter cleanz	8448222	Beckmann Coulter, Krefeld, Germany
Vi-Cell Reagent Isoton II	8448011	Beckmann Coulter, Krefeld, Germany

3.1.8. Consumables

Table 39: Consumables

Article	Cat. No.	Supplier
Chromatography Paper "Whatman™ CHR 3 mm"	3030-917	GE Healthcare, Little Chalfont, UK
Conic tube, 15 ml	188271	ThermoFisher Scientific Inc., Waltham, MA, USA
Conic tube, 50 ml	2098	ThermoFisher Scientific Inc., Waltham, MA, USA
Corning® cell lifter	CLS3008	Sigma-Aldrich, Munich, Germany
Corning® Costar® TC-Treated Multiple Well Plates, 12 wells	3512	Sigma-Aldrich, Munich, Germany
Cryo Vials 2 ml	E315.1	Carl Roth, Karlsruhe, Germany
Falcon® 5mL Round Bottom Polystyrene Test Tube (FACS Tubes)	10186360	ThermoFisher Scientific Inc., Waltham, MA, USA
Falcon™ Polystyrene Microplates, 6 well	353046	ThermoFisher Scientific Inc., Waltham, MA, USA
Falcon™ Standard Tissue Culture Dishes, 10 cm	353003	ThermoFisher Scientific Inc., Waltham, MA, USA
Glassware	divers	SCHOTT AG, Mainz, Germany
Immun-Blot® PVDF Membrane	1620177	Bio-Rad, Munich, Germany
MicroAmp™ Optical Adhesive Film for PCR	4311971	ThermoFisher Scientific Inc., Waltham, MA, USA
Microplate, 96 well for PCR	652260	Greiner Bio-One GmbH, Frickenhausen, Germany
Microplates, 96 well plate, black	655076	Greiner Bio-One GmbH, Frickenhausen, Germany
Microplates, 96 well plate, clear	821581	Sarstedt, Nürnbrecht, Germany
Microplates, 384 well plate, flat bottom, black with clear bottom	781091	Greiner Bio-One GmbH, Frickenhausen, Germany
Microplates, 384 well plate, round bottom, black with clear bottom	3830	Corning, Corning, NY, USA
Millex-GS Syringe Filter 0.22 µm, sterile	SLGS033SS	Sigma-Aldrich, Munich, Germany
Pasteurpipettes, Glas 230 mm	12908	WU Mainz, Bamberg, Germany
Pipet tips, refillable, 10 µl	961-001-20	Steinbrenner Laborsysteme, Wiesenbach, Germany
Pipet tips, refillable, 1000 µl	961-1002-7	Steinbrenner Laborsysteme, Wiesenbach, Germany
Pipet tips, refillable, 200 µl	961-201-20	Steinbrenner Laborsysteme, Wiesenbach, Germany
Pipet tips, sterile, 10 µl	07-613-8300	nerbe plus, Winsen/Luhe, Germany
Pipet tips, sterile, 100 µl	07-642-8300	nerbe plus, Winsen/Luhe, Germany
Pipet tips, sterile, 1000 µl	06-693-5300	nerbe plus, Winsen/Luhe, Germany
Pipet tips, sterile, 20 µl	07-622-8300	nerbe plus, Winsen/Luhe, Germany
Pipet tips, sterile, 200 µl	07-662-8300	nerbe plus, Winsen/Luhe, Germany
Reaction tubes, 0.5 ml	0030121023	Eppendorf, Hamburg, Germany
Reaction tubes, 1.5 ml	72.690.001	Sarstedt, Nürnbrecht, Germany
Reaction tubes, 1.5 ml	0030120086	Eppendorf, Hamburg, Germany
Reaction tubes, 2 ml	0030120094	Eppendorf, Hamburg, Germany

Article	Cat. No.	Supplier
Sapphire PCR tubes, 0.2 ml	683201	Greiner Bio-One GmbH, Frickenhausen, Germany
Serological pipettes, 10 ml	4488	Sigma-Aldrich, Munich, Germany
Serological pipettes, 25 ml	4489	Sigma-Aldrich, Munich, Germany
Serological pipettes, 5 ml	4487	Sigma-Aldrich, Munich, Germany
Serological pipettes, 50 ml	4490	Sigma-Aldrich, Munich, Germany
T175 Tissue Culture Flask	660175	Greiner Bio-One GmbH, Frickenhausen, Germany
T25 Tissue Culture Flask	690175	Greiner Bio-One GmbH, Frickenhausen, Germany
T75 Tissue Culture Flask	658175	Greiner Bio-One GmbH, Frickenhausen, Germany
Vi-CELL® 4 ml Sample Vials	383721	Beckmann Coulter, Krefeld, Germany

3.1.9. Kits

Table 40: Kits

Article	Cat. No.	Supplier
Amersham ECL Prime Western Blotting Detection Reagent	RPN2232	GE Healthcare, Little Chalfont, UK
CellTiterGlo 2.0	G9243	Promega, Madison, WI, USA
First Strand cDNA Synthesis Kit	K1612	ThermoFisher Scientific Inc., Waltham, MA, USA
Pierce™ BCA Protein Assay Kit	23227	ThermoFisher Scientific Inc., Waltham, MA, USA
PlasmoTest™ Mycoplasma Detection Kit	Rep_ptrk	InvivoGen, Toulouse, France
QIAmp® DNA Mini Kit	51304	QIAGEN, Hilden, Germany
qPCR MasterMix for SYBR Green I	RT-SN2x-03T	Eurogentec, Seraing, Belgium
Radiance Q HRP Substrate for CCD Imaging	512101	Biozym Biotech Trading GmbH, Wien, Austria
RNeasy® Mini Kit	74106	QIAGEN, Hilden, Germany
Venor®GeM Classic Mycoplasma Detection Kit	11-1250	Minerva Biolabs, Berlin, Germany

3.1.10. Equipment and instruments

Table 41: Equipment and Instruments

Instrument	Supplier
7500 Real Time PCR System	ThermoFisher Scientific Inc., Waltham, MA, USA
Azure Imaging System 400	Azure Biosystems, Dublin, CA, USA
Bench top centrifuge Allegra® X-12	Beckman Coulter, Krefeld, Germany
Biometra T3000 Thermocycler	LabRepCo, Horsham, PA, USA
Corning® CoolCell® cryogenic storage box	Corning, NY, USA
D300e digital drug dispenser	Tecan, Männedorf, Switzerland
Electrophoresis Power Supply EV231	PEQLab, Erlangen, Germany
FACSCanto II	BD Biosciences, Heidelberg, Germany
FLUOstar OPTIMA plate reader	BMG Labtech, Ortenberg, Germany

Instrument	Supplier
Heating block Mixer HC	STARLAB, Hamburg, Germany
ImageXpress Micro Confocal high content microscope	Molecular Devices, San Jose, CA, USA
Light microscope CKX31	Olympus, Hamburg, Germany
Microcentrifuge 5417 R	Eppendorf, Hamburg, Germany
Micropipette 10 µl	Eppendorf, Hamburg, Germany
Micropipette 100 µl	Eppendorf, Hamburg, Germany
Micropipette 1000 µl	Gilson, Middleton, WI, USA
Micropipette 200 µl	Eppendorf, Hamburg, Germany
Mini-PROTEAN Tetra Vertical Electrophoresis Cell	Bio-Rad, Munich, Germany
NanoDrop 2000 Spectrophotometer	ThermoFisher Scientific Inc., Waltham, MA, USA
Perfection V700 photo	Epson, Tokyo, Japan
pH-Meter SevenEasy	Mettler-Toledo, Gießen, Germany
Pipet controller accu-jet® pro	BRAND, Wertheim, Germany
Precision balance 440-47N	KERN & SOHN, Balingen, Germany
Precision balance AB54	Mettler-Toledo, Gießen, Germany
Rocking Platform WT16	Biometra, Göttingen, Germany
Spark plate reader	Tecan, Männedorf, Switzerland
Tube roller RS-TR05	Phoenix Instruments, Garbsen, Germany
Vi-CELL® XR cell viability analyzer	Beckman Coulter, Krefeld, Germany
Waterbath SWB20	P-D Industriegesellschaft mbH, Dresden, Germany

3.1.11. Software

Table 42: Software

Software	Version
BD DIVA	8.0.x
BMG Reader Control Software	V2.20 R2
D300eControl	3.3.1
FlowJo	10.x
ImageJ	1.53e
MARS Data Analysis Software	V3.01 R2
PCR 7500 Software v2.3	v2.3
R	4.0.3
R studio	1.2.1335
Vi-CELL XR	2.03

Table 43: R packages

R package	Version
base	4.0.3
datasets	4.0.3
dendextend	1.15.1
dplyr	1.0.4
drc	3.0-1
ggforce	0.3.2

R package	Version
ggplot2	3.3.5
ggpubr	0.4.0
graphics	4.0.3
grDevices	4.0.3
gtools	3.8.2
methods	4.0.3
outliers	0.14
PharmacoGx	2.2.4
plyr	1.8.6
RankProd	3.14
readxl	1.3.1
reshape2	1.4.4
stats	4.0.3
stringr	1.4.0
utils	4.0.3
xlsx	0.6.5

3.1.12. Databases and datasets

Table 44: Databases

Database	URL	Reference
R2	http://r2.amc.nl	Ref [233]
Reactome	https://reactome.org/	Ref [234]

Table 45: Datasets used in RankProd gene expression analysis

Dataset	Author	n	Date downloaded	Reference
Tumor Pediatric Inform - Pilot / Registry - 483 - MAS5.0 - u133p2	INFORM	483	2018-05-08	Refs [235] and [236]
Tumor Ependymoma - Pfister - 209 - MAS5.0 - u133p2	Pfister	209	2018-05-08	GSE64415; Ref [237]
Tumor Glioma (combined - v3) - Jones - 216 - MAS5.0 - u133p2	Jones	216	2018-05-08	Unpublished data by David T.W. Jones, DKFZ, Heidelberg
Tumor Neuroblastoma public - Versteeg - 88 - MAS5.0 - u133p2	Versteeg	88	2018-05-08	GSE16476; Ref [238]
Tumor Osteosarcoma - Kobayashi - 27 - MAS5.0 - u133p2	Kobayashi	27	2018-05-08	GSE14827; Ref [239]
Tumor Rhabdomyosarcoma - Barr - 58 - MAS5.0 - u133p2	Barr	58	2018-05-08	GSE66533; Ref [240]

Table 46: Datasets used in validation analyses

Dataset	Author	n	Date downloaded	Reference
Tumor Neuroblastoma Prim Relapse - Schramm - 18 - custom - ag44kcwolf	Schramm	18	2021-09-09	GSE65303; Ref [241]
Cell line Neuroblastoma - Jagannathan - 38 - custom - ilmnhwg6v2	Jagannathan	38	2021-06-08	GSE19274; Ref [242]
Cell line CCLE Cancer Cell Line Encyclopedia - Broad - 917 - MAS5.0 - u133p2	Broad	917	2021-06-08	GSE36133; Ref [243]
Cell line Neuroblastoma - Versteeg - 24 - MAS5.0 - u133p2	Versteeg	24	2021-01-07	GSE28019
Cell line Neuroblastoma - Utnes - 10 - deseq2 - ravi002	Utnes	10	2021-01-07	GSE148700; Ref [244]
Cell line Neuroblastoma - Maris - 41 - FPKM - rsg001	Maris	41	2021-01-07	GSE89413; Ref [174]
Tumor Pediatric Inform - pilot / registry - 1645 - fpkm - gencode19	INFORM	1645	2021-08-25	Refs [235] and [236]

3.2. Methods

3.2.1. Analysis of Gene Expression Data

3.2.1.1. Differential gene expression analysis between primary and relapsed pediatric tumors

To investigate expression differences between primary and relapsed pediatric tumors, I downloaded the gene expression datasets detailed in Table 45 from R2[233] and subdivided them to ensure that I compared similar molecular subgroups (Table 49). To ensure similar variance between the groups being compared I plotted the log2 transformed data using the standard boxplot function from R graphics package. I controlled that there was no batch effect by calculating the Euclidean distance between samples and performing hierarchical clustering with the stats package. To identify up- and downregulated genes between the primary and relapse groups I used the RankProd package from Bioconductor.[245,246] This package facilitates the calculation of the Rank Product, a non-parametric statistical test, which is based on the rank of a gene in a dataset rather than its absolute expression value. This allowed me to compare primary and relapsed tumors from different datasets. I accepted genes as up- or downregulated with a percentage of false prediction (PFP) < 0.05 and a fold change (FC) > 2 between primary and relapse.

I used the online platform Reactome to perform pathway enrichment analysis.[234] Reactome uses a hypergeometric distribution test to calculate which pathways are over-represented in a submitted list of genes. It uses the Benjamini-Hochberg method to correct the resulting p-values for false discovery rate (FDR). I used three list of genes to perform the pathway enrichment analysis for each tumor entity: I analyzed up- and downregulated genes separately as well as all regulated genes together. I then complied all pathways that were enriched at $p < 0.05$. In cases where pathways were enriched in more than one gene set I used the lowest p-value. I manually sorted the resulting list of pathways into six groups: Pathways concerned with the extracellular matrix (ECM), pathways involved in ERBB family signaling, cell cycle pathways, pathways concerned with the immune system, other signaling pathways and other pathways.

3.2.1.2. Validation with neuroblastoma datasets

To validate my findings from the gene expression analysis and functional screen I used the neuroblastoma cell line and patient datasets from R2 detailed in Table 46.
The dataset by Schramm contains paired gene expression data from the same patients before and after relapse. The version of the INFORM dataset I used for the validation analysis contains more samples than the one with which I performed the initial gene expression analysis, due to the later download date. Also, due to a change in the INFORM pipeline, this dataset contains RNA sequencing data rather than gene expression data from an affymetrix array. As the INFORM dataset contains only relapsed tumors I compared the neuroblastoma cohort to all other entities in the dataset.

For the cell line datasets, I included only those cell lines that I could positively identify as having been derived before or after the patient had received chemotherapy and defined these as primary and relapse, respectively.
I only included members of the ABC family of transmembrane transporters and the four ERBB family members into my validation analysis. I used ANOVA followed by Tukey's post-test to determine differences between the respective groups (primary vs. relapse and relapsed neuroblastoma vs. other relapsed pediatric entities, respectively).
Where paired samples were available (Schramm and Utnes datasets) I calculated the FC from the respective primary (tumor) to relapse samples for the ERBB family and *ABCB1*. I used Student's t-test against 0 on the log transformed values of the relapsed samples to determine statistical significance.

3.2.2. Cell Culture

3.2.2.1. Propagation and seeding of cells

All cell lines were kept at standard cell culture conditions, at 37°C in humidified atmosphere containing 5% CO_2. All cell culture reagents were warmed to room temperature prior to use. Cells were usually kept in T75 tissue culture flasks and passaged once or twice a week, when they reached 70-80% confluence. Approximate splitting ratios for all cell lines can be found in Table 47.
For passaging, the supernatant of adherent cell lines (compare Table 47) was discarded and cells were either washed off with 8 ml fresh medium (CHP-134, SIMA, SMS-KAN), or incubated 3-4 min at 34°C with 3 ml versene (SK-N-BE(1)) or trypsin-EDTA (all other adherent cell lines). To stop the dissociation reaction, 5 ml fresh medium was added and cells were further separated by careful pipetting.
The supernatant of semi-adherent cell lines was collected along with all cells that were easily washed off. For NB-S-124 and SMS-KANR this was sufficient to collect all cells, while LA-N-5 were incubated with 3 ml versene for 3-4 min at 37°C and collected with medium. Semi-adherent cells were then centrifuged 5 min at 335 x *g*. The supernatant was discarded completely (NB-S-124 and SMS-KANR) or reduced to roughly 1/2 – 1/3 of total volume (LA-N-5) and cells were carefully re-suspended in (additional) fresh medium.
Prior to seeding, cell count and viability of the single cell suspension was assessed by trypan blue exclusion using the Vi-CELL XR automated cell counter. All cell lines were seeded in their respective growth medium, with the exception of the VCR resistant cell lines (rVCR), which were seeded in IMDM + 10% FCS without addition of VCR.

3.2.2.2. Freezing and defrosting of cells

Cells were frozen at low passage numbers and stored at -80°C for short term use or in liquid nitrogen for long term storage. For freezing, cells were counted and viability was assessed with the Vi-CELL XR automated cell counter. Cells were only frozen if the viability exceeded 85%. The cell suspension was centrifuged 5 min at 335 x *g* and re-suspended at 2-5 x 10^6 cells/ml in their respective culture medium (compare Table 47) supplemented with 10% DMSO. 1 ml aliquots were transferred to cryovials and frozen at -80°C in a cryogenic storage box (Corning® CoolCell®) at a constant rate of -1°C/minute for at

least 24 h before being transferred to their normal storage place at -80°C or in liquid nitrogen. All cell lines intended for long term storage were tested by Multiplex contamination and authentication analysis (compare 3.2.2.3 Contamination control and cell line authentication, p. 34) prior to placement in liquid nitrogen.

For defrosting, cells were quickly warmed to 37°C and diluted in 10 ml of their respective growth medium. They were then centrifuged 5 min at 335 x *g* and the supernatant containing DMSO was discarded. The cell pellet was re-suspended in 4 ml medium + 1 ml FCS and transferred to a T25 tissue culture flask.

Table 47: Culture conditions of cell lines. SN = supernatant.

Cell line	Medium	Adherent	Dissociation	Split ratios	SN transferred
CHP-134	RPMI-1640 + 10 % FCS	Yes	Pipetting	1:8-1:16 2x/week	No
IMR-32	DMEM + 10 % FCS + 1% NEAA	Yes	Trypsin – EDTA	1:4-1:8 2x/week	No
Kelly	RPMI-1640 + 10 % FCS + 1% NEAA	Yes	Trypsin – EDTA	1:4-1:8 2x/week	No
LA-N-5	RPMI-1640 + 10 % FCS	Semi-adherent	Versene	1:2-1:3 1-2x/week	Yes
MHH-NB-11 ctrl	IMDM + 10% FCS	Yes	Trypsin – EDTA	1:4-1:8 2x/week	No
MHH-NB-11 rVCR	IMDM + 10% FCS + 20 ng/ml VCR (freshly added)	Yes	Trypsin – EDTA	1:2 1x/week	No
NB-1	RPMI-1640 + 10 % FCS	Yes	Trypsin – EDTA	1:2-1:3 1-2x/week	No
NB8 / NB-S-124	Neurobasal A + 2% B27 + 0.5 mM L-Glutamin + 2 µg/ml Heparin+ 20 ng/ml FGFb + 20 ng/ml EGF	Semi-adherent	Pipetting	1:2 1-2x/week	Only for centrifugation
NB-S-124 ctrl	IMDM + 10% FCS	Yes	Trypsin – EDTA	1:10-1:20 2x/week	No
NB-S-124 rVCR	IMDM + 10% FCS + 100 ng/ml VCR (freshly added)	Yes	Trypsin – EDTA	1:5-1:10 2x/week	No
NGP ctrl	IMDM + 10% FCS	Yes	Trypsin – EDTA	1:4-1:8 2x/week	No
NGP rVCR	IMDM + 10% FCS + 20 ng/ml VCR (freshly added)	Yes	Trypsin – EDTA	1:4-1:8 2x/week	No

Cell line	Medium	Adherent	Dissociation	Split ratios	SN transferred
SIMA	RPMI-1640 + 10% FCS	Yes	Pipetting	1:2 1-2x/week	No
SK-N-BE(1)	RPMI-1640 + 10% FCS	Yes	Versene	1:2-1:3 1-2x/week	No
SK-N-BE(2)	RPMI-1640 + 10 % FCS	Yes	Trypsin – EDTA	1:4-1:8 2x/week	No
SK-N-BE(2)-C	DMEM + 10% FCS + 1% NEAA	Yes	Trypsin – EDTA	1:3-1:6 2x/week	No
SK-N-BE(2)-C ctrl	IMDM + 10% FCS	Yes	Trypsin – EDTA	1:4-1:8 2x/week	No
SK-N-BE(2)-C rVCR	IMDM + 10% FCS + 20 ng/ml VCR (freshly added)	Yes	Trypsin – EDTA	1:3-1:6 2x/week	No
SMS-KAN	RPMI-1640 + 10% FCS	Yes	Pipetting	1:2 1-2x/week	No
SMS-KANR	RPMI-1640 + 10% FCS	Semi-adherent	Pipetting	1:2 1x/week	Only for centrifugation

3.2.2.3. Contamination control and cell line authentication

All cell lines were checked for mycoplasma contamination by polymerase chain reaction (PCR) once a month using the Venor®GeM kit (Minerva Biolabs) or with the PlasmoTest™ Mycoplasma Detection Kit (InvivoGen) in all other weeks. For this, an aliquot of the supernatant of all cell lines in culture was transferred to a 1.5 ml reaction tube and incubated 5 min at 95°C or 10 min at 99°C, respectively. The supernatants were stored at 4°C until testing.

Cells were also checked for a broad range of contaminations with the Multiplex cell Contamination Test (McCT)[247] and authenticated by Multiplex Cell Line Authentication (MCA) test (Multiplexion GmbH, Friedrichshafen, Germany). For this, two aliquots of 10^6 cells were collected, transferred to a 1.5 ml reaction tube and centrifuged at 6,800 x *g* for 5 min. For McCT, one pellet was resuspended in 100 µl DPBS and incubated 25 min at 95°C. It was centrifuged at 20,800 x *g* for 5 min to pellet cellular debris and the supernatant was transferred into a new reaction tube. For MCA, DNA was extracted from the second aliquot with the QIAmp DNA Mini Kit according to the manufacturer's protocol, using DNase and RNase free water as eluent. DNA content was measured by NanoDrop and diluted to 30 ng/ml in 30 µl. Both McCT and MCA samples were stored at 4°C until they were sent for analysis.

3.2.2.4. Generation of VCR resistant cell lines

The VCR resistant cell lines (SK-N-BE(2)-C rVCR, MHH-NB-11 rVCR, NB-S-124 rVCR and NGP rVCR) were a kind gift of M. Michaelis. For their generation the sensitive parental cell lines were continuously exposed to step-wise increasing concentrations of VCR, as described previously,[248] and derived from the Resistant Cancer Cell Line (RCCL) Collection.[249] To sustain the resistant phenotype, VCR resistant cell lines were propagated in VCR containing medium (compare Table 47).

3.2.3. Knock-down of *ERBB4* and *ABCB1*

Depending on the following readout, I used different seeding numbers and plates for the knock-down (KD) of *ERBB4* and *ABCB1*. For KD followed by a viability assay, I seeded 60,000 cells/well in 6 well plates. For colony assays I seeded 800 cells/well in 6 well plates. For calcein efflux assays and for KD control by western blot I seeded 200,000 cells/plate in 10 cm dishes. I allowed the cells to attach overnight and then transfected them with 25 nM of the respective siRNAs in OptiMEM with 0.5% HiPerFect. The *ERBB4* siRNAs and control siRNAs (Table 9) were pooled to 25 nM total siRNA concentration. The next day I performed a medium change with the respective treatments and continued with the respective experiments as detailed below.

3.2.4. Detection of cell death and cell viability

3.2.4.1. Viability assay

Cell death and cell viability were detected by trypan blue staining. Trypan blue is a diazo die that cannot enter cells with an intact membrane. Dead and dying cells cannot uphold membrane integrity, thus allowing trypan blue to enter and stain the cells.
For the detection of cell death by trypan blue exclusion, cells were seeded in 12 well plates at 2 x 10^5 cells/well in 0.5 ml medium. They were left to attach overnight and were treated in technical duplicates the next day in a final volume of 1 ml. Unless stated otherwise, cells were treated for 48 h. Cells were harvested by collecting the supernatant containing dead cells in a 15 ml tube and detaching viable cells with the respective dissociation reagent (compare Table 47). The dissociation reaction was stopped with medium, cells were combined with their respective supernatant and centrifuged 5 min at 335 x *g*. The supernatant was discarded, cells resuspended in 1 ml medium and transferred to Vi-CELL vials. Cell lines that could be detached by simple pipetting (CHP-134, SMS-KAN, SMS-KANR, SIMA) were directly transferred into Vi-CELL vials. Cell viability was assessed with the Vi-CELL XR automated cell counter. For this, cells were aspirated by the Vi-CELL and mixed with trypan blue for three cycles. 50 images were acquired per sample and the number of viable (unstained) and dead (stained) cells were detected by the Vi-CELL XR 2.03 software. The integrated algorithm for the detection of stained and unstained cells was adjusted where necessary to account for different cell size and forms (Table 48). Relative viable cell number (1) and cell death (2) were calculated according to the following formulas:

$$Viable\ cells\ [\%] = 100\% \times \left(\frac{Number\ of\ viable\ cell\ in\ sample}{Number\ of\ viable\ cells\ in\ solvent\ control}\right) \quad (1)$$

$$Cell\ death\ [\%] = 100\% \times \left(1 - \frac{Number\ of\ viable\ cells\ in\ sample}{Number\ of\ total\ cells\ in\ sample}\right) \quad (2)$$

Table 48: Settings of the Vi-CELL automated cell counting for the different cell lines

Cell line	Diameter [microns] Min – Max	Cell bright-ness [%]	Cell sharp-ness	Viable cell spot bright-ness [%]	Viable cell spot area [%]	Minimum circularity	De-cluster degreee
SK-N-BE(1), SK-N-BE(2) and all its subclones	7 – 50	85	100	85	10	0	Medium
NB-1	5 – 50	85	65	70	5	0	High
LA-N-5	2 – 25	90	100	95	10	0	Medium
CHP-134	5 – 50	90	100	85	10	0.5	High
All other cell lines	5 – 50	85	100	65	5	0	Medium

3.2.4.2. CellTiter-Glo (CTG)

To assess metabolic activity a CellTiter-Glo (CTG) assay was used. This assay detects the presence of ATP by a luminescence reaction, which correlates to the metabolic activity of the cells. I seeded cells in 384 round bottom plates at 1000 cell/well in 25 µl and collected them by centrifugation at 500 x *g* for 3 min. After allowing the cells to settle overnight, I treated them using a TECAN D300e digital drug dispenser. 0.1% DMSO and 1000 nM STS were included on all plates as controls. I assessed metabolic activity after 48 h using the CellTiter-Glo 2.0 kit by adding 15 µl of CTG reagent to each well. The plates were mixed by shaking 5 min at 450 rounds per minute (rpm), followed by additional 15 min incubation at room temperature. I measured luminescence at a TECAN Spark plate reader pre-warmed to 28°C. I calculated metabolic activity (3) and percent inhibition (4) by the following formulas, where DMSO is the mean of all healthy controls (0.1% DMSO), STS is the mean of all dead controls (1000 nM STS) and x are the individual data points:

$$Metabolic\ activity\ [\%] = 100 * \left(1 - \frac{DMSO - x}{DMSO - STS}\right) \quad (3)$$

$$Inhibition\ of\ activity\ [\%] = 100 * \left(1 - \frac{x - DMSO}{STS - DMSO}\right) \quad (4)$$

3.2.4.3. Caspase activity assay

Caspases are proteases that are activated by auto-cleavage upon the induction of apoptotic cell death and continue the apoptotic cascade by cleaving their downstream targets. The different members of the caspase family recognize and cleave different amino acid motifs. When active caspases are incubated with fluorescent dyes coupled to the right peptide sequence, they release the active fluorophore by cleaving the peptide sequence, thus allowing to measure caspase activity. I used two different caspase substrates in my analyses: Ac-DEVD-AFC and Ac-IETD-AFC, detecting caspases-3/7 and caspase-8, respectively.

I seeded 2 x 10^6 cells per treatment in 10 cm dishes and allowed them to attach overnight before treatment. Unless stated otherwise, treatment time was 48 h. I harvested the cells, including all cells floating in the supernatant, according to the respective cell line (compare Table 47) and collected the cell pellet by 5 min centrifugation at 500 x *g* and 4°C. From this time on samples were always kept on ice. I washed the cell pellets once with ice cold DPBS and collected them by 3 min centrifugation at 9,000 rpm (8,500 x *g*) and 4°C. Cell pellets were lysed in 65 µl ice cold caspase assay cell lysis buffer and incubated on ice for 10 min. Lysates were stored at -80°C overnight or a maximum of 5 days before the activity assay was performed.
For the caspase activity assay I defrosted the samples on ice and assessed protein concentration of the 1:2 diluted lysates by bicinchoninic acid (BCA) assay (compare chapter 3.2.6.2 Determination of protein concentrations, p. 40). Samples were then diluted to equal amounts of protein (10 µg unless stated otherwise) in 50 µl cell lysis buffer, including cell lysis buffer as blank, and the same volume 2x reaction buffer with freshly added 10 mM DTT was added. Finally, I prepared a stock solution of 1 mg/ml caspase substrate in DMSO and added it at a final concentration of 50 µg/ml to the prepared samples. I transferred the samples in technical duplicates of 50 µl each to a black flat bottom 96 well plate and measured fluorescent emission at a pre-warmed FLUOstar OPTIMA plate reader every 10 min for 3 h (20 cycles) at 37°C. The plate reader was set to 380 nm excitation, 520 nm emission and a gain of 1400. After the run, the time window of linear increase in fluorescent signal was determined and the slope of the linear increase calculated by the integrated BMG Reader Control Software.

3.2.4.4. Bodipy Lipid Peroxidation staining

A marker of ferroptosis is an increase of lipid peroxidation in the cell. This can easily be measured by staining with the BODIPY 581/591 Lipid Peroxidation Sensor stain, which intercalates with cellular membranes. In its reduced state BODIPY 581/591 emits light at 590 nm, which shifts to 510 nm upon oxidation. The increase of green fluorescence can be measured by flow cytometry or microscopy.
I seeded 500,000 cells/well in 6 well plates and allowed them to attach overnight before treatment. I treated wells in duplicates, including an untreated autofluorescence control. Unless otherwise indicated treatment time was 48 h. I harvested the cells, including all cells floating in the supernatant, according to the respective cell line (compare Table 47) and collected the cell pellet by 5 min centrifugation at 500 x *g* and 4°C. I resuspended the cell pellets in phenol red-free RPMI medium with 10% FCS and 20 µM BODIPY, excluding the autofluorescence control, which was resupended in phenol red-free RPMI medium with 10% FCS without stain, and incubated them at 37°C for 30 min in the dark. I collected the cells by 5 min centrifugation at 10,000 rpm (ca. 10,500 x *g*) at 4°C and washed once with ice cold DPBS. From this time on samples were always kept on ice and care was taken to reduce exposure to light. Collecting the cells again, I resuspended them in 200 µl phenol red-free RPMI medium with 10% FCS and measured the oxidized BODIPY using a FACSCanto II flow cytometric analyzer with an excitation at 488 nm and 502 nm longpass and 530/30 nm bandpass filters.

3.2.4.5. Colony formation assay

For the colony formation assay I seeded 800 cells/well in 6 well plates and allowed them to attach overnight. I then performed *ABCB1* KD as described in chapter 3.2.3 Knock-down of *ERBB4* and *ABCB1* (p. 35). 24 h after the KD I treated the cells for 72 h, at which time I changed the medium and allowed the cells to continue to grow and form colonies for 9 additional days. I then discarded the supernatant and stained the cells with a crystal violet staining solution (Table 37). Superfluous stain was removed by washing with ddH_2O. After drying the plates overnight, I scanned them with a Perfection V700 photo scanner and analyzed colony growth with the ITCN plugin in ImageJ.

3.2.5. Measurement of surface ERBB4 and P-gp

3.2.5.1. Immunfluorescence of ERBB4 and P-gp

For immunofluorescence microscopy I seeded 2,500 cells/well in a flat bottom 384 well plate and allowed them to attach overnight. I fixed the cells with 4% paraformaldehyde in DPBS and washed the cells once with DPBS. I then permeabilized the cells with 0.1% TritonX100 in DPBS (Table 35) for 10 min and blocked them in blocking solution (Table 36) for 1 h to avoid unspecific antibody binding. Primary antibodies against ERBB4 and P-gp respectively were diluted in blocking solution as stated in Table 7 and incubated overnight at 4°C. Cells were washed 3x with DPBS before I added the secondary antibodies in blocking solution for 1h at room temperature, diluted as detailed in Table 7. The cells were concurrently stained with 0.5 µg/ml of the nuclear marker Hoechst3334. I took the images using an ImageXpress Micro Confocal high content microscope using the Cy3 (ERBB4), FITC (P-gp), DAPI (Hoechst33342) and brightfield channels.

3.2.5.2. Measuring surface P-gp by FACS

To measure P-gp surface expression, I seeded 2 x 10^6 cells in 10 cm dishes. To harvest the cells I discarded the supernatant and dissociated the cells using versene (Table 3) for 5 min at 37°C. I collected the cells using phenol-red free RPMI medium containing 10% FCS and determined the cell number. I collected the cells by 5 min centrifugation at 230 x *g* at 4°C, resuspended them at 15 x 10^5 cells/ml in phenol-red free medium and aliquoted them into a 96 well plate at 3 x 10^5 cells/well for antibody staining. After this step, the cells were kept on ice at all times. I collected the cells at the bottom of the 96 well plate by 3 min centrifugation at 180 x *g* at 4°C, removed the supernatant and incubated them with the primary antibody on ice for 2 h. I washed the cells 3x with ice cold phenol-red free medium and incubated them with the secondary antibody on ice for 1 h. The antibodies and their dilutions can be found in Table 8. After three more washing steps, I collected the cells in 130 µl phenol-red free medium and analyzed the fluorescence at a FACSCanto II, with excitation at 640 nm and a 670/14 nm bandpass filter to detect the emission at 660 nm.

3.2.6. Western Blot

3.2.6.1. Preparation of cell lysates

The preparation of cell lysates for western blot analysis differed according to the proteins of interest. For the analysis of proteins indicating the cell death mechanisms apoptosis or ferroptosis (Poly(ADP-ribose) polymerase (PARP), BID, TfR) I harvested the cells including the supernatant, to ensure that dead or dying cells were not lost. For these proteins as well as total ERBB4 and P-gp I used a buffer containing SDS to obtain whole cell lysates (Table 11). For all phosphoproteins as well as their respective total protein I used a slightly milder buffer using the detergent NP-40 (Table 12 and Table 13).
For all western blots lysates I seeded 10^6 cells in 10 cm dishes and allowed the cells to attach overnight before treatment. Unless otherwise stated, treatment time for cell death analysis was 48 h and for phosphoprotein analysis 6 h. All protein lysates were stored at -80°C.

For the generation of SDS whole cell lysates for cell death analysis, I harvested the cells, including all cells floating in the supernatant, according to the respective cell line (compare Table 47) and collected the cell pellet by 5 min centrifugation at 500 x *g* and 4°C. I washed the cells twice with ice cold DPBS, collecting them by centrifugation at 8,000 rpm (6,800 x *g*) for 5 min at 4°C.
For the generation of SDS whole cell lysates for total analysis of ERBB4 or P-gp, I harvested the cells by discarding the supernatant, washing the cells twice with ice cold DPBS and collecting them by carefully scraping them off the culture dish on ice in 1 ml ice cold DPBS. I collected the cells by centrifugation at 8,000 rpm (6,800 x *g*) for 5 min at 4°C.
The resulting washed pellets were lysed in 100-150 µl SDS lysis buffer (Table 11), followed by 5 min incubation at 95°C. Debris resulting from cell lysis was collected by centrifugation at 10,000 x *g* for 10 min at 10°C and the supernatant containing the proteins was collected. Protein concentration was determined by BCA assay (compare chapter 3.2.6.2 Determination of protein concentrations, p. 40) and prior to loading 1 µl of a saturated bromophenol blue solution was added to each sample.

For the generation of NP-40 lysates for phosphoprotein analysis, cells were harvested without their supernatant. The supernatant was removed on ice, cells were washed twice with ice cold DPBS and collected by carefully scraping them off the culture dish in 1 ml ice cold DPBS. I collected the cells by 5 min centrifugation at 8,000 rpm (6,800 x *g*) at 4°C and lysed them in 80 µl freshly prepared 1x NP-40 buffer (Table 13) per sample. Cells were broken up by gently pipetting 8-10x, followed by 10 min incubation on ice, a brief vortex and another 10 min incubation on ice. Debris was collected by 15 min centrifugation at 14,000 rpm (20,800 x *g*) at 4°C. The supernatant containing the proteins was collected and protein concentration was determined by BCA assay (compare chapter 3.2.6.2 Determination of protein concentrations, p. 40). Sample aliquots were diluted to equal protein amounts in 1x NP-40 buffer (Table 13), mixed 3:1 with 4x Laemmli buffer (Table 14) and incubated 5 min at 95°C prior to loading.

3.2.6.2. Determination of protein concentrations

Protein concentrations were determined by using the Pierce™ BCA Protein Assay Kit according to the manufacturer's instructions. A protein standard of the supplied albumin ranging from 2000 µg/ml to 25 µg/ml was prepared using the respective lysis buffer (SDS buffer, NP-40 buffer or caspase assay cell lysis buffer). The standard was always kept on ice and stored at -20°C between uses. Samples were diluted 1:2-1:6 in their appropriate lysis buffers to ensure the measured concentrations were within the standard range. I added 5 µl of sample or standard to a clear, flat bottom 96 well plate in triplicates and added 200 µl of the BCA working reagent (reagent A mixed to reagent B in a 50:1 ratio). After 30 min incubation at 37°C the colorimetric change, corresponding to the protein amount present in the sample, was determined at a FLUOstar OPTIMA plate reader by measuring the absorbance at 570 nm.

3.2.6.3. SDS-polyacrylamide gel electrophoresis (SDS-PAGE)

To separate the proteins by size I performed SDS-polyacrylamide gel electrophoresis (SDS-PAGE). Depending on the size of the protein of interest I prepared gels containing either 8% (ERBB4, P-gp, PARP and TfR) or 10% (all other proteins) acrylamide (Table 17), topped by a stacking gel (Table 18) to collect the samples prior to protein separation. Whenever possible I loaded 20 µg of protein per sample. In the rare cases when protein concentrations were too low, I normalized the protein amount to the sample with the lowest concentration to allow comparability between samples. I used the Precision Plus Protein™ Kaleidoscope™ Prestained Protein Standard as marker for protein size. I ran the gel electrophoresis in an electrophoresis chamber filled with 1x Running buffer (Table 20) at 80 V while the samples passed through the stacking gel and at 120 V during protein separation in the running gel.

3.2.6.4. Western Blotting and Immunodetection

To be able to detect proteins by incubation with antibodies, I transferred the proteins from the SDS-polyacrylamide gel to a PVDF membrane with 0.2 µm pore size using a semi-dry system. The PVDF membrane was activated in methanol, washed in ddH_2O and in 1x transfer buffer (Table 22) prior to transfer. Membrane and gel were surrounded by 5 layers of chromatography whatman papers soaked in 1x transfer buffer and care was taken to avoid air bubbles. Transfer occurred at 35 mA per gel for 2-3 h depending on protein size.

After the completed transfer I stained the remaining protein on the SDS-polyacrylamide gel by a coomassie stain (Table 25) for 30 min, followed by washing the stained gel overnight in water. The total transferred protein on the PVDF membrane was stained with a ponceau solution (Table 26) for 5-10 min, followed by a short wash in water and immediate imaging. The ponceau solution was then washed off by incubation with 1x TBS-T for 5-10 min. Both coomassie and ponceau images were scanned using a Perfection V700 photo scanner or the Azure Imaging System 600.

To avoid unspecific antibody binding, I blocked the membrane for 1 h at room temperature in either 2% milk/TBS-T (Table 28) or 5% BSA/TBS-T (Table 29). All phosphoproteins and their respective total protein were blocked in BSA, all other proteins (ERBB4, P-gp, PARP, BID, TfR) were blocked in milk. All primary antibodies were diluted as detailed in Table 5 in their respective blocking buffer. Secondary antibodies were diluted as detailed in Table 6 in 2% milk/TBS-T.

Binding of the primary antibodies occurred overnight at 4°C, while secondary antibodies conjugated to horseradish peroxidase (HRP) were incubated at room temperature for 1 h. All antibody incubations were followed by three washing steps in TBS-T for 10 min at room temperature. Antibody binding was determined by the chemoluminescence emitted by enhanced chemiluminescence (ECL) substrates when in contact with HRP and detected using an Azure Imaging System 400. Images were quantified in ImageJ.

3.2.7. Realtime-PCR

To measure the expression of genes of interest in cell lines I performed real-time reverse transcriptase PCR. For this, I collected 10^6 cells and isolated the RNA with the RNease Mini Kit following the manufacturer's instructions, including the optional on column DNase digestion step and eluting in RNase free water. I measured RNA content using a NanoDrop spectrometer and reverse transcribed 1 µg RNA to cDNA using the First Strand cDNA Synthesis kit according to the manufacturer's instructions. For real-time PCR I added 25 ng cDNA and 0.4 µM each of the respective forward and reverse primer (Table 10) to the qPCR MasterMix for SYBR Green I. I measured the amplification of signal with a 7500 Real Time PCR System under the following cycling conditions: 2 min at 50°C and 10 min at 95°C, followed by 40 cycles of 15 s at 95°C and 1 min at 60°C, ending with 30 s at 95°C and 15 s at 60°C. I calculated the FC based on the $2^{-\Delta\Delta C_T}$ method,[250] using *SDHA* and *HPRT* expression as housekeeping genes.[251] Unless stated otherwise, a mixture of cDNA from untreated LA-N-5, NB-1, IMR-32, Kelly and SK-N-BE(2)-C was used as internal reference to which all values were normalized.

3.2.8. P-gp function assay by calcein efflux

Calcein AM is a membrane permeable dye that is cleaved by cellular esterases, leading to the fluorescent product calcein, which is a substrate of P-gp. Loss of calcein signal is therefore a measure of P-gp activity in living cells. To assess P-gp function I seeded 500,000 cells/well in 6 well plates for drug treatments or 200,000 cells/plate in 10 cm dishes for *ABCB1* KD (compare chapter 3.2.3 Knock-down of *ERBB4* and *ABCB1*, p.35). I allowed them to attach overnight before treatment or KD. Treatment time, unless stated otherwise, was 24 h. After treatment I stained the cells with 10 nM calcein AM for 15 min at 37°C. After KD I stained the cells with 100 nM calcein AM for 30 min at 37°C. I then discarded the supernatant and washed the cells 3x with ice cold DPBS. I carefully scraped the cells off the culture dish in 1 ml ice cold DBPS and collected them by 5 min centrifugation at 800 x *g* at 4°C. I resuspended the cells in phenol red-free RPMI containing 10% FCS and measured calcein signal at a FACSCanto II with excitation at 488 nm and 502 nm longpass and 530/30 nm bandpass filters.

3.2.9. Statistical Analysis of experiments

For the synergy score calculation following CTG measurements I used the online tool SynergyFinder (https://synergyfinder.fimm.fi)[252] based on the Bliss reference model, which assumes independent modes of action of the two drugs under investigation. I calculated all other statistics in R (version 4.0.3). I calculated significance with the core "stats" package using ANOVA followed by Tukeys's post-test or t-test as indicated. I calculated curve fits and IC50s with the "drc" package using a four-parameter log-logistic function. For the area under the curve (AUC) calculation after the functional screen I used the "PharmacoGx" package. I performed outlier calculations with the Grubbs test of the "outliers" package, if necessary. I generated the figures using the "ggplot2" package.

4. Results

4.1. ERBB4 is identified as possible target in chemotherapy resistance by gene expression data

The first aim of my thesis was to identify novel vulnerabilities in relapsed pediatric tumors that might be used to overcome the chemotherapy resistance that is very common in this group. I therefore compared data from relapsed patients available via the INFORM registry[235,236] to data from tumor samples at primary diagnosis. I analyzed gene expression data of five tumor entities. To ensure that I compared only similar molecular subtypes, I further subdivided some entities into molecular subtypes, yielding six individual comparison groups. Table 49 summarizes the datasets used. For ependymoma I focused on the PF-EPN-A subtype (anaplastic ependymoma group A found in the posterior fossa). In high grade gliomas (HGG) I analyzed only data from glioblastomas and diffuse intrinsic pontine gliomas (DIPGs). For the neuroblastoma dataset at primary diagnosis I only included samples from patients with an INSS stage 4 tumor, as these are most likely to relapse. This raised the likelihood of differences between the primary and relapse neuroblastoma datasets being in fact due to treatment, and not due to differences between different tumor stages. I divided the primary rhabdomyosarcoma (RMS) dataset into tumors with a *PAX3-FOXO1* or *PAX7-FOXO1* fusion, which correspond to alveolar RMS, versus fusion negative tumors, which correspond to embryonal RMS. I did not subdivide the osteosarcoma data.

Table 49: Datasets and their subsets used in gene expression analysis. All data was downloaded from R2 (http://r2.amc.nl) in May 2018. HGG: high grade glioma; RMS: rhabdomyosarcoma.

Entity	**Primary dataset from R2**	**Subgroup primary**	**Sample no. primary**	**Tumor class in INFORM (relapse) Ref** [235,236]	**Subgroup in INFORM**	**Sample no. relapse**
Ependy-moma	Tumor Ependymoma - Pfister - 209 - MAS5.0 - u133p2 Ref [237] *GSE64415*	primary and PF-EPN-A	56	Ependy-moma	PF-EPN-A	16
HGG	Tumor Glioma (combined - v3) - Jones - 216 - MAS5.0 - u133p2 *Jones et al., unpublished data*	hgg_dipg or hgg_glio-blastoma	17	High Grade Glioma	hgg_dipg or hgg_glio-blastoma	57
Neuro-blastoma	Tumor Neuroblastoma public - Versteeg - 88 - MAS5.0 - u133p2 Ref [238] *GSE16476*	inss stage 4 and neither recurrence nor progression	13	Neuro-blastoma	-	58

Entity	Primary dataset from R2	Subgroup primary	Sample no. primary	Tumor class in INFORM (relapse) Ref [235,236]	Subgroup in INFORM	Sample no. relapse
Osteo-sarcoma	Tumor Osteosarcoma – Kobayashi - 27 - MAS5.0 - u133p2 Ref [239] *GSE14827*	-	27	Osteo-sarcoma	-	41
Alveolar RMS	Tumor Rhabdomyosarcoma - Barr - 58 - MAS5.0 - u133p2 Ref [240] *GSE66533*	pax3-foxo1 fusion or pax7-foxo1 fusion	33	Rhabdo-myosarcoma	alveolar	34
Embryonal RMS	Tumor Rhabdomyosarcoma - Barr - 58 - MAS5.0 - u133p2 Ref [240] *GSE66533*	fusion-negative	25	Rhabdo-myosarcoma	embryonal	13

As it is problematic and error prone to directly compare data from different gene expression datasets, I used a ranked approach. The RankProd package in R utilizes the Rank Product to obtain differentially expressed genes between two groups. An important assumption of this method is that the measurement variance should be about equal for all samples. Boxplots of the neuroblastoma data showed that, apart from very few outliers, the vast majority of genes were expressed at similar levels, with only minor differences in median and quartiles (Figure 1A). The other entities showed the same tendency (Appendix Figure 1-Appendix Figure 5). To further ensure that there was no over-pronounced batch effect to bias the analysis, I calculated and plotted the Euclidean distance for all samples. As primary and relapsed samples did not cluster as two entirely separate clusters (Figure 1B and Appendix Figure 1-Appendix Figure 5), I concluded that the assumption was fulfilled and proceeded with the analysis.

With the RankProd analysis I generated two lists of results: one identifying upregulated genes in one group over the other and one identifying downregulated genes. The percentage of false prediction (PFP) was computed for all genes in both lists (Figure 1C and Appendix Figure 6) and up or downregulated genes were identified by a PFP < 0.05 in the respective list. To increase biological relevance, I further applied a threshold > 2 for the FC between primary and relapse. I thus generated lists of differentially regulated genes for each entity, ranging from 589 genes in HGG to 2927 genes in osteosarcoma (Figure 1D).

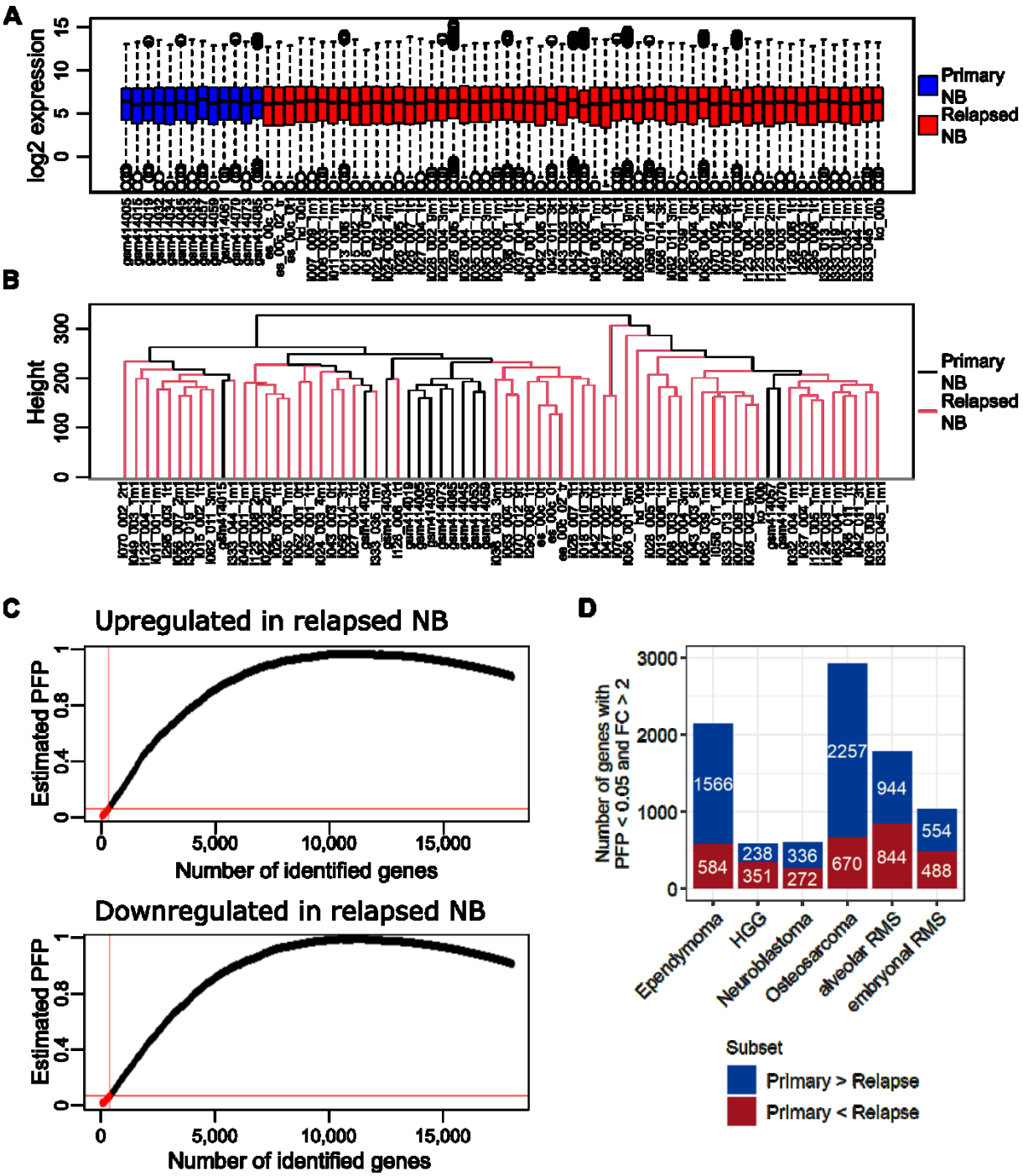

Figure 1: Differentially expressed genes are identified by RankProd analysis. ***(A)*** *Log2 expression data of the neuroblastoma (NB) primary (blue) and relapsed (red) datasets. Indicated are the median with first and third quartiles, as well as the strongest outliers.* ***(B)*** *Histogram of the primary (black) and relapsed (red) neuroblastoma samples. Hierarchical clustering was computed by Euclidian distance.* ***(C)*** *Up and downregulated genes of relapsed neuroblastoma were estimated by RankProd analysis. Genes with PFP < 0.05 (marked in red) were considered differentially regulated.* ***(D)*** *Summary of the final list of differentially expressed genes per entity with PFP < 0.05 and FC > 2.*

I then performed a pathway enrichment analysis to find out to with cellular pathways the differentially regulated genes belong. I used the online platform Reactome (www.reactome.org)[234] to perform an over-representation analysis, allowing me to determine which pathways were enriched (Appendix Table 1). I manually sorted the resulting pathways into broader categories: pathways involved with the ECM, pathways involved in ERBB signaling, cell cycle, immune system, other signaling and other

pathways (Figure 2A). While some entities had a great number of enriched pathways in individual categories (e.g. ependymoma with > 50 enriched pathways involved in cell cycle), pathways concerned with ERBB signaling and the ECM were enriched across different entities. A closer look at the pathways involved in ERBB signaling revealed that most of them were involved with two specific members of the family: ERBB2 and ERBB4 (Figure 2B). The four members of the ERBB family were either downregulated or not significantly different between primary and relapse in both subtypes of RMS and ependymoma (Figure 2C). In relapsed osteosarcoma only *ERBB3* was upregulated and in relapsed HGG a strong combination of *ERBB3* and *ERBB4* might indicate an interaction. In neuroblastoma only *ERBB4* was upregulated in the relapsed samples compared to primary. I therefore chose to investigate the involvement of *ERBB4* in chemotherapy resistance in relapsed neuroblastoma.

4.1.1. Validation of *ERBB4* as target for chemotherapy resistance in relapsed neuroblastoma

In a first step of validation, I wanted to ensure that my models reflect the upregulation of *ERBB4* I had observed in the gene expression analysis. My main model consisted of the relapsed, high-risk neuroblastoma cell line SK-N-BE(2)-C and a subline, which had been made resistant to VCR. I will refer to the two cell lines as BE(2)-C ctrl and BE(2)-C rVCR respectively.
Realtime-PCR analysis of the members of the ERBB family revealed that both *ERBB3* and *ERBB4* were upregulated at mRNA level in BE(2)-C rVCR compared to their sensitive counterpart (Figure 3A). Significant upregulation of ERBB4 at protein level was confirmed by western blot analysis (Figure 3B) and immunofluorescent staining (Figure 3C).
The SK-N-BE(2)-C are a subclone of the cell line SK-N-BE(2), which was derived at relapse from the same patient from whom SK-N-BE(1) had been derived at primary diagnosis. Confirming the results from the BE(2)-C ctrl / rVCR pair, *ERBB3* and *ERBB4* were upregulated at mRNA level between SK-N-BE(2) and SK-N-BE(1) (Figure 3D).
To broaden the spectrum of neuroblastoma cell lines from this single genotype, I performed realtime-PCR of the ERBB family on a panel of seven neuroblastoma cell lines that I could identify as having been derived before (primary) or after (relapse) the patient had received chemotherapy. In this panel, no member of the ERBB family was significantly up or downregulated between the two groups, but a slight trend could be seen for increased *ERBB4* levels in the cell lines derived at relapse (Figure 3E). Of note, the two cell lines in the panel with the highest *ERBB4* expression - CHP-134 and SIMA - were both derived at relapse.
As the BE(2)-C ctrl / rVCR pair, as well as CHP-134 and SIMA, seemed to best reflect the upregulation of *ERBB4*, which I observed in the initial gene expression analysis, I concentrated my further validation on these cell lines.

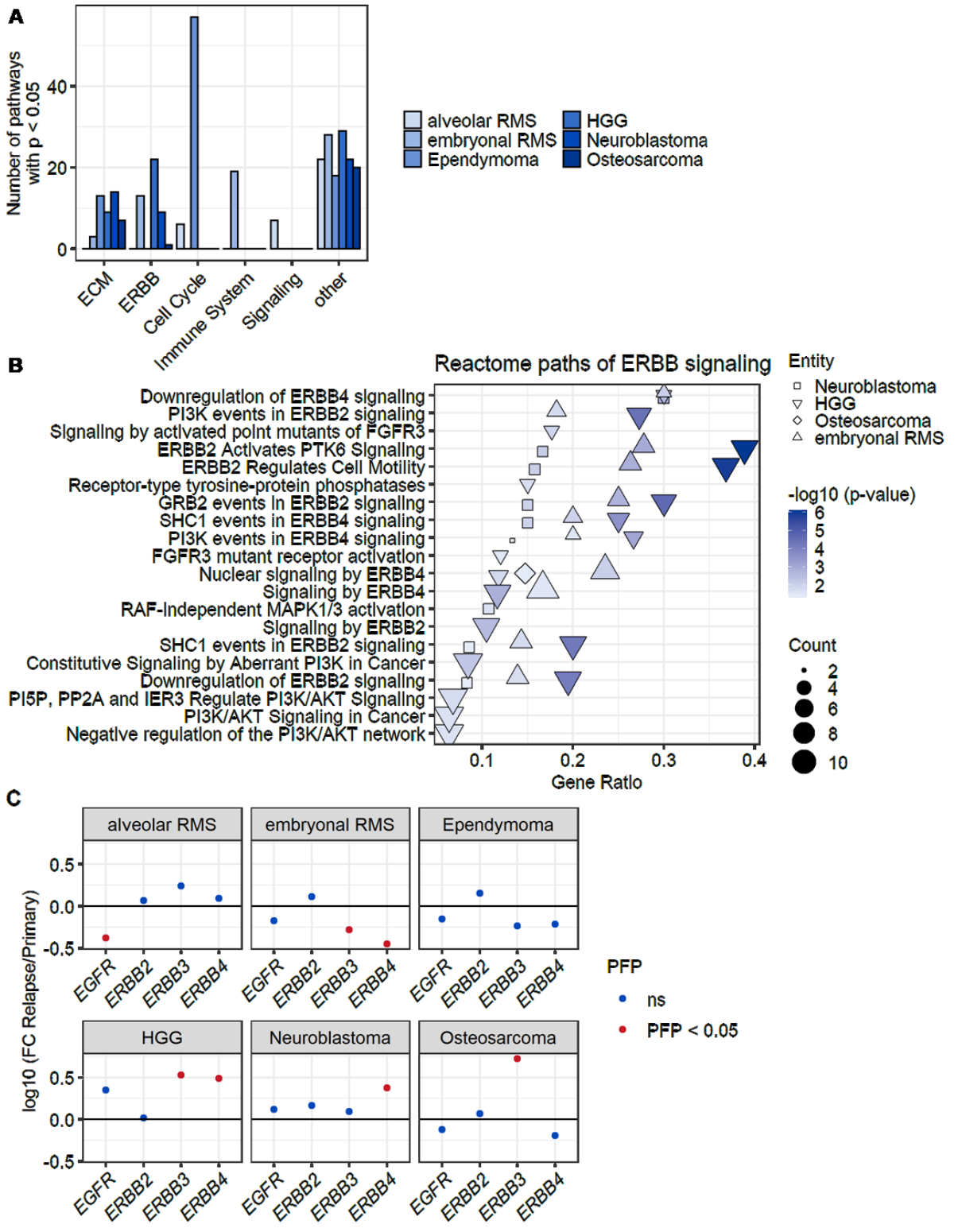

Figure 2: ERBB pathways are enriched across entities and ERBB4 is upregulated in neuroblastoma. ***(A)*** *A pathway enrichment analysis of the differentially expressed genes was performed with Reactome (www.reactome.org).*[234] *Enriched pathways were manually sorted into six categories. Presented are the numbers of enriched pathways per category and entity.* ***(B)*** *The enriched pathways sorted into the ERBB signaling category are plotted against gene ratio (number of enriched genes compared to total number of genes in each term). Shape represents entity, dot size represents the number of enriched genes and color represents the p-value in each term.* ***(C)*** *Expression of the members of the ERBB family as FC between relapse and primary samples. Red dots indicate significantly differentially regulated genes.*

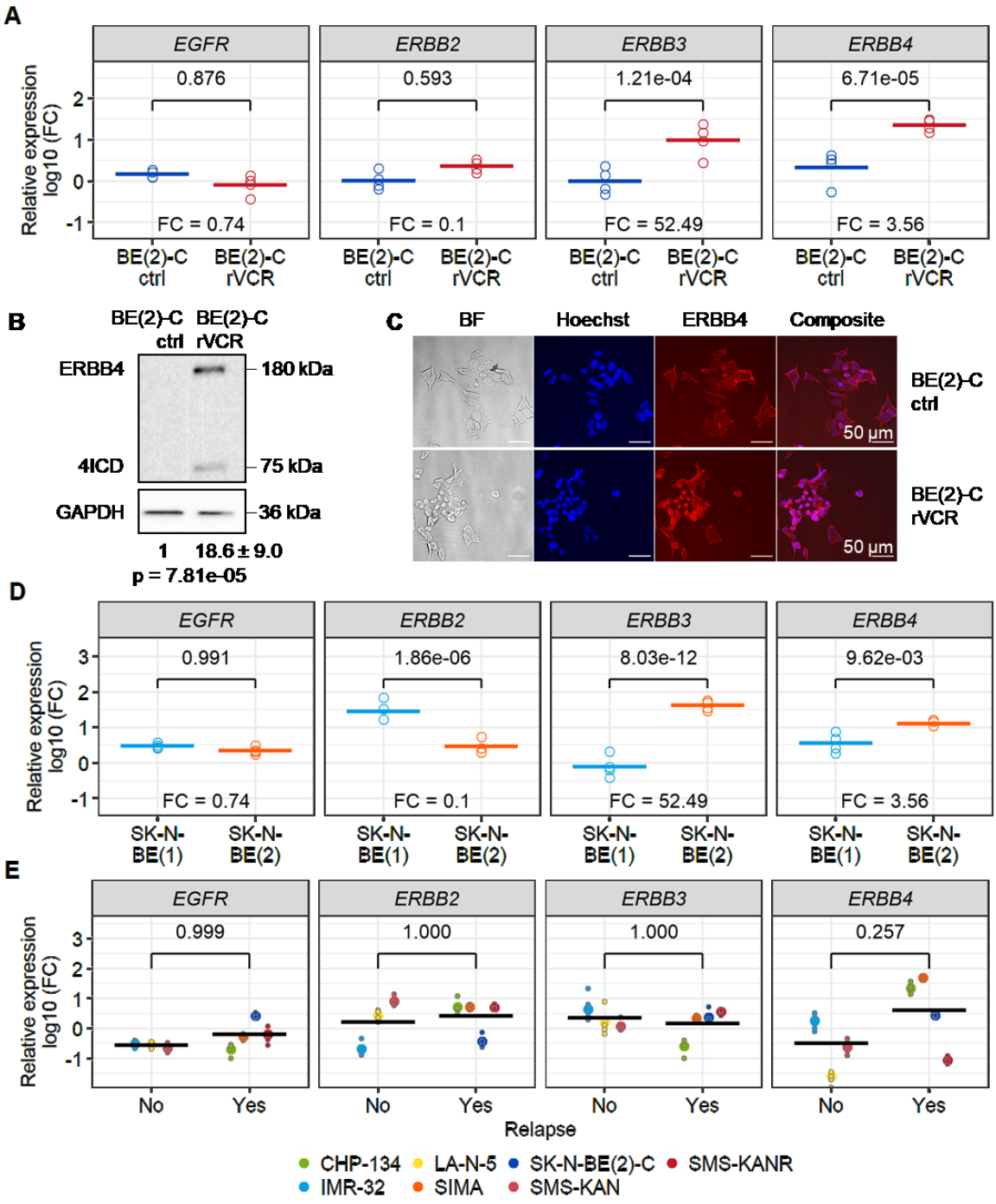

Figure 3: ERBB3 and ERBB4 are upregulated in VCR resistant BE(2)-C and SK-N-BE(2). ***(A)*** *Realtime-PCR of the ERBB family was performed with untreated BE(2)-C ctrl and BE(2)-C rVCR. Expression was normalized to a mix of five neuroblastoma cell lines. Statistics were calculated with ANOVA followed by Tukey's post-test. The FC between control and resistant BE(2)-C is indicated. Shown are biological replicates (n = 4) and their mean.* ***(B)*** *Western blot against ERBB4 was performed with untreated BE(2)-C ctrl and BE(2)-C rVCR. Shown are representative blots of six biological replicates. Quantifications were normalized first to the respective GAPDH and then to BE(2)-C ctrl. The mean of the replicates and their standard deviation are indicated. Significance was calculated by Student's t-test against 0 of the log10 transformed FC values of BE(2)-C rVCR.* ***(C)*** *Representative immunofluorescence images of untreated BE(2)-C ctrl and BE(2)-C rVCR. Cells were labeled with an ERBB4 primary antibody and stained with an Alexa Fluor 508 labeled secondary antibody, as well as the DNA intercalating dye Hoechst33342. The white scale bar represents 50 µm. BF = bright field.* ***(D)*** *Realtime-PCR of the ERBB family was performed on untreated SK-N-BE(1) and SK-N-BE(2). Expression was normalized to a mix of five neuroblastoma cell lines. Statistics were calculated by ANOVA followed by Tukey's post-test. The FC between SK-N-BE(1) and SK-N-BE(2) is indicated. Presented are four biological replicates and their mean.* ***(E)*** *Realtime-PCR of the ERBB*

family was performed on a panel of three non-relapsed and four relapsed neuroblastoma cell lines. Expression was normalized to a mix of five neuroblastoma cell lines. Shown are the biological replicates of each cell line (n ≥ 3), the mean relative expression of each cell line and the group means. P-values between group means are indicated and were calculated by ANOVA followed by Tukey's post-test. This figure was adapted from Rösch et al.[253] *All work presented therein is my own.*

As I only tested a panel of 11 neuroblastoma cell lines by real-time PCR analysis, I used gene expression datasets of neuroblastoma patient and cell line samples from R2 to extent my field of samples. The first dataset I investigated was compiled by Schramm *et al.* (GSE65303)[241] and consists of gene expression data from seven neuroblastoma patients at primary diagnosis and after relapse. While *EGFR* and *ERBB2* expression was very similar between primary diagnosis and relapse, there was slightly more variation for *ERBB3* and *ERBB4* expression (Figure 4A). Both genes were upregulated at relapse in some patients and downregulated in others. Overall, this led to no coherent up or downregulation between the groups primary diagnosis and relapse.

I complemented this analysis by analyzing a cell line dataset by Utnes *et al.* (GSE148700)[244], which consists of five cell pairs that were derived from the same patients at primary diagnosis or relapse. Similar to the results from Figure 4A, there was no differential regulation of any member of the ERBB family between the primary/relapse groups (Figure 4B). Of note, there was a single cell line pair with strong *ERBB4* upregulation at relapse: The SK-N-BE(1)/SK-N-BE(2) pair, supporting my real-time PCR results in Figure 3D.

I then analyzed four further datasets with neuroblastoma cell lines provided by Jagannathan *et al.* (GSE19274)[242], Versteeg *et al.* (GSE28019), Maris *et al.* (GSE89413)[174] and the Cell Line Encyclopedia from the Broad Institute (GSE36133)[243]. In these datasets I included only those cell lines, which I could identify as having been derived before the patient received chemotherapy (primary diagnosis) or afterwards (relapse/progression). In the datasets by Maris and Versteeg there was a slight, but not significant trend to increased *ERBB4* at relapse. No other member of the ERBB family was differentially regulated in these datasets or in the datasets by Jagannathan and the Broad Institute (Figure 4C-F).

Finally, I once more returned to the INFORM dataset to test how expression of the ERBB family behaves in relapsed neuroblastoma compared to other relapsed pediatric entities. Interestingly, *EGFR*, *ERBB2* and *ERBB3* were all expressed lower in relapsed neuroblastoma than other entities, while *ERBB4* was unchanged (Figure 4G).

Overall, the gene expression data from neuroblastoma cell lines and patient samples indicates that *ERBB4* upregulation might be important in a subset of neuroblastoma patients, but is very divers across different cohorts.

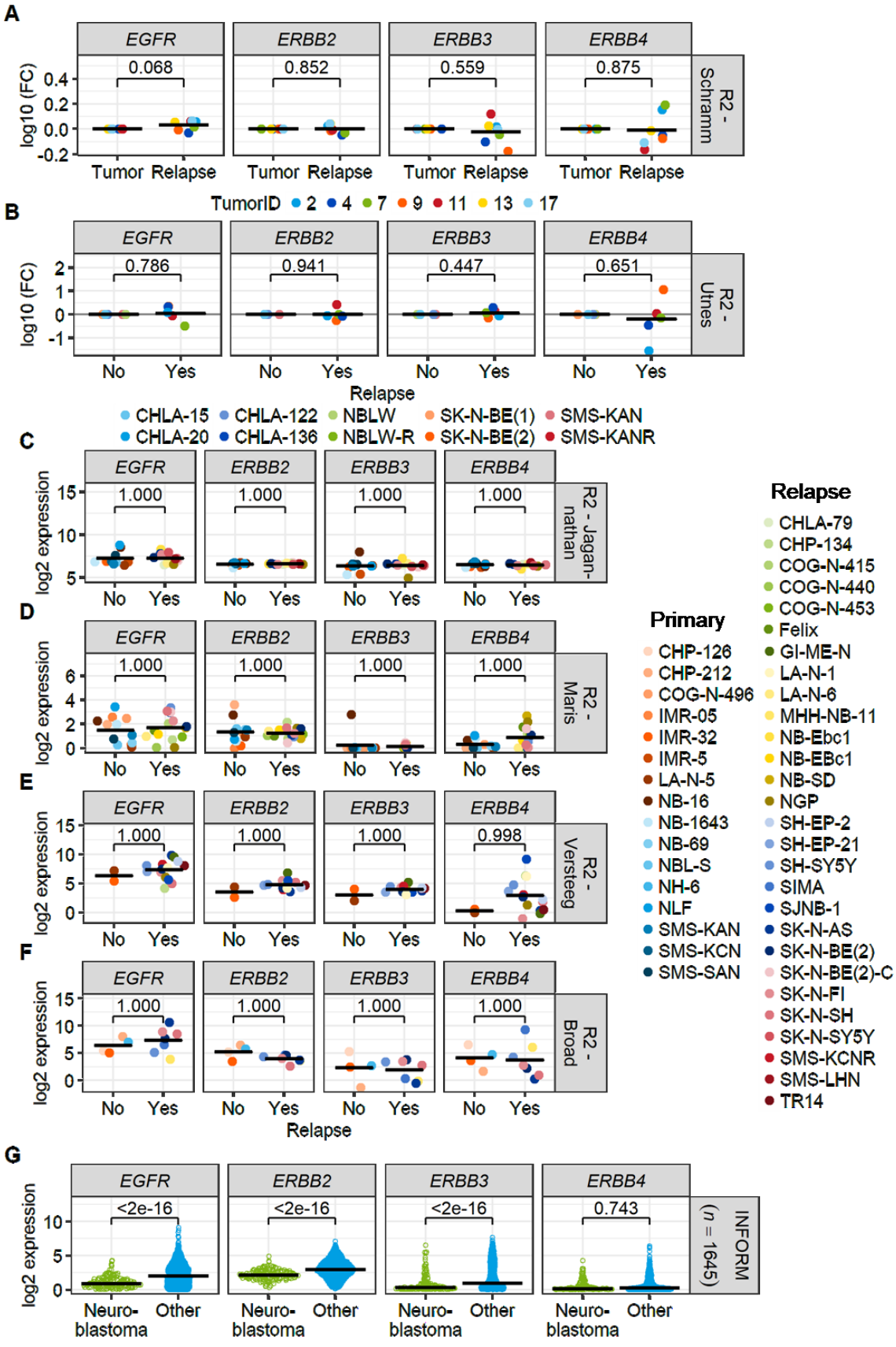

Figure 4: The ERBB family is not regulated in neuroblastoma cell lines and relapsed tumors. ***(A)*** *Gene expression data of 18 tumor samples from the dataset by Schramm et al. (GSE65303)*[241] *was downloaded from R2 (http://r2.amc.nl, 09 September 2021). Only paired samples with data at primary diagnosis (Tumor) and at*

Relapse were included (n = 7 pairs). ***(B)*** *Gene expression data of 10 paired neuroblastoma cell lines from the dataset by Utnes et al. (GSE148700)*[244] *was downloaded from R2 (07 January 2021). This dataset consists of five cell line pairs derived from the same patients at primary diagnosis and after relapse.* ***(A&B)*** *Statistics of log transformed relapse values were calculated with Student's t-test against 0. Matched pairs are indicated by color.* ***(C)*** *Gene expression data of 38 neuroblastoma cell lines from the dataset by Jagannathan et al. (GSE19274)*[242] *was downloaded from R2 (08 June 2021). All cell lines that could not be positively identified as having been derived before (n = 10) or after (n = 12) the patient had received chemotherapy (Relapse No/Yes) were excluded from the analysis.* ***(D)*** *Gene expression data of 41 neuroblastoma cell lines from the dataset by Maris et al. (GSE89413)*[174] *was downloaded from R2 (07 January 2021). All cell lines that could not be positively identified as having been derived before (n = 12) or after (n = 15) the patient had received chemotherapy (Relapse No/Yes) were excluded from the analysis.* ***(E)*** *Gene expression data of 24 neuroblastoma cell lines from the dataset by Versteeg et al. (GSE28019) was downloaded from R2 (07 January 2021). All cell lines that could not be positively identified as having been derived before (n = 2) or after (n = 14) the patient had received chemotherapy (Relapse No/Yes) were excluded from the analysis.* ***(F)*** *Gene expression data of 917 cell lines from the cell line encyclopedia dataset from the Broad Institute (GSE19274)*[243]*, which included 17 neuroblastoma cell lines, was downloaded from R2 (08 June 2021). Neuroblastoma cell lines that could not be positively identified as having been derived before (n = 4) or after (n = 7) the patient had received chemotherapy (Relapse No/Yes) were excluded from the analysis.* ***(G)*** *Gene expression data from the INFORM registry*[235,236] *(n = 1645). Comparison of neuroblastoma cases (n = 162) vs. all other entities.* ***(C-G)*** *Statistics were calculated by ANOVA followed by Tukey's post-test including all genes of the ERBB and the ABC families present in the respective datasets. This figure was adapted from Rösch et al.*[253] *The analysis presented therein is my own.*

I further tested whether inhibition of the ERBB family by small molecule inhibitors could break resistance and act synergistically with VCR to decrease viability. A viability assay by trypan blue exclusion confirmed that BE(2)-C rVCR were more resistant to VCR treatment than BE(2)-C ctrl (Figure 5A and C). This resistance was broken by the addition of afatinib, an inhibitor of the ERBB family with a particularly high affinity for EGFR and ERBB4 (Figure 5A). Synergism analysis at metabolic activity level using the Bliss synergy model indicated strong synergism (Bliss synergy score > 10) between VCR and afatinib for both BE(2)-C ctrl and rVCR (Figure 5A and B and Appendix Figure 7A). Combining VCR with another pan-ERBB inhibitor, lapatinib, confirmed that resistance of BE(2)-C rVCR was broken by inhibitors of the ERBB family (Figure 5C).

The combination of VCR and afatinib also decreased viability in CHP-134 and SIMA in a trypan blue exclusion assay (Figure 5D and E), which metabolic activity confirmed to be synergistic after the Bliss model of synergism (Figure 5B, D and E and Appendix Figure 7A). To further complement these results, I tested three more sensitive/resistant neuroblastoma cell line pairs: MHH-NB-1 ctrl/rVCR, NB-S-124 ctrl/rVCR and NGP ctrl/rVCR. In all three cell line pairs VCR resistance was effectively and synergistically broken by the addition of afatinib (Figure 5B and E and Appendix Figure 7B) with synergy scores that were much higher in the resistant cell lines compared to their sensitive parental line.

ERBB signaling can act through a number of different pathways in the cell, the most common being PI3K/AKT signaling, the MAPK pathway or signaling through SRC. To identify which of the downstream pathways are involved with chemotherapy resistance in relapsed neuroblastoma, I analyzed the effect of afatinib on these three pathways. Surprisingly, in BE(2)-C ctrl and rVCR afatinib had no effect on the phosphorylation levels of AKT, ERK and SRC (Figure 6A). While all three proteins were phosphorylated in the untreated controls - indicating at least partial activation of these pathways - phosphorylation was not attenuated by treatment with afatinib.

In the CHP-134 cells, only SRC was phosphorylated in the untreated cells (Figure 6B). Of note, while SRC and ERK phosphorylation levels remained unchanged in response to afatinib treatment in CHP-134, phosphorylation of AKT increased.

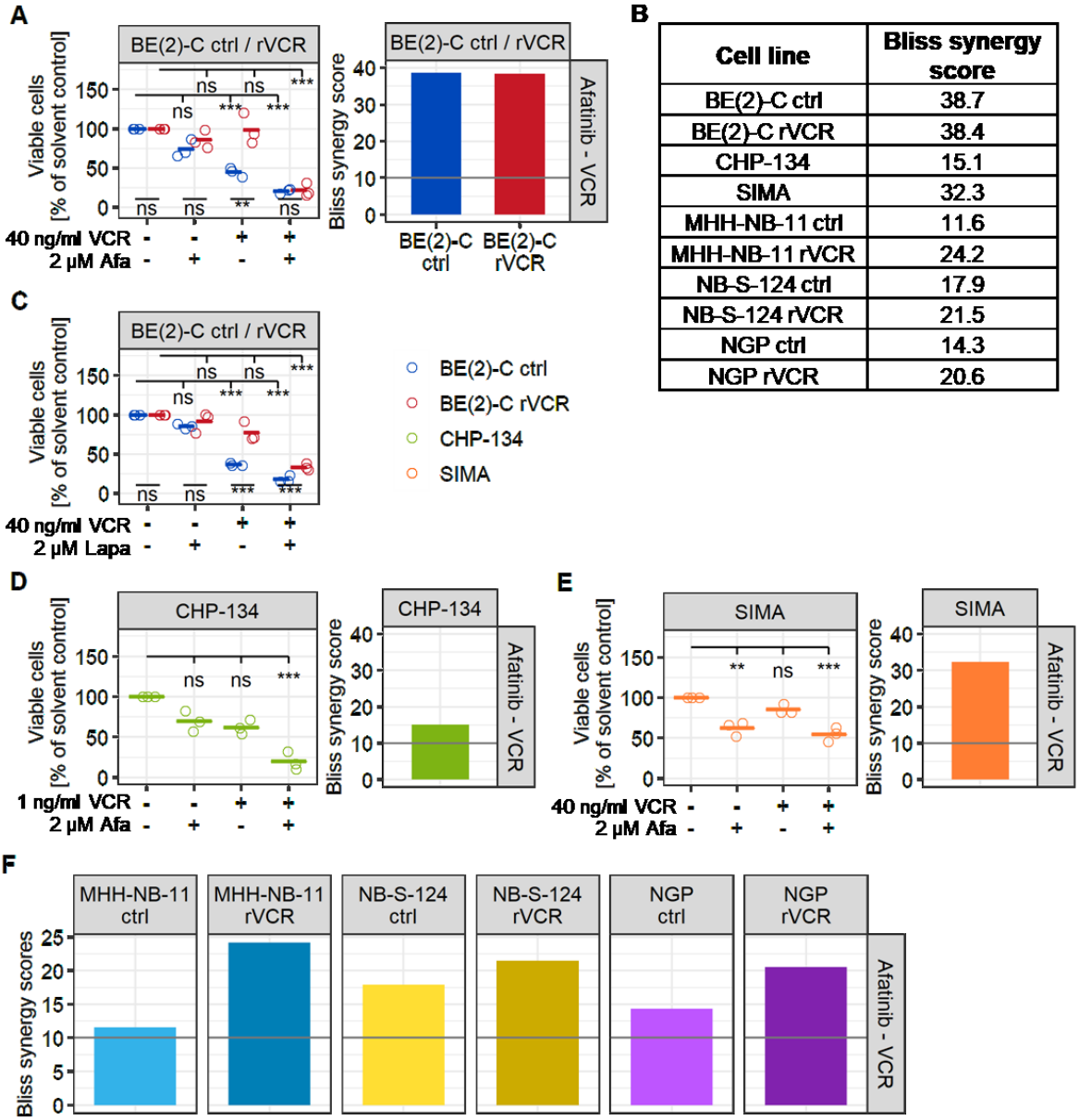

Cell line	Bliss synergy score
BE(2)-C ctrl	38.7
BE(2)-C rVCR	38.4
CHP-134	15.1
SIMA	32.3
MHH-NB-11 ctrl	11.6
MHH-NB-11 rVCR	24.2
NB-S-124 ctrl	17.9
NB-S-124 rVCR	21.5
NGP ctrl	14.3
NGP rVCR	20.6

Figure 5: Inhibitors of the ERBB family break resistance in neuroblastoma. ***(A)*** *BE(2)-C control and rVCR were treated with 40 ng/ml VCR and 2 µM of the ERBB inhibitor afatinib for 48 h.* ***(B)*** *Bliss synergy scores were calculated from metabolic activity data (0, 10, 20, 40, 100 ng/ml VCR +/- 0, 0.5, 1, 2 µM afatinib for 48 h in all cell lines) using SynergyFinder.*[252] *A score > 10 indicates synergy.* ***(C)*** *BE(2)-C control and rVCR were treated with 40 ng/ml VCR and 2 µM of the ERBB inhibitor laptinib for 48 h.* ***(D)*** *CHP-134 cells were treated with 1 ng/ml VCR and 2 µM afatinib for 48 h.* ***(E)*** *SIMA cells were treated with 40 ng/ml VCR and 2 µM afatinib for 48 h.* ***(A,C-E)*** *Dead cells were stained with trypan blue and only viable cells were counted. Percent of viable cells to the solvent control of each cell line was calculated. Shown are three biological replicates and their mean. Statistics were calculated using the log10 transformed values by ANOVA followed by Tukey's post-test. Presented are the comparisons between the cell lines at each concentration (bottom) for BE(2)-C ctrl/rVCR as well as the comparisons to solvent control for each cell line (top).* ***(A,D-F)*** *Bliss synergy scores were calculated as described in (B). A score > 10 (grey line) indicates synergy. *** p < 0.001, ** p < 0.01, * p < 0.05, ns = not significant. Afa = afatinib, Lapa = lapatinib. This figure was adapted from Rösch et al.*[253] *All work presented therein is my own.*

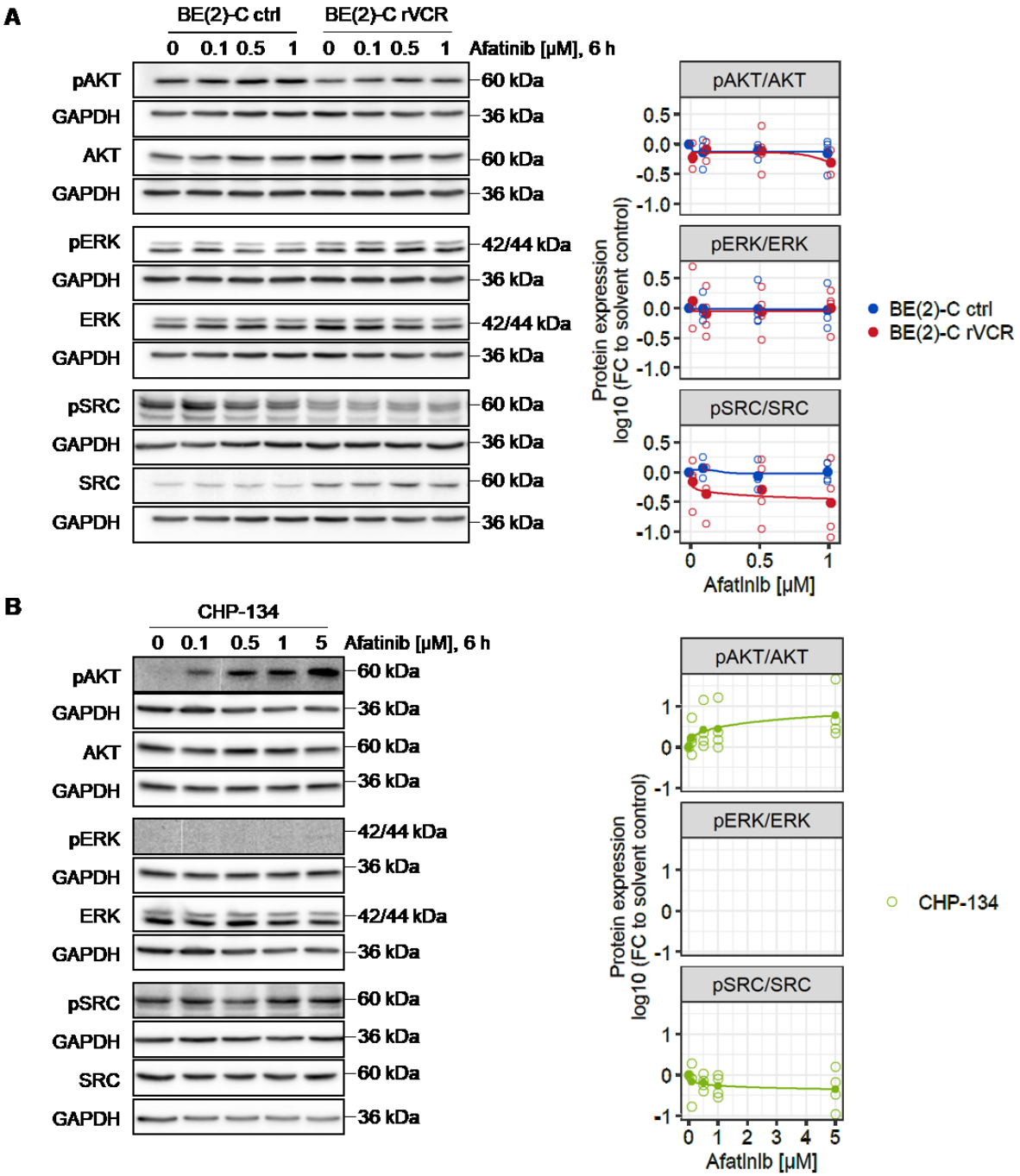

Figure 6: Afatinib does not decrease phosphorylation of ERBB downstream pathways. ***(A)*** *BE(2)-C ctrl and BE(2)-C rVCR were treated with 0, 0.1, 0.5 and 1 µM afatinib for 6 h. The same GAPDH control applies for AKT/pERK and pAKT/ERK/SRC, respectively.* ***(B)*** *CHP-134 were treated with 0, 0.1, 0.5, 1, 5 µM afatinib for 6 h. The same GAPDH control applies for AKT/pERK and pAKT/ERK, respectively.* ***(A&B)*** *Protein levels of AKT, ERK and SRC and their phosphorylation were assessed by western blot. Representative blots of four biological replicates are shown. Quantification of the phosphoprotein expression was normalized first to the respective GAPDH, then to GAPDH normalized total protein and finally to solvent control. Both BE(2)-C ctrl and rVCR were normalized to solvent control of BE(2)-C ctrl. Part (A) of this figure was adapted from Rösch et al.*[253] *All work presented in this figure is my own.*

As the ERBB family are not the only kinases that activate the PI3K/AKT, MAPK and SRC signaling pathways, I analyzed the phosphorylation levels of these pathways after specific activation of the ERBB family by its ligand neuregulin-1 (NRG-1), which binds and activates ERBB3 and ERBB4. However, instead of increasing phosphorylation levels, NRG-1 decreased phosphorylation of AKT and ERK in BE(2)-C ctrl and even stronger in BE(2)-C rVCR (Figure 7A). Addition of afatinib even increased this effect for pERK in BE(2)-C rVCR, but did not have any effect on pAKT in BE(2)-C rVCR or BE(2)-C ctrl. Phosphorylation of SRC remained unchanged in both BE(2)-C lines.
In the CHP-134 cell line, phosphorylation of AKT also decreased after 5 and 10 min of NRG-1 treatment (Figure 7B). While this decrease was also seen with the addition of afatinib in the early time points, after 1 h of NRG-1 treatment pAKT was as strongly phosphorylated as in afatinib single treatment, which was increased compared to untreated, corroborating the results in Figure 6B. The strongest effect of NRG-1 in CHP-134 was observed in the phosphorylation of ERK. After 10 min of NRG-1 treatment, ERK showed increased levels of phosphorylation. After 1 h, pERK returned almost to basal levels, and addition of afatinib lessened the increase of pERK upon NRG-1 treatment. Phosphorylation of SRC was not affected by NRG-1 treatment.
Overall, the functional analysis indicates that NRG-1 treatment in BE(2)-C ctrl and rVCR initiates negative feedback signaling, which leads to the observed decrease in phosphorylation of AKT and ERK. In CHP-134 cells, a negative feedback loop is also observed for the phosphorylation of AKT, while ERK responds as expected, with activation after NRG-1 treatment, which is attenuated by co-treatment with afatinib.

As afatinib had not affected phosphorylation of the ERBB downstream pathways in BE(2)-C ctrl and rVCR, I wanted to ensure that phosphorylation of AKT, ERK and SRC could in principle be regulated by small molecule inhibitors in these cell lines. Indeed, treatments with PI3K inhibitor BKM120, MEK inhibitor trametinib and SRC inhibitor dasatinib were very efficient in reducing phosphorylation levels of AKT, ERK and SRC respectively (Figure 8A-C, left and middle panels). However, none of these inhibitors were able to breaks resistance with the same efficiency observed in afatinib (Figure 8A-C, right most panels).

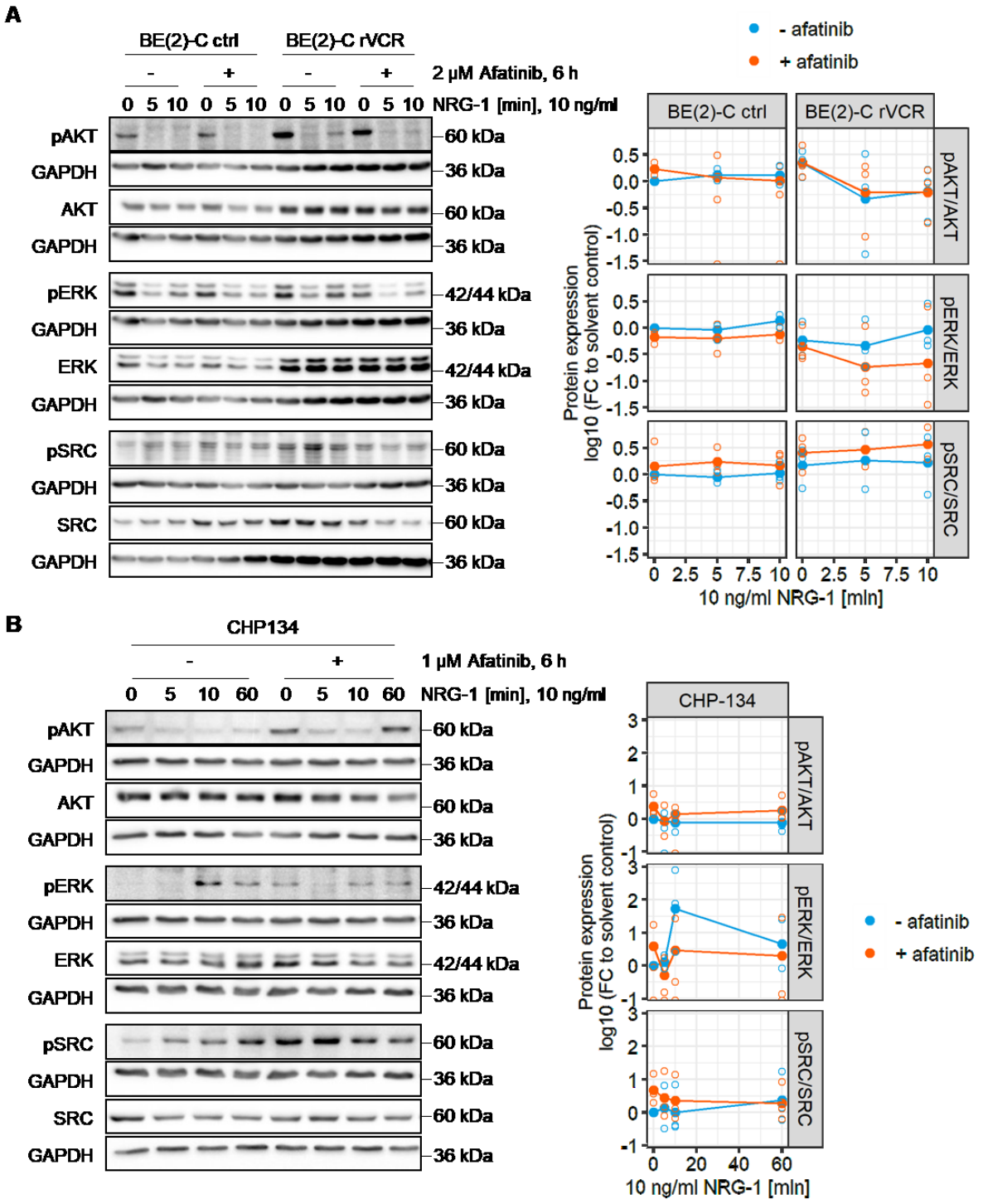

Figure 7: Afatinib and NRG-1 combination treatment. ***(A)*** *Control BE(2)-C and BE(2)-C rVCR were treated with 2 µM afatinib or solvent control for 6 h, followed by treatment with 10 ng/ml NRG-1 for 0, 5 and 10 min. The same GAPDH control applies for pAKT/ERK and AKT/pERK, respectively.* ***(B)*** *CHP-134 were treated with 1 µM afatinib or solvent control for 6 h, followed by treatment with 10 ng/ml NRG-1 for 0, 5, 10 and 60 min. The same GAPDH control applies to pAKT/pERK and ERK/pSRC, respectively.* ***(A&B)*** *Phosphorylation of AKT, ERK and SRC, as well as total protein levels, were assessed by western blot. Representative blots of three biological replicates are shown. Quantified phosphoprotein expression was normalized first to the respective GAPDH, then to GAPDH normalized complete protein and finally to solvent control. Both BE(2)-C ctrl and rVCR were normalized to solvent control of BE(2)-C ctrl.*

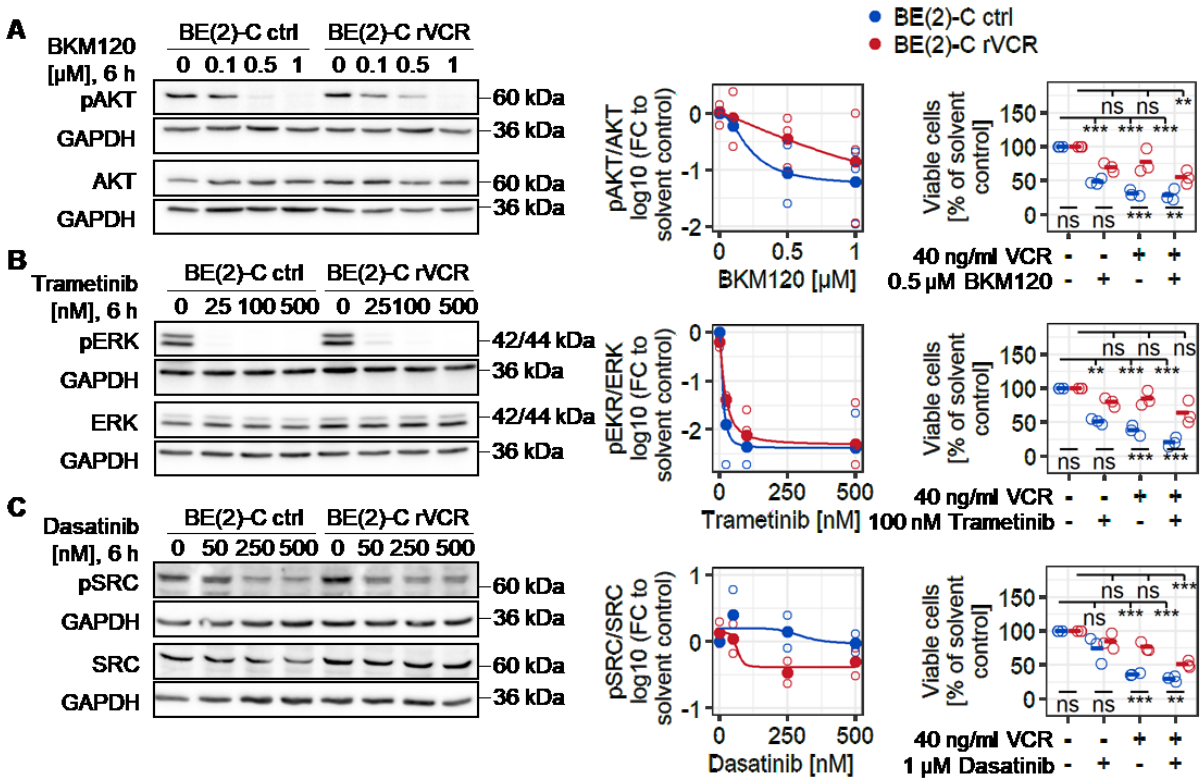

Figure 8: Direct inhibition of PI3K/AKT, MAPK and SRC signaling does not break resistance efficiently. ***(A-C)*** *Control BE(2)-C and BE(2)-C rVCR were treated with the indicated concentrations BKM120, trametinib or dasatinib, respectively, for 6 h for western blot or 48 h in combination with 40 ng/ml VCR for viability assay (right most panels). Phosphorylation and complete protein levels of AKT, ERK and SRC respectively were assessed by western blot. Representative blots of three biological replicates are shown. Phosphoprotein expression was normalized first to the respective GAPDH, then to GAPDH normalized complete protein and finally to solvent control of control BE(2)-C. The quantifications are presented in the middle panels. Viability was assessed by trypan blue exclusion. Dead cells were stained with trypan blue and only viable cells were counted. Percent of viable cells to the solvent control of each cell line was calculated. Presented are n = 3 biological replicates and their mean. Statistics were calculated with ANOVA followed by Tukey's post-test. Shown are the comparisons between the cell lines (bottom) as well as the comparisons to solvent control for each cell line (top). This figure was adapted from Rösch et al.*[253] *All work presented therein is my own.*

As I showed above, treatment with afatinib was very efficient in breaking resistance in BE(2)-C rVCR, but in spite of *ERBB4* upregulation, it did not influence activity of the ERBB downstream pathways. I therefore performed an *ERBB4* KD to investigate whether it was indeed ERBB4, which conferred resistance in BE(2)-C rVCR.

Even though I achieved an efficient KD, it did not attenuate viability in VCR single or VCR and afatinib double treatment compared to a control KD (Figure 9A). Furthermore, the treatment sensitizing effect of adding afatinib to VCR treatment was not abolished by *ERBB4* KD. Similarly, blocking ERBB4 signaling with an ERBB4 blocking antibody, also did not influence the sensitivity of BE(2)-C rVCR to VCR single treatment (Figure 9B).

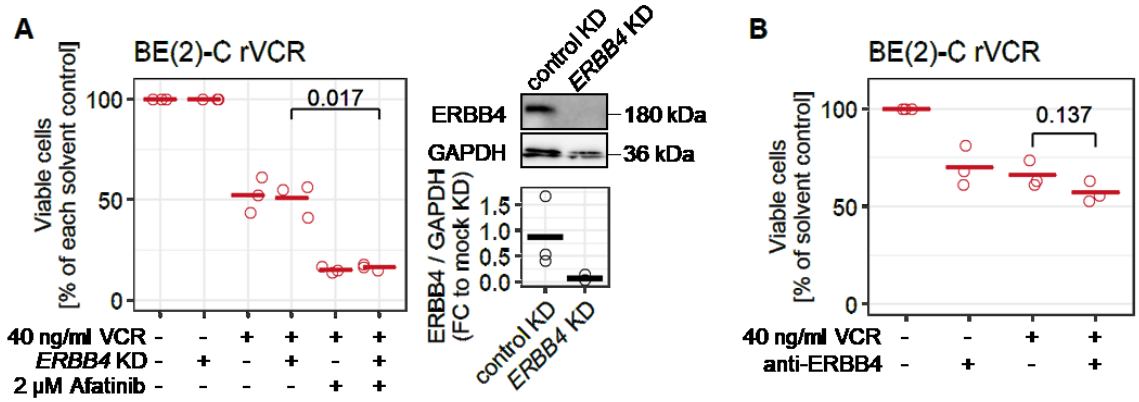

Figure 9: Afatinib breaks VCR resistance independently of ERBB4. ***(A)*** *ERBB4 KD and control KD were performed on BE(2)-C rVCR cells, which were treated 24 h later with 40 ng/ml VCR and/or 2 µM afatinib for 48 h. Dead cells were stained with trypan blue and only viable cells were counted. Percent of viable cells to the solvent control of each KD was calculated. Presented are n = 3 biological replicates and their mean. Statistic was calculated with Student's t-test. KD efficiency was validated by western blot. Quantifications were normalized to GAPDH and mock KD.* ***(B)*** *BE(2)-C rVCR were treated with 1 µg/ml anti-ERBB4 blocking antibody and/or 40 ng/ml VCR for 48 h. Dead cells were stained with trypan blue and only viable cells were counted. Percent of viable cells to the solvent control was calculated. Presented are n = 3 biological replicates and their mean. Statistic was calculated with Student's t-test. This figure was adapted from Rösch et al.*[253] *All work presented therein is my own.*

Having identified ERBB4 as a possible target for chemotherapy resistance in neuroblastoma by a gene expression analysis done with patient data, I showed that ERBB4 is upregulated in some relapsed and chemotherapy resistant neuroblastoma cell lines. Although treatment with the ERBB family inhibitor afatinib efficiently broke resistance and acted synergistically with VCR, I could not find any evidence that afatinib acted on-target by reduced activity of the most common ERBB family downstream pathways. Indeed, a KD of afatinib-target ERBB4 in BE(2)-C rVCR did not affect the viability of the cells. All together these data lead to the conclusion that the resistance breaking effect of afatinib is an off-target effect that has little to do with ERBB4 signaling.

4.2. A metabolic activity screen identifies P-glycoprotein as possible target

As I could find no evidence that the resistance breaking effect of afatinib in BE(2)-C rVCR was mediated by ERBB4, I wanted to broaden my approach in understanding resistance in this cell line. For this, I performed a metabolic activity screen, in which I combined VCR with concentration ranges of 14 clinically approved drugs targeting cancer relevant pathways. As drug resistance mediated by the transmembrane pump P-gp is also known to affect VCR, I further included the P-gp inhibitor tariquidar, which has been studied in clinical trials.[254] I treated BE(2)-C rVCR with five concentrations of each drug alone or in combination with VCR (Figure 10A) and calculated the area under the curves (AUC). The greatest difference between the AUCs of single and combination treatment (ΔAUC) was found for P-gp inhibitor tariquidar, followed by afatinib (Figure 10B). I therefore continued by taking a closer look at P-gp in relapsed neuroblastoma.

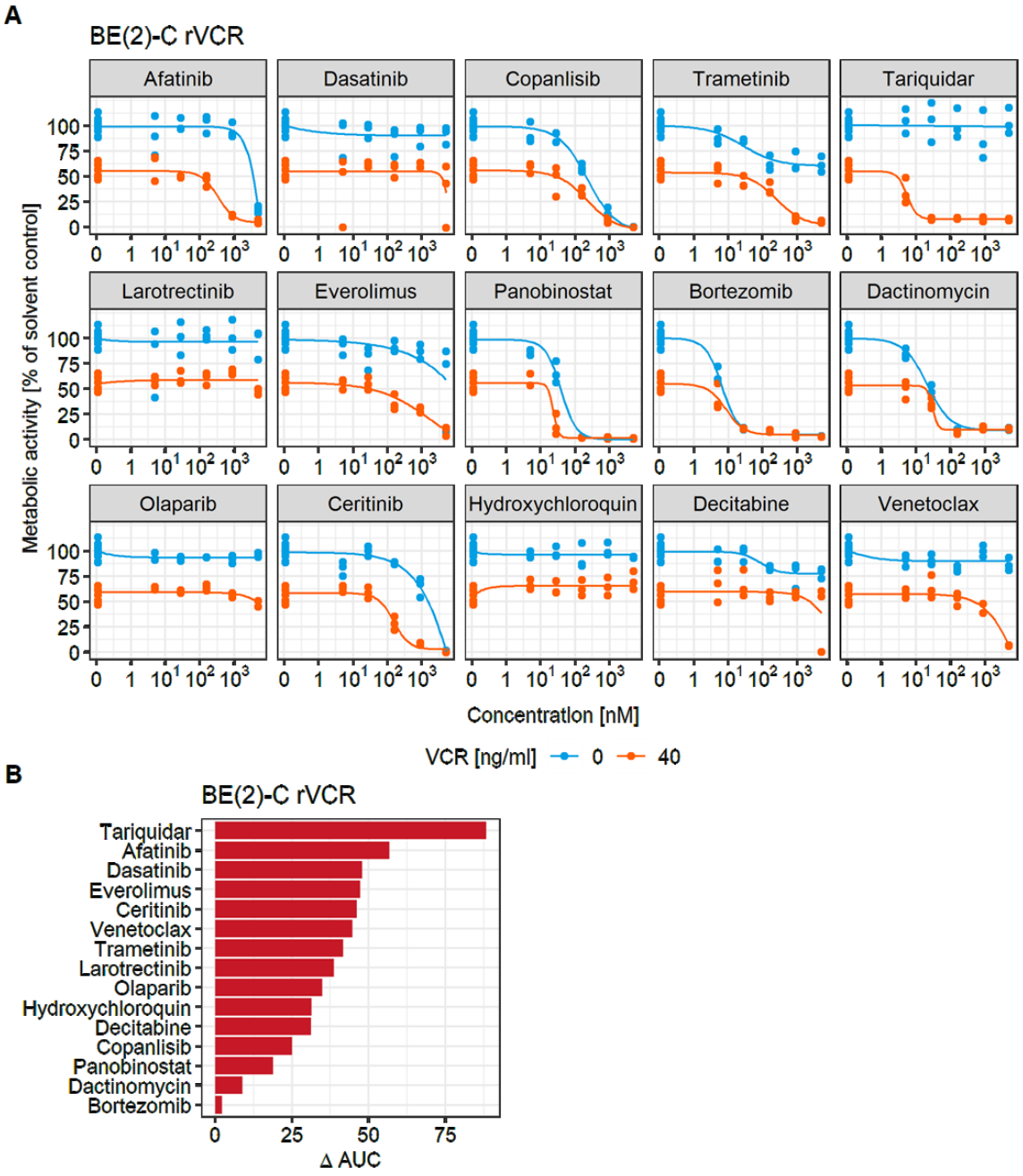

Figure 10: An inhibitor of P-gp breaks resistance in BE(2)-C rVCR. ***(A)*** *A metabolic activity screen (CTG) of combination treatment of VCR with 15 anti-cancer drugs (14 clinically approved) was performed with BE(2)-C rVCR. Cells were treated with 0, 5, 28, 158, 889 and 5000 nM of the 15 drugs alone (blue) or in combination with 40 ng/ml VCR (orange) for 48 h. Presented are technical replicates and a curve fit calculated by an L4 model.* ***(B)*** *The difference in AUC between single and combination treatment (ΔAUC) was calculated. This figure was adapted from Rösch et al.*[253] *All work presented therein is my own.*

4.2.1. Validation of P-glycoprotein as mediator of chemotherapy resistance in relapsed neuroblastoma

Having identified the P-gp inhibitor tariquidar as a potential drug to break resistance in relapsed neuroblastoma, I took a closer look at P-gp/*ABCB1* in neuroblastoma cell lines. In the VCR resistant BE(2)-C subline, *ABCB1* was not differentially expressed at mRNA level compared to BE(2)-C ctrl (Figure 11A). Total P-gp protein expression by western blot was also not significantly upregulated in BE(2)-C rVCR (Figure 11B). However, immunofluorescence imaging as well as staining of surface P-gp show that P-gp is significantly higher expressed at the surface of BE(2)-C rVCR (Figure 11C and D).
The primary/relapse cell line pair from the same patient - SK-N-BE(1) and SK-N-BE(2) - showed no upregulation of *ABCB1* at mRNA level (Figure 11E), again mirroring the expression pattern of BE(2)-C ctrl/rVCR as they had done for the expression of the ERBB family proteins.
To expand my view to further cell lines, I also analyzed *ABCB1* expression in a panel of three primary and four relapsed neuroblastoma cell lines. At mRNA level, *ABCB1* was higher in relapsed cell lines compared to primary, however, statistical significance was not reached (Figure 11F).

To further expand the amount of samples, I analyzed gene expression datasets of neuroblastoma cell lines and patient samples from R2. *ABCB1* was not significantly upregulated in the patient sample dataset by Schramm *et al.*[241] when comparing the overall means. However, when looking at every paired sample individually, all were either upregulated or unchanged at relapse, while none was downregulated (Figure 12A). This was corroborated by the matched primary/relapsed cell line pairs compiled by Utnes *et al.*[244] (Figure 12B). In the four cell line datasets I analyzed, *ABCB1* was significantly upregulated in cell lines derived at relapse in the datasets by Jagannathan,[242] Maris[174] and Versteeg (Figure 12C-E). In the dataset from the Broad institute,[243] *ABCB1* upregulation did not reach statistical significance (Figure 12F). Finally, when comparing relapsed neuroblastoma to other relapsed pediatric entities in INFORM,[235,236] *ABCB1* was strongly upregulated in neuroblastoma (Figure 12G).

As *ABCB1* is only one member of a large family of transporters - many of which are involved in drug resistance - I had a closer look at the other members of the ABC family in the datasets above. In the cell line datasets and the patient dataset by Schramm *et al.*, no ABC family member other than *ABCB1* was differentially regulated (Appendix Figure 8-Appendix Figure 13). When comparing neuroblastoma to other relapsed pediatric entities from the INFORM dataset, two other transporters - *ABCA3* and *ABCG4* - were also significantly ($p < 0.05$) and relevantly ($FC > 2$) upregulated (Appendix Figure 14). However, of the three transporters *ABCB1* had the strongest difference between neuroblastoma and other entities with a FC of 3.3.
Taken together, analyses of these datasets point towards a prominent role of *ABCB1* in relapsed neuroblastoma.

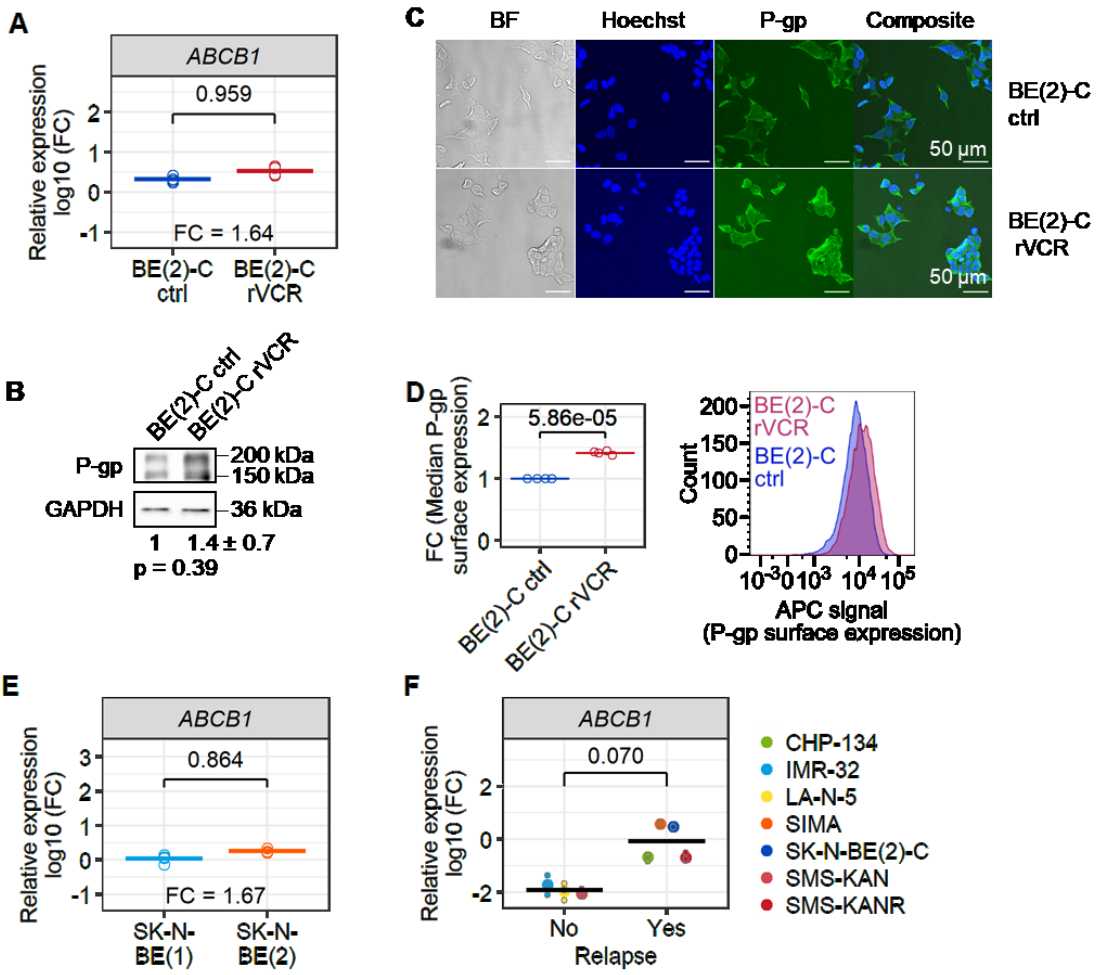

Figure 11: Surface P-gp is upregulated in BE(2)-C rVCR. ***(A)*** *Real-time PCR of ABCB1 was performed on untreated BE(2)-C ctrl and BE(2)-C rVCR. Expression was normalized to a mix of five neuroblastoma cell lines. Statistics were calculated with ANOVA followed by Tukey's post-test. The FC between control and resistant BE(2)-C is indicated. Shown are four biological replicates and their mean.* ***(B)*** *Western blot against P-gp was performed with untreated BE(2)-C ctrl and BE(2)-C rVCR. Shown is a representative blot of four biological replicates. Quantifications were normalized first to the respective GAPDH and then to control BE(2)-C. The mean of the replicates and their standard deviation are indicated. Significance was calculated by Student's t-test against 0 of the log10 transformed FC values of BE(2)-C rVCR.* ***(C)*** *Representative immunofluorescence images of untreated control BE(2)-C and BE(2)-C rVCR. Cells were labeled with a P-gp primary antibody and stained with an Alexa Fluor 488 labeled secondary antibody, as well as the DNA intercalating dye Hoechst33342. The white scale bar indicates 50 µm. BF = bright field.* ***(D)*** *Surface expression of P-gp was measured by flow cytometric analysis. BE(2)-C ctrl and rVCR were stained with P-gp primary antibody and allophycocyanin (APC) labeled secondary antibody. Median APC signal relative to BE(2)-C ctrl is shown in the left panel, a representative signal distribution of four biological replicates is shown on the right. Statistic was calculated by Student's t-test against 0 of the log10 transformed FC values of BE(2)-C rVCR.* ***(E)*** *Realtime-PCR of ABCB1 was performed on untreated SK-N-BE(1) and SK-N-BE(2). Expression was normalized to a mix of five neuroblastoma cell lines. Statistics were calculated by ANOVA followed by Tukey's post-test. The FC between SK-N-BE(1) and SK-N-BE(2) is indicated. Shown are four biological replicates and their mean.* ***(F)*** *Real-time PCR of ABCB1 was performed on a panel of three non-relapsed and four relapsed neuroblastoma cell lines. Expression was normalized to a mix of five neuroblastoma cell lines. Presented are the biological replicates of each cell line ($n \geq 3$, small dots), the mean relative expression of each cell line (big dots) and the group means (black bars). P-values between group means are indicated and were calculated by ANOVA followed by Tukey's post-test. This figure was adapted from Rösch et al.*[253] *All work presented therein is my own.*

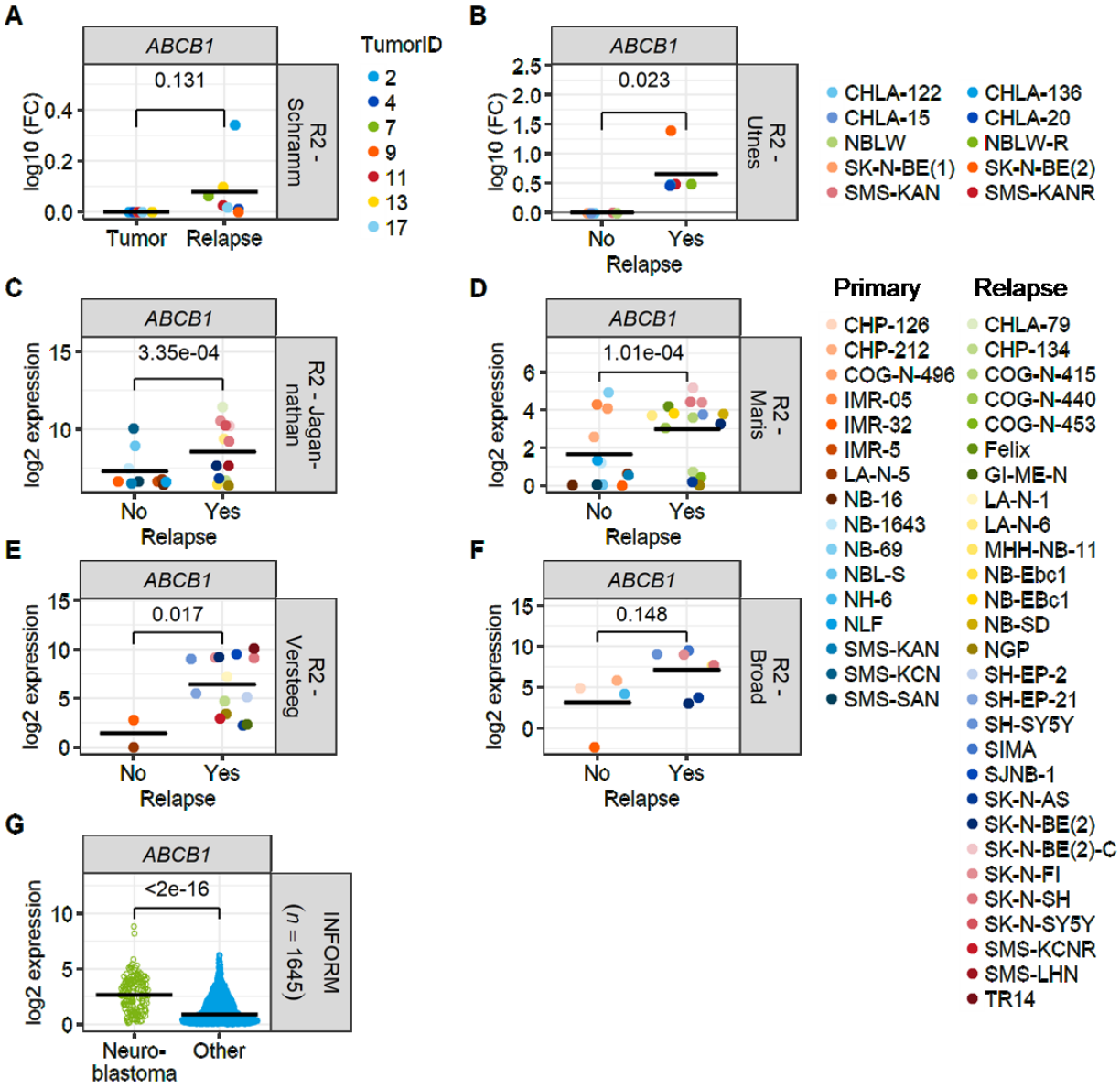

Figure 12: ABCB1 is upregulated in neuroblastoma cell lines and relapsed tumors. ***(A)*** *Gene expression data of 18 tumor samples from the dataset by Schramm et al. (GSE65303)*[241] *was downloaded from R2 (http://r2.amc.nl, 09 September 2021). Only paired samples with data at primary diagnosis (Tumor) and at Relapse were included (n = 7 pairs).* ***(B)*** *Gene expression data of 10 paired neuroblastoma cell lines from the dataset by Utnes et al. (GSE148700)*[244] *was downloaded from R2 (07 January 2021). This dataset consists of five cell line pairs derived from the same patients at primary diagnosis and after relapse.* ***(A&B)*** *Statistics of log transformed relapse values were calculated with Student's t-test against 0. Matched pairs are indicated by color.* ***(C)*** *Gene expression data of 38 neuroblastoma cell lines from the dataset by Jagannathan et al. (GSE19274)*[242] *was downloaded from R2 (08 June 2021). All cell lines that could not be positively identified as having been derived before (n = 10) or after (n = 12) the patient had received chemotherapy (Relapse No/Yes) were excluded from the analysis.* ***(D)*** *Gene expression data of 41 neuroblastoma cell lines from the dataset by Maris et al. (GSE89413)*[174] *was downloaded from R2 (07 January 2021). All cell lines that could not be positively identified as having been derived before (n = 12) or after (n = 15) the patient had received chemotherapy (Relapse No/Yes) were excluded from the analysis.* ***(E)*** *Gene expression data of 24 neuroblastoma cell lines from the dataset by Versteeg et al. (GSE28019) was downloaded from R2 (07 January 2021). All cell lines that could not be positively identified as having been derived before (n = 2) or after (n = 14) the patient had received chemotherapy (Relapse No/Yes) were excluded from the analysis.* ***(F)*** *Gene expression data of 917 cell lines from the cell line encyclopedia dataset from the Broad Institute (GSE19274)*[243]*, which included 17 neuroblastoma cell lines, was downloaded from R2 (08 June 2021). Neuroblastoma cell lines that could not be positively identified as having been derived before (n = 4) or after (n = 7) the patient had received chemotherapy (Relapse No/Yes) were excluded from the analysis.* ***(G)*** *Gene*

expression data from the INFORM registry[235,236] *(n = 1645). Comparison of neuroblastoma cases (n = 162) vs. all other entities.* ***(C-G)*** *Statistics were calculated by ANOVA followed by Tukey's post-test including all genes of the ERBB and the ABC families present in the respective datasets. This figure was adapted from Rösch et al.*[253] *The analysis presented therein is my own.*

Having shown that *ABCB1* is upregulated in relapsed neuroblastoma, I tested whether inhibition of P-gp breaks chemotherapy resistance. Trypan blue exclusion of BE(2)-C cells showed that combining VCR with the P-gp inhibitor tariquidar efficiently killed the VCR resistant subline (Figure 13A). Bliss synergy analysis following a metabolic activity assay indicated strong synergy between the two drugs for the BE(2)-C ctrl and rVCR (Figure 13A and B and Appendix Figure 15A). Combining VCR with another P-gp inhibitor, verapamil, confirmed that resistance was broken by P-gp inhibition (Figure 13C).
In two other relapsed, neuroblastoma cell lines, CHP-134 and SIMA, viability was likewise reduced upon combination treatment of VCR with tariquidar (Figure 13D and E). A metabolic activity assay followed by Bliss synergy analysis also indicated synergism for the combination of VCR with tariquidar in these cell lines (Figure 13B, D and E and Appendix Figure 15A).
In addition, I complemented these data by analysis of the three sensitive/resistant cell line pairs MHH-NB-11 ctrl/rVCR, NB-S-124 ctrl/rVCR and NGP ctrl/rVCR. They all showed synergism between tariquidar and VCR, with stronger effects for the resistant cell lines (Figure 13B and F and Appendix Figure 15B).

Having shown that P-gp inhibition by small molecule inhibitors in combination with VCR treatment led to synergistic loss of viability, I performed an *ABCB1* KD to ensure the specificity of the effect. Indeed, in BE(2)-C rVCR colony number was significantly reduced when VCR treatment was combined with *ABCB1* KD, compared to VCR treatment in a control KD (Figure 14A). To analyze P-gp function, I stained BE(2)-C ctrl and rVCR with the P-gp substrate calcein and measured calcein content in the cells by flow cytometric analysis. Calcein signal was reduced in BE(2)-C rVCR compared to BE(2)-C ctrl, indicating increased P-gp activity (Figure 14B). Blocking P-gp function in BE(2)-C ctrl and rVCR by tariquidar significantly increased calcein signal in both cell lines (Figure 14C). This effect was stronger in the resistant cell line than the sensitive one. Finally, I performed an *ABCB1* KD in BE(2)-C rVCR, which significantly increased calcein in the cells, indicating that the efflux of calcein is indeed mainly mediated by P-gp (Figure 14D).

Having identified P-gp as a potential target in a functional resistance breaking screen, I found it to be upregulated in a wide number of neuroblastoma cell lines derived at relapse. I showed that the VCR resistant BE(2)-C cells had increased P-gp surface expression and increased P-gp function compared to BE(2)-C ctrl. Finally, *ABCB1* KD efficiently sensitized BE(2)-C rVCR to VCR treatment and reduced P-gp function. Taken together these results indicate the importance of P-gp mediated drug efflux in chemotherapy resistance in relapsed neuroblastoma.

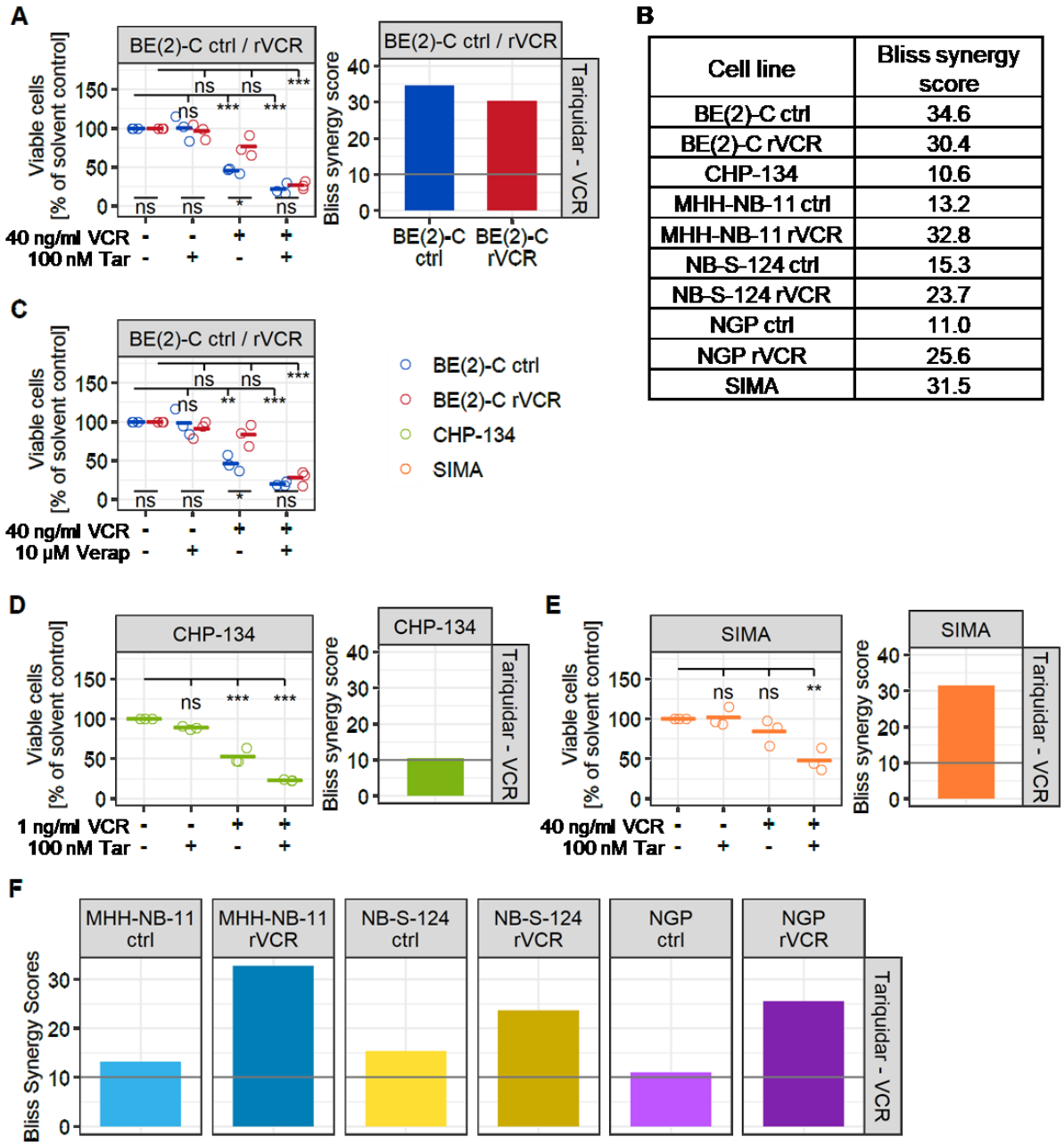

Cell line	Bliss synergy score
BE(2)-C ctrl	34.6
BE(2)-C rVCR	30.4
CHP-134	10.6
MHH-NB-11 ctrl	13.2
MHH-NB-11 rVCR	32.8
NB-S-124 ctrl	15.3
NB-S-124 rVCR	23.7
NGP ctrl	11.0
NGP rVCR	25.6
SIMA	31.5

Figure 13: Inhibitors of P-gp break VCR resistance in neuroblastoma. ***(A)*** *BE(2)-C control and rVCR were treated with 40 ng/ml VCR and 100 nM of the P-gp inhibitor tariquidar for 48 h.* ***(B)*** *Bliss synergy scores were calculated from metabolic activity data (0, 10, 20, 40, 100 ng/ml VCR +/- 0, 1, 10, 1000 nM tariquidar for 48 h in all cell lines) using SynergyFinder.*[252] *A score > 10 indicates synergy.* ***(C)*** *BE(2)-C control and rVCR were treated with 40 ng/ml VCR and 10 µM of the P-gp inhibitor verapamil for 48 h.* ***(D)*** *CHP-134 cells were treated with 1 ng/ml VCR and 100 nM tariquidar for 48 h.* ***(E)*** *SIMA cells were treated with 40 ng/ml VCR and 100 nM tariquidar for 48 h.* ***(A,C-E)*** *Dead cells were stained with trypan blue and only viable cells were counted. Percent of viable cells to the solvent control of each cell line was calculated. Presented are biological replicates (n = 3) and their mean. Statistics were calculated with ANOVA followed by Tukey's post-test. Shown are the comparisons between the cell lines (bottom) as well as the comparisons to solvent control for each cell line (top).* ***(A,D-F)*** *Bliss synergy scores were calculated as described in (B). A score > 10 (grey line) indicates synergy. *** p < 0.001, ** p < 0.01, * p < 0.05, ns = not significant. Tar = tariquidar, Verap = verapamil. This figure was adapted from Rösch et al.*[253] *All work presented therein is my own.*

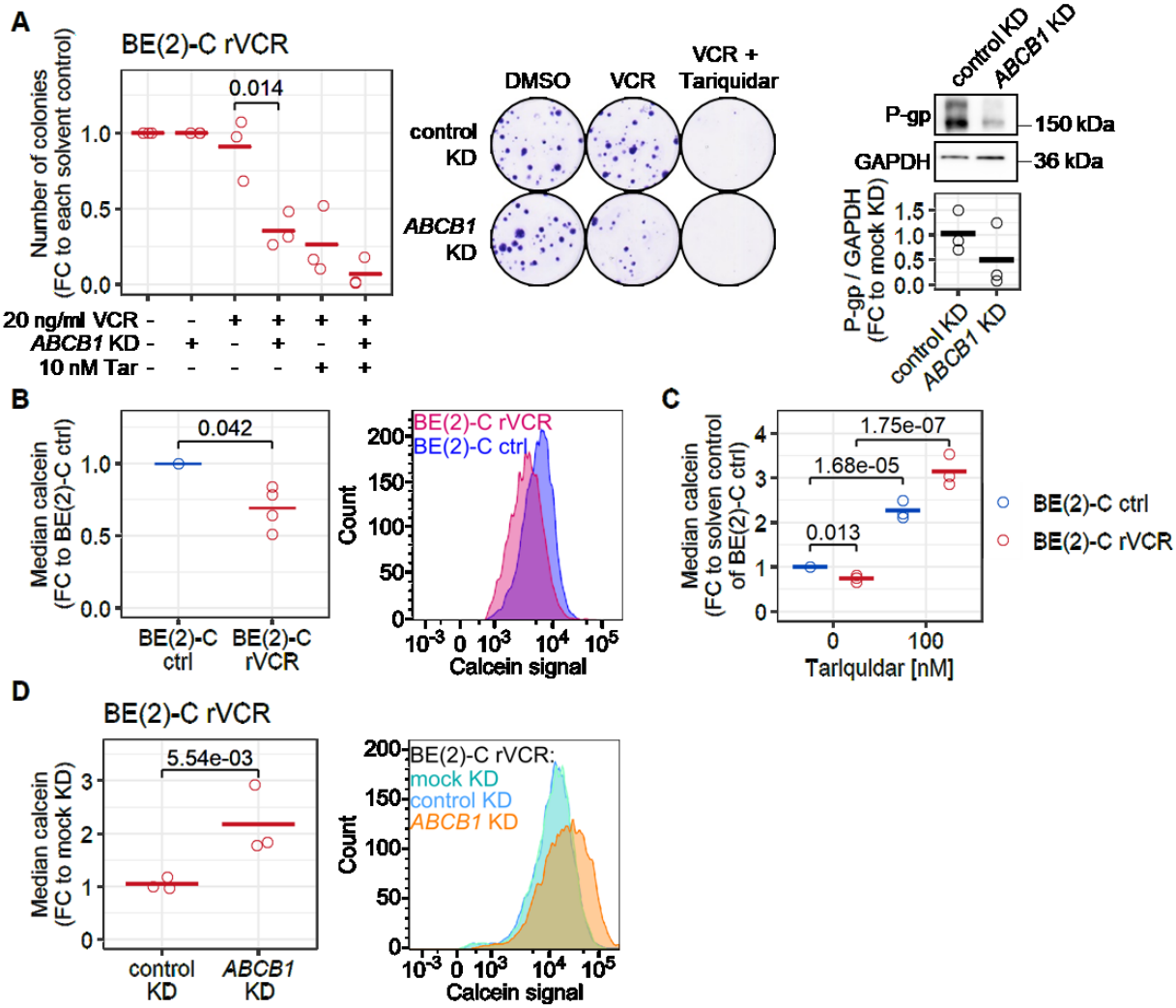

Figure 14: P-gp KD breaks VCR resistance and P-gp function is increased in VCR resistant cells. ***(A)*** *ABCB1 and control KD were induced in BE(2)-C rVCR for 24 h, followed by treatment with 20 ng/ml VCR and 10 nM tariquidar as indicated for 72 h. Medium was changed and colonies were allowed to grow for 9 days before staining. Colony number was assessed by ImageJ and is shown normalized to the solvent control of each KD. Shown are biological replicates and their mean. Statistic was calculated by Student's t-test of the log transformed values. In the middle panel, representative images of three biological replicates are presented. Efficient KD was confirmed by WB. Quantifications were normalized to GAPDH and mock KD.* ***(B)*** *P-gp function assay by calcein efflux. Untreated BE(2)-C ctrl and rVCR were stained with 10 nM calcein for 15 min. Intracellular calcein was analyzed by flow cytometry. A representative calcein signal distribution of four biological replicates is presented in the right panel. Quantified was median calcein signal normalized to BE(2)-C ctrl, the biological replicates and their mean are presented in the left panel. Statistic was calculated on log transformed values with Student's t-test.* ***(C)*** *BE(2)-C ctrl and rVCR were treated with 100 nM tariquidar for 24 h and P-gp function was assessed as described in (B). Three biological replicates and their mean are depicted. Statistics were computed by ANOVA of the log transformed values followed by Tukey's post-test.* ***(D)*** *BE(2)-C rVCR were induced with ABCB1 or control KD for a total of 48 h. Cells were stained with 100 nM calcein for 30 min and intracellular calcein was assessed by flow cytometry. A representative calcein signal distribution of three biological replicates is presented in the right panel. Median calcein signal was normalized to mock KD. Presented are the three biological replicates and their mean. Statistic was calculated on log transformed values with Student's t-test. This figure was adapted from Rösch et al.*[253] *All work presented therein is my own.*

4.3. Cell death analysis

In my analysis of programmed cell death I chose to focus on two mechanisms in particular, which are known to play a role in neuroblastoma: apoptosis and ferroptosis. Apoptosis is the longest known and best studied mechanism of regulated cell death and acts through the activation of caspases. Ferroptosis on the other hand has only been termed as a distinct mechanism and studied for about 10 years.[193] Its defining features are a dependency on intracellular iron and oxidation of the intracellular lipids.[215]

To establish the methods to detect apoptosis and ferroptosis, I analyzed the effect of the pan-HDAC inhibitor panobinostat, which is known to induce cell death in neuroblastoma and well-characterized in our research group, and focused on four neuroblastoma cell lines: IMR-32, LA-N-5, NB-1 and SK-N-BE(2)-C. To ensure comparable effects of panobinostat on these cell lines I analyzed viability after 48 h panobinostat treatment with the exception of IMR-32, which were much more susceptible than the other cell lines and were consequently only treated for 24 h. Viability was significantly reduced in all cell lines, although in LA-N-5 cells viability remained above 50% (Figure 15A). IMR-32 not only died at an earlier time point than the other cell lines, but also showed stronger reduction of viability at lower concentrations. Overall, I induced cell death to comparable effects in all four cell lines with the adaptation in treatment time.

To detect apoptosis I performed caspase activity assays. In a first step, I tested in NB-1 cells which protein concentration of the whole cell lysate allowed me to best detect the increase of caspase activation in response to panobinostat treatment. 50 µg protein led to a saturation of caspase-3/7 signal at only 10 nM panobinostat (Figure 15B). Using 30 µg protein allowed the discrimination between 10 nM and 50 nM panobinostat, however, the assay showed the strongest effect in caspase-3/7 activation if only 10 µg protein were used. Similar results were obtained for caspase-8 activation and 10 µg protein showed the strongest sensitivity in the assay. I therefore continued all caspase activity assays with 10 µg protein generated from whole cell lysates including the floating cells from the supernatant.

Following panobinostat treatment, IMR-32 and particularly NB-1 cells strongly activated caspases-3/7 and caspase-8 (Figure 15C). LA-N-5 and SK-N-BE(2)-C cells moderately activated caspase-3/7 upon treatment and did not activate caspase-8. To ensure the specificity of the assay, I treated the two cell lines with the strongest caspase activation - IMR-32 and NB-1 - with a combination of panobinostat and the caspase inhibitor Z-VAD-FMK. The addition of Z-VAD-FMK completely abolished caspase-8 activation in both cell lines and caspase-3/7 activation in IMR-32 (Figure 15C). Caspase-3/7 activation in NB-1 was greatly reduced

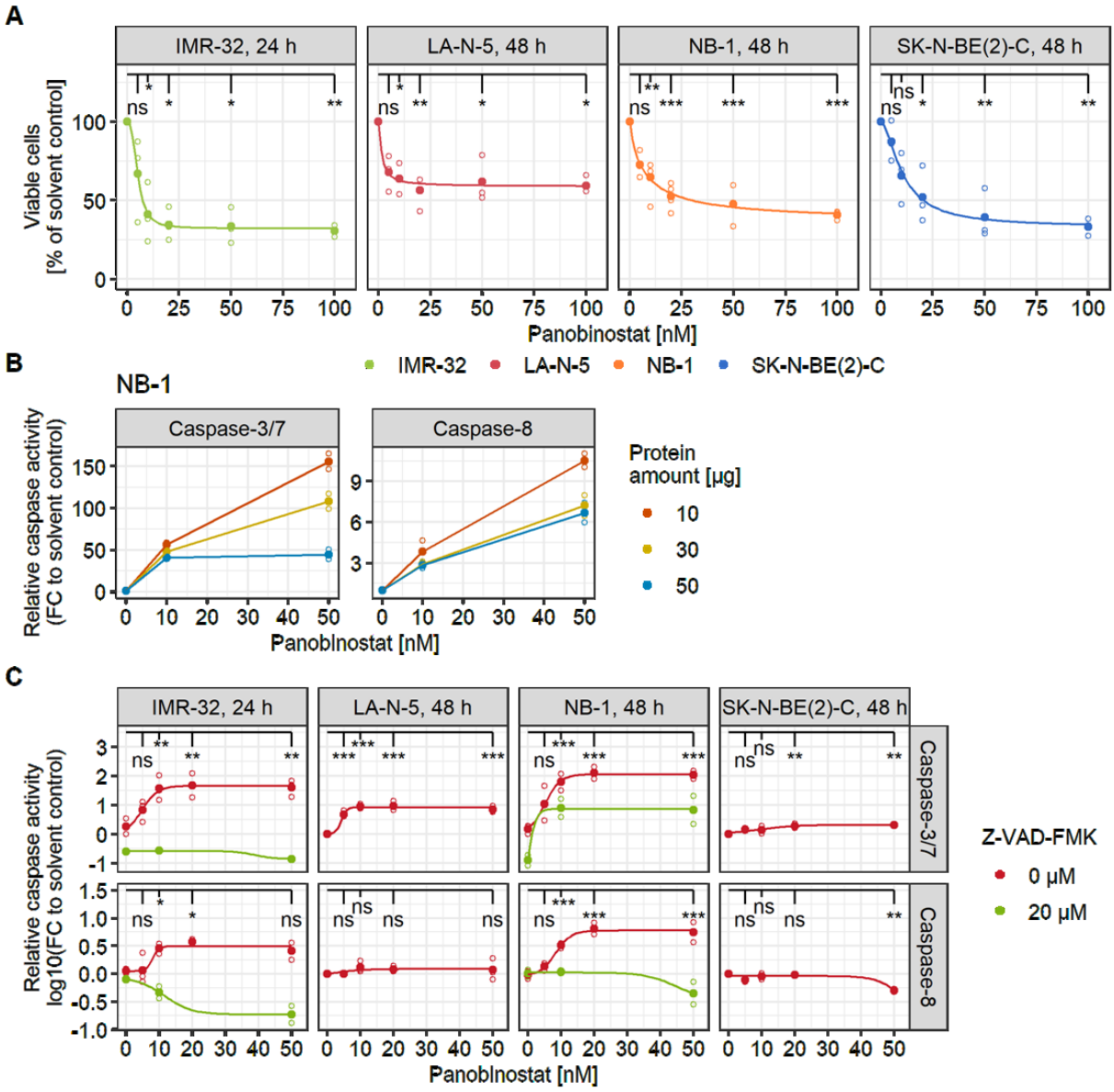

Figure 15: Caspases are activated in IMR-32 and NB-1 upon panobinostat treatment. ***(A)*** *IMR-32, LA-N-5, NB-1 and SK-N-BE(2)-C were treated with 0, 5, 10, 20, 40 and 100 nM panobinostat for 24 h or 48 h, as indicated. Viability was assessed by trypan blue exclusion assay and viable cells were normalized to the solvent control of each cell line. Presented are three biological replicates and their means. Curve fits were calculated with an LL4 model. Statistics were calculated by ANOVA on log10 transformed values followed by Tukey's post-test.* ***(B)*** *NB-1 cells were treated with 0, 10 and 50 nM panobinostat for 48 h. Caspase-3/7 and caspase-8 activity assays were performed with 10 µg, 30 µg or 50 µg added protein. Relative caspase activation is expressed in relation to the solvent control of each protein concentration.* ***(C)*** *Caspase-3/7 and caspase-8 activity assays were performed in IMR-32, LA-N-5, NB-1 and SK-N-BE(2)-C cells following treatment with 0, 5, 10, 20 and 50 nM panobinostat for 24 h or 48 h, as indicated (n = 3). IMR-32 and NB-1 were also treated with 0, 10 and 50 nM panobinostat in combination with 20 µM Z-VAD-FMK (n = 2). Relative caspase activation is expressed in relation to the solvent control of each cell line. Presented are biological replicates and their mean. The curve fits were calculated by an L4 model. Statistics were calculated by ANOVA followed by Tukey's post-test. ns = not significant, * $p < 0.05$; ** $p<0.01$, *** $p < 0.001$.*

Having shown that caspases are activated in the tested neuroblastoma cell lines after panobinostat treatment, I then investigated the outcome of caspase activation in these cells by detecting the cleavage of their target proteins. I therefore performed western blot analysis of PARP, which is cleaved by caspases during the onset of apoptosis. The ratio of cleaved PARP to full length PARP is an indicator for caspase activation and was changed most drastically for IMR-32 cells following panobinostat treatment (Figure 16A). LA-N-5 cells showed a much weaker cleavage that only reached statistical significance at 50 nM. In spite of the very strong activation of caspases shown in Figure 15C, NB-1 cells only showed a medium strong PARP cleavage as compared to IMR-32.
I also treated IMR-32 and NB-1 with a combination of panobinostat and the caspase inhibitor Z-VAD-FMK. In IMR-32 Z-VAD-FMK was able to significantly reduce PARP cleavage under panobinostat treatment (Figure 16B). In NB-1 cells, however, Z-VAD-FMK had no effect on PARP cleavage.
I then analyzed BID, another caspase substrate, which can potentiate apoptosis. Similar to PARP, BID was most strongly cleaved in IMR-32 (Figure 16C). Surprisingly, considering that NB-1 cells displayed a much stronger caspase activation than LA-N-5 cell (Figure 15C), this was followed by LA-N-5, which showed earlier trends for BID cleavage than NB-1 cells. Statistical significance was reached at 50 nM panobinostat in LA-N-5. Due to large interexperimental differences, no statistical significance was reached for BID cleavage in NB-1.

To detect ferroptosis, I performed lipid peroxidation measurement by flow cytometry. As IMR-32 had been previously shown to die by ferroptosis under certain conditions, I used this cell line to establish the assay. In a first step I checked that IMR-32 cells die when treated with the lipid peroxide inducing compound cumene hydroperoxide (CuOOH). Indeed, viability is decreased very efficiently upon CuOOH treatment (Figure 17A). I then performed the lipid peroxidation measurement with CuOOH concentrations that reduced viability by at least 50% and saw a concentration dependent increase in lipid peroxidation in IMR-32 (Figure 17B). Treatment with 20 nM panobinostat increased lipid peroxidation significantly in IMR-32, but not in NB-1 cells (Figure 17C). As a secondary ferroptosis readout I used expression of TfR. In IMR-32, panobinostat treatment increased TfR expression almost 5 fold, showing that this readout can also be used to detect ferroptosis (Figure 17D).

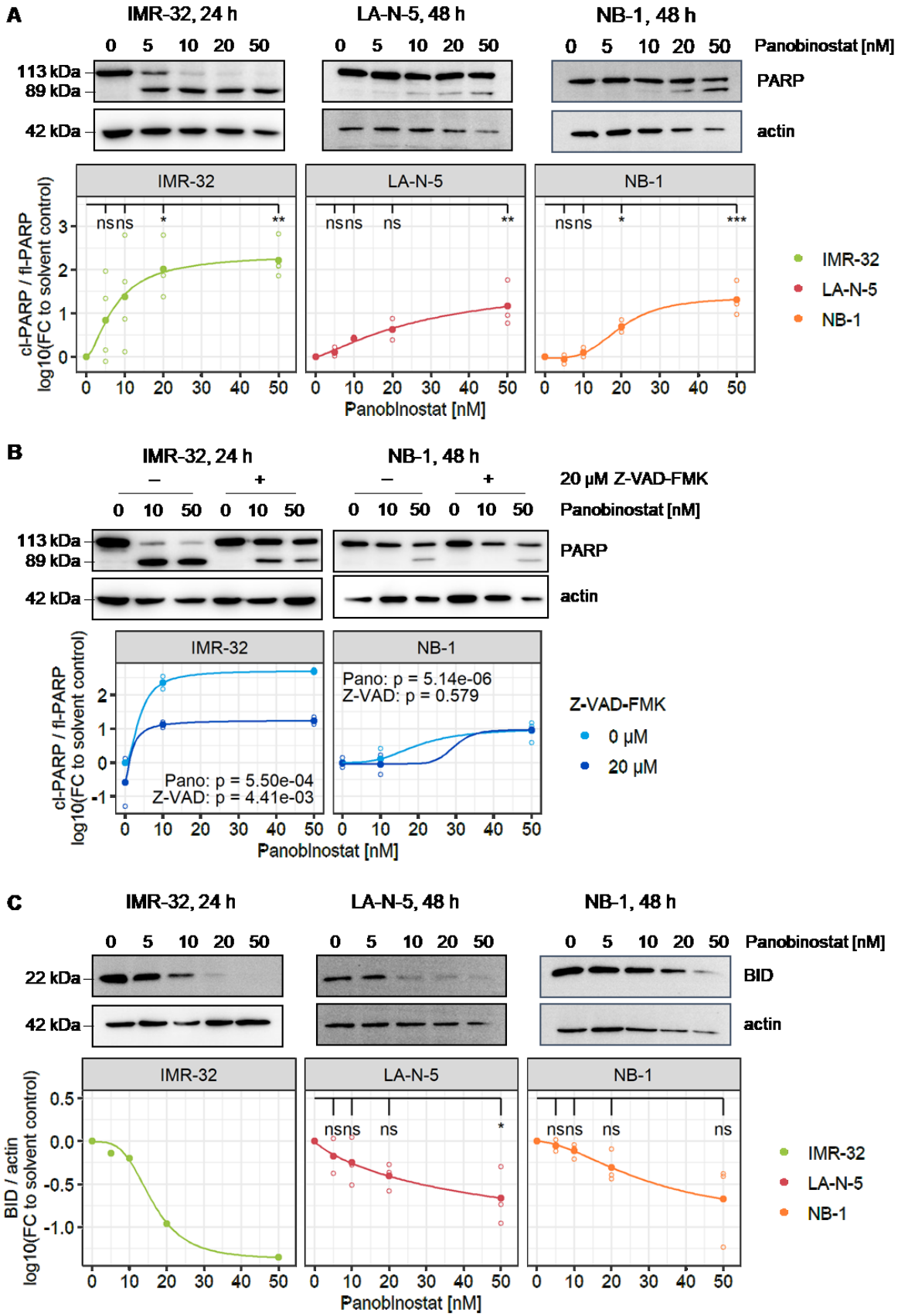

Figure 16: IMR-32 shows strongest cleavage of caspase substrates. ***(A)*** *IMR-32, LA-N-5 and NB-1 cells were treated with 0, 5, 10, 20 and 50 nM panobinostat for the indicated times. Western blots against PARP and actin were performed. Presented are representative blots of three biological replicates. PARP signal was quantified and the ratio of cleaved PARP (cl-PARP) over full length PARP (fl-PARP) was normalized to each cell line's solvent control. Shown are the replicates and their means. Statistics were calculated by ANOVA followed by Tukey's post-*

test. ***(B)*** *IMR-32 and NB-1 cells were treated with 0, 10 and 50 nM panobinostat in combination with 20 µM Z-VAD-FMK for 24 h and 48 h, respectively. NB-1 cells were re-treated with 20 µM Z-VAD-FMK after 24 h. Western blots against PARP and actin were performed. Presented are representative blots of two and three biological replicates for IMR-32 and NB-1, respectively. PARP signal was quantified and the ratio of cl-PARP over fl-PARP was normalized to each cell line's solvent control. Shown are the replicates and their means. Statistics were calculated by ANOVA.* ***(C)*** *IMR-32, LA-N-5 and NB-1 cells were treated with 0, 5, 10, 20 and 50 nM panobinostat for the indicated times. Western blots against BID and actin were performed. Presented are representative blots of three biological replicates for LA-N-5 and NB-1 and a single replicate for IMR-32. The quantified BID signal was normalized to actin and the respective cell line's solvent control. Shown are the replicates and their means. Statistics were calculated by ANOVA followed by Tukey's post-test. ns = not significant, * p < 0.05; ** p<0.01, *** p < 0.001.*

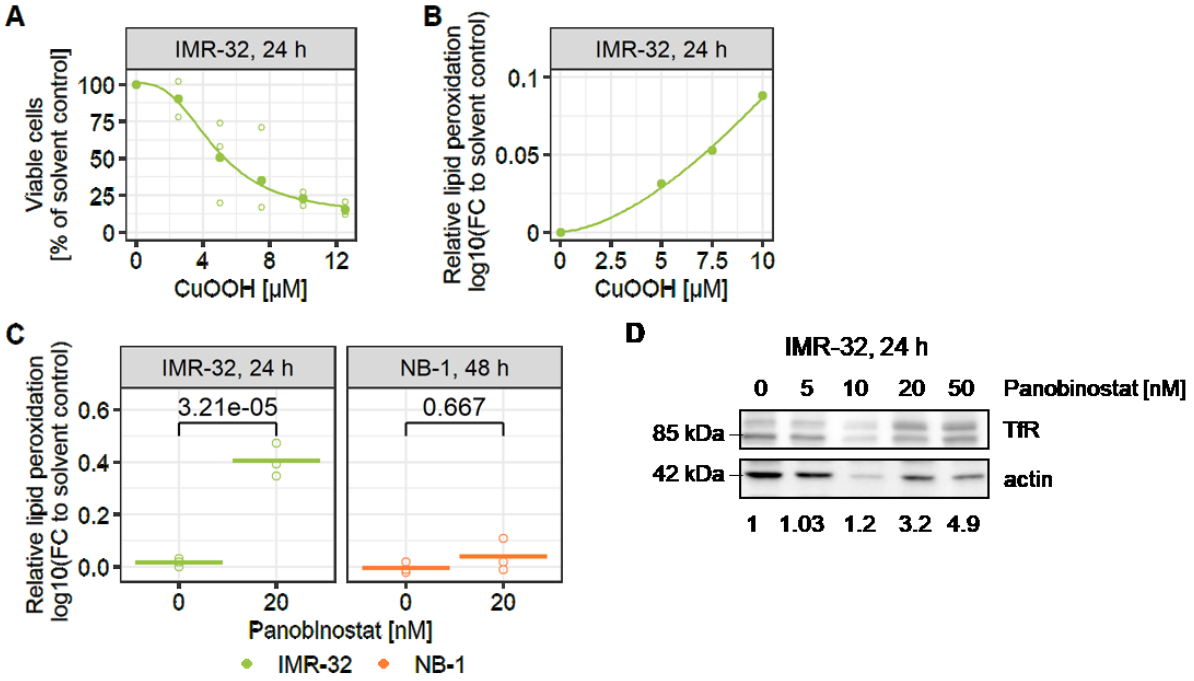

Figure 17: Panobinostat treatment induces ferroptosis in IMR-32, but not in NB-1. ***(A)*** *IMR-32 cells were treated with 0, 2.5, 5, 7.5, 10 and 12.5 µM CuOOH for 24 h. Viable cells were counted by trypan blue exclusion and their number normalized to solvent control. Three biological replicates and their mean are shown.* ***(B)*** *IMR-32 cells were treated with 0, 5, 7.5 and 10 µM CuOOH for 24 h. Cells were stained with 20 µM BODIPY 581/591 for 30 min and oxidized BODIPY measured by flow cytometric analysis. Values were normalized to solvent control.* ***(C)*** *IMR-32 and NB-1 were treated with solvent control and 20 nM panobinostat for 24 h and 48 h, respectively. Cells were stained with 20 µM BODIPY 581/591 for 30 min and oxidized BODIPY measured by flow cytometric analysis. Values were normalized to untreated control. Three biological replicates and their mean are shown. Statistics were calculated by ANOVA followed by Tukey's post-test.* ***(D)*** *IMR-32 were treated with 0, 5, 10, 20 and 50 nM panobinostat for 24 h. Western blot against TfR and actin was performed. Quantified TfR signal was normalized to actin and solvent control. The FCs of one replicate are shown underneath the blot.*

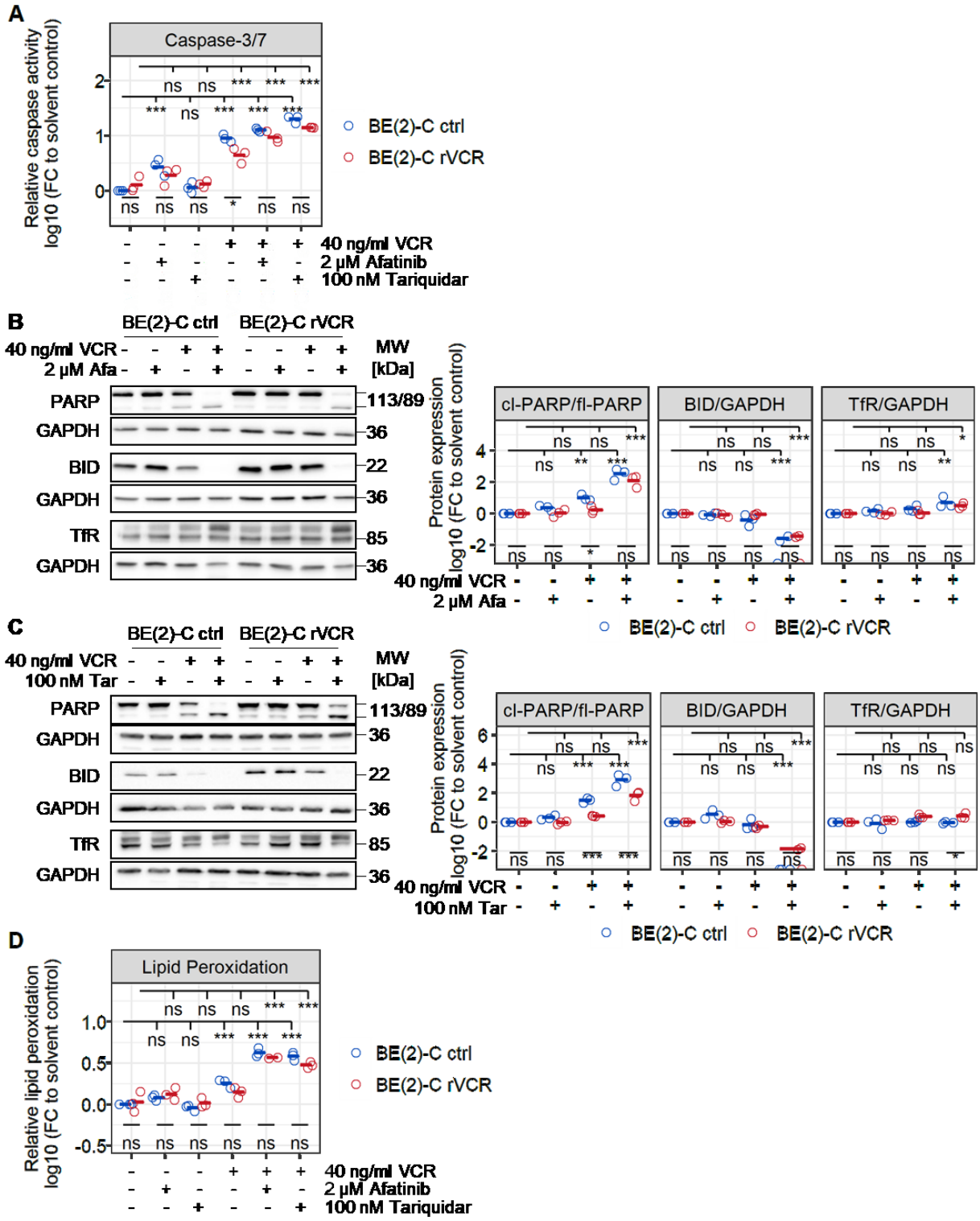

Figure 18: Combination treatment of VCR with afatinib or tariquidar induces apoptosis in BE(2)-C. ***(A)*** *BE(2)-C control and rVCR were treated with 40 ng/ml VCR, 2 µM afatinb, 100 nM tariquidar or combinations as indicated for 48 h. Caspase-3/7 activity was normalized to solvent control of BE(2)-C ctrl. Three biological replicates and their means are shown. Statistics were calculated by ANOVA followed by Tukey's post-test.* ***(B)*** *BE(2)-C ctrl and rVCR were treated for 48 h with 40 ng/ml VCR and 2 µM afatinib.* ***(C)*** *BE(2)-C ctrl and rVCR were treated for 48 h with 40 ng/ml VCR and 100 nM tariquidar.* ***(B&C)*** *Western Blot against PARP, BID, TfR and GAPDH. Representative blots of three biological replicates are shown. Signal quantifications are shown in the right panels. Signal was normalized to the respective GAPDH and solvent control of each cell line. Statistics were calculated by ANOVA followed by Tukey's post-test.* ***(D)*** *BE(2)-C control and rVCR were treated with 40 ng/ml VCR, 2 µM afatinb, 100 nM tariquidar or combinations as indicated for 48 h. Cells were stained with 20 µM BODIPY 581/591 for 30 min and*

*oxidized BODIPY measured by flow cytometric analysis. Values were normalized to solvent control. Three biological replicates and their means are shown. Statistics were calculated by ANOVA followed by Tukey's post-test. ns = not significant, * p < 0.05; ** p < 0.01, *** p < 0.001. This figure was adapted from Rösch et al.*[253] *All work presented therein is my own.*

Finally, I used the methods I had established to detect apoptosis and ferroptosis to analyze the combination of VCR with afatinib or tariquidar in control and VCR resistant BE(2)-C cells. Caspase activity assays showed strong activation of caspase-3/7 in response to VCR single treatment as well as both combinations (Figure 18A). Notably, the VCR resistance of BE(2)-C rVCR was confirmed by caspase activity, as caspases-3/7 were significantly stronger induced in control BE(2)-C than BE(2)-C rVCR. Caspase targets PARP and BID were cleaved in both cell lines in the combination treatments with VCR and afatinib or tariquidar (Figure 18B and C). Here, the VCR resistance of BE(2)-C rVCR was reflected by the cleavage of PARP, which occurred in VCR single treatment for control BE(2)-C, but not for BE(2)-C rVCR.
Ferroptosis marker TfR was only slightly increased in the combination treatments and unchanged in the single treatments for both cell lines (Figure 18B and C). Lipid peroxidation was significantly, but not strongly increased in the single treatment of BE(2)-C ctrl, but not BE(2)-C rVCR, and in both cell lines in the combination treatments (Figure 18D).
Taken together, these results suggest that apoptosis is the predominant mechanism of cell death in BE(2)-C in response to VCR treatment in combination with afatinib or tariquidar.

In this thesis I present data that underlines the importance of both detailed validation and functional approaches in targeted medicine. I performed differential gene and pathway enrichment analyses in relapsed pediatric tumor, which indicated the ERBB family, particularly ERBB4, as potential interesting targets in relapsed high-risk neuroblastoma. Validation analyses, however, did not yield any evidence that ERBB4 mediates chemotherapy resistance in relapsed high-risk neuroblastoma. A functional approach, on the other hand, indicated P-gp to play a major role in breaking resistance. Indeed, further validation experiments showed that both P-gp expression and function were increased in resistant neuroblastoma. Additionally, I was interested in different methods of programmed cell death and was able to show the induction of both apoptosis and ferroptosis in neuroblastoma cell lines. Finally, I showed that when VCR resistance was broken by the addition of P-gp inhibitors, apoptosis was induced.

5. Discussion

Chemotherapy resistance in relapsed pediatric tumors is a persistent clinical problem. As the example of neuroblastoma shows, high-risk patients after relapse still have very poor outcomes with a 5 year overall survival under 10%.[31] These cases are often accompanied by strong chemotherapy resistance, which needs to be overcome to improve treatment of these patients.

In my thesis I combined two approaches to identify a way to overcome chemotherapy resistance: an analysis of gene expression data of primary and relapsed tumors to find a targetable gene or pathway, and a functional metabolic activity screen with selected drugs to find a drug that is able to overcome resistance in a given chemoresistance model. The first approach is related to static targeted medicine, in which a fixed property is measured to determine a target gene or - preferably - target pathway. Functional precision medicine on the other hand measures the response of living cells to an intervention, usually a panel of drugs. This makes it possible to find treatment options for patients even without a clear and actionable driver mutation.[255] While static targeted therapy analyses are becoming increasingly established, functional precision medicine is still being introduced in clinical settings, which includes setting up a pipeline to obtain viable tumor material directly from the individual patient. Functional assays that are performed on established cell lines are less suitable and informative, as they might not reflect the original tumor precisely any longer and of course can give no information on a specific patient.

Both the static and the functional approaches have their advantages and disadvantages, but complement each other well. The gene expression analysis allowed me to include bulk data from many patients and indeed from several pediatric tumor entities. I later focused my validation on one entity - neuroblastoma - but was able to start with a very broad analysis. Furthermore, the gene expression analysis included over 18,000 genes, allowing an unbiased approach and making the discovery of new and unexpected target pathways possible. The functional approach using a metabolic activity screen, on the other hand, gives much more direct insight into the actual question under consideration: how can I overcome chemotherapy resistance in the given model? Even though the number of targets and models analyzed must be limited for practical reasons, the results allow a more immediate conclusion that a certain drug can indeed break resistance. Of course, the actual on-target activity of the drug must still be carefully validated. A disadvantage of the functional approach as I have performed it is that I used a cell line model, which was artificially created to be chemotherapy resistant, instead of a recently cultured patient sample.

In the course of my thesis I identified two possible targets in chemotherapy resistant, relapsed neuroblastomas. Following the gene expression analysis I focused on the ERBB family of receptor tyrosine kinases, with a particular emphasis on ERBB4, while the functional analysis indicated a great importance for the transmembrane pump P-gp. Validation analyses showed that it was indeed P-gp, which conferred chemotherapy resistance in my models.

5.1. Gene expression analysis of primary and relapsed pediatric tumors

In the gene expression analysis I compared gene expression data from primary (n > 13) and relapsed (n > 13) tumors for six pediatric tumor (sub)entities.

Ependymoma is a neuroepithelial cancer of the central nervous system that befalls both children and adults.[256] The subtype PF-EPN-A occurs only in children and is one of two ependymoma subtypes with a particularly poor outcome.[257] A pathway enrichment analysis of PF-EPN-A samples against other ependymoma subtypes and normal brain showed, amongst others, enrichment in cell migration and adhesion and the ECM, cell proliferation and differentiation, and development of the forebrain and the central nervous system.[257] This fits well with the results from my own pathway enrichment analysis of primary versus relapsed PF-EPN-A, where I identified pathways of the ECM, neuronal signaling and the cell cycle.

HGG and DIPG are malignant brain tumors that are responsible for the greatest number of pediatric tumor related deaths.[258] A characteristic feature of pediatric HGGs are the common occurrence of mutations in histone 3.[259,260] A study comparing different HGG subgroups found pathway enrichments that included many signaling pathways (particularly PI3K and MAPK signaling), associations with development and the central nervous system, cell migration, immune response and the cell cycle.[261] In the comparison between primary and relapsed HGGs I similarly found many pathways involved in signaling, with an emphasis on ERBB and PI3K signaling, as well as pathways involved in transcription and the ECM.

Osteosarcomas are malignant tumors of the bone, most often occurring in the long bones of the body. They are characterized by chromosomal instability and many osteosarcomas have *TP53* mutations.[262] While a majority of patients have a good outcome, this changes dramatically if a patient relapses, with 5 year survival rates below 20%.[263] Compared to the other tumor entities I analyzed, osteosarcoma had much fewer enriched pathways. The only discernible grouping were seven pathways concerned with the ECM. Indeed, the complex genomics and great heterogeneity between osteosarcoma patients complicate the analysis. Nevertheless, the importance of the tumor microenvironment has been suggested.[262]

RMS are malignant, soft tissue sarcomas. The most common types of RMS in children and adolescents are embryonal RMS and alveolar RMS. Alveolar RMS is very aggressive and is characterized by *FOXO1* fusions, mostly *PAX3-FOXO1* or *PAX7-FOXO1*. Embryonal RMS on the other hand, is less aggressive. While approximately 50% of embryonal RMS have a loss of function in *TP53*, no consistent molecular driver is known.[264] In my analysis of primary and relapsed RMS, I found relapsed alveolar RMS to be enriched in cell cycle and few signaling related pathways, while relapsed embryonal RMS was enriched in signaling events in the cells and the immune system. A study comparing a mixed set of RMS samples to normal muscle samples found pathways involved in the cell cycle, p53 signaling, the ECM and viral carcinogenesis upregulated in the tumor samples.[265] However, as this study did not distinguish between RMS subtypes, comparisons to my own data need to be made with caution.

In relapsed neuroblastoma I identified the ECM and ERBB signaling as enriched pathways. A study with chemotherapy resistant *MYCN* amplified mice showed that resistant neuroblastoma cells transition to a migratory and invasive phenotype, in which changes in the ECM play an integral role.[266] Of the four members of the ERBB family, only *ERBB4* was upregulated in relapsed neuroblastoma in my analysis.

The importance of ERBB4 on chemotherapy resistance in neuroblastoma has been suggested before,[137,267] but has not been studied in great detail.
Many pathway enrichment analyses compare different tumor subentities, or tumor tissue with a normal tissue control.[257,261,265] In contrast to this, I laid a particular focus on the differences between primary and relapsed tumors in my thesis. Still, I found many of the same pathways enriched, which are already known to play a role in the respective entity, thus supporting my analysis.

5.2. Functional resistance breaking screen

In contrast to the gene expression analysis, in which I analyzed different tumor entities, I focused only on relapsed neuroblastoma in the functional screen. Specifically, I asked the question how I could overcome the VCR resistance in the resistant cell line model BE(2)-C rVCR by combining VCR treatment with 14 approved drugs targeting different cancer relevant pathways and with tariquidar, a P-gp inhibitor that has been studied in clinical trials.[254] A limitation of the functional screen was using only one VCR concentration. While one concentration was sufficient to find which combination partner was beneficial and would break resistance, it hindered the discrimination between additive and synergistic effects. I therefore performed synergy analyses for the two top hits of the functional screen (afatinib and tariquidar) in a second step and applied several cell lines in the course of my validation analysis. This revealed strong synergism for both combinations, VCR with afatinib or tariquidar, in all tested VCR resistant cell lines. Hence, even though the initial functional screen was very focused in the number of samples and concentrations, it gave valid output.

5.3. ERBB4 in relapsed high-risk neuroblastoma

Both the gene expression analysis of primary and relapsed neuroblastomas and the functional assay indicated an importance for the ERBB family, in particular ERBB4, in chemotherapy resistant, relapsed neuroblastoma. I therefore studied this in closer detail.
Few studies have systematically examined the role of the individual members of the ERBB family in neuroblastoma. Two studies applying immunohistochemistry (IHC) staining and real-time PCR in neuroblastoma tumor tissue, respectively, found ERBB4 to be expressed, albeit at low levels.[268,269] Another study, also with an IHC readout, found high ERBB4 expression in ca. 50% of the examined neuroblastic tumors (70% neuroblastomas, 30% ganglioneuroblastomas and ganglioneuromas), with higher ERBB4 expression in the high-risk group and in metastatic rather than localized disease.[270] None of these studies examined the difference in ERBB family expression between primary and relapsed neuroblastoma. My own results were varied. I found significant ERBB4 upregulation in both my main model of VCR resistant BE(2)-C compared to control BE(2)-C and between their parental cell line SK-N-BE(2) and its corresponding cell line from the primary tumor, SK-N-BE(1). However, my bulk analysis of different gene expression datasets of neuroblastoma tumor samples and cell lines showed no significant upregulation of any member of the ERBB family at relapse when comparing group means. Individual samples or cell lines with a comparatively high *ERBB4* expression were offset by others with no or very low *ERBB4* expression. This indicates that *ERBB4* overexpression is not a general resistance mechanism in relapsed neuroblastoma, but occurs only in specific samples.

A neuroblastoma cell line that was made resistant to the ALK inhibitor lorlatinib, also upregulated ERBB4 in a similar manner.[271] However, and in concordance with my own results, ERBB4 was not the driver of resistance in this study. Rather, several acquired mutations, particularly a heterozygous *NF1* mutation, led to an overactivation of the MAPK pathway. Similarly, my validation studies clearly showed that the strong upregulation of ERBB4 in BE(2)-C rVCR per se had no effect on VCR resistance, as KD of *ERBB4* did not sensitize to VCR treatment. This indicates that upregulation of ERBB4 might rather be a side effect of the resistance generated in these models. Nevertheless, I investigated ERBB4 signaling more closely to confirm its mechanistic role in chemotherapy resistance in relapsed neuroblastoma.

5.3.1. Inhibition of ERBB4 and its downstream pathways

As there are no exclusive ERBB4 inhibitors, I chose the ERBB family inhibitors afatinib and lapatinib to investigate ERBB4 signaling. Afatinib is a drug approved by the U.S. Food and Drug Administration (FDA) for EGFR mutated NSCLC and has a very high affinity for ERBB4, with an IC50 in cell free assays of 1 nM.[272,273] It also inhibits EGFR (IC50 0.5 nM) and, with slightly lower affinity, ERBB2 (IC50 14 nM).[273] In a functional screen with fresh patient samples from relapsed or progressing pediatric tumors, 5.6% (5 of 88) of patients reacted strongly to afatinib, including one neuroblastoma patient (I. Oehme, Translational Drug Screening Unit, KiTZ, Heidelberg, personal communication, April 05, 2022). Afatinib was also among the two strongest hits in my functional drug screen using the VCR resistant BE(2)-C. Lapatinib is approved for advanced or metastatic breast cancer by the FDA and has slightly lower affinities to the ERBB family than afatinib, with IC50s of 10 nM (EGFR), 9 nM (ERBB2) and 367 nM (ERBB4).[272,274] The last member of the ERBB family, ERBB3, is kinase impaired and its reduced phosphorylation capabilities are not affected by ERBB family inhibitors.[101] In addition, afatinib and lapatinib are both substrates of P-gp and competitively inhibit the transporter at higher concentrations (> 1 μM).[273,275]

The combination of afatinib with VCR was synergistic for all n = 10 cell lines tested. The Bliss synergy scores of the four artificially resistant cell line pairs were generally higher for the VCR resistant sublines than their sensitive counterpart. The only exception were BE(2)-C ctrl, which had a similar synergy score to BE(2)-C rVCR. BE(2)-C ctrl were more resistant to VCR single treatment with an IC50 that was 10 fold higher than those of the other sensitive cell lines MHH-NB-11 ctrl, NB-S-124 ctrl and NGP ctrl. As uniform VCR concentrations were chosen for all synergy experiments, the high sensitivity of MHH-NB-11 ctrl, NB-S-124 ctrl and NGP ctrl to VCR single treatment led to a very strong loss in viability, which was not augmented greatly by the addition of afatinib. The higher relative resistance of BE(2)-C ctrl to VCR allowed for a much greater additional effect of afatinib at the chosen concentrations, which is reflected in the higher Bliss synergy score.

Surprisingly, in CHP-134 cells, the treatment with afatinib for 6 h induced AKT phosphorylation, indicating pathway activation. In the PI3K/AKT signaling pathway, mTOR and S6 kinase induce a negative feedback loop towards AKT, which can lead to paradoxical activation of AKT phosphorylation when interrupted.[276,277] If the lack of basal AKT phosphorylation in the CHP-134 cell line is due to such a negative feedback loop, and afatinib - by interfering in the cellular signaling pathways - were to lead

to decreased mTOR activity, this would disrupt the negative feedback loop and might lead to the observed increase in AKT phosphorylation. Such paradoxical activation is also well documented in other signaling pathways, e.g. MAPK signaling, where first generation RAF inhibitors stabilize the formation of RAS-RAF dimers, leading to increased phosphorylation of downstream ERK.[278,279]
Another, more direct, negative regulator of PI3K/AKT is PTEN, the loss of which has been shown to increase AKT phosphorylation.[280,281] Loss of PTEN was observed upon treatment with the ERBB family inhibitors erlotinib, gefitinib or afatinib in relapsed or progressing NSCLC patients harboring activating EGFR mutations.[282] Such an afatinib induced loss of PTEN activity might therefore interrupt the negative regulation of AKT phosphorylation and lead to the observed increase in AKT phosphorylation in CHP-134 cells. Indeed, in an experimental setting, 6 h were sufficient time to allow degradation of PTEN,[283] indicating a short half-life of PTEN and making a connection between afatinib treatment and decreased PTEN activity plausible. To confirm this hypothesis it might be interesting to follow up on PTEN expression and activity in CHP-134 cells following afatinib treatment.
In contrast to the paradoxical activation of AKT in the CHP-134 cells, I did not observe any change in the phosphorylation levels of downstream ERBB signaling in response to afatinib treatment in BE(2)-C ctrl and rVCR. Also different to CHP-134 cells, AKT and ERK were phosphorylated in BE(2)-C cells in their untreated state. BE(2)-C cells harbor a mutation of the tumor suppressor gene *NF1*.[231] NF1 is a negative regulator of RAS, *NF1* mutations therefore lead to an overactivation of the MAPK pathway.[284]
A possible explanation for the lack of afatinib effect on phosphorylation levels in BE(2)-C ctrl and rVCR is therefore the presence of strong upregulation of the pathways downstream of the receptor that would negate receptor inhibition. However, if this were the resistance mechanism, afatinib would not reduce viability. This was indeed observed in a study by Redaelli *et al.*, in which a neuroblastoma cell line with ERBB4 upregulation and *NF1* mutation showed little attenuation of viability in response to afatinib.[271] While a strong upregulation of ERBB family downstream pathways might therefore explain the lack of afatinib effect on phosphorylation in the BE(2)-C cell lines, it also strengthens the conclusion that resistance is mediated by P-gp in these models.

I showed that it is possible to reduce phosphorylation of the ERBB family downstream pathways by specific inhibitors (SRC inhibitor dasatinib, MEK inhibitor trametinib and PI3K inhibitor BKM120). However, the inhibitors of the three downstream pathways did not reduce viability upon VCR co-treatment as efficiently as afatinib.
Of the three compounds, dasatinib had the strongest effect on viability, and indeed, dasatinib was also a high hit in my functional resistance breaking screen. Still, even dasatinib did not restore VCR sensitivity at the level of afatinib. Of note, like afatinib, dasatinib is a P-gp substrate. However, dasatinib inhibits P-gp at much higher concentrations than afatinib. While afatinib inhibits P-gp at concentrations < 1 µM,[273] dasatinib requires up to 10 µM.[285,286] While dasatinib showed a small effect towards restoring sensitivity, its comparatively low affinity for P-gp also precluded an efficient P-gp inhibition at the chosen concentrations.
Trametinib inhibits P-gp at concentrations around 5 µM.[85] As trametinib inhibits MEK in the nanomolar range, the tested concentrations did not reach the levels required to inhibit P-gp, which is reflected in the low additional effect of trametinib on VCR that I observed. BKM120 is not a P-gp substrate and

accordingly did not reduce viability further.[287] This data also supports P-gp as the main driver of resistance in BE(2)-C rVCR.

The *ERBB4* KD, which decreased expression more than 85%, had no additional effect on viability in combination with VCR treatment or the combination treatment VCR and afatinib. This shows that the cells do not depend on ERBB4 for survival and VCR resistance is not mediated by ERBB4. However, 75% of neuroblastomas express more than one member of the ERBB family,[270] and indeed, *ERBB3* was also strongly upregulated in BE(2)-C rVCR compared to control BE(2)-C, while *EGFR* and *ERBB2* were expressed at similar levels in both sublines. Hence, it is possible that upon KD of *ERBB4*, another ERBB family member would have compensated for the lack of ERBB4. Indeed, heterodimers make up a significant part of ERBB family signaling.[288] It is conceivable that formation of EGFR monodimers or EGFR-ERBB2, EGFR-ERBB3 or ERBB2-ERBB3 heterodimers would have increased upon the loss of ERBB4 and compensated the diminished ERBB4 signaling, which might be interesting to follow up on. Inhibition of ERBB4 by a blocking antibody did not affect viability either. Taken together this indicates that ERBB4 or the other members of the ERBB family are not mainly responsible for the VCR resistance in BE(2)-C rVCR. The restored VCR sensitivity observed in combination with both afatinib and lapatinib are most likely an off-target effect on P-gp.

5.4. P-gp in high-risk relapsed neuroblastoma

P-gp mediated chemotherapy resistance is a well-established resistance mechanism in cancer, however its role in neuroblastoma is not so clear. Several studies showed that *ABCB1* expression does not predict outcome in mixed or primary neuroblastoma cohorts,[289–292] whereas its upregulation in aggressive, relapsed neuroblastoma has been shown by others.[293,294] This is in line with my own analysis of the INFORM dataset of relapsed pediatric entities, where I found *ABCB1* to be higher expressed in the neuroblastoma subset compared to the whole cohort of relapsed pediatric tumors. The comparison of *ABCB1* expression between cell lines derived at primary diagnosis or after the patient had received chemotherapy, which revealed upregulation of *ABCB1* at relapse, further highlights that high *ABCB1* expression might indeed be most relevant in the relapsed, high-risk neuroblastoma subset, rather than neuroblastoma in general. This is supported by the fact that *ABCB1* is regulated by MYCN, which is often amplified in high-risk neuroblastomas.[289]

Moreover, expression levels alone might be insufficient to predict P-gp activity. P-gp functions as a transporter at the cell surface, hence, cell surface expression and transporting function might be as relevant as overall expression. In the VCR resistant BE(2)-C cell line, with which I performed the majority of my experiments, total *ABCB1* mRNA and P-gp protein levels were not significantly upregulated compared to control BE(2)-C. However, surface staining of P-gp showed increased expression at the plasma membrane in BE(2)-C rVCR. While P-gp is most commonly expressed at the surface of the cell, it can also be found in different cellular compartments, e.g. in the endoplasmic reticulum, the golgi apparatus or in lysosomes.[295,296] Although I did not perform detailed analysis of the expression of P-gp in different cellular compartments of the BE(2)-C cell lines, the comparison of total and surface P-gp make it plausible that a rearrangement of P-gp localization within the cell

occurred in the VCR resistant subline. This is in line with the observed increase of P-gp function in BE(2)-C rVCR. The transport efficiency of P-gp can be affected by several mechanisms: P-gp mutations that influence the rate of transport through P-gp,[75,297] the cholesterol content of the membrane[298] and finally the differing binding affinities of different compounds to P-gp, leading to variable rates of transport.[299] In my case increased surface P-gp seems the most plausible explanation for the observed increase of P-gp function in BE(2)-C rVCR, although I cannot fully exclude the possibility of a P-gp mutation or shift in cholesterol content of the membranes between control BE(2)-C and BE(2)-C rVCR, as I did not measure it.

Notably, the addition of the P-gp inhibitor tariquidar to VCR treatment led to a synergistic decrease in viability in the resistant model, but also in the BE(2)-C ctrl model. This is not surprising, as P-gp is also highly expressed and functional in BE(2)-C ctrl cells. Similarly, the cell line SIMA combined very high *ABCB1* expression levels with high a synergy score. The cell line CHP-134 had the lowest *ABCB1* expression amongst the relapsed cell lines I tested, and also showed the weakest indication for synergism between VCR and tariquidar. However, it must be taken into consideration that CHP-134 are much more sensitive to VCR than either the BE(2)-C cell lines or SIMA. Since the synergy analysis was performed with the same concentrations for all cell lines, the lower synergy scores for CHP-134 might stem from this higher sensitivity to the single VCR treatment.

5.4.1. P-gp inhibition in clinical trials

P-gp inhibition by several 2nd and 3rd generation inhibitors has been studied in several clinical trials with high expectations, however most of those trials came to an unsatisfactory end, showing toxicity in the patients, high variability in response rates or interaction between P-gp inhibitors and other drugs.[75,300] This led to great discouragement in the field of P-gp research.[301] However, it has more recently been pointed out that most clinical trials concerning P-gp inhibition did not sufficiently stratify patients into high or low *ABCB1* expression.[83,300] At a time where detailed molecular analyses are available for many patients and not only the expression of *ABCB1*, but also of other members of the ABC transporter family involved in drug resistance, can be easily accessed, transporter mediated drug resistance might be an interesting topic once more.

I identified the P-gp inhibitor tariquidar as the most efficient compound to overcome VCR resistance in BE(2)-C rVCR in the functional screen. Tariquidar is a third generation inhibitor of P-gp and was specifically developed for this purpose. Unlike many other P-gp inhibitors, tariquidar acts non-competitively on P-gp by inhibiting its ATPase activity.[302,303] In addition to its non-competitive inhibition of P-gp, tariquidar is a substrate of BCRP/*ABCG2*, which it inhibits at concentrations > 100 nM.[304] In clinical trials tariquidar has shown no toxicity in adults, nor in children and adolescents.[254,305] However, increased toxicity of the chemotherapeutic partner compound was reported for the combination of tariquidar with vinorelbine, paclitaxel and carboplatin in NSCLC trials, which led to these trials being closed early.[305] The only currently active trial with tariquidar is for the treatment of neuropathic pain (NCT04603066, www.clinicaltrials.gov, accessed March 21, 2022).

5.4.2. Other ABC family members

P-gp is only one member of a large family of transmembrane transporters. Within the ABC family, over 40 members are known, which are categorized into 7 subfamilies. Their physiological functions are divers, ranging from antigen processing, over osmotic homeostasis, iron metabolism and lipid trafficking to efficient efflux of xenobiotics.[75,306] Apart from P-gp, the ABCC subfamily - especially *ABCC1* - and *ABCG2* are best described for their contribution to chemotherapy resistance.

BCRP/*ABCG2* is associated with a bad outcome in breast cancer, NSCLC, acute myeloid leukemia and pancreatic cancer.[307–312] Its substrates overlap with P-gp, but notably do not include VCR or cisplatin among the chemotherapeutics.[75] Both afatinib and tariquidar inhibit BCRP.[75,313] *ABCG2* is regulated by MYCN, however, it is a low *ABCG2* expression that correlates with an adverse outcome in neuroblastoma.[289] This makes it an unlikely candidate for involvement in transport mediated chemotherapy resistant in relapsed neuroblastoma. Indeed, I saw no changes in *ABCG2* expression between primary and relapse in any of the neuroblastoma datasets I analyzed. The association between low *ABCG2* expression and adverse outcome might be through its influence on the migratory abilities of cells. It was shown in lung cancer that high *ABCG2* led to higher E-cadherin expression and attenuated migration, whereas low *ABCG2* expression increased motility, making migration and the formation of metastasis easier.[314]

High MRP-1/*ABCC1* expression is associated with bad outcome in several cancer types, including breast cancer, NSCLC, acute myeloid leukemia, acute lymphoid leukemia and neuroblastoma.[289,292,315–320] MRP-1 substrates include common chemotherapeutics, including VCR, but also targeted drugs like kinase inhibitors, including afatinib.[75,321] Interestingly for neuroblastoma, *ABCC1* expression is regulated by MYCN, a well-established risk factor in neuroblastoma.[289,319] In a neuroblastoma mouse model, knock out of *ABCC1* was sufficient to restore sensitivity to chemotherapeutics,[322] however, roles outside of drug efflux have also been suggested. Loss of *ABCC1*, independently of drug treatments, was associated with increased apoptosis, increased differentiation, decreased migratory ability and delayed tumor growth in neuroblastomas.[319,323–325] While other members of the ABCC subfamily have also been implicated in drug resistance, it is interesting to note that Henderson *et al.* identified high *ABCC1* and *ABCC4* expression in combination with low *ABCC3* expression as a risk signature for neuroblastoma.[319] This finding also highlights the more complex role of the ABC family, which is not restricted to drug transport.
In my own data analyses I found no upregulation of *ABCC1* in relapsed compared to primary neuroblastoma, indicating that its role in acquired chemotherapy resistance after relapse might be minor. Interestingly, *ABCC3* was higher expressed in relapsed neuroblastoma compared to other pediatric entities. However, as low *ABCC3* is associated with bad outcome in neuroblastoma, this also does not seem to imply a major role of *ABCC3* in chemotherapy resistance of relapsed neuroblastomas.

Overall, among all ABC family members I saw the strongest and most consistent differences between primary and relapsed neuroblastoma for *ABCB1*. Even though *ABCB1* expression is not as clearly

correlated with adverse outcome in neuroblastoma as *ABCC1*, my analysis focused on the difference between primary and relapsed cases and suggests a more prominent role of *ABCB1* in the acquisition of chemotherapy resistance than for other members of the ABC family.

5.5. Cell death mechanisms in neuroblastoma cell lines

In the analysis of cell death mechanisms I focused on apoptosis and ferroptosis. Apoptosis, and in particular resistance to apoptosis, has been a much studied subject in neuroblastoma research. Especially in relapsed, chemotherapy resistant neuroblastoma cases, increased apoptosis resistance occurs, e.g. by aberrant p53 signaling.[162–165] Apoptosis is characterized by caspase activation, release of cytochrome c from the mitochondria, plasma membrane blebbing, externalization of phosphatidylserine to the outside of the plasma membrane, nuclear fragmentation and chromatin condensation.

In my analysis of apoptosis I focused on caspase activation, measuring the activity of key caspases directly and by the cleavage of the caspase substrates PARP and BID. Different caspases recognize and cleave different peptide sequences.[326] Although there are some overlaps, this allows to differentiate in caspase activity assays which caspases are active. The main effector caspase of apoptosis, caspase-3, recognizes the peptide sequence DEVD, which is also recognized by caspase-7.[326] In addition I analyzed cleavage of the peptide sequence IETD, which is mainly recognized by caspase-8, but also to some extent by caspase-9 and caspase-10.[184,326]

For the analysis of caspase downstream targets I focused on cleavage of PARP and BID. PARP is involved in DNA repair, sensing DNA damage and facilitating the recruitment of the necessary DNA repair proteins.[327] At the onset of apoptosis, PARP is quickly and efficiently cleaved by caspase-3, losing its catalytic ability and actively inhibiting the activity of full length PARP.[190] This promotes apoptosis by preventing further DNA repair and conserves energy necessary for the execution of apoptosis.

BID is a pro-apoptotic member of the BCL-2 family of proteins, which regulate the permeabilization of the mitochondrial membrane during apoptosis.[172] At the onset of apoptosis, BID is cleaved by caspases (e.g. caspase-8) or other proteases and its truncated version, tBID, translocates to the mitochondrial outer membrane to induce membrane permeabilization by BAK and BAX, leading to cytochrome c release and caspase activation.[328] Thus, BID is an important link between extrinsic apoptosis and mitochondrial involvement, but also serves as an amplifier within the caspase activation cascade.[185,187]

Ferroptosis has been described as a cell death mechanism fairly recently.[193] The defining characteristics of ferroptosis are a dependency on intracellular iron and the oxidation of intracellular lipid membranes.[215] Peroxidation of intracellular lipids can be easily measured by the stain BODIPY 581/591. It integrates into cellular membranes and changes its fluorescent emission from red to green upon oxidation. Another, more indirect measure is the expression levels of TfR.[329] TfR transports iron from extracellular iron pools into the cell, overexpression of TfR therefore contributes to and facilitates ferroptosis.[207,329]

Several studies have shown that ferroptosis can be induced in neuroblastoma cell lines.[166–169] Particularly neuroblastomas with *MYCN* amplification, a high risk characteristic, have been suggested to be vulnerable to ferroptosis induction.[169,330–332] The role of MYCN in this context is twofold. MYCN

has been shown to increase expression of TfR, which leads to enhanced iron uptake into the cell and consequently to increased lipid ROS.[169,330] This increase in lipid ROS is detoxified by glutathione, requiring high levels of intracellular cysteine, which are achieved through high uptake of cystine as well as generation of cysteine from methionine through the transsulfuration pathway. Both cystine uptake and the transsulfuration pathway have been shown to be increased in *MYCN* amplified neuroblastomas.[169,331,332] This constitutes a vulnerability in *MYCN* amplified neuroblastoma, as cysteine depletion leads to cell death via ferroptosis.[332]

I used four neuroblastoma cell lines in my study of apoptosis and ferroptosis, all of them with an *MYCN* amplification. In addition, IMR-32 and NB-1 are *ALK* amplified, while LA-N-5 have an activating *ALK* mutation.[220] SK-N-BE(2)-C - the only cell line among the four derived at relapse - have non-functional p53 and NF1.[164,231]
IMR-32 have previously been shown to be susceptible to cell death by ferroptosis,[167] and indeed I showed that ferroptosis markers were increased in IMR-32 when cell death was induced by panobinostat. In a previous study from our group, IMR-32 were shown to have very high basal levels of ROS compared to other neuroblastoma cell lines.[333] This might make them more sensitive to further iron dependent increase of lipid ROS, which is defining for ferroptosis. However, caspases were also activated in IMR-32 in response to panobinostat and led to a strong cleavage of both BID and PARP, which was attenuated by caspase inhibition. Therefore, the line between ferroptosis and apoptosis is not very clear cut in IMR-32, but the two mechanisms seem rather to act in parallel to cause cell death. This might explain the higher sensitivity of IMR-32 to panobinostat compared to the other cell lines tested.
NB-1 showed even stronger caspase activation than IMR-32, which could not even be entirely suppressed by repeated administration of a caspase inhibitor. However, downstream cleavage of PARP and BID was less pronounced in NB-1 than IMR-32. Indeed, cleavage of the downstream proteins was comparable to LA-N-5, which had much weaker caspase activity. A less efficient execution of cell death in NB-1 might therefore also be a reason why NB-1 respond later to panobinostat treatment than IMR-32, in addition to a lack of ferroptosis induction.
Moreover, I analyzed apoptosis and ferroptosis induction in the VCR resistant and control BE(2)-C sublines. This analysis showed apoptosis to be the dominant cell death mechanism in SK-N-BE(2)-C cells.

Overall, I was able to show both the induction of ferroptosis and apoptosis in neuroblastoma cell lines. Although I have not performed a detailed study with many different compounds, the results from NB-1 and IMR-32 cells seem to suggest that the inherent capability of a certain cell line to undergo ferroptosis is not only dependent on the type of treatment, but also on an inherent susceptibility of a cell line to this type of cell death. Apoptosis on the other hand was induced in all cell lines I studied, making a sharp distinction between the two cell death mechanisms difficult. Indeed, as mentioned above, my data support the possibility that the two cell death mechanisms might at times run in parallel and contribute together to enhanced sensitivity.

6. Conclusion and outlook

In this thesis, I aimed to identify novel vulnerabilities in relapsed pediatric tumors, with a focus on neuroblastoma. By analyzing gene expression data, I identified the ERBB receptor tyrosine kinase family, especially ERBB4, as a possible target. Using a functional approach, inhibitors of the transmembrane transporter P-gp and the ERBB family were most effective in breaking chemotherapy resistance.

Validating ERBB4 on its impact on chemotherapy resistance in relapsed neuroblastoma, I found it to be inconsistently upregulated in this subgroup compared to primary or chemotherapy sensitive neuroblastoma. Functional studies confirmed that, although resistance was broken by the ERBB family inhibitor afatinib, this was not due to its inhibitory function on the ERBB downstream pathways, but rather an off-target effect on P-gp. While my data can therefore not support an integral role of ERBB4 in the development of chemotherapy resistance in relapsed neuroblastoma, further study might be warranted concerning the interplay of the entire ERBB family. ERBB3 is an interesting target to study in neuroblastoma research due to its important role in the development of Schwann cells and neuroblasts.[5,334]

The validation of P-gp as a contributing factor in chemotherapy resistance in relapsed neuroblastoma showed higher P-gp expression compared to primary or chemotherapy-sensitive samples. KD and functional analyses confirmed that P-gp was the essential contributor to chemotherapy resistance in this study. Previous studies did not find a consistent correlation of *ABCB1* expression with outcome in neuroblastoma; however, they did not specifically analyze relapsed tumors. I therefore hypothesize that P-gp plays a more important role in the subset of relapsed neuroblastoma than in the entire cohort of neuroblastoma patients. This would be an interesting point to study further.

The final aim of my thesis was the analysis of the two programmed cell death mechanisms apoptosis and ferroptosis in neuroblastoma cell lines. I showed that treatment with panobinostat was able to induce apoptosis in all cell line models studied and that one model, IMR-32, showed ferroptosis as well. This lends itself to the conclusion that it is not only the compound or environment that determines the mechanism by which cells die, but also that the inherent susceptibilities of the cell lines play a role. Indeed, my data seem to indicate that both apoptosis and ferroptosis can at times complement each other. To fully determine the separate effects of apoptosis and ferroptosis, a much larger study with more cell lines and different treatments would be necessary.

7. Appendix

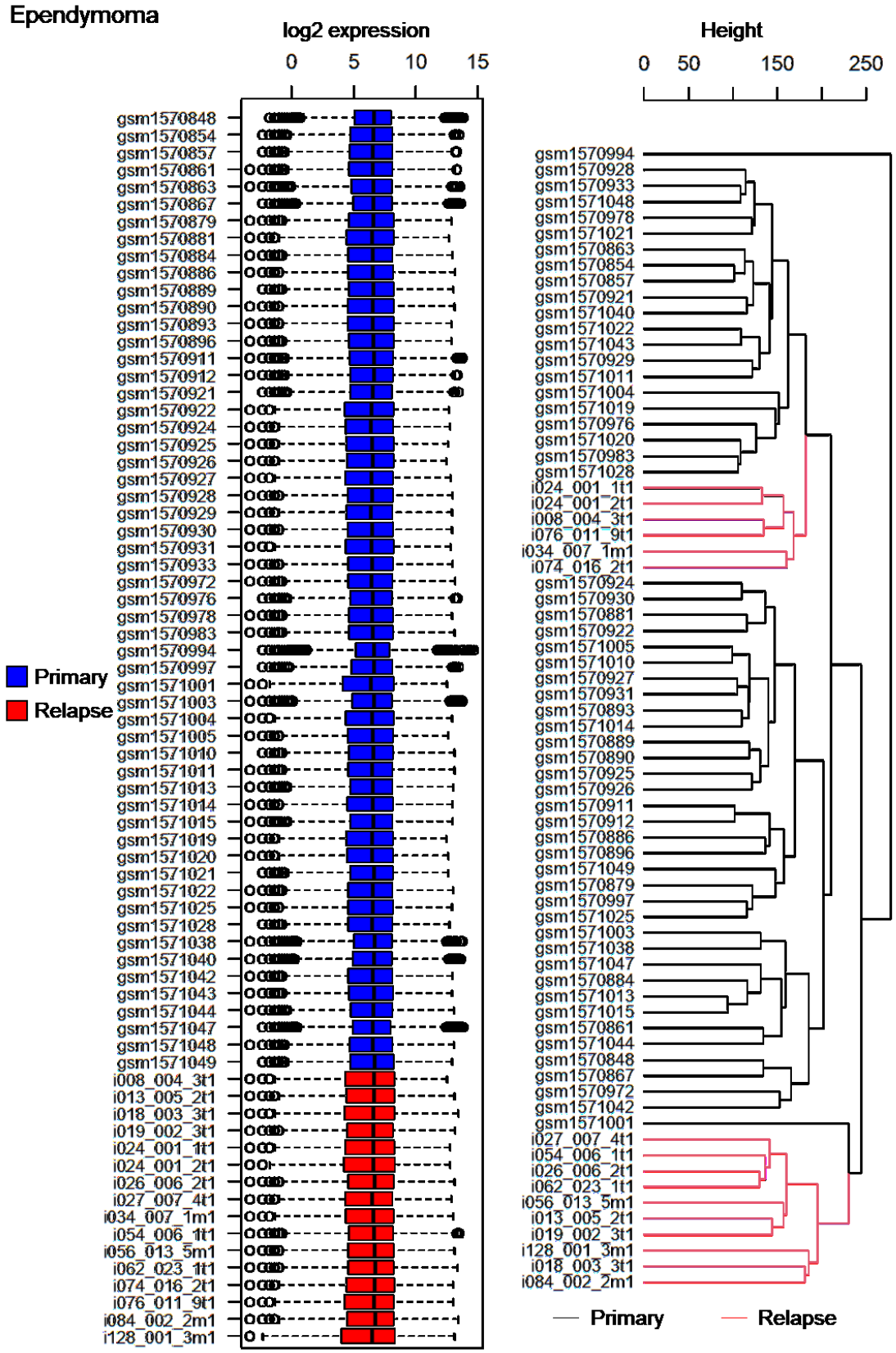

Appendix Figure 1: RankProd analysis quality control in ependymoma. ***(A)*** *Log2 expression data of the primary (blue) and relapsed (red) datasets. Indicated are the median with first and third quartiles, as well as the strongest outliers.* ***(B)*** *Histogram of the primary (black) and relapsed (red) neuroblastoma samples. Hierarchical clustering was computed by the Euclidian distance.*

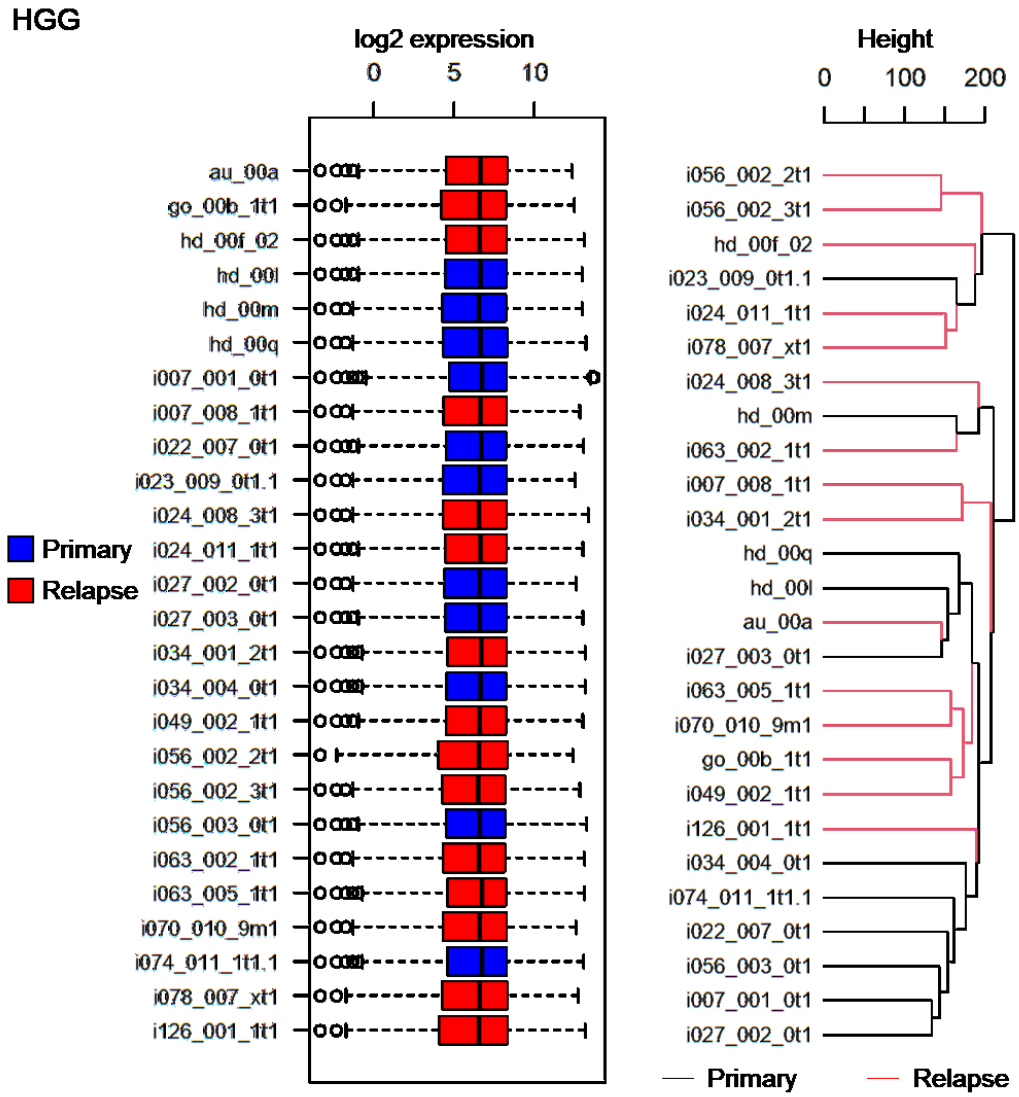

Appendix Figure 2: RankProd analysis quality control in high grade glioma. ***(A)*** *Log2 expression data of the primary (blue) and relapsed (red) datasets. Indicated are the median with first and third quartiles, as well as the strongest outliers.* ***(B)*** *Histogram of the primary (black) and relapsed (red) neuroblastoma samples. Hierarchical clustering was computed by the Euclidian distance.*

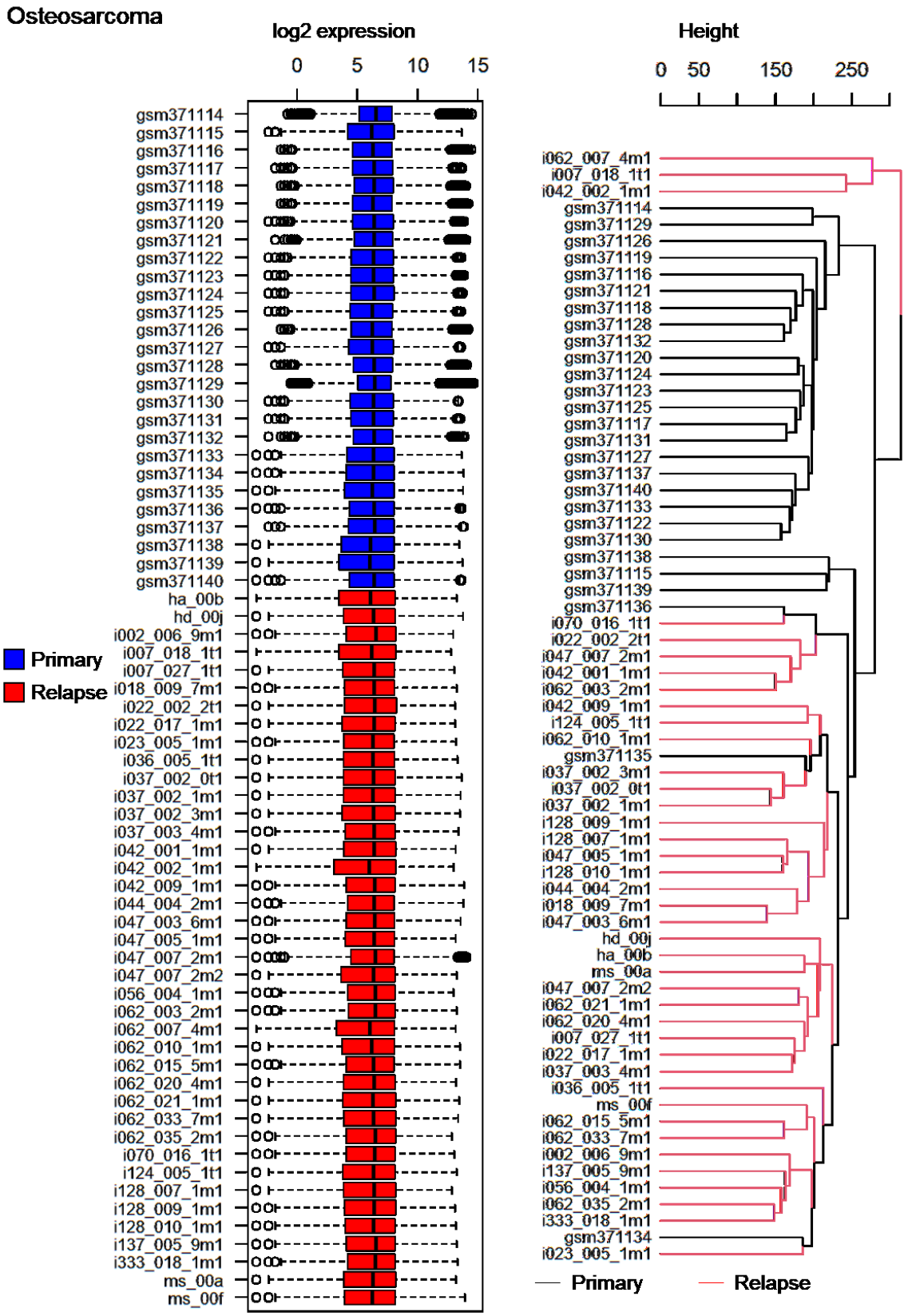

Appendix Figure 3: RankProd analysis quality control in osteosarcoma. ***(A)*** *Log2 expression data of the primary (blue) and relapsed (red) datasets. Indicated are the median with first and third quartiles, as well as the strongest outliers.* ***(B)*** *Histogram of the primary (black) and relapsed (red) neuroblastoma samples. Hierarchical clustering was computed by the Euclidian distance.*

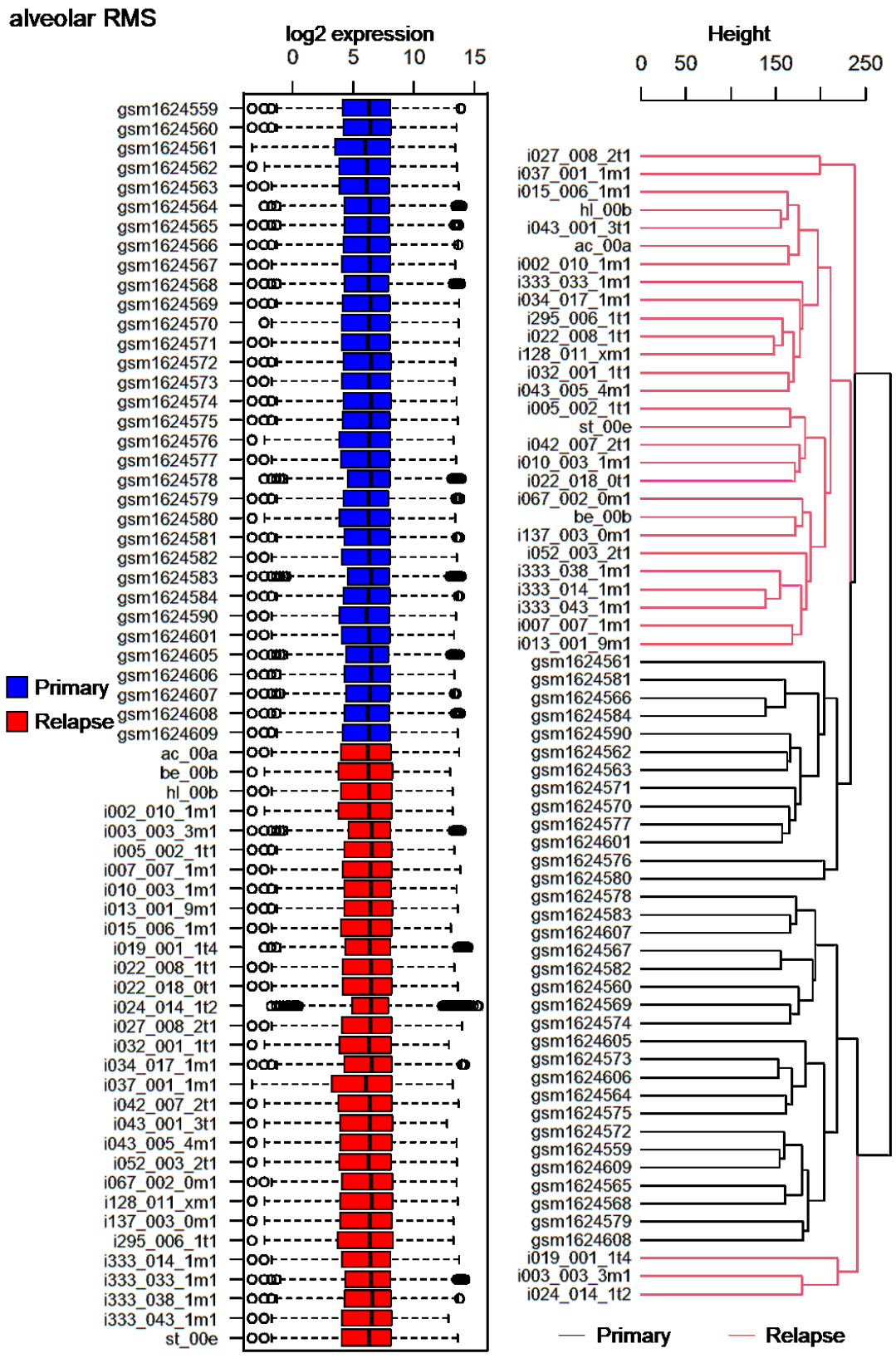

Appendix Figure 4: RankProd analysis quality control in alveolar rhabdomyosarcoma. ***(A)*** *Log2 expression data of the primary (blue) and relapsed (red) datasets. Indicated are the median with first and third quartiles, as well as the strongest outliers.* ***(B)*** *Histogram of the primary (black) and relapsed (red) neuroblastoma samples. Hierarchical clustering was computed by the Euclidian distance.*

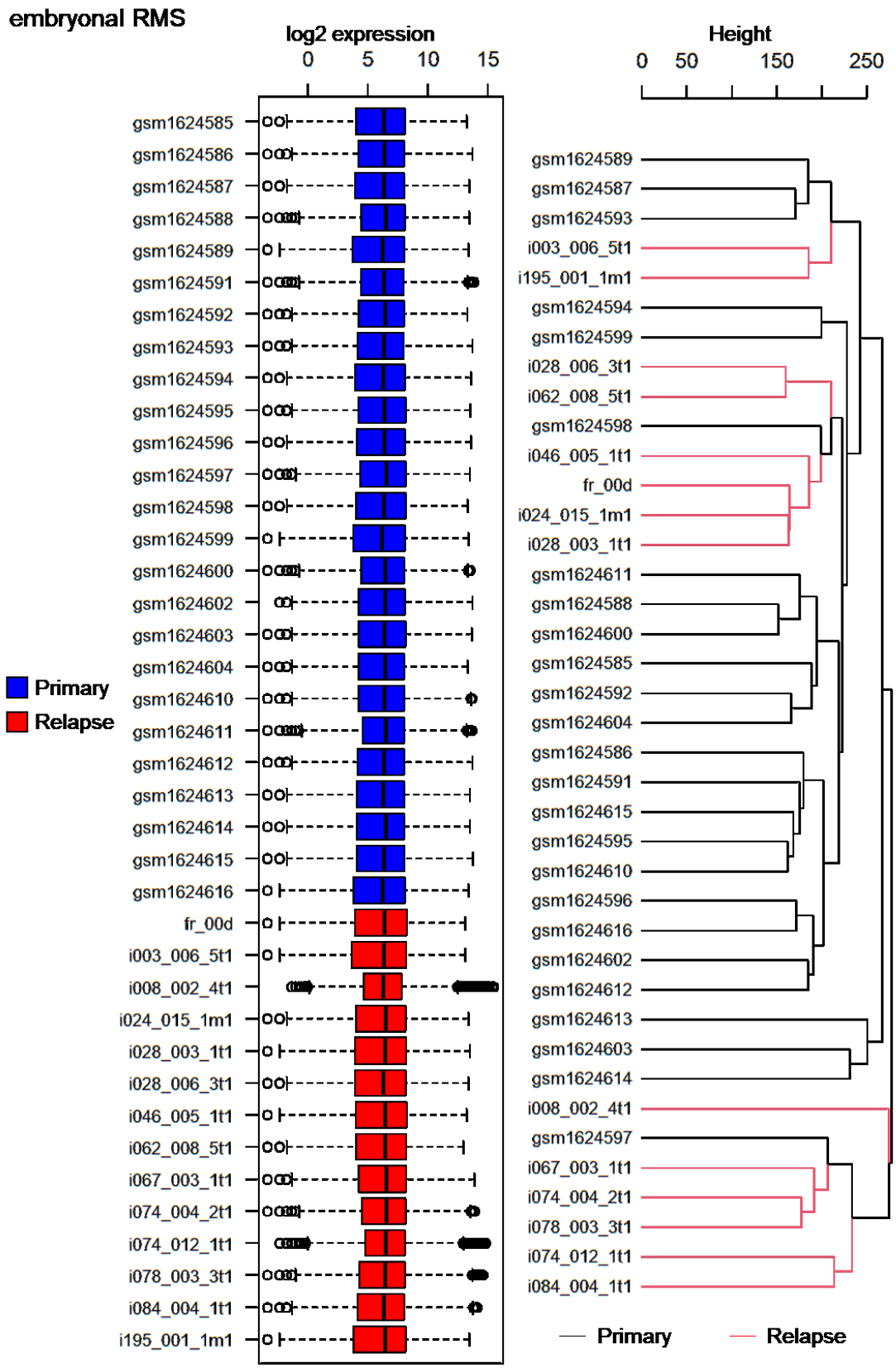

Appendix Figure 5: RankProd analysis quality control in embryonal rhabdomyosarcoma. ***(A)*** *Log2 expression data of the primary (blue) and relapsed (red) datasets. Indicated are the median with first and third quartiles, as well as the strongest outliers.* ***(B)*** *Histogram of the primary (black) and relapsed (red) neuroblastoma samples. Hierarchical clustering was computed by the Euclidian distance.*

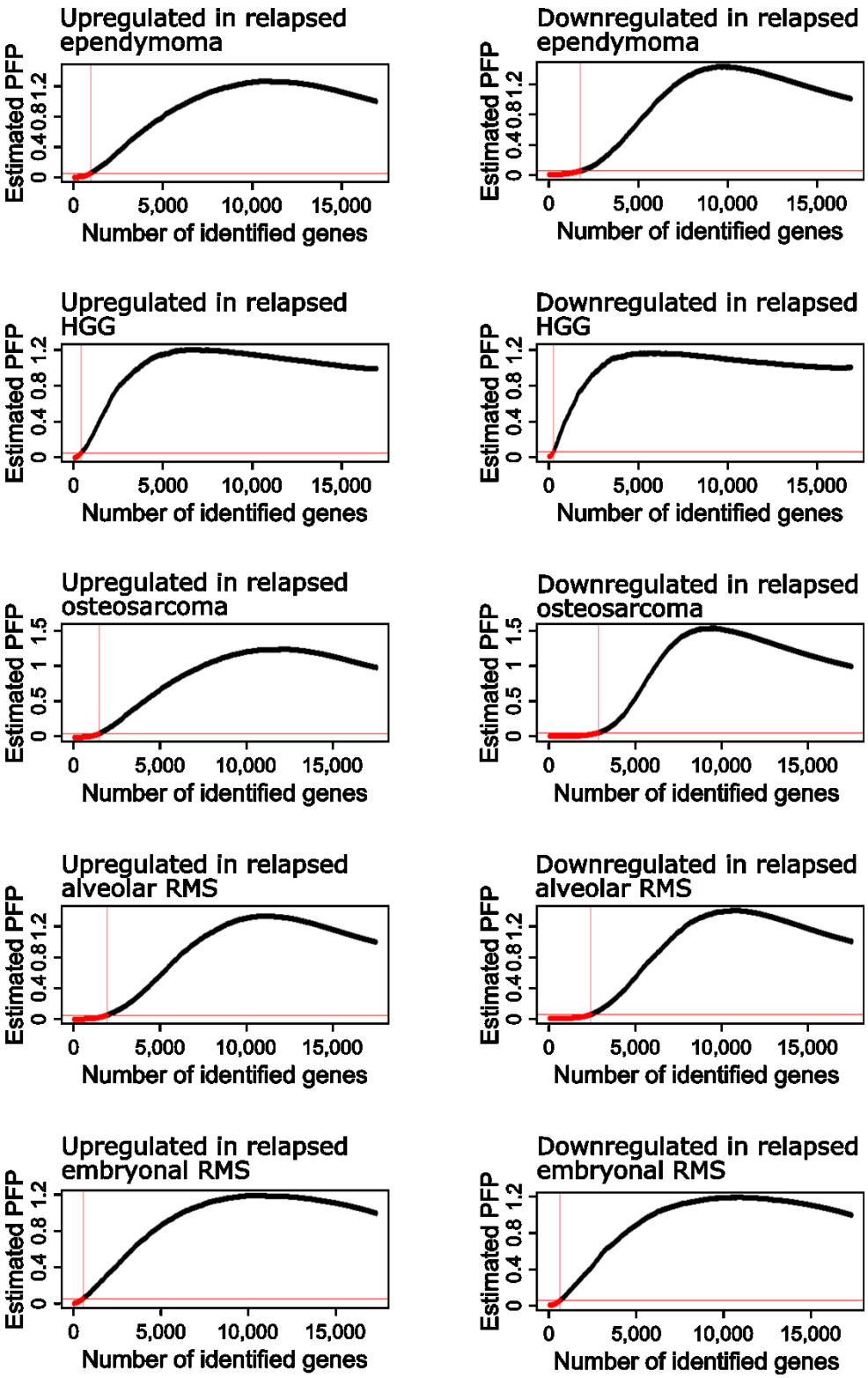

Appendix Figure 6: Up and downregulated genes of the indicated entities were estimated by RankProd analysis. Genes with PFP < 0.05 (marked in red) were considered differentially regulated. HGG = high grade glioma; RMS = rhabdomyosarcoma

Appendix Table 1: Enriched Reactome pathways. FDR = false discovery rate

Entity	Pathway Name	Pathway Identifier	p-value	FDR	Category
Neuroblastoma	Assembly of collagen fibrils and other multimeric structures	R-HSA-2022090	2.67E-06	1.49E-03	ECM
Neuroblastoma	Collagen chain trimerization	R-HSA-8948216	6.58E-06	1.84E-03	ECM
Neuroblastoma	Collagen formation	R-HSA-1474290	2.10E-05	3.35E-03	ECM
Neuroblastoma	Collagen degradation	R-HSA-1442490	2.41E-05	3.35E-03	ECM
Neuroblastoma	Collagen biosynthesis and modifying enzymes	R-HSA-1650814	5.05E-05	5.60E-03	ECM
Neuroblastoma	Degradation of the extracellular matrix	R-HSA-1474228	1.13E-04	9.68E-03	ECM
Neuroblastoma	Extracellular matrix organization	R-HSA-1474244	1.23E-04	9.68E-03	ECM
Neuroblastoma	Integrin cell surface interactions	R-HSA-216083	6.46E-04	0.045	ECM
Neuroblastoma	ECM proteoglycans	R-HSA-3000178	7.90E-03	0.308	ECM
Neuroblastoma	NCAM1 interactions	R-HSA-419037	0.016	0.460	ECM
Neuroblastoma	Laminin interactions	R-HSA-3000157	0.030	0.516	ECM
Neuroblastoma	SDK interactions	R-HSA-373756	0.042	0.516	ECM
Neuroblastoma	Non-integrin membrane-ECM interactions	R-HSA-3000171	0.044	0.516	ECM
Neuroblastoma	O-linked glycosylation of mucins	R-HSA-913709	0.049	0.743	ECM
Neuroblastoma	Downregulation of ERBB4 signaling	R-HSA-1253288	1.41E-03	0.086	ERBB
Neuroblastoma	ERBB2 Activates PTK6 Signaling	R-HSA-8847993	7.27E-03	0.308	ERBB
Neuroblastoma	ERBB2 Regulates Cell Motility	R-HSA-6785631	8.42E-03	0.309	ERBB
Neuroblastoma	GRB2 events in ERBB2 signaling	R-HSA-1963640	9.66E-03	0.309	ERBB
Neuroblastoma	SHC1 events in ERBB4 signaling	R-HSA-1250347	9.66E-03	0.309	ERBB
Neuroblastoma	RAF-independent MAPK1/3 activation	R-HSA-112409	0.023	0.516	ERBB
Neuroblastoma	SHC1 events in ERBB2 signaling	R-HSA-1250196	0.041	0.516	ERBB
Neuroblastoma	PI3K events in ERBB4 signaling	R-HSA-1250342	0.042	0.516	ERBB
Neuroblastoma	Downregulation of ERBB2 signaling	R-HSA-8863795	0.044	0.516	ERBB
Neuroblastoma	Class B/2 (Secretin family receptors)	R-HSA-373080	1.57E-03	0.086	other
Neuroblastoma	RUNX1 regulates genes involved in megakaryocyte differentiation and platelet function	R-HSA-8936459	7.45E-03	0.308	other
Neuroblastoma	Common Pathway of Fibrin Clot Formation	R-HSA-140875	7.78E-03	0.824	other

Entity	Pathway Name	Pathway Identifier	p-value	FDR	Category
Neuroblastoma	TRKA activation by NGF	R-HSA-187042	8.07E-03	0.743	other
Neuroblastoma	RUNX1 regulates transcription of genes involved in BCR signaling	R-HSA-8939245	0.010	0.319	other
Neuroblastoma	Calcitonin-like ligand receptors	R-HSA-419812	0.017	0.824	other
Neuroblastoma	Formation of Fibrin Clot (Clotting Cascade)	R-HSA-140877	0.019	0.824	other
Neuroblastoma	Ca2+ activated K+ channels	R-HSA-1296052	0.020	0.516	other
Neuroblastoma	Hypusine synthesis from eIF5A-lysine	R-HSA-204626	0.028	0.516	other
Neuroblastoma	Activation of TRKA receptors	R-HSA-187015	0.030	0.743	other
Neuroblastoma	Ca2+ pathway	R-HSA-4086398	0.031	0.516	other
Neuroblastoma	Platelet degranulation	R-HSA-114608	0.032	0.743	other
Neuroblastoma	MET activates PTK2 signaling	R-HSA-8874081	0.033	0.516	other
Neuroblastoma	Extrinsic Pathway of Fibrin Clot Formation	R-HSA-140834	0.034	0.824	other
Neuroblastoma	RUNX2 regulates genes involved in cell migration	R-HSA-8941332	0.037	0.516	other
Neuroblastoma	Ethanol oxidation	R-HSA-71384	0.040	0.743	other
Neuroblastoma	Response to elevated platelet cytosolic Ca2+	R-HSA-76005	0.041	0.743	other
Neuroblastoma	Interaction With Cumulus Cells	R-HSA-2534343	0.042	0.516	other
Neuroblastoma	GABA A receptor activation	R-HSA-977441	0.042	0.516	other
Neuroblastoma	GABA receptor activation	R-HSA-977443	0.047	0.516	other
Neuroblastoma	Norepinephrine Neurotransmitter Release Cycle	R-HSA-181430	0.047	0.743	other
Neuroblastoma	Serotonin receptors	R-HSA-390666	0.047	0.743	other
Ependymoma	Cell Cycle, Mitotic	R-HSA-69278	4.44E-16	5.54E-13	Cell Cycle
Ependymoma	Cell Cycle	R-HSA-1640170	8.39E-14	5.24E-11	Cell Cycle
Ependymoma	Activation of E2F1 target genes at G1/S	R-HSA-539107	7.60E-10	2.37E-07	Cell Cycle
Ependymoma	G1/S-Specific Transcription	R-HSA-69205	7.60E-10	2.37E-07	Cell Cycle
Ependymoma	Amplification of signal from unattached kinetochores via a MAD2 inhibitory signal	R-HSA-141444	2.93E-09	6.10E-07	Cell Cycle

Entity	Pathway Name	Pathway Identifier	p-value	FDR	Category
Ependymoma	Amplification of signal from the kinetochores	R-HSA-141424	2.93E-09	6.10E-07	Cell Cycle
Ependymoma	Mitotic Spindle Checkpoint	R-HSA-69618	1.02E-08	1.81E-06	Cell Cycle
Ependymoma	Mitotic G1-G1/S phases	R-HSA-453279	1.43E-08	2.23E-06	Cell Cycle
Ependymoma	Resolution of Sister Chromatid Cohesion	R-HSA-2500257	2.44E-08	3.37E-06	Cell Cycle
Ependymoma	Cell Cycle Checkpoints	R-HSA-69620	7.19E-08	8.92E-06	Cell Cycle
Ependymoma	G1/S Transition	R-HSA-69206	5.53E-07	5.31E-05	Cell Cycle
Ependymoma	Mitotic Anaphase	R-HSA-68882	7.71E-07	6.86E-05	Cell Cycle
Ependymoma	Mitotic Metaphase and Anaphase	R-HSA-2555396	8.46E-07	7.02E-05	Cell Cycle
Ependymoma	Mitotic Prometaphase	R-HSA-68877	1.92E-06	1.50E-04	Cell Cycle
Ependymoma	G0 and Early G1	R-HSA-1538133	3.70E-06	2.70E-04	Cell Cycle
Ependymoma	Separation of Sister Chromatids	R-HSA-2467813	5.70E-06	3.93E-04	Cell Cycle
Ependymoma	M Phase	R-HSA-68886	1.16E-05	7.54E-04	Cell Cycle
Ependymoma	Cyclin A/B1/B2 associated events during G2/M transition	R-HSA-69273	3.48E-05	2.16E-03	Cell Cycle
Ependymoma	Transcription of E2F targets under negative control by DREAM complex	R-HSA-1362277	3.87E-05	2.28E-03	Cell Cycle
Ependymoma	Activation of ATR in response to replication stress	R-HSA-176187	1.53E-04	8.59E-03	Cell Cycle
Ependymoma	TP53 Regulates Transcription of Genes Involved in G2 Cell Cycle Arrest	R-HSA-6804114	6.45E-04	0.031	Cell Cycle
Ependymoma	Mitotic G2-G2/M phases	R-HSA-453274	9.02E-04	0.038	Cell Cycle
Ependymoma	Condensation of Prometaphase Chromosomes	R-HSA-2514853	9.23E-04	0.038	Cell Cycle

Entity	Pathway Name	Pathway Identifier	p-value	FDR	Category
Ependymoma	Activation of the pre-replicative complex	R-HSA-68962	2.14E-03	0.073	Cell Cycle
Ependymoma	CDC6 association with the ORC:origin complex	R-HSA-68689	2.20E-03	0.073	Cell Cycle
Ependymoma	Unwinding of DNA	R-HSA-176974	3.00E-03	0.093	Cell Cycle
Ependymoma	G2/M Transition	R-HSA-69275	3.93E-03	0.114	Cell Cycle
Ependymoma	E2F mediated regulation of DNA replication	R-HSA-113510	4.76E-03	0.129	Cell Cycle
Ependymoma	G2 Phase	R-HSA-68911	5.06E-03	0.131	Cell Cycle
Ependymoma	G2/M DNA replication checkpoint	R-HSA-69478	5.06E-03	0.131	Cell Cycle
Ependymoma	Deposition of new CENPA-containing nucleosomes at the centromere	R-HSA-606279	5.47E-03	0.131	Cell Cycle
Ependymoma	Nucleosome assembly	R-HSA-774815	5.47E-03	0.131	Cell Cycle
Ependymoma	Phosphorylation of Emi1	R-HSA-176417	7.28E-03	0.160	Cell Cycle
Ependymoma	Initiation of Nuclear Envelope Reformation	R-HSA-2995383	8.16E-03	0.171	Cell Cycle
Ependymoma	Nuclear Envelope Reassembly	R-HSA-2995410	8.16E-03	0.171	Cell Cycle
Ependymoma	Breakdown of the nuclear lamina	R-HSA-352238	9.61E-03	0.190	Cell Cycle
Ependymoma	SUMOylation of DNA replication proteins	R-HSA-4615885	9.84E-03	0.190	Cell Cycle
Ependymoma	Activation of NIMA Kinases NEK9, NEK6, NEK7	R-HSA-2980767	0.010	0.190	Cell Cycle
Ependymoma	E2F-enabled inhibition of pre-replication complex formation	R-HSA-113507	0.010	0.190	Cell Cycle
Ependymoma	DNA Replication	R-HSA-69306	0.010	0.196	Cell Cycle
Ependymoma	DNA strand elongation	R-HSA-69190	0.011	0.205	Cell Cycle
Ependymoma	DNA Replication Pre-Initiation	R-HSA-69002	0.012	0.205	Cell Cycle

Entity	Pathway Name	Pathway Identifier	p-value	FDR	Category
Ependymoma	M/G1 Transition	R-HSA-68874	0.012	0.205	Cell Cycle
Ependymoma	Nuclear Envelope Breakdown	R-HSA-2980766	0.013	0.221	Cell Cycle
Ependymoma	APC/C-mediated degradation of cell cycle proteins	R-HSA-174143	0.014	0.223	Cell Cycle
Ependymoma	Regulation of mitotic cell cycle	R-HSA-453276	0.014	0.223	Cell Cycle
Ependymoma	Interaction between PHLDA1 and AURKA	R-HSA-8854521	0.017	0.265	Cell Cycle
Ependymoma	Transcription of E2F targets under negative control by p107 (RBL1) and p130 (RBL2) in complex with HDAC1	R-HSA-1362300	0.017	0.274	Cell Cycle
Ependymoma	G2/M Checkpoints	R-HSA-69481	0.020	0.305	Cell Cycle
Ependymoma	NCAM signaling for neurite out-growth	R-HSA-375165	0.021	0.315	Cell Cycle
Ependymoma	Clearance of Nuclear Envelope Membranes from Chromatin	R-HSA-2993913	0.021	0.320	Cell Cycle
Ependymoma	MASTL Facilitates Mitotic Progression	R-HSA-2465910	0.021	0.320	Cell Cycle
Ependymoma	APC/C:Cdc20 mediated degradation of Cyclin B	R-HSA-174048	0.027	0.376	Cell Cycle
Ependymoma	S Phase	R-HSA-69242	0.030	0.419	Cell Cycle
Ependymoma	Chromosome Maintenance	R-HSA-73886	0.035	0.487	Cell Cycle
Ependymoma	Chk1/Chk2(Cds1) mediated inactivation of Cyclin B:Cdk1 complex	R-HSA-75035	0.038	0.525	Cell Cycle
Ependymoma	Nuclear Pore Complex (NPC) Disassembly	R-HSA-3301854	0.047	0.637	Cell Cycle
Ependymoma	Extracellular matrix organization	R-HSA-1474244	2.19E-04	0.012	ECM
Ependymoma	Degradation of the extracellular matrix	R-HSA-1474228	4.46E-04	0.023	ECM
Ependymoma	Assembly of collagen fibrils and other multimeric structures	R-HSA-2022090	5.43E-04	0.027	ECM
Ependymoma	Collagen degradation	R-HSA-1442490	6.88E-04	0.032	ECM

Entity	Pathway Name	Pathway Identifier	p-value	FDR	Category
Ependymoma	Collagen formation	R-HSA-1474290	7.20E-04	0.032	ECM
Ependymoma	Collagen biosynthesis and modifying enzymes	R-HSA-1650814	1.48E-03	0.058	ECM
Ependymoma	Collagen chain trimerization	R-HSA-8948216	6.29E-03	0.145	ECM
Ependymoma	NCAM1 interactions	R-HSA-419037	6.29E-03	0.145	ECM
Ependymoma	Elastic fibre formation	R-HSA-1566948	7.92E-03	0.166	ECM
Ependymoma	Molecules associated with elastic fibres	R-HSA-2129379	0.011	0.205	ECM
Ependymoma	ECM proteoglycans	R-HSA-3000178	0.017	0.264	ECM
Ependymoma	Integrin cell surface interactions	R-HSA-216083	0.027	0.376	ECM
Ependymoma	Activation of Matrix Metalloproteinases	R-HSA-1592389	0.029	0.410	ECM
Ependymoma	RHO GTPases Activate Formins	R-HSA-5663220	1.36E-07	1.53E-05	other
Ependymoma	Polo-like kinase mediated events	R-HSA-156711	2.85E-07	2.97E-05	other
Ependymoma	RHO GTPase Effectors	R-HSA-195258	9.85E-04	0.039	other
Ependymoma	GABA A receptor activation	R-HSA-977441	2.41E-03	0.972	other
Ependymoma	Signaling by Rho GTPases	R-HSA-194315	2.48E-03	0.079	other
Ependymoma	Smooth Muscle Contraction	R-HSA-445355	3.32E-03	0.100	other
Ependymoma	Deregulated CDK5 triggers multiple neurodegenerative pathways in Alzheimers disease models	R-HSA-8862803	4.46E-03	0.125	other
Ependymoma	Neurodegenerative Diseases	R-HSA-8863678	4.46E-03	0.125	other
Ependymoma	TP53 Regulates Transcription of Cell Cycle Genes	R-HSA-6791312	5.10E-03	0.131	other
Ependymoma	Depolymerisation of the Nuclear Lamina	R-HSA-4419969	5.72E-03	0.137	other
Ependymoma	Synthesis of active ubiquitin: roles of E1 and E2 enzymes	R-HSA-8866652	5.99E-03	0.144	other
Ependymoma	Receptor-type tyrosine-protein phosphatases	R-HSA-388844	7.38E-03	0.971	other
Ependymoma	Transcriptional Regulation by E2F6	R-HSA-8953750	7.92E-03	0.166	other
Ependymoma	Transport of glycerol from adipocytes to the liver by Aquaporins	R-HSA-432030	9.61E-03	0.190	other
Ependymoma	Protein-protein interactions at synapses	R-HSA-6794362	0.018	0.972	other

Entity	Pathway Name	Pathway Identifier	p-value	FDR	Category
Ependymoma	Calcitonin-like ligand receptors	R-HSA-419812	0.039	0.971	other
Ependymoma	Axonal growth inhibition (RHOA activation)	R-HSA-193634	0.044	0.972	other
Ependymoma	NOTCH3 Activation and Transmission of Signal to the Nucleus	R-HSA-9013507	0.049	0.637	other
HGG	Assembly of collagen fibrils and other multimeric structures	R-HSA-2022090	1.62E-03	0.102	ECM
HGG	Collagen formation	R-HSA-1474290	0.013	0.299	ECM
HGG	ECM proteoglycans	R-HSA-3000178	0.016	0.304	ECM
HGG	Collagen chain trimerization	R-HSA-8948216	0.017	0.514	ECM
HGG	Degradation of the extracellular matrix	R-HSA-1474228	0.020	0.366	ECM
HGG	Integrin cell surface interactions	R-HSA-216083	0.022	0.373	ECM
HGG	Anchoring fibril formation	R-HSA-2214320	0.031	0.471	ECM
HGG	Collagen degradation	R-HSA-1442490	0.039	0.474	ECM
HGG	NCAM1 interactions	R-HSA-419037	0.048	0.474	ECM
HGG	ERBB2 Activates PTK6 Signaling	R-HSA-8847993	8.88E-07	1.95E-04	ERBB
HGG	ERBB2 Regulates Cell Motility	R-HSA-6785631	1.27E-06	1.95E-04	ERBB
HGG	GRB2 events in ERBB2 signaling	R-HSA-1963640	2.31E-05	2.69E-03	ERBB
HGG	PI3K events in ERBB2 signaling	R-HSA-1963642	3.92E-05	3.60E-03	ERBB
HGG	SHC1 events in ERBB2 signaling	R-HSA-1250196	6.27E-05	4.83E-03	ERBB
HGG	Downregulation of ERBB2 signaling	R-HSA-8863795	7.47E-05	4.93E-03	ERBB
HGG	SHC1 events in ERBB4 signaling	R-HSA-1250347	2.59E-04	0.012	ERBB
HGG	GPCR ligand binding	R-HSA-500792	2.74E-04	0.026	ERBB
HGG	Signaling by Non-Receptor Tyrosine Kinases	R-HSA-9006927	6.20E-04	0.024	ERBB
HGG	PI3K events in ERBB4 signaling	R-HSA-1250342	8.55E-04	0.030	ERBB
HGG	Signaling by ERBB4	R-HSA-1236394	1.53E-03	0.050	ERBB
HGG	Downregulation of ERBB4 signaling	R-HSA-1253288	2.80E-03	0.082	ERBB
HGG	Signaling by ERBB2	R-HSA-1227986	2.82E-03	0.082	ERBB
HGG	Constitutive Signaling by Aberrant PI3K in Cancer	R-HSA-2219530	5.27E-03	0.142	ERBB
HGG	Signaling by activated point mutants of FGFR3	R-HSA-1839130	0.012	0.275	ERBB
HGG	G alpha (i) signalling events	R-HSA-418594	0.015	0.304	ERBB
HGG	Nuclear signaling by ERBB4	R-HSA-1251985	0.015	0.317	ERBB

Entity	Pathway Name	Pathway Identifier	p-value	FDR	Category
HGG	PI5P, PP2A and IER3 Regulate PI3K/AKT Signaling	R-HSA-6811558	0.018	0.348	ERBB
HGG	Receptor-type tyrosine-protein phosphatases	R-HSA-388844	0.018	0.348	ERBB
HGG	Negative regulation of the PI3K/AKT network	R-HSA-199418	0.025	0.415	ERBB
HGG	PI3K/AKT Signaling in Cancer	R-HSA-2219528	0.025	0.415	ERBB
HGG	FGFR3 mutant receptor activation	R-HSA-2033514	0.032	0.514	ERBB
HGG	Peptide ligand-binding receptors	R-HSA-375276	5.21E-09	1.98E-06	other
HGG	Class A/1 (Rhodopsin-like receptors)	R-HSA-373076	2.06E-05	3.92E-03	other
HGG	Negative regulation of activity of TFAP2 (AP-2) family transcription factors	R-HSA-8866904	5.72E-05	7.21E-03	other
HGG	Activation of anterior HOX genes in hindbrain development during early embryogenesis	R-HSA-5617472	1.13E-04	5.77E-03	other
HGG	Activation of HOX genes during differentiation	R-HSA-5619507	1.13E-04	5.77E-03	other
HGG	Signaling by PTK6	R-HSA-8848021	6.20E-04	0.024	other
HGG	Activation of the TFAP2 (AP-2) family of transcription factors	R-HSA-8866907	1.49E-03	0.102	other
HGG	TFAP2 (AP-2) family regulates transcription of other transcription factors	R-HSA-8866906	3.93E-03	0.196	other
HGG	GABA synthesis, release, reuptake and degradation	R-HSA-888590	4.17E-03	0.196	other
HGG	Negative regulation of TCF-dependent signaling by WNT ligand antagonists	R-HSA-3772470	5.35E-03	0.284	other
HGG	TFAP2 (AP-2) family regulates transcription of cell cycle factors	R-HSA-8866911	5.59E-03	0.233	other
HGG	SUMOylation of transcription factors	R-HSA-3232118	6.18E-03	0.233	other
HGG	TFAP2 (AP-2) family regulates transcription of growth factors and their receptors	R-HSA-8866910	7.06E-03	0.233	other

Entity	Pathway Name	Pathway Identifier	p-value	FDR	Category
HGG	Synthesis of bile acids and bile salts via 24-hydroxycholesterol	R-HSA-193775	7.16E-03	0.179	other
HGG	GABA synthesis	R-HSA-888568	7.52E-03	0.233	other
HGG	Neurotransmitter release cycle	R-HSA-112310	0.010	0.299	other
HGG	Regulation of gene expression in endocrine-committed (NEUROG3+) progenitor cells	R-HSA-210746	0.012	0.299	other
HGG	Chemokine receptors bind chemokines	R-HSA-380108	0.012	0.299	other
HGG	Axonal growth inhibition (RHOA activation)	R-HSA-193634	0.015	0.497	other
HGG	POU5F1 (OCT4), SOX2, NANOG repress genes related to differentiation	R-HSA-2892245	0.015	0.304	other
HGG	Synthesis of bile acids and bile salts via 27-hydroxycholesterol	R-HSA-193807	0.015	0.317	other
HGG	Transcriptional regulation by the AP-2 (TFAP2) family of transcription factors	R-HSA-8864260	0.016	0.304	other
HGG	p75NTR regulates axonogenesis	R-HSA-193697	0.018	0.514	other
HGG	Tachykinin receptors bind tachykinins	R-HSA-380095	0.023	0.563	other
HGG	RUNX1 regulates transcription of genes involved in WNT signaling	R-HSA-8939256	0.026	0.415	other
HGG	G alpha (q) signalling events	R-HSA-416476	0.031	0.471	other
HGG	Voltage gated Potassium channels	R-HSA-1296072	0.034	0.514	other
HGG	Transmission across Chemical Synapses	R-HSA-112315	0.041	0.474	other
HGG	Regulation of commissural axon pathfinding by SLIT and ROBO	R-HSA-428542	0.044	0.612	other
Osteosarcoma	Apoptotic cleavage of cell adhesion proteins	R-HSA-351906	3.45E-03	0.579	ECM
Osteosarcoma	Extracellular matrix organization	R-HSA-1474244	0.017	0.774	ECM
Osteosarcoma	Molecules associated with elastic fibres	R-HSA-2129379	0.020	0.774	ECM
Osteosarcoma	ECM proteoglycans	R-HSA-3000178	0.033	0.774	ECM
Osteosarcoma	Cell-cell junction organization	R-HSA-421270	0.034	0.774	ECM

Entity	Pathway Name	Pathway Identifier	p-value	FDR	Category
Osteosarcoma	Collagen chain trimerization	R-HSA-8948216	0.037	0.774	ECM
Osteosarcoma	Cell junction organization	R-HSA-446728	0.038	0.774	ECM
Osteosarcoma	Elastic fibre formation	R-HSA-1566948	0.044	0.774	ECM
Osteosarcoma	Nuclear signaling by ERBB4	R-HSA-1251985	0.042	0.774	ERBB
Osteosarcoma	Metallothioneins bind metals	R-HSA-5661231	3.02E-04	0.241	other
Osteosarcoma	Diseases associated with surfactant metabolism	R-HSA-5687613	5.59E-04	0.241	other
Osteosarcoma	Surfactant metabolism	R-HSA-5683826	8.70E-04	0.241	other
Osteosarcoma	Defective CSF2RA causes pulmonary surfactant metabolism dysfunction 4 (SMDP4)	R-HSA-5688890	1.10E-03	0.241	other
Osteosarcoma	Defective CSF2RB causes pulmonary surfactant metabolism dysfunction 5 (SMDP5)	R-HSA-5688849	1.10E-03	0.241	other
Osteosarcoma	Response to metal ions	R-HSA-5660526	1.23E-03	0.241	other
Osteosarcoma	Formation of the cornified envelope	R-HSA-6809371	3.70E-03	0.994	other
Osteosarcoma	Alternative complement activation	R-HSA-173736	4.68E-03	0.688	other
Osteosarcoma	Defective pro-SFTPC causes pulmonary surfactant metabolism dysfunction 2 (SMDP2) and respiratory distress syndrome (RDS)	R-HSA-5688354	5.63E-03	0.737	other
Osteosarcoma	Neutrophil degranulation	R-HSA-6798695	0.012	0.774	other
Osteosarcoma	Transport of glycerol from adipocytes to the liver by Aquaporins	R-HSA-432030	0.012	0.774	other
Osteosarcoma	Advanced glycosylation endproduct receptor signaling	R-HSA-879415	0.012	0.774	other
Osteosarcoma	DEx/H-box helicases activate type I IFN and inflammatory cytokines production	R-HSA-3134963	0.012	0.774	other
Osteosarcoma	SMAD2/SMAD3:SMAD4 heterotrimer regulates transcription	R-HSA-2173796	0.022	0.774	other

Entity	Pathway Name	Pathway Identifier	p-value	FDR	Category
Osteosarcoma	TRAF6 mediated NF-kB activation	R-HSA-933542	0.030	0.774	other
Osteosarcoma	Keratinization	R-HSA-6805567	0.031	0.994	other
Osteosarcoma	Transcriptional activity of SMAD2/SMAD3:SMAD4 heterotrimer	R-HSA-2173793	0.035	0.774	other
Osteosarcoma	Metal sequestration by antimicrobial proteins	R-HSA-6799990	0.036	0.774	other
Osteosarcoma	Calcitonin-like ligand receptors	R-HSA-419812	0.043	0.994	other
alveolar RMS	Deposition of new CENPA-containing nucleosomes at the centromere	R-HSA-606279	1.42E-03	0.725	Cell Cycle
alveolar RMS	Nucleosome assembly	R-HSA-774815	1.42E-03	0.725	Cell Cycle
alveolar RMS	CREB3 factors activate genes	R-HSA-8874211	0.028	0.941	Cell Cycle
alveolar RMS	Packaging Of Telomere Ends	R-HSA-171306	0.030	0.725	Cell Cycle
alveolar RMS	G0 and Early G1	R-HSA-1538133	0.047	0.725	Cell Cycle
alveolar RMS	Clearance of Nuclear Envelope Membranes from Chromatin	R-HSA-2993913	0.049	0.725	Cell Cycle
alveolar RMS	Adherens junctions interactions	R-HSA-418990	0.011	0.725	ECM
alveolar RMS	HDACs deacetylate histones	R-HSA-3214815	4.53E-03	0.725	other
alveolar RMS	ERCC6 (CSB) and EHMT2 (G9a) positively regulate rRNA expression	R-HSA-427389	6.28E-03	0.725	other
alveolar RMS	Striated Muscle Contraction	R-HSA-390522	6.74E-03	0.725	other
alveolar RMS	Formation of the beta-catenin:TCF transactivating complex	R-HSA-201722	7.02E-03	0.725	other
alveolar RMS	ESR-mediated signaling	R-HSA-8939211	7.80E-03	0.725	other
alveolar RMS	Estrogen-dependent gene expression	R-HSA-9018519	9.95E-03	0.725	other
alveolar RMS	PRC2 methylates histones and DNA	R-HSA-212300	0.011	0.725	other
alveolar RMS	DNA methylation	R-HSA-5334118	0.013	0.725	other

Entity	Pathway Name	Pathway Identifier	p-value	FDR	Category
alveolar RMS	Cross-presentation of particulate exogenous antigens (phagosomes)	R-HSA-1236973	0.013	0.725	other
alveolar RMS	Transport of glycerol from adipocytes to the liver by Aquaporins	R-HSA-432030	0.018	0.725	other
alveolar RMS	RNA Polymerase I Promoter Opening	R-HSA-73728	0.027	0.725	other
alveolar RMS	Transcription of E2F targets under negative control by DREAM complex	R-HSA-1362277	0.029	0.725	other
alveolar RMS	Neutrophil degranulation	R-HSA-6798695	0.030	0.725	other
alveolar RMS	Inwardly rectifying K+ channels	R-HSA-1296065	0.030	0.725	other
alveolar RMS	Binding of TCF/LEF:CTNNB1 to target gene promoters	R-HSA-4411364	0.032	0.725	other
alveolar RMS	Activation of G protein gated Potassium channels	R-HSA-1296041	0.039	0.725	other
alveolar RMS	G protein gated Potassium channels	R-HSA-1296059	0.039	0.725	other
alveolar RMS	Inhibition of voltage gated Ca2+ channels via Gbeta/gamma subunits	R-HSA-997272	0.039	0.725	other
alveolar RMS	RNA Polymerase I Transcription	R-HSA-73864	0.041	0.725	other
alveolar RMS	Translocation of GLUT4 to the plasma membrane	R-HSA-1445148	0.043	0.725	other
alveolar RMS	Positive epigenetic regulation of rRNA expression	R-HSA-5250913	0.050	0.725	other
alveolar RMS	Activation of TRKA receptors	R-HSA-187015	5.14E-03	0.725	Signaling
alveolar RMS	NGF-independant TRKA activation	R-HSA-187024	8.30E-03	0.725	Signaling
alveolar RMS	Advanced glycosylation endproduct receptor signaling	R-HSA-879415	0.025	0.725	Signaling
alveolar RMS	Nuclear signaling by ERBB4	R-HSA-1251985	0.030	0.725	Signaling
alveolar RMS	RUNX3 regulates WNT signaling	R-HSA-8951430	0.032	0.725	Signaling
alveolar RMS	TRKA activation by NGF	R-HSA-187042	0.046	0.725	Signaling
alveolar RMS	RHO GTPases activate PKNs	R-HSA-5625740	0.050	0.725	Signaling
embryonal RMS	Activation of Matrix Metalloproteinases	R-HSA-1592389	1.14E-04	9.27E-03	ECM

Entity	Pathway Name	Pathway Identifier	p-value	FDR	Category
embryonal RMS	Collagen degradation	R-HSA-1442490	1.57E-04	0.012	ECM
embryonal RMS	Degradation of the extracellular matrix	R-HSA-1474228	1.33E-03	0.092	ECM
embryonal RMS	ERBB2 Activates PTK6 Signaling	R-HSA-8847993	1.11E-03	0.119	ERBB
embryonal RMS	ERBB2 Regulates Cell Motility	R-HSA-6785631	1.41E-03	0.130	ERBB
embryonal RMS	GPCR ligand binding	R-HSA-500792	1.46E-03	0.095	ERBB
embryonal RMS	GRB2 events in ERBB2 signaling	R-HSA-1963640	1.76E-03	0.141	ERBB
embryonal RMS	Nuclear signaling by ERBB4	R-HSA-1251985	8.28E-03	0.779	ERBB
embryonal RMS	Downregulation of ERBB4 signaling	R-HSA-1253288	9.14E-03	0.585	ERBB
embryonal RMS	SHC1 events in ERBB4 signaling	R-HSA-1250347	0.011	0.628	ERBB
embryonal RMS	G alpha (i) signalling events	R-HSA-418594	0.013	0.456	ERBB
embryonal RMS	PI3K events in ERBB2 signaling	R-HSA-1963642	0.015	0.728	ERBB
embryonal RMS	SHC1 events in ERBB2 signaling	R-HSA-1250196	0.017	0.762	ERBB
embryonal RMS	Downregulation of ERBB2 signaling	R-HSA-8863795	0.019	0.762	ERBB
embryonal RMS	PI3K events in ERBB4 signaling	R-HSA-1250342	0.026	0.762	ERBB
embryonal RMS	Signaling by ERBB4	R-HSA-1236394	0.030	0.902	ERBB
embryonal RMS	Interleukin-10 signaling	R-HSA-6783783	2.22E-16	2.17E-13	Immune System
embryonal RMS	Chemokine receptors bind chemokines	R-HSA-380108	3.16E-11	1.54E-08	Immune System
embryonal RMS	Cytokine Signaling in Immune system	R-HSA-1280215	3.00E-09	9.74E-07	Immune System
embryonal RMS	Signaling by Interleukins	R-HSA-449147	4.34E-08	8.46E-06	Immune System

Entity	Pathway Name	Pathway Identifier	p-value	FDR	Category
embryonal RMS	Interleukin-4 and 13 signaling	R-HSA-6785807	2.88E-07	4.67E-05	Immune System
embryonal RMS	Immune System	R-HSA-168256	1.97E-06	2.74E-04	Immune System
embryonal RMS	Neutrophil degranulation	R-HSA-6798695	2.12E-05	2.05E-03	Immune System
embryonal RMS	Alternative complement activation	R-HSA-173736	2.00E-03	0.121	Immune System
embryonal RMS	Cross-presentation of particulate exogenous antigens (phagosomes)	R-HSA-1236973	2.12E-03	0.121	Immune System
embryonal RMS	CLEC7A/inflammasome pathway	R-HSA-5660668	4.48E-03	0.228	Immune System
embryonal RMS	Innate Immune System	R-HSA-168249	5.90E-03	0.283	Immune System
embryonal RMS	Interferon alpha/beta signaling	R-HSA-909733	9.51E-03	0.415	Immune System
embryonal RMS	Interferon Signaling	R-HSA-913531	0.010	0.415	Immune System
embryonal RMS	Interleukin-18 signaling	R-HSA-9012546	0.011	0.415	Immune System
embryonal RMS	Initial triggering of complement	R-HSA-166663	0.011	0.415	Immune System
embryonal RMS	Interferon gamma signaling	R-HSA-877300	0.016	0.512	Immune System
embryonal RMS	Translocation of ZAP-70 to Immunological synapse	R-HSA-202430	0.030	0.717	Immune System
embryonal RMS	Activation of C3 and C5	R-HSA-174577	0.033	0.717	Immune System
embryonal RMS	Phosphorylation of CD3 and TCR zeta chains	R-HSA-202427	0.038	0.717	Immune System
embryonal RMS	Muscle contraction	R-HSA-397014	1.92E-09	1.05E-06	other
embryonal RMS	Striated Muscle Contraction	R-HSA-390522	3.24E-09	1.05E-06	other
embryonal RMS	Peptide ligand-binding receptors	R-HSA-375276	1.51E-08	3.68E-06	other
embryonal RMS	Class A/1 (Rhodopsin-like receptors)	R-HSA-373076	5.25E-06	5.79E-04	other

Entity	Pathway Name	Pathway Identifier	p-value	FDR	Category
embryonal RMS	Metallothioneins bind metals	R-HSA-5661231	5.36E-06	5.79E-04	other
embryonal RMS	Response to metal ions	R-HSA-5660526	3.02E-05	2.66E-03	other
embryonal RMS	Ion homeostasis	R-HSA-5578775	1.15E-04	0.025	other
embryonal RMS	Cardiac conduction	R-HSA-5576891	3.16E-04	0.051	other
embryonal RMS	RHO GTPases Activate NADPH Oxidases	R-HSA-5668599	3.86E-03	0.209	other
embryonal RMS	Reduction of cytosolic Ca++ levels	R-HSA-418359	4.03E-03	0.286	other
embryonal RMS	Transport of glycerol from adipocytes to the liver by Aquaporins	R-HSA-432030	6.84E-03	0.315	other
embryonal RMS	Formyl peptide receptors bind formyl peptides and many other ligands	R-HSA-444473	0.011	0.415	other
embryonal RMS	Inactivation of CDC42 and RAC1	R-HSA-428543	0.015	0.728	other
embryonal RMS	Regulation of Insulin-like Growth Factor (IGF) transport and uptake by Insulin-like Growth Factor Binding Proteins (IGFBPs)	R-HSA-381426	0.016	0.524	other
embryonal RMS	Metabolism of Angiotensinogen to Angiotensins	R-HSA-2022377	0.023	0.698	other
embryonal RMS	Physiological factors	R-HSA-5578768	0.024	0.902	other
embryonal RMS	Ion channel transport	R-HSA-983712	0.033	0.762	other
embryonal RMS	Ion transport by P-type ATPases	R-HSA-936837	0.033	0.762	other
embryonal RMS	RUNX1 regulates transcription of genes involved in BCR signaling	R-HSA-8939245	0.033	0.717	other
embryonal RMS	Activation of AMPA receptors	R-HSA-399710	0.036	0.762	other

Entity	Pathway Name	Pathway Identifier	p-value	FDR	Category
embryonal RMS	RUNX2 regulates chondrocyte maturation	R-HSA-8941284	0.036	0.762	other
embryonal RMS	Response to elevated platelet cytosolic Ca2+	R-HSA-76005	0.036	0.717	other
embryonal RMS	Acyl chain remodelling of PS	R-HSA-1482801	0.039	0.717	other
embryonal RMS	Defective CSF2RA causes pulmonary surfactant metabolism dysfunction 4 (SMDP4)	R-HSA-5688890	0.043	0.717	other
embryonal RMS	Defective CSF2RB causes pulmonary surfactant metabolism dysfunction 5 (SMDP5)	R-HSA-5688849	0.043	0.717	other
embryonal RMS	ATF4 activates genes	R-HSA-380994	0.043	0.717	other
embryonal RMS	ChREBP activates metabolic gene expression	R-HSA-163765	0.046	0.762	other
embryonal RMS	The fatty acid cycling model	R-HSA-167826	0.046	0.762	other

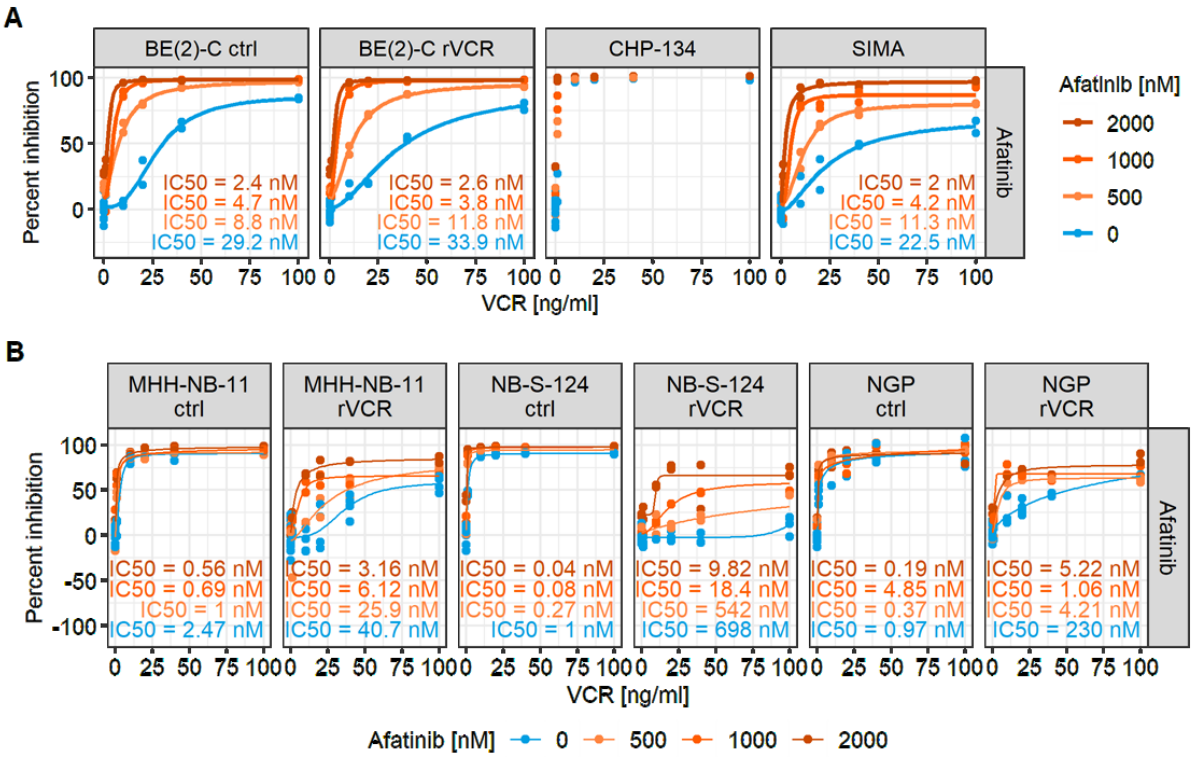

Appendix Figure 7: Combining VCR with afatinib results in synergistic reduction of viability. ***(A&B)*** *The indicated cell lines were treated with 0, 10, 20, 40, 100 ng/ml VCR +/- 0, 0.5, 1, 2 µM afatinib for 48 h. Metabolic activity was assessed by CTG and Percent inhibition was calculated relative to controls (1 µM staurosporine and DMSO). IC50s were calculated with a LL4 model. This figure was adapted from Rösch et al.*[253] *All work presented therein is my own.*

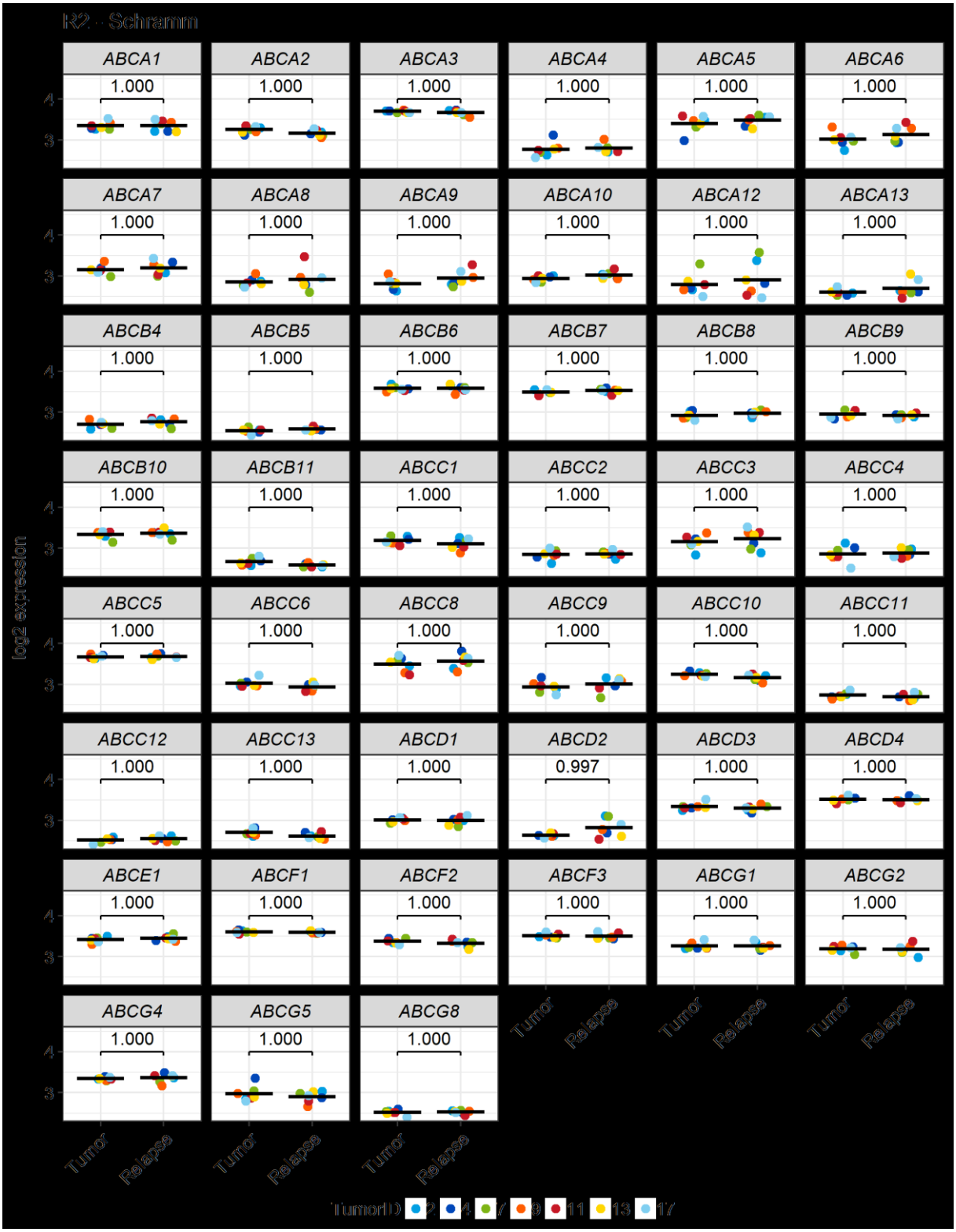

Appendix Figure 8: Expression of the ABC gene family in gene expression data of paired samples of patients at primary diagnosis and at relapse. Gene expression data of 18 tumor samples from the dataset by Schramm et al. (GSE65303)[241] *was downloaded from R2 (http://r2.amc.nl, 09 September 2021). Only paired samples with data at primary diagnosis (Tumor) and at Relapse were included (n = 7 pairs). Statistics were calculated by ANOVA followed by Tukey's post-test including all genes of the ERBB and the ABC families present in the dataset. This figure was adapted from Rösch et al.*[253] *The analysis presented therein is my own.*

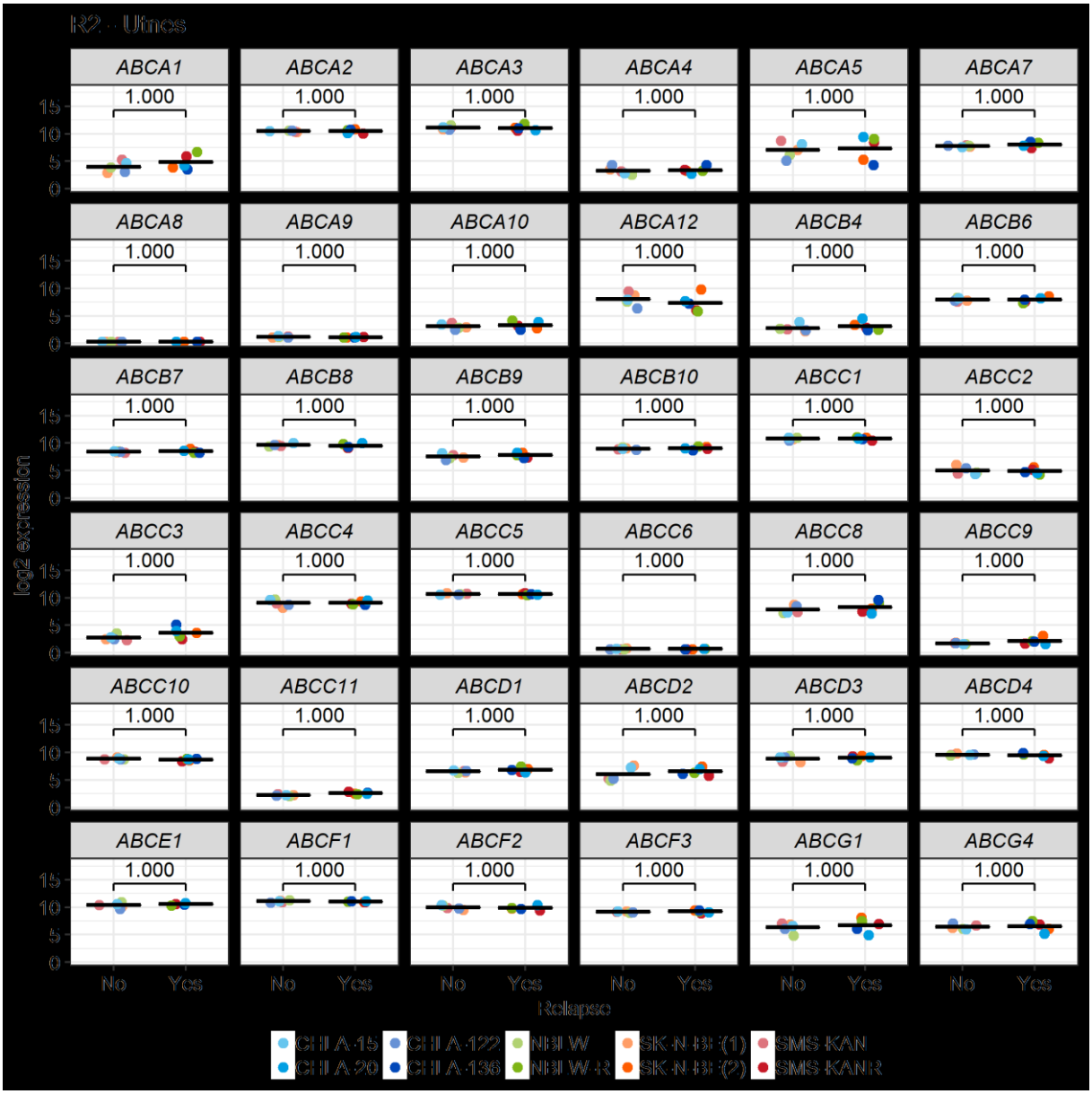

Appendix Figure 9: Expression of the ABC gene family in gene expression data of paired cell lines (Utnes et al.) derived at primary diagnosis and at relapse. Gene expression data of 10 paired neuroblastoma cell lines from the dataset by Utnes et al. (GSE148700)[244] *was downloaded from R2 (http://r2.amc.nl, 07 January 2021). This dataset is made up of five cell line pairs derived from the same patients at primary diagnosis and after relapse. Matched pairs are indicated by color. Statistics were calculated by ANOVA followed by Tukey's post-test including all genes of the ERBB and the ABC families present in the dataset. This figure was adapted from Rösch et al.*[253] *The analysis presented therein is my own.*

Appendix Figure 10: Expression of the ABC gene family in gene expression data of cell lines (Jagannathan et al.) derived at primary diagnosis and at relapse. Gene expression data of 38 neuroblastoma cell lines from the dataset by Jagannathan et al. (GSE19274)[242] was downloaded from R2 (http://r2.amc.nl, 08 June 2021). All cell lines that could not be positively identified as having been derived before (n = 10) or after (n = 12) the patient had received chemotherapy (Relapse No/Yes) were excluded from the analysis. Statistics were calculated by ANOVA followed by Tukey's post-test including all genes of the ERBB and the ABC families present in the dataset. This figure was adapted from Rösch et al.[253] The analysis presented therein is my own.

Appendix Figure 11: Expression of the ABC gene family in gene expression data of cell lines (Maris et al.) derived at primary diagnosis and at relapse. Gene expression data of 41 neuroblastoma cell lines from the dataset by Maris et al. (GSE89413)[174] *was downloaded from R2 (http://r2.amc.nl, 07 January 2021). All cell lines that could not be positively identified as having been derived before (n = 12) or after (n = 15) the patient had received chemotherapy (Relapse No/Yes) were excluded from the analysis. Statistics were calculated by ANOVA followed by Tukey's post-test including all genes of the ERBB and the ABC families present in the dataset. This figure was adapted from Rösch et al.*[253] *The analysis presented therein is my own.*

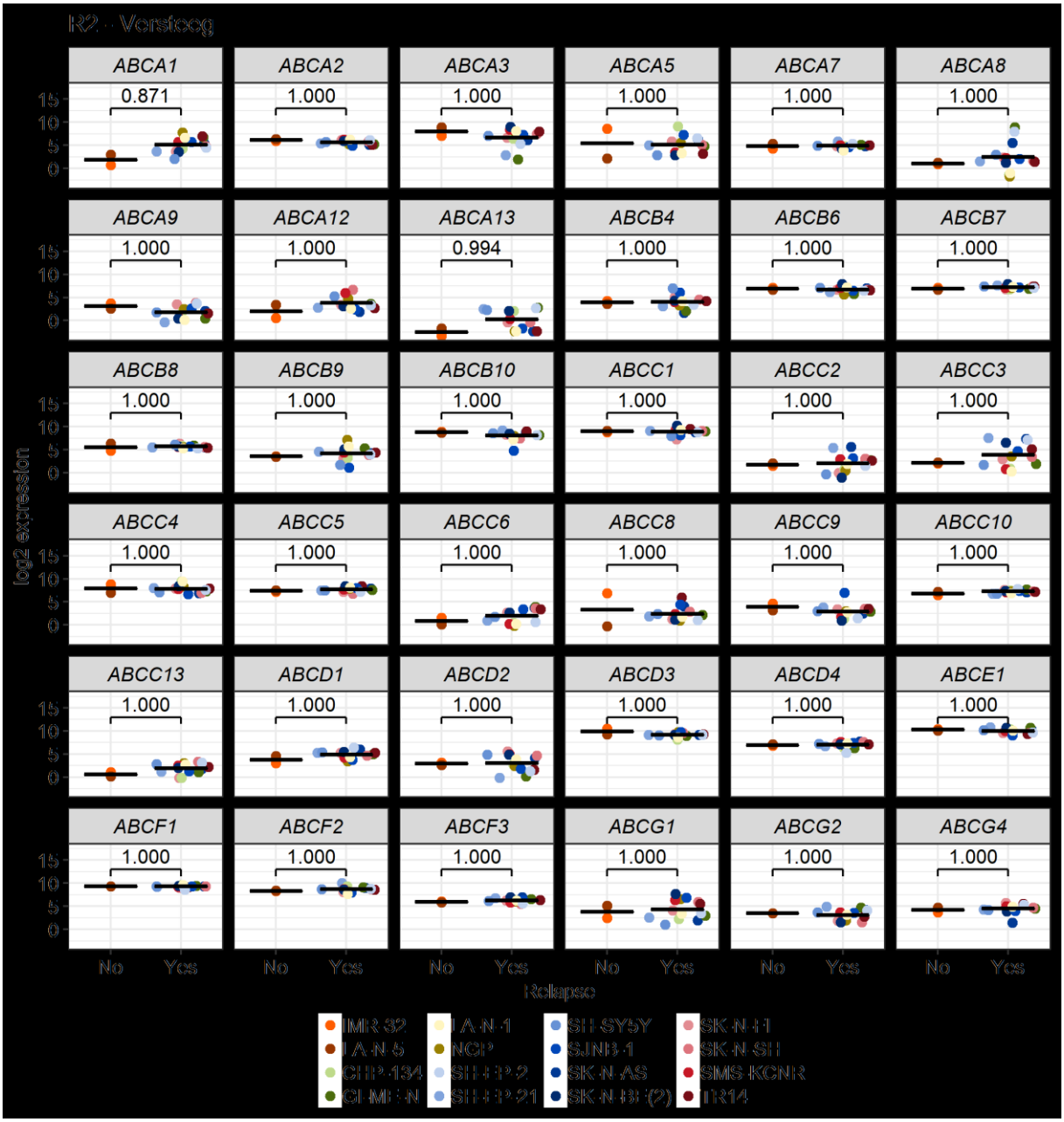

Appendix Figure 12: Expression of the ABC gene family in gene expression data of cell lines (Versteeg et al.) derived at primary diagnosis and at relapse. Gene expression data of 24 neuroblastoma cell lines from the dataset by Versteeg et al. (GSE28019) was downloaded from R2 (http://r2.amc.nl, 07 January 2021). All cell lines that could not be positively identified as having been derived before (n = 2) or after (n = 14) the patient had received chemotherapy (Relapse No/Yes) were excluded from the analysis. Statistics were calculated by ANOVA followed by Tukey's post-test including all genes of the ERBB and the ABC families present in the dataset. This figure was adapted from Rösch et al.[253] The analysis presented therein is my own.

Appendix Figure 13: Expression of the ABC gene family in gene expression data of cell lines (Broad Institute) derived at primary diagnosis and at relapse. Gene expression data of 917 cell lines from the cell line encyclopedia dataset from the Broad Institute (GSE19274)[243]*, which comprised 17 neuroblastoma cell lines, was downloaded from R2 (http://r2.amc.nl, 08 June 2021). All cell lines that could not be positively identified as having been derived before (n = 4) or after (n = 7) the patient had received chemotherapy (Relapse No/Yes) were excluded from the analysis. Statistics were calculated by ANOVA followed by Tukey's post-test including all genes of the ERBB and the ABC families present in the dataset. This figure was adapted from Rösch et al.*[253] *The analysis presented therein is my own.*

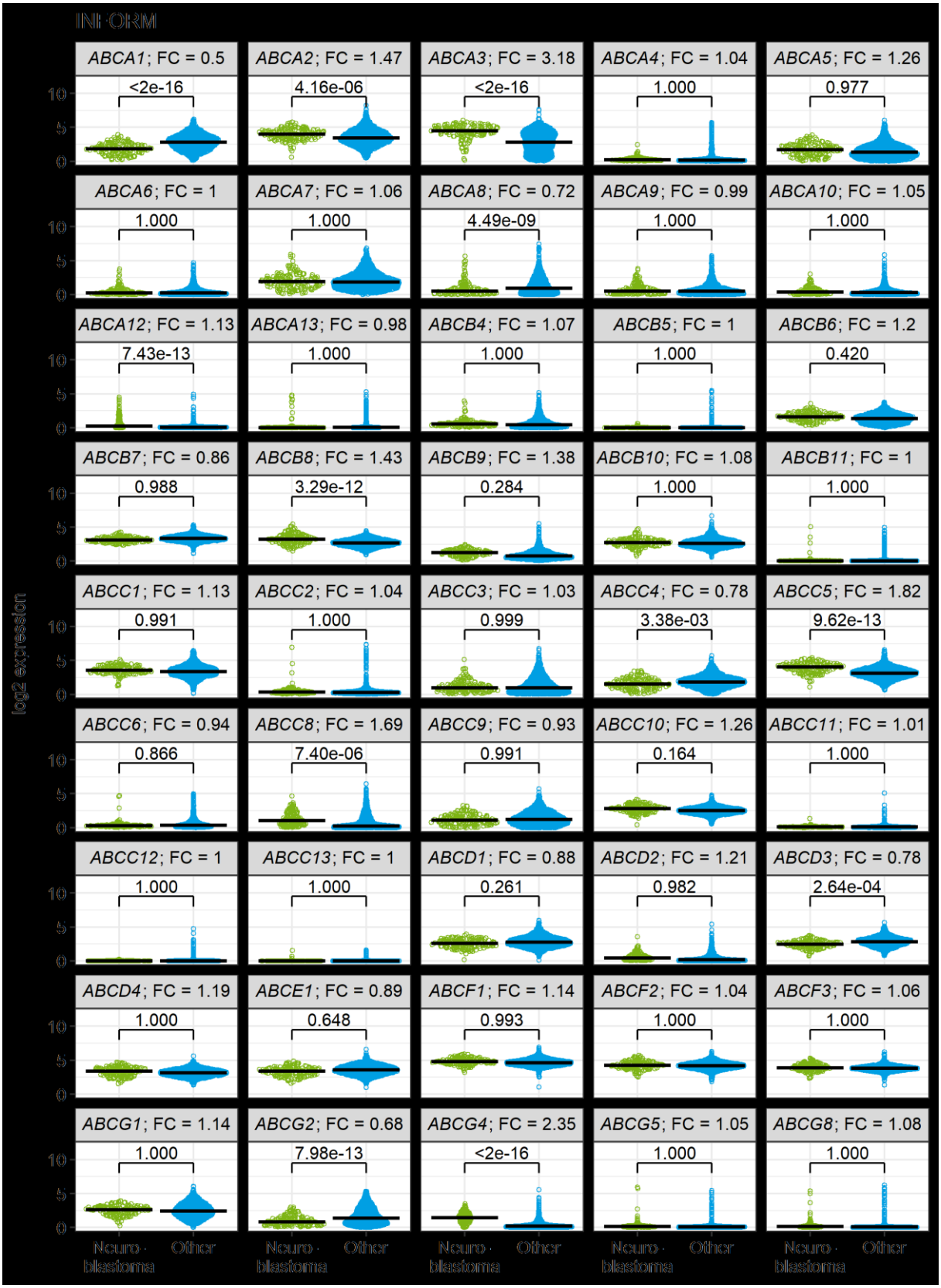

Appendix Figure 14: Expression of the ABC gene family in gene expression data of relapsed neuroblastoma compared to other relapsed pediatric tumor entities. Gene expression data from the INFORM registry[235,236] *(n = 1645) was downloaded from R2 (http://r2.amc.nl). Comparison of neuroblastoma cases (n = 162) vs. all other entities. FC between the group means is indicated in the panel titles. Statistics were calculated by ANOVA followed by Tukey's post-test including all genes of the ERBB and the ABC families present in the dataset. This figure was adapted from Rösch et al.*[253] *The analysis presented therein is my own.*

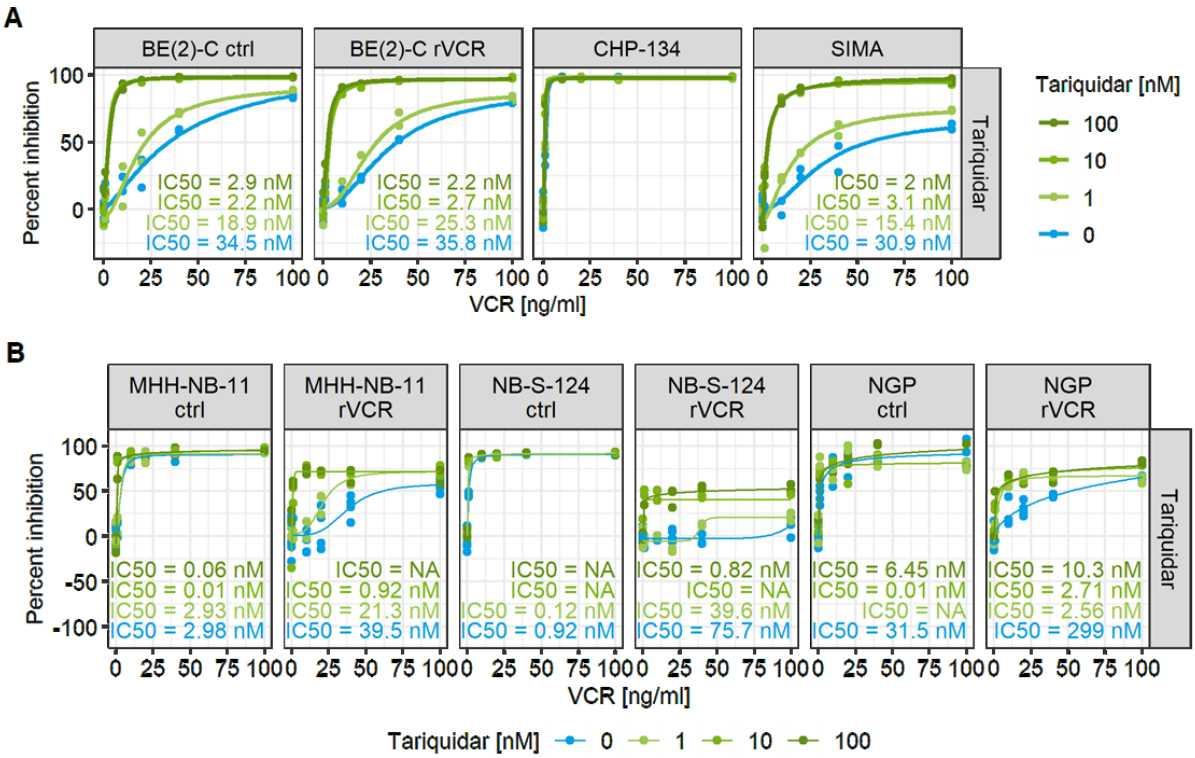

Appendix Figure 15: Combining VCR with tariquidar results in synergistic reduction of viability. ***(A&B)*** *The indicated cell lines were treated with 0, 10, 20, 40, 100 ng/ml VCR +/- 0, 1, 10, 100 nM tariquidar for 48 h. Metabolic activity was assessed by CTG and Percent inhibition was calculated relative to controls (1 µM staurosporine and DMSO). IC50s were calculated with a LL4 model. NA = no IC50 could be computed. This figure was adapted from Rösch et al.*[253] *All work presented therein is my own.*

8. References

1. Erdmann, F., Kaatsch, P., Grabow, D. & Spix, C. *German Childhood Cancer Registry - Annual Report 2019 (1980-2018)*. (Institute of Medical Biostatistics, Epidemiology and Informatics (IMBEI) at the University Medical Center of the Johannes Gutenberg University Mainz, 2020).
2. Marshall, G. M. *et al.* The prenatal origins of cancer. *Nat. Rev. Cancer* **14**, 277–289 (2014). doi:10.1038/nrc3679.
3. Kathryn A, Z. *et al.* Differential expression of myc family genes during murine development. *Nature* **319**, 780-783. (1986). doi:10.1038/319780a0.
4. Wartiovaara, K., -Heider, F. B., Miller, F. D. & Kaplan, D. R. N-myc promotes survival and induces S-phase entry of postmitotic sympathetic neurons. *J. Neurosci.* **22**, 815–824 (2002). doi:10.1523/jneurosci.22-03-00815.2002.
5. Jansky, S. *et al.* Single-cell transcriptomic analyses provide insights into the developmental origins of neuroblastoma. *Nat. Genet.* (2021) doi:10.1038/s41588-021-00806-1. doi:10.1038/s41588-021-00806-1.
6. Cohn, S. L. *et al.* The International Neuroblastoma Risk Group (INRG) classification system: An INRG task force report. *J. Clin. Oncol.* **27**, 289–297 (2009). doi:10.1200/JCO.2008.16.6785.
7. Brodeur, G. M. *et al.* Revisions of the international criteria for neuroblastoma diagnosis, staging and response to treatment. *Prog. Clin. Biol. Res.* **385**, 363–369 (1994).
8. Monclair, T. *et al.* The International Neuroblastoma Risk Group (INRG) staging system: An INRG Task Force report. *J. Clin. Oncol.* **27**, 298–303 (2009). doi:10.1200/JCO.2008.16.6876.
9. Hero, B. *et al.* Localized infant neuroblastomas often show spontaneous regression: Results of the prospective trials NB95-S and NB97. *J. Clin. Oncol.* **26**, 1504–1510 (2008). doi:10.1200/JCO.2007.12.3349.
10. Simon, T. *et al.* 2017 GPOH Guidelines for Diagnosis and Treatment of Patients with Neuroblastic Tumors. *Klin. Padiatr.* **229**, 147–167 (2017). doi:10.1055/s-0043-103086.
11. Pinto, N. R. *et al.* Advances in risk classification and treatment strategies for neuroblastoma. *J. Clin. Oncol.* **33**, 3008–3017 (2015). doi:10.1200/JCO.2014.59.4648.
12. Murphy, D. J. *et al.* Distinct Thresholds Govern Myc's Biological Output In Vivo. *Cancer Cell* **14**, 447–457 (2008). doi:10.1016/j.ccr.2008.10.018.
13. Valentijn, L. J. *et al.* TERT rearrangements are frequent in neuroblastoma and identify aggressive tumors. *Nat. Genet.* **47**, 1411–1414 (2015). doi:10.1038/ng.3438.
14. Peifer, M. *et al.* Telomerase activation by genomic rearrangements in high-risk neuroblastoma. *Nature* **526**, 700–704 (2015). doi:10.1038/nature14980.
15. Mossé, Y. P. *et al.* Identification of ALK as a major familial neuroblastoma predisposition gene. *Nature* **455**, 930–935 (2008). doi:10.1038/nature07261.
16. Mosse, Y. P. *et al.* Germline PHOX2B mutation in hereditary neuroblastoma. *Am. J. Hum. Genet.* **75**, 727–730 (2004). doi:10.1086/424530.
17. Reiff, T. *et al.* Neuroblastoma Phox2b variants stimulate proliferation and dedifferentiation of immature sympathetic neurons. *J. Neurosci.* **30**, 905–915 (2010). doi:10.1523/JNEUROSCI.5368-09.2010.
18. Carén, H., Abel, F., Kogner, P. & Martinsson, T. High incidence of DNA mutations and gene amplifications of the ALK gene in advanced sporadic neuroblastoma tumours. *Biochem. J.* **416**, 153–159 (2008). doi:10.1042/BJ20081834.
19. Schleiermacher, G. *et al.* Emergence of new ALK mutations at relapse of neuroblastoma. *J. Clin. Oncol.* **32**, 2727–2734 (2014). doi:10.1200/JCO.2013.54.0674.
20. Hallberg, B. & Palmer, R. H. The role of the ALK receptor in cancer biology. *Ann. Oncol.* **27**, iii4–iii15 (2016). doi:10.1093/annonc/mdw301.
21. Schönherr, C. *et al.* Anaplastic Lymphoma Kinase (ALK) regulates initiation of transcription of MYCN in neuroblastoma cells. *Oncogene* **31**, 5193–5200 (2012). doi:10.1038/onc.2012.12.
22. Berry, T. *et al.* The ALKF1174L Mutation Potentiates the Oncogenic Activity of MYCN in

Neuroblastoma. *Cancer Cell* **22**, 117–130 (2012). doi:10.1016/j.ccr.2012.06.001.
23. Zhu, S. *et al.* Activated ALK Collaborates with MYCN in Neuroblastoma Pathogenesis. *Cancer Cell* **21**, 362–373 (2012). doi:10.1016/j.ccr.2012.02.010.
24. Hanahan, D. & Weinberg, R. A. Hallmarks of cancer: The next generation. *Cell* **144**, 646–674 (2011). doi:10.1016/j.cell.2011.02.013.
25. Cheung, N. K. V. *et al.* Association of age at diagnosis and genetic mutations in patients with neuroblastoma. *JAMA - J. Am. Med. Assoc.* **307**, 1062–1071 (2012). doi:10.1001/jama.2012.228.
26. Heaphy, C. M. *et al.* Altered telomeres in tumors with ATRX and DAXX mutations. *Science (80-.).* **333**, 425 (2011). doi:10.1126/science.1207313.
27. Ackermann, S. *et al.* A mechanistic classification of clinical phenotypes in neuroblastoma. *Science (80-.).* **362**, 1165–1170 (2018). doi:10.1126/science.aat6768.
28. Van Groningen, T. *et al.* Neuroblastoma is composed of two super-enhancer-associated differentiation states. *Nat. Genet.* **49**, 1261–1266 (2017). doi:10.1038/ng.3899.
29. Gartlgruber, M. *et al.* Super enhancers define regulatory subtypes and cell identity in neuroblastoma. *Nat. Cancer* **2**, 114–128 (2021). doi:10.1038/s43018-020-00145-w.
30. Ponzoni, M. *et al.* Recent advances in the developmental origin of neuroblastoma: an overview. *J. Exp. Clin. Cancer Res.* **41**, 1–28 (2022). doi:10.1186/s13046-022-02281-w.
31. Basta, N. O. *et al.* Factors associated with recurrence and survival length following relapse in patients with neuroblastoma. *Br. J. Cancer* **115**, 1048–1057 (2016). doi:10.1038/bjc.2016.302.
32. London, W. B. *et al.* Clinical and biologic features predictive of survival after relapse of neuroblastoma: A report from the International Neuroblastoma Risk Group Project. *J. Clin. Oncol.* **29**, 3286–3292 (2011). doi:10.1200/JCO.2010.34.3392.
33. Santana, V. M., Furman, W. L., McGregor, L. M. & Billups, C. A. Disease control intervals in high-risk neuroblastoma. *Cancer* **112**, 2796–2801 (2008). doi:10.1002/cncr.23507.
34. Bukowski, K., Kciuk, M. & Kontek, R. Mechanisms of multidrug resistance in cancer chemotherapy. *Int. J. Mol. Sci.* **21**, (2020). doi:10.3390/ijms21093233.
35. Mantovani, F., Collavin, L. & Del Sal, G. Mutant p53 as a guardian of the cancer cell. *Cell Death Differ.* **26**, 199–212 (2019). doi:10.1038/s41418-018-0246-9.
36. Duesberg, P., Stindl, R. & Hehlmann, R. Origin of multidrug resistance in cells with and without multidrug resistance genes: Chromosome reassortments catalyzed by aneuploidy. *Proc. Natl. Acad. Sci. U. S. A.* **98**, 11283–11288 (2001). doi:10.1073/pnas.201398998.
37. Olsson, M., Beck, S., Kogner, P., Martinsson, T. & Carén, H. Genome-wide methylation profiling identifies novel methylated genes in neuroblastoma tumors. *Epigenetics* **11**, 74–84 (2016). doi:10.1080/15592294.2016.1138195.
38. Mohammad, H. P., Barbash, O. & Creasy, C. L. Targeting epigenetic modifications in cancer therapy: erasing the roadmap to cancer. *Nat. Med.* **25**, 403–418 (2019). doi:10.1038/s41591-019-0376-8.
39. Feng, Q. *et al.* An epigenomic approach to therapy for tamoxifen-resistant breast cancer. *Cell Res.* **24**, 809–819 (2014). doi:10.1038/cr.2014.71.
40. Gerlinger, M. *et al.* Intratumor Heterogeneity and Branched Evolution Revealed by Multiregion Sequencing. *N. Engl. J. Med.* **366**, 883–892 (2012). doi:10.1056/nejmoa1113205.
41. Ramos, P. & Bentires-Alj, M. Mechanism-based cancer therapy: Resistance to therapy, therapy for resistance. *Oncogene* **34**, 3617–3626 (2015). doi:10.1038/onc.2014.314.
42. Klein, C. A. Selection and adaptation during metastatic cancer progression. *Nature* **501**, 365–372 (2013). doi:10.1038/nature12628.
43. Conze, D. *et al.* Autocrine production of interleukin 6 causes multidrug resistance in breast cancer cells. *Cancer Res.* **61**, 8851–8858 (2001).
44. Wang, Y. *et al.* Autocrine production of interleukin-8 confers cisplatin and paclitaxel resistance in ovarian cancer cells. *Cytokine* **56**, 365–375 (2011). doi:10.1016/j.cyto.2011.06.005.
45. Wilson, T. R. *et al.* Widespread potential for growth-factor-driven resistance to anticancer kinase inhibitors. *Nature* **487**, 505–509 (2012). doi:10.1038/nature11249.

46. Huang, C. *et al.* B1 Integrin Mediates an Alternative Survival Pathway in Breast Cancer Cells Resistant To Lapatinib. *Breast Cancer Res.* **13**, 1–15 (2011). doi:10.1186/bcr2936.
47. Muranen, T. *et al.* Inhibition of PI3K/mTOR Leads to Adaptive Resistance in Matrix-Attached Cancer Cells. *Cancer Cell* **21**, 227–239 (2012). doi:10.1016/j.ccr.2011.12.024.
48. Rosell, R. *et al.* Molecular Predictors of Response to Chemotherapy in Lung Cancer. *Semin. Oncol.* **31**, 20–27 (2004). doi:10.1053/j.seminoncol.2003.12.011.
49. Gentile, F. *et al.* Computer-aided drug design of small molecule inhibitors of the ERCC1-XPF protein–protein interaction. *Chem. Biol. Drug Des.* **95**, 460–471 (2020). doi:10.1111/cbdd.13660.
50. Shah, N. P. *et al.* Multiple BCR-ABL kinase domain mutations confer polyclonal resistance to the tyrosine kinase inhibitor imatinib (STI571) in chronic phase and blast crisis chronic myeloid leukemia. *Cancer Cell* **2**, 117–125 (2002). doi:10.1016/S1535-6108(02)00096-X.
51. Ercan, D. *et al.* Amplification of EGFR T790M causes resistance to an irreversible EGFR inhibitor. *Oncogene* **29**, 2346–2356 (2010). doi:10.1038/onc.2009.526.
52. Corcoran, R. B. *et al.* BRAF gene amplification can promote acquired resistance to MEK inhibitors in cancer cells harboring the BRAF V600E mutation. *Sci. Signal.* **3**, 1–11 (2010). doi:10.1126/scisignal.2001148.
53. Emery, C. M. *et al.* MEK1 mutations confer resistance to MEK and B-RAF inhibition. *Proc. Natl. Acad. Sci. U. S. A.* **106**, 20411–20416 (2009). doi:10.1073/pnas.0905833106.
54. Chandarlapaty, S. *et al.* Frequent mutational activation of the PI3K-AKT pathway in trastuzumab-resistant breast cancer. *Clin. Cancer Res.* **18**, 6784–6791 (2012). doi:10.1158/1078-0432.CCR-12-1785.
55. Nagata, Y. *et al.* PTEN activation contributes to tumor inhibition by trastuzumab, and loss of PTEN predicts trastuzumab resistance in patients. *Cancer Cell* **6**, 117–127 (2004). doi:10.1016/j.ccr.2004.06.022.
56. Grant, S. Cotargeting survival signaling pathways in cancer. *J. Clin. Invest.* **118**, 3003–3006 (2008). doi:10.1172/JCI36898.
57. McCubrey, J. A. *et al.* Therapeutic resistance resulting from mutations in Raf/MEK/ERK and PI3K/PTEN/Akt/mTOR signaling pathways. *J. Cell. Physiol.* **226**, 2762–2781 (2011). doi:10.1002/jcp.22647.
58. Carracedo, A. *et al.* Inhibition of mTORC1 leads to MAPK pathway activation through a PI3K-dependent feedback loop in human cancer. *J. Clin. Invest.* **118**, 3065–3074 (2008). doi:10.1172/JCI34739.
59. Kinkade, C. W. *et al.* Targeting AKT/mTOR and ERK MAPK signaling inhibits hormone-refractory prostate cancer in a preclinical mouse model. *J. Clin. Invest.* **118**, 3051–3064 (2008). doi:10.1172/JCI34764.
60. Wee, S. *et al.* PI3K pathway activation mediates resistance to MEK inhibitors in KRAS mutant cancers. *Cancer Res.* **69**, 4286–4293 (2009). doi:10.1158/0008-5472.CAN-08-4765.
61. Hoeflich, K. P. *et al.* In vivo antitumor activity of MEK and phosphatidylinositol 3-kinase inhibitors in basal-like breast cancer models. *Clin. Cancer Res.* **15**, 4649–4664 (2009). doi:10.1158/1078-0432.CCR-09-0317.
62. Pan, S. T., Li, Z. L., He, Z. X., Qiu, J. X. & Zhou, S. F. Molecular mechanisms for tumour resistance to chemotherapy. *Clin. Exp. Pharmacol. Physiol.* **43**, 723–737 (2016). doi:10.1111/1440-1681.12581.
63. Watanabe, A. *et al.* BCL2 and BCLxL are key determinants of resistance to antitubulin chemotherapeutics in melanoma cells. *Exp. Dermatol.* **22**, 518–523 (2013). doi:10.1111/exd.12185.
64. Liu, Y. *et al.* Resistance to bortezomib in breast cancer cells that downregulate Bim through FOXA1 O-GlcNAcylation. *J. Cell. Physiol.* **234**, 17527–17537 (2019). doi:10.1002/jcp.28376.
65. Fujimoto, A. *et al.* Allelic Imbalance of 12q22-23 Associated with APAF-1 Locus Correlates with Poor Disease Outcome in Cutaneous Melanoma. *Cancer Res.* **64**, 2245–2250 (2004). doi:10.1158/0008-5472.CAN-03-2932.

66. Jung, J. *et al.* Interaction of translationally controlled tumor protein with Apaf-1 is involved in the development of chemoresistance in HeLa cells. *BMC Cancer* **14**, 1–13 (2014). doi:10.1186/1471-2407-14-165.
67. Yang, W. Z., Zhou, H. & Yan, Y. XIAP underlies apoptosis resistance of renal cell carcinoma cells. *Mol. Med. Rep.* **17**, 125–130 (2018). doi:10.3892/mmr.2017.7925.
68. Julien, O. & Wells, J. A. Caspases and their substrates. *Cell Death Differ.* **24**, 1380–1389 (2017). doi:10.1038/cdd.2017.44.
69. Scott, F. L. *et al.* XIAP inhibits caspase-3 and -7 using two binding sites: Evolutionary conserved mechanism of IAPs. *EMBO J.* **24**, 645–655 (2005). doi:10.1038/sj.emboj.7600544.
70. Zhao, M. *et al.* Cytochrome p450 enzymes and drug metabolism in humans. *Int. J. Mol. Sci.* **22**, 1–16 (2021). doi:10.3390/ijms222312808.
71. Zhang, J. *et al.* Metabolism and transport of oxazaphosphorines and the clinical implications. *Drug Metab. Rev.* **37**, 611–703 (2005). doi:10.1080/03602530500364023.
72. van Eijk, M., Boosman, R. J., Schinkel, A. H., Huitema, A. D. R. & Beijnen, J. H. Cytochrome P450 3A4, 3A5, and 2C8 expression in breast, prostate, lung, endometrial, and ovarian tumors: relevance for resistance to taxanes. *Cancer Chemother. Pharmacol.* **84**, 487–499 (2019). doi:10.1007/s00280-019-03905-3.
73. Egbelakin, A. *et al.* Increased risk of vincristine neurotoxicity associated with low CYP3A5 expression genotype in children with acute lymphoblastic leukemia. *Pediatr. Blood Cancer* **56**, 361–367 (2011). doi:10.1002/pbc.22845.
74. Pathania, S., Bhatia, R., Baldi, A., Singh, R. & Rawal, R. K. Drug metabolizing enzymes and their inhibitors' role in cancer resistance. *Biomed. Pharmacother.* **105**, 53–65 (2018). doi:10.1016/j.biopha.2018.05.117.
75. Liu, X. ABC Family Transporters. in *Drug Transporters in Drug Disposition, Effects and Toxicity* (eds. Liu, X. & Pan, G.) 13–100 (Springer Singapore, 2019). doi:10.1007/978-981-13-7647-4_2. doi:10.1007/978-981-13-7647-4_2.
76. Juliano, R. L. & Ling, V. A surface glycoprotein modulating drug permeability in Chinese hamster ovary cell mutants. *BBA - Biomembr.* **455**, 152–162 (1976). doi:10.1016/0005-2736(76)90160-7.
77. Szakács, G., Paterson, J. K., Ludwig, J. A., Booth-Genthe, C. & Gottesman, M. M. Targeting multidrug resistance in cancer. *Nat. Rev. Drug Discov.* **5**, 219–234 (2006). doi:10.1038/nrd1984.
78. Thiebaut, F. *et al.* Cellular localization of the multidrug-resistance gene product P-glycoprotein in normal human tissues. *Proc. Natl. Acad. Sci. U. S. A.* **84**, 7735–7738 (1987). doi:10.1073/pnas.84.21.7735.
79. Dombrowski, S. M. *et al.* Overexpression of multiple drug resistance genes in endothelial cells from patients with refractory epilepsy. *Epilepsia* **42**, 1501–1506 (2001). doi:10.1046/j.1528-1157.2001.12301.x.
80. St.-Pierre, M. V. *et al.* Expression of members of the multidrug resistance protein family in human term placenta. *Am. J. Physiol. - Regul. Integr. Comp. Physiol.* **279**, 1495–1503 (2000). doi:10.1152/ajpregu.2000.279.4.r1495.
81. Melaine, N. *et al.* Multidrug resistance genes and P-glycoprotein in the testis of the rat, mouse, guinea pig, and human. *Biol. Reprod.* **67**, 1699–1707 (2002). doi:10.1095/biolreprod.102.003558.
82. Esser, L. *et al.* Structures of the Multidrug Transporter P-glycoprotein Reveal Asymmetric ATP Binding and the Mechanism of Polyspecificity. *J. Biol. Chem.* **292**, 446–461 (2017). doi:10.1074/jbc.M116.755884.
83. Robey, R. W. *et al.* Revisiting the role of ABC transporters in multidrug-resistant cancer. *Nat. Rev. Cancer* **18**, 452–464 (2018). doi:10.1038/s41568-018-0005-8.
84. Zhang, Y. *et al.* Afatinib Decreases P-Glycoprotein Expression to Promote Adriamycin Toxicity of A549T Cells. *J. Cell. Biochem.* **119**, 414–423 (2018). doi:10.1002/jcb.26194.
85. Vaidhyanathan, S., Mittapalli, R. K., Sarkaria, J. N. & Elmquist, W. F. Factors influencing the

CNS distribution of a novel MEK-1/2 inhibitor: Implications for combination therapy for melanoma brain metastases. *Drug Metab. Dispos.* **42**, 1292–1300 (2014). doi:10.1124/dmd.114.058339.

86. Essodaïgui, M., Broxterman, H. J. & Garnier-Suillerot, A. Kinetic analysis of calcein and calcein-acetoxymethylester efflux mediated by the multidrug resistance protein and P-glycoprotein. *Biochemistry* **37**, 2243–2250 (1998). doi:10.1021/bi9718043.
87. Palmeira, A. *et al.* New uses for old drugs: Pharmacophore-based screening for the discovery of P-glycoprotein inhibitors. *Chem. Biol. Drug Des.* **78**, 57–72 (2011). doi:10.1111/j.1747-0285.2011.01089.x.
88. Abolhoda, A. *et al.* Rapid Activation of MDR1 Gene Expression in Human Metastatic Sarcoma after in Vivo Exposure to Doxorubicin. *Clin. Cancer Res.* **5**, 3352–3356 (1999).
89. Chevillard, S. *et al.* Sequential assessment of multidrug resistance phenotype and measurement of S-phase fraction as predictive markers of breast cancer response to neoadjuvant chemotherapy. *Cancer* **77**, 292–300 (1996). doi:10.1002/(SICI)1097-0142(19960115)77:2<292::AID-CNCR11>3.0.CO;2-X.
90. van der Zee, A. G. *et al.* Value of P-glycoprotein, glutathione S-transferase pi, c-erbB-2, and p53 as prognostic factors in ovarian carcinomas. *J. Clin. Oncol. Off. J. Am. Soc. Clin. Oncol.* **13**, 70–78 (1995). doi:10.1200/JCO.1995.13.1.70.
91. Patch, A. M. *et al.* Whole-genome characterization of chemoresistant ovarian cancer. *Nature* **521**, 489–494 (2015). doi:10.1038/nature14410.
92. Nakagawa, M. *et al.* Clinical significance of multi-drug resistance associated protein and P-glycoprotein in patients with bladder cancer. *J. Urol.* **157**, 1260–1265 (1997). doi:10.1016/S0022-5347(01)64944-9.
93. Abe, T. *et al.* Expression of multidrug resistance protein gene in patients with glioma after chemotherapy. *J. Neurooncol.* **40**, 11–18 (1998). doi:10.1023/a:1005954406809.
94. Han, K. *et al.* Expression of functional markers in acute nonlymphoblastic leukemia. *Acta Haematol.* **104**, 174–180 (2000). doi:10.1159/000046511.
95. Chauncey, T. R. *et al.* A phase I study of induction chemotherapy for older patients with newly diagnosed acute myeloid leukemia (AML) using mitoxantrone, etoposide, and the MDR modulator PSC 833: A Southwest Oncology Group study 9617. *Leuk. Res.* **24**, 567–574 (2000). doi:10.1016/S0145-2126(00)00024-2.
96. Dai, C. L. *et al.* Lapatinib (Tykerb, GW572016) reverses multidrug resistance in cancer cells by inhibiting the activity of ATP-binding cassette subfamily B member 1 and G member 2. *Cancer Res.* **68**, 7905–7914 (2008). doi:10.1158/0008-5472.CAN-08-0499.
97. Mi, Y. J. *et al.* Apatinib (YN968D1) reverses multidrug resistance by inhibiting the efflux function of multiple ATP-binding cassette transporters. *Cancer Res.* **70**, 7981–7991 (2010). doi:10.1158/0008-5472.CAN-10-0111.
98. Tiwari, A. K. *et al.* Nilotinib (AMN107, Tasigna®) reverses multidrug resistance by inhibiting the activity of the ABCB1/Pgp and ABCG2/BCRP/MXR transporters. *Biochem. Pharmacol.* **78**, 153–161 (2009). doi:10.1016/j.bcp.2009.04.002.
99. Yarden, Y. & Pines, G. The ERBB network: At last, cancer therapy meets systems biology. *Nat. Rev. Cancer* **12**, 553–563 (2012). doi:10.1038/nrc3309.
100. Citri, A., Skaria, K. B. & Yarden, Y. The deaf and the dumb: The biology of ErbB-2 and ErbB-3. *Exp. Cell Res.* **284**, 54–65 (2003). doi:10.1016/S0014-4827(02)00101-5.
101. Shi, F., Telesco, S. E., Liu, Y., Radhakrishnan, R. & Lemmona, M. A. ErbB3/HER3 intracellular domain is competent to bind ATP and catalyze autophosphorylation. *Proc. Natl. Acad. Sci. U. S. A.* **107**, 7692–7697 (2010). doi:10.1073/pnas.1002753107.
102. Arteaga, C. L. & Engelman, J. A. ERBB receptors: From oncogene discovery to basic science to mechanism-based cancer therapeutics. *Cancer Cell* **25**, 282–303 (2014). doi:10.1016/j.ccr.2014.02.025.
103. Roskoski, R. The ErbB/HER family of protein-tyrosine kinases and cancer. *Pharmacol. Res.* **79**, 34–74 (2014). doi:10.1016/j.phrs.2013.11.002.

104. Segers, V. F. M., Dugaucquier, L., Feyen, E., Shakeri, H. & Keulenaer, G. W. The role of ErbB4 in cancer. *Cell. Oncol.* (2020) doi:https://doi.org/10.1007/s13402-020-00499-4. doi:https://doi.org/10.1007/s13402-020-00499-4.
105. Wallasch, C. *et al.* Heregulin-dependent regulation of HER2/neu oncogenic signaling by heterodimerization with HER3. *EMBO J.* **14**, 4267–4275 (1995). doi:10.1002/j.1460-2075.1995.tb00101.x.
106. Black, L. E., Longo, J. F. & Carroll, S. L. Mechanisms of Receptor Tyrosine-Protein Kinase ErbB-3 (ERBB3) Action in Human Neoplasia. *Am. J. Pathol.* **189**, 1898–1912 (2019). doi:10.1016/j.ajpath.2019.06.008.
107. Vaught, D. B. *et al.* HER3 is required for HER2-induced preneoplastic changes to the breast epithelium and tumor formation. *Cancer Res.* **72**, 2672–2682 (2012). doi:10.1158/0008-5472.CAN-11-3594.
108. Lee-Hoeflich, S. T. *et al.* A central role for HER3 in HER2-amplified breast cancer: Implications for targeted therapy. *Cancer Res.* **68**, 5878–5887 (2008). doi:10.1158/0008-5472.CAN-08-0380.
109. Engelman, J. A. *et al.* ErbB-3 mediates phosphoinositide 3-kinase activity in gefitinib-sensitive non-small cell lung cancer cell lines. *Proc. Natl. Acad. Sci. U. S. A.* **102**, 3788–3793 (2005). doi:10.1073/pnas.0409773102.
110. Mattoon, D. R., Lamothe, B., Lax, I. & Schlessinger, J. The docking protein Gab1 is the primary mediator of EGF-stimulated activation of the PI-3K/Akt cell survival pathway. *BMC Biol.* **2**, 1–12 (2004). doi:10.1186/1741-7007-2-24.
111. Turke, A. B. *et al.* Preexistence and Clonal Selection of MET Amplification in EGFR Mutant NSCLC. *Cancer Cell* **17**, 77–88 (2010). doi:10.1016/j.ccr.2009.11.022.
112. Engelman, J. A. Targeting PI3K signalling in cancer: Opportunities, challenges and limitations. *Nat. Rev. Cancer* **9**, 550–562 (2009). doi:10.1038/nrc2664.
113. Vanhaesebroeck, B., Stephens, L. & Hawkins, P. PI3K signalling: The path to discovery and understanding. *Nat. Rev. Mol. Cell Biol.* **13**, 195–203 (2012). doi:10.1038/nrm3290.
114. Wilson, K. J., Gilmore, J. L., Foley, J., Lemmon, M. A. & Riese II, D. J. Functional Selectivity of EGF Family Peptide Growth Factors: Implications for Cancer. *Pharmacol. Ther.* **122**, 1–8 (2009). doi:10.1016/j.pharmthera.2008.11.008.
115. Kaushansky, A. *et al.* System-Wide Investigation of ErbB4 Reveals 19 Sites of Tyr Phosphorylation that Are Unusually Selective in their Recruitment Properties. *Chem. Biol.* **15**, 808–817 (2008). doi:10.1016/j.chembiol.2008.07.006.System-Wide.
116. Maa, M. C., Leu, T. H., Mccarley, D. J., Schatzman, R. C. & Parsons, S. J. Potentiation of epidermal growth factor receptor-mediated oncogenesis by c-Src: Implications for the etiology of multiple human cancers. *Proc. Natl. Acad. Sci. U. S. A.* **92**, 6981–6985 (1995). doi:10.1073/pnas.92.15.6981.
117. Guarino, M. Src signaling in cancer invasion. *J. Cell. Physiol.* **223**, 14–26 (2010). doi:10.1002/jcp.22011.
118. Forget, A. *et al.* Aberrant ERBB4-SRC Signaling as a Hallmark of Group 4 Medulloblastoma Revealed by Integrative Phosphoproteomic Profiling. *Cancer Cell* **34**, 379-395.e7 (2018). doi:10.1016/j.ccell.2018.08.002.
119. Lynch, T. J. *et al.* Activating Mutations in the Epidermal Growth Factor Receptor Underlying Responsiveness of Non–Small-Cell Lung Cancer to Gefitinib. *N. Engl. J. Med.* **350**, 2129–2139 (2004). doi:10.1056/nejmoa040938.
120. Paez, J. G. *et al.* EGFR mutations in lung, cancer: Correlation with clinical response to gefitinib therapy. *Science (80-.).* **304**, 1497–1500 (2004). doi:10.1126/science.1099314.
121. Pao, W. *et al.* EGF receptor gene mutations are common in lung cancers from 'never smokers' and are associated with sensitivity of tumors to gefitinib and erlotinib. *Proc. Natl. Acad. Sci. U. S. A.* **101**, 13306–13311 (2004). doi:10.1073/pnas.0405220101.
122. Mok, T. S. *et al.* Gefitinib or Carboplatin–Paclitaxel in Pulmonary Adenocarcinoma. *N. Engl. J. Med.* **361**, 947–957 (2009). doi:10.1056/nejmoa0810699.

123. Rosell, R. *et al.* Erlotinib versus standard chemotherapy as first-line treatment for European patients with advanced EGFR mutation-positive non-small-cell lung cancer (EURTAC): A multicentre, open-label, randomised phase 3 trial. *Lancet Oncol.* **13**, 239–246 (2012). doi:10.1016/S1470-2045(11)70393-X.
124. Sequist, L. V. *et al.* Phase III study of afatinib or cisplatin plus pemetrexed in patients with metastatic lung adenocarcinoma with EGFR mutations. *J. Clin. Oncol.* **31**, 3327–3334 (2013). doi:10.1200/JCO.2012.44.2806.
125. Slamon, D. J. *et al.* Human breast cancer: Correlation of relapse and survival with amplification of the HER-2/neu oncogene. *Science (80-.).* **235**, 182–191 (1987). doi:10.1126/science.3798106.
126. Beji, A., Horst, D., Engel, J., Kirchner, T. & Ullrich, A. Toward the prognostic significance and therapeutic potential of HER3 receptor tyrosine kinase in human colon cancer. *Clin. Cancer Res.* **18**, 956–968 (2012). doi:10.1158/1078-0432.CCR-11-1186.
127. Maurer, C. A. *et al.* Increased expression of erbB3 in colorectal cancer is associated with concomitant increase in the level of erbB2. *Hum. Pathol.* **29**, 771–777 (1998). doi:10.1016/S0046-8177(98)90444-0.
128. Lee, Y. *et al.* Role of erbB3 receptors in cancer therapeutic resistance. *Acta Biochim. Biophys. Sin. (Shanghai).* **46**, 190–198 (2014). doi:10.1093/abbs/gmt150.
129. Plowman, G. D. *et al.* Ligand-specific activation of HER4/p180erbB4, a fourth member of the epidermal growth factor receptor family. *Proc. Natl. Acad. Sci. U. S. A.* **90**, 1746–1750 (1993). doi:10.1073/pnas.90.5.1746.
130. Elenius, K. *et al.* Characterization of a naturally occurring ErbB4 isoform that does not bind or activate phosphatidyl inositol 3-kinase. *Oncogene* **18**, 2607–2615 (1999). doi:10.1038/sj.onc.1202612.
131. Sawyer, C., Hiles, I., Page, M., Crompton, M. & Dean, C. Two erbB-4 transcripts are expressed in normal breast and in most breast cancers. *Oncogene* **17**, 919–924 (1998). doi:10.1038/sj.onc.1202015.
132. Elenius, K. *et al.* A novel juxtamembrane domain isoform of HER4/ErbB4. Isoform-specific tissue distribution and differential processing in response to phorbol ester. *J. Biol. Chem.* **272**, 26761–26768 (1997). doi:10.1074/jbc.272.42.26761.
133. Veikkolainen, V. *et al.* Function of ERBB4 is determined by alternative splicing. *Cell Cycle* **10**, 2647–2657 (2011). doi:10.4161/cc.10.16.17194.
134. Gilbertson, R. *et al.* Novel ERBB4 juxtamembrane splice variants are frequently expressed in childhood medulloblastoma. *Genes Chromosom. Cancer* **31**, 288–294 (2001). doi:10.1002/gcc.1146.
135. Zeng, N. *et al.* Real-time quantitative polymerase chain reaction (qPCR) analysis with fluorescence resonance energy transfer (FRET) probes reveals differential expression of the four ERBB4 juxtamembrane region variants between medulloblastoma and pilocytic astrocytoma. *Neuropathol. Appl. Neurobiol.* **35**, 353–366 (2009). doi:10.1111/j.1365-2990.2008.01001.x.
136. Gilmour, L. M. *et al.* Expression of erbB-4/HER-4 growth factor receptor isoforms in ovarian cancer. *Cancer Res.* **61**, 2169–2176 (2001).
137. Richards, K. N. *et al.* Signaling of ERBB receptor tyrosine kinases promotes neuroblastoma growth in vitro and in vivo. *Cancer* **116**, 3233–3243 (2010). doi:10.1002/cncr.25073.
138. Sundvall, M. *et al.* Isoform-specific monoubiquitination, endocytosis, and degradation of alternatively spliced ErbB4 isoforms. *Proc. Natl. Acad. Sci. U. S. A.* **105**, 4162–4167 (2008). doi:10.1073/pnas.0708333105.
139. Kainulainen, V. *et al.* A natural ErbB4 isoform that does not activate phosphoinositide 3-kinase mediates proliferation but not survival or chemotaxis. *J. Biol. Chem.* **275**, 8641–8649 (2000). doi:10.1074/jbc.275.12.8641.
140. Rio, C., Buxbaum, J. D., Peschon, J. J. & Corfas, G. Tumor necrosis factor-α-converting enzyme is required for cleavage of erbB4/HER4. *J. Biol. Chem.* **275**, 10379–10387 (2000).

doi:10.1074/jbc.275.14.10379.
141. Ni, C. Y., Murphy, M. P., Golde, T. E. & Carpenter, G. γ-secretase cleavage and nuclear locatization of ErbB-4 receptor tyrosine kinase. *Science (80-.).* **294**, 2179–2181 (2001). doi:10.1126/science.1065412.
142. Lee, H. J. *et al.* Presenilin-dependent γ-secretase-like intramembrane cleavage of ErbB4. *J. Biol. Chem.* **277**, 6318–6323 (2002). doi:10.1074/jbc.M110371200.
143. Komuro, A., Nagai, M., Navin, N. E. & Sudol, M. WW domain-containing protein YAP associates with ErbB-4 and acts as a co-transcriptional activator for the carboxyl-terminal fragment of ErbB-4 that translocates to the nucleus. *J. Biol. Chem.* **278**, 33334–33341 (2003). doi:10.1074/jbc.M305597200.
144. Williams, C. C. *et al.* The ERBB4/HER4 receptor tyrosine kinase regulates gene expression by functioning as a STAT5A nuclear chaperone. *J. Cell Biol.* **167**, 469–478 (2004). doi:10.1083/jcb.200403155.
145. Han, W., Sfondouris, M. E. & Jones, F. E. Direct coupling of the HER4 intracellular domain (4ICD) and STAT5A signaling is required to induce mammary epithelial cell differentiation. *Biochem. Biophys. Reports* **7**, 323–327 (2016). doi:10.1016/j.bbrep.2016.07.015.
146. Linggi, B. & Carpenter, G. ErbB-4 s80 intracellular domain abrogates ETO2-dependent transcriptional repression. *J. Biol. Chem.* **281**, 25373–25380 (2006). doi:10.1074/jbc.M603998200.
147. Sundvall, M. *et al.* Cell death or survival promoted by alternative isoforms of ErbB4. *Mol. Biol. Cell* **21**, 4275–4286 (2010). doi:10.1091/mbc.E10-04-0332.
148. Ishibashi, K. *et al.* Nuclear ErbB4 signaling through H3K9me3 is antagonized by EGFR-activated c-Src. *J. Cell Sci.* **126**, 625–637 (2013). doi:10.1242/jcs.116277.
149. Naresh, A. *et al.* The ERBB4/HER4 intracellular domain 4ICD is a BH3-only protein promoting apoptosis of breast cancer cells. *Cancer Res.* **66**, 6412–6420 (2006). doi:10.1158/0008-5472.CAN-05-2368.
150. Tidcombe, H. *et al.* Neural and mammary gland defects in Erbb4 knockout mice genetically rescued from embryonic lethality. *Proc. Natl. Acad. Sci. U. S. A.* **100**, 8281–8286 (2003). doi:10.1073/pnas.1436402100.
151. Schroeder, J. A. & Lee, D. C. Dynamic expression and activation of ERBB receptors in the developing mouse mammary gland. *Cell Growth Differ.* **9**, 451–464 (1998).
152. Muraoka-Cook, R. S., Feng, S. M., Strunk, K. E. & Earp, S. H. ErbB4/HER4: Role in mammary gland development, differentiation and growth inhibition. *J. Mammary Gland Biol. Neoplasia* **13**, 235–246 (2008). doi:10.1007/s10911-008-9080-x.
153. Vermeulen, Z. *et al.* Inhibitory actions of the NRG-1/ErbB4 pathway in macrophages during tissue fibrosis in the heart, skin, and lung. *Am. J. Physiol. - Hear. Circ. Physiol.* **313**, H934–H945 (2017). doi:10.1152/ajpheart.00206.2017.
154. Schumacher, M. A. *et al.* ErbB4 signaling stimulates pro-inflammatory macrophage apoptosis and limits colonic inflammation. *Cell Death Dis.* **8**, e2622-12 (2017). doi:10.1038/cddis.2017.42.
155. Deng, C., Pan, B., Engel, M. & Huang, X. F. Neuregulin-1 signalling and antipsychotic treatment: Potential therapeutic targets in a schizophrenia candidate signalling pathway. *Psychopharmacology (Berl).* **226**, 201–215 (2013). doi:10.1007/s00213-013-3003-2.
156. Thybusch-Bernhardt, A., Beckmann, S. & Juhl, H. Comparative analysis of the EGF-receptor family in pancreatic cancer: expression of HER-4 correlates with a favourable tumor stage. *Int. J. Surg. Investig.* **2**, 393–400 (2001).
157. Liu, Y. *et al.* ERBB4 acts as a suppressor in the development of hepatocellular carcinoma. *Carcinogenesis* **38**, 465–473 (2017). doi:10.1093/carcin/bgx017.
158. Prickett, T. D. *et al.* Analysis of the tyrosine kinome in melanoma reveals recurrent mutations in ERBB4. *Nat. Genet.* **41**, 1127–1132 (2009). doi:10.1038/ng.438.
159. Singh, R., Letai, A. & Sarosiek, K. Regulation of apoptosis in health and disease: the balancing act of BCL-2 family proteins. *Nat. Rev. Mol. Cell Biol.* **20**, 175–193 (2019). doi:10.1038/s41580-

018-0089-8.
160. Kerr, J. F. R., Wyllie, A. H. & Currie, A. R. Apoptosis: A basic biological phenomenon with wide-ranging implications in human disease. *Br. J. Cancer* **26**, 239–257 (1972).
161. Galluzzi, L. *et al.* Molecular mechanisms of cell death: recommendations of the Nomenclature Committee on Cell Death 2018. *Cell Death Differ.* (2018) doi:10.1038/s41418-017-0012-4. doi:10.1038/s41418-017-0012-4.
162. Carr, J. *et al.* Increased frequency of aberrations in the p53/MDM2/p14ARF pathway in neuroblastoma cell lines established at relapse. *Cancer Res.* **66**, 2138–2145 (2006). doi:10.1158/0008-5472.CAN-05-2623.
163. Keshelava, N. *et al.* Loss of p53 function confers high-level multidrug resistance in neuroblastoma cell lines. *Cancer Res.* **61**, 6185–6193 (2001).
164. Tweddle, D. A., Malcolm, A. J., Bown, N., Pearson, A. D. J. & Lunec, J. Evidence for the Development of p53 Mutations after Cytotoxic Therapy in a Neuroblastoma Cell Line. *Cancer Res.* **61**, 8–13 (2001).
165. Maris, J. M., Hogarty, M. D., Bagatell, R. & Cohn, S. L. Neuroblastoma. *Lancet* **369**, 2106–2120 (2007). doi:10.1016/S0140-6736(07)60983-0.
166. Kabiraj, P. *et al.* The Neuroprotective Role of Ferrostatin-1 Under Rotenone-Induced Oxidative Stress in Dopaminergic Neuroblastoma Cells. *Protein J.* **34**, 349–358 (2015). doi:10.1007/s10930-015-9629-7.
167. Hassannia, B., Vandenabeele, P. & Vanden Berghe, T. Nano-targeted induction of dual ferroptotic mechanisms eradicates high-risk neuroblastoma Graphical abstract The Journal of Clinical Investigation. *J Clin Invest* **128**, 3341–3355 (2018). doi:10.1172/JCI99032.
168. Geng, N. *et al.* Knockdown of ferroportin accelerates erastin-induced ferroptosis in neuroblastoma cells. *Eur. Rev. Med. Pharmacol. Sci.* **22**, 3826–3836 (2021). doi:10.26355/eurrev_201806_15267.
169. Floros, K. V. *et al.* MYCN -amplified neuroblastoma is addicted to iron and vulnerable to inhibition of the system xc-/glutathione axis. *Cancer Res.* **81**, 1896–1908 (2021). doi:10.1158/0008-5472.CAN-20-1641.
170. Pihán, P., Carreras-Sureda, A. & Hetz, C. BCL-2 family: Integrating stress responses at the ER to control cell demise. *Cell Death Differ.* **24**, 1478–1487 (2017). doi:10.1038/cdd.2017.82.
171. Brumatti, G., Salmanidis, M. & Ekert, P. G. Crossing paths: Interactions between the cell death machinery and growth factor survival signals. *Cell. Mol. Life Sci.* **67**, 1619–1630 (2010). doi:10.1007/s00018-010-0288-8.
172. Moldoveanu, T., Follis, A. V., Kriwacki, R. W. & Green, D. R. Many players in BCL-2 family affairs. *Trends Biochem. Sci.* **39**, 101–111 (2014). doi:10.1016/j.tibs.2013.12.006.
173. Tait, S. W. G. & Green, D. R. Mitochondria and cell death: Outer membrane permeabilization and beyond. *Nat. Rev. Mol. Cell Biol.* **11**, 621–632 (2010). doi:10.1038/nrm2952.
174. Harenza, J. L. *et al.* Transcriptomic profiling of 39 commonly used neuroblastoma cell lines. *Sci. Data* **4**, 1–8 (2017). doi:10.1038/sdata.2017.33.
175. Edlich, F. *et al.* Bcl-xL retrotranslocates Bax from the mitochondria into the cytosol. *Cell* **145**, 104–116 (2011). doi:10.1016/j.cell.2011.02.034.
176. Schellenberg, B. *et al.* Bax Exists in a Dynamic Equilibrium between the Cytosol and Mitochondria to Control Apoptotic Priming. *Mol. Cell* **49**, 959–971 (2013). doi:10.1016/j.molcel.2012.12.022.
177. Li, P. *et al.* Cytochrome c and dATP-dependent formation of Apaf-1/caspase-9 complex initiates an apoptotic protease cascade. *Cell* **91**, 479–489 (1997). doi:10.1016/S0092-8674(00)80434-1.
178. Du, C., Fang, M., Li, Y., Li, L. & Wang, X. Smac, a mitochondrial protein that promotes cytochrome c-dependent caspase activation by eliminating IAP inhibition. *Cell* **102**, 33–42 (2000). doi:10.1016/S0092-8674(00)00008-8.
179. Strasser, A., Jost, P. J. & Nagata, S. The Many Roles of FAS Receptor Signaling in the Immune System. *Immunity* **30**, 180–192 (2009). doi:10.1016/j.immuni.2009.01.001.

180. Gibert, B. & Mehlen, P. Dependence receptors and cancer: Addiction to trophic ligands. *Cancer Res.* **75**, 5171–5175 (2015). doi:10.1158/0008-5472.CAN-14-3652.
181. Negulescu, A. M. & Mehlen, P. Dependence receptors – the dark side awakens. *FEBS J.* **285**, 3909–3924 (2018). doi:10.1111/febs.14507.
182. Dickens, L. S., Powley, I. R., Hughes, M. A. & MacFarlane, M. The 'complexities' of life and death: Death receptor signalling platforms. *Exp. Cell Res.* **318**, 1269–1277 (2012). doi:10.1016/j.yexcr.2012.04.005.
183. Sprick, M. R. *et al.* Caspase-10 is recruited to and activated at the native TRAIL and CD95 death-inducing signalling complexes in a FADD-dependent manner but can not functionally substitute caspase-8. *EMBO J.* **21**, 4520–4530 (2002). doi:10.1093/emboj/cdf441.
184. Wachmann, K. *et al.* Activation and Specificity of human Caspase-10. *Biochemistry* **49**, 8307–8315 (2010). doi:10.1021/bi100968m.Activation.
185. Shelton, S. N., Shawgo, M. E. & Robertson, J. D. Cleavage of Bid by executioner caspases mediates feed forward amplification of mitochondrial outer membrane permeabilization during genotoxic stress-induced apoptosis in Jurkat cells. *J. Biol. Chem.* **284**, 11247–11255 (2009). doi:10.1074/jbc.M809392200.
186. Kim, W. S. *et al.* The caspase-8/Bid/cytochrome c axis links signals from death receptors to mitochondrial reactive oxygen species production. *Free Radic. Biol. Med.* **112**, 567–577 (2017). doi:10.1016/j.freeradbiomed.2017.09.001.
187. Li, H., Zhu, H., Xu, C.-J. & Yuan, J. Cleavage of BID by Caspase 8 Mediates the Mitochondrial Damage in the Fas Pathway of Apoptosis. *Cell* **94**, 491–501 (1998). doi:10.1016/S0092-8674(00)81590-1.
188. Luo, X., Budihardjo, I., Zou, H., Slaughter, C. & Wang, X. Bid, a Bcl2 interacting protein, mediates cytochrome c release from mitochondria in response to activation of cell surface death receptors. *Cell* **94**, 481–490 (1998). doi:10.1016/S0092-8674(00)81589-5.
189. Agard, N. J. *et al.* Global kinetic analysis of proteolysis via quantitative targeted proteomics. *Proc. Natl. Acad. Sci. U. S. A.* **109**, 1913–1918 (2012). doi:10.1073/pnas.1117158109.
190. D'Amours, D., Sallmann, F. R., Dixit, V. M. & Poirier, G. G. Gain-of-function of poly(ADP-ribose) polymerase-1 upon cleavage by apoptotic proteases: implications for apoptosis. *J. Cell Sci.* **114**, 3771–3778 (2001).
191. Green, D. R., Oguin, T. H. & Martinez, J. The clearance of dying cells: Table for two. *Cell Death Differ.* **23**, 915–926 (2016). doi:10.1038/cdd.2015.172.
192. Berghe, T. Vanden *et al.* Necroptosis, necrosis and secondary necrosis converge on similar cellular disintegration features. *Cell Death Differ.* **17**, 922–930 (2010). doi:10.1038/cdd.2009.184.
193. Dixon, S. J. *et al.* Ferroptosis: An iron-dependent form of nonapoptotic cell death. *Cell* **149**, 1060–1072 (2012). doi:10.1016/j.cell.2012.03.042.
194. Dixon, S. J. & Stockwell, B. R. The Hallmarks of Ferroptosis. *Annu. Rev. Cancer Biol.* **3**, 35–54 (2019). doi:10.1146/annurev-cancerbio-030518-055844.
195. Kagan, V. E. *et al.* Oxidized arachidonic and adrenic PEs navigate cells to ferroptosis. *Nat. Chem. Biol.* **13**, 81–90 (2017). doi:10.1038/nchembio.2238.
196. Gaschler, M. M. & Stockwell, B. R. Lipid peroxidation in cell death. *Biochem. Biophys. Res. Commun.* **482**, 419–425 (2017). doi:10.1016/j.bbrc.2016.10.086.
197. Skouta, R. *et al.* Ferrostatins inhibit oxidative lipid damage and cell death in diverse disease models. *J. Am. Chem. Soc.* **136**, 4551–4556 (2014). doi:10.1021/ja411006a.
198. Yang, W. S. *et al.* Peroxidation of polyunsaturated fatty acids by lipoxygenases drives ferroptosis. *Proc. Natl. Acad. Sci. U. S. A.* **113**, E4966–E4975 (2016). doi:10.1073/pnas.1603244113.
199. Seiler, A. *et al.* Glutathione Peroxidase 4 Senses and Translates Oxidative Stress into 12/15-Lipoxygenase Dependent- and AIF-Mediated Cell Death. *Cell Metab.* **8**, 237–248 (2008). doi:10.1016/j.cmet.2008.07.005.
200. Torii, S. *et al.* An essential role for functional lysosomes in ferroptosis of cancer cells. *Biochem.*

J. **473**, 769–777 (2016). doi:10.1042/BJ20150658.
201. Kurz, T., Gustafsson, B. & Brunk, U. T. Intralysosomal iron chelation protects against oxidative stress-induced cellular damage. *FEBS J.* **273**, 3106–3117 (2006). doi:10.1111/j.1742-4658.2006.05321.x.
202. Feng, H. & Stockwell, B. R. Unsolved mysteries: How does lipid peroxidation cause ferroptosis? *PLOS Biol.* **4**, 1–15 (2018). doi:10.1371/journal.pbio.2006203.
203. Abeysinghe, R. D. *et al.* The environment of the lipoxygenase iron binding site explored with novel hydroxypyridinone iron chelators. *J. Biol. Chem.* **271**, 7965–7972 (1996). doi:10.1074/jbc.271.14.7965.
204. Winterbourn, C. C. Toxicity of iron and hydrogen peroxide: the Fenton reaction. *Toxicol. Lett.* **82**–**83**, 969–974 (1995). doi:10.1016/0378-4274(95)03532-X.
205. Stockwell, B. R. *et al.* Ferroptosis: A Regulated Cell Death Nexus Linking Metabolism, Redox Biology, and Disease. *Cell* **171**, 273–285 (2017). doi:10.1016/j.cell.2017.09.021.
206. Gao, M., Monian, P., Quadri, N., Ramasamy, R. & Jiang, X. Glutaminolysis and Transferrin Regulate Ferroptosis. *Mol. Cell* **59**, 298–308 (2015). doi:10.1016/j.molcel.2015.06.011.
207. Yang, W. S. & Stockwell, B. R. Synthetic Lethal Screening Identifies Compounds Activating Iron-Dependent, Nonapoptotic Cell Death in Oncogenic-RAS-Harboring Cancer Cells. *Chem. Biol.* **15**, 234–245 (2008). doi:10.1016/j.chembiol.2008.02.010.
208. Ursini, F., Maiorino, M. & Gregolin, C. The selenoenzyme phospholipid hydroperoxide glutathione peroxidase. *BBA - Gen. Subj.* **839**, 62–70 (1985). doi:10.1016/0304-4165(85)90182-5.
209. Ingold, I. *et al.* Selenium Utilization by GPX4 Is Required to Prevent Hydroperoxide-Induced Ferroptosis. *Cell* **172**, 409-422.e21 (2018). doi:10.1016/j.cell.2017.11.048.
210. Yang, W. S. *et al.* Regulation of ferroptotic cancer cell death by GPX4. *Cell* **156**, 317–331 (2014). doi:10.1016/j.cell.2013.12.010.
211. Friedmann Angeli, J. P. *et al.* Inactivation of the ferroptosis regulator Gpx4 triggers acute renal failure in mice. *Nat. Cell Biol.* **16**, 1180–1191 (2014). doi:10.1038/ncb3064.
212. Dixon, S. J. *et al.* Pharmacological inhibition of cystine-glutamate exchange induces endoplasmic reticulum stress and ferroptosis. *Elife* **2014**, 1–25 (2014). doi:10.7554/eLife.02523.
213. Viswanathan, V. S. *et al.* Dependency of a therapy-resistant state of cancer cells on a lipid peroxidase pathway. *Nature* **547**, 453–457 (2017). doi:10.1038/nature23007.
214. Matsushita, M. *et al.* T cell lipid peroxidation induces ferroptosis and prevents immunity to infection. *J. Exp. Med.* **212**, 555–568 (2015). doi:10.1084/jem.20140857.
215. Cao, J. Y. & Dixon, S. J. Mechanisms of ferroptosis. *Cell. Mol. Life Sci.* **73**, 2195–2209 (2016). doi:10.1007/s00018-016-2194-1.
216. Wang, L. *et al.* High-Throughput Functional Genetic and Compound Screens Identify Targets for Senescence Induction in Cancer. *Cell Rep.* **21**, 773–783 (2017). doi:10.1016/j.celrep.2017.09.085.
217. Schlesinger, H. R., Gerson, J. M., Moorhead, P. S., Maguire, H. & Hummeler, K. Establishment and Characterization of Human Neuroblastoma Cell Lines. *Cancer Res.* **36**, 3094–3100 (1976).
218. Thiele, C. J. Neuroblastoma Cell Lines -- Molecular Features.pdf. in *Kluwer Academic Publishers* (ed. Masters, J.) vol. 1 21–53 (Kluwer Academic Publishers, 1998).
219. Tumilowicz, J. J., Nichols, W. W., Cholon, J. J. & Greene, A. E. Definition of a continuous human cell line derived from neuroblastoma. *Cancer Res.* **30**, 2110–2118 (1970).
220. De Brouwer, S. *et al.* Meta-analysis of neuroblastomas reveals a skewed ALK mutation spectrum in tumors with MYCN amplification. *Clin. Cancer Res.* **16**, 4353–4362 (2010). doi:10.1158/1078-0432.CCR-09-2660.
221. Shen, J. *et al.* A kinome-wide RNAi screen identifies ALK as a target to sensitize neuroblastoma cells for HDAC8-inhibitor treatment. *Cell Death Differ.* 1–18 (2018) doi:10.1038/s41418-018-0080-0. doi:10.1038/s41418-018-0080-0.
222. COG Cell Line & Xenograft Repository. LA-N-5 Cell Line Data Sheet. 1–4

https://www.cccells.org/dl/NB_Data_Sheets/LA-N-5_Cell_Line_Data_Sheet_COGcell_org.pdf.
223. Pietsch, T. *et al.* Characterization of a continuous cell line (MHH-NB-11) derived from advanced neuroblastoma. *Anticancer Res.* **8**, 1329–1333 (1988).
224. Imashuku, S., Inui, A., Nakamura, T., Tanaka, J. & Miyake, S. Catecholamine metabolism in tissue culture cells of a neuroblastoma. *J. Clin. Endocrinol. Metab.* **36**, 931–936 (1973). doi:10.1210/jcem-36-5-931.
225. Kondo, T., Oka, T., Sato, H., Shinnou, Y. & Washio, K. MYCN downregulates integrin α1 to promote invasion of human neuroblastoma cells. *Int. J. Oncol.* **33**, 815–821 (2008). doi:10.3892/ijo_00000069.
226. Kolbinger, F. R. *et al.* The HDAC6/8/10 inhibitor TH34 induces DNA damage-mediated cell death in human high-grade neuroblastoma cell lines. *Arch. Toxicol.* **0**, 0 (2018). doi:10.1007/s00204-018-2234-8.
227. Brodeur, G. M. *et al.* Cytogenetic Features of Human Neuroblastomas and Cell Lines. *Cancer Res.* **41**, 4678–4686 (1981).
228. Brodeur, G. M., Sekhin, G. S. & Goldstein, M. N. Chromosomal aberrations in human neuroblastomas. *Cancer* **40**, 2256–2263 (1977). doi:10.1002/1097-0142(197711)40:5<2256::aid-cncr2820400536>3.0.co;2-1.
229. Marini, P. *et al.* SiMa, a new neuroblastoma cell line combining poor prognostic cytogenetic markers with high adrenergic differentiation. *Cancer Genet. Cytogenet.* **112**, 161–164 (1999). doi:10.1016/S0165-4608(98)00269-6.
230. Schachner, M. & Freedman, L. S. Multiple Neurotransmitter Synthesis by Human Neuroblastoma Cell Lines and Clones. *Cancer Res.* 3751–3757 (1978).
231. DepMap 20Q1 Public. *Broad Institute* https://figshare.com/articles/DepMap_20Q1_Public/11791698/2 (2020) doi:10.6084/m9.figshare.11791698.v2. doi:10.6084/m9.figshare.11791698.v2.
232. Reynolds, C. P. *et al.* Characterization of human neuroblastoma cell lines established before and after therapy. *J. Natl. Cancer Inst.* **76**, 375–87 (1986).
233. R2: Genomics Analysis and Visualization Platform (http://r2.amc.nl).
234. Fabregat, A. *et al.* The reactome pathway knowledgebase. *Nucleic Acids Res.* **44**, D481–D487 (2016). doi:10.1093/nar/gkv1351.
235. Worst, B. C. *et al.* Next-generation personalised medicine for high-risk paediatric cancer patients - The INFORM pilot study. *Eur. J. Cancer* **65**, 91–101 (2016). doi:10.1016/j.ejca.2016.06.009.
236. van Tilburg, C. M. *et al.* The pediatric precision oncology INFORM registry: clinical outcome and benefit for patients with very high-evidence targets. *Cancer Discov.* candisc.0094.2021 (2021) doi:10.1158/2159-8290.cd-21-0094. doi:10.1158/2159-8290.cd-21-0094.
237. Pajtler, K. W. *et al.* Molecular Classification of Ependymal Tumors across All CNS Compartments, Histopathological Grades, and Age Groups. *Cancer Cell* **27**, 728–743 (2015). doi:10.1016/j.ccell.2015.04.002.
238. Molenaar, J. J. *et al.* Sequencing of neuroblastoma identifies chromothripsis and defects in neuritogenesis genes. *Nature* **483**, 589–593 (2012). doi:10.1038/nature10910.
239. Kobayashi, E. *et al.* Reduced Argininosuccinate Synthetase Is a Predictive Biomarker for the Development of Pulmonary Metastasis in Patients with Osteosarcoma. *Mol. Cancer Ther.* **9**, 535–544 (2010). doi:10.1158/1535-7163.MCT-09-0774.
240. Sun, W. *et al.* Distinct methylation profiles characterize fusion-positive and fusion-negative rhabdomyosarcoma. *Mod. Pathol.* **28**, 1214–1224 (2015). doi:10.1038/modpathol.2015.82.
241. Schramm, A. *et al.* Mutational dynamics between primary and relapse neuroblastomas. *Nat. Genet.* **47**, 872–877 (2015). doi:10.1038/ng.3349.
242. Cole, K. A. *et al.* RNAi screen of the protein kinome identifies checkpoint kinase 1 (CHK1) as a therapeutic target in neuroblastoma. *Proc. Natl. Acad. Sci. U. S. A.* **108**, 3336–3341 (2011). doi:10.1073/pnas.1012351108.
243. Barretina, J. *et al.* The Cancer Cell Line Encyclopedia enables predictive modelling of

anticancer drug sensitivity. *Nature* **483**, 603–607 (2012). doi:10.1038/nature11003.
244. Utnes, P., Løkke, C., Flægstad, T. & Einvik, C. Clinically Relevant Biomarker Discovery in High-Risk Recurrent Neuroblastoma. *Cancer Inform.* **18**, 117693511983291 (2019). doi:10.1177/1176935119832910.
245. Hong, F. *et al.* RankProd: A bioconductor package for detecting differentially expressed genes in meta-analysis. *Bioinformatics* **22**, 2825–2827 (2006). doi:10.1093/bioinformatics/btl476.
246. Del Carratore, F. *et al.* RankProd 2.0: a refactored bioconductor package for detecting differentially expressed features in molecular profiling datasets. *Bioinformatics* **33**, 2774–2775 (2017). doi:10.1093/bioinformatics/btx292.
247. Schmitt, M. & Pawlita, M. High-throughput detection and multiplex identification of cell contaminations. *Nucleic Acids Res.* **37**, (2009). doi:10.1093/nar/gkp581.
248. Michaelis, M. *et al.* Adaptation of cancer cells from different entities to the MDM2 inhibitor nutlin-3 results in the emergence of p53-mutated multi-drug-resistant cancer cells. *Cell Death Dis.* **2**, (2011). doi:10.1038/cddis.2011.129.
249. Michaelis, M., Wass, M. N. & Cinatl, J. Drug-adapted cancer cell lines as preclinical models of acquired resistance. *Cancer Drug Resist.* **2**, 447–456 (2019). doi:10.20517/cdr.2019.005.
250. Livak, K. J. & Schmittgen, T. D. Analysis of relative gene expression data using real-time quantitative PCR and the 2-ΔΔCT method. *Methods* **25**, 402–408 (2001). doi:10.1006/meth.2001.1262.
251. Fischer, M., Skowron, M. & Berthold, F. Reliable transcript quantification by real-time reverse transcriptase-polymerase chain reaction in primary neuroblastoma using normalization to averaged expression levels of the control genes HPRT1 and SDHA. *J. Mol. Diagnostics* **7**, 89–96 (2005). doi:10.1016/S1525-1578(10)60013-X.
252. Ianevski, A., Giri, A. K. & Aittokallio, T. SynergyFinder 2.0: Visual analytics of multi-drug combination synergies. *Nucleic Acids Res.* **48**, W488–W493 (2021). doi:10.1093/NAR/GKAA216.
253. Rösch, L. *et al.* ERBB and P-glycoprotein inhibitors break resistance in relapsed neuroblastoma models through P-glycoprotein. *Mol. Oncol.* **n/a**, (2022). doi:https://doi.org/10.1002/1878-0261.13318.
254. Fox, E. *et al.* Pharmacokinetic and pharmacodynamic study of tariquidar (XR9576), a P-glycoprotein inhibitor, in combination with doxorubicin, vinorelbine, or docetaxel in children and adolescents with refractory solid tumors. *Cancer Chemother. Pharmacol.* **76**, 1273–1283 (2015). doi:10.1007/s00280-015-2845-1.
255. Letai, A., Bhola, P. & Welm, A. L. Functional precision oncology: Testing tumors with drugs to identify vulnerabilities and novel combinations. *Cancer Cell* **40**, 26–35 (2022). doi:10.1016/j.ccell.2021.12.004.
256. Korshunov, A. *et al.* Molecular staging of intracranial ependymoma in children and adults. *J. Clin. Oncol.* **28**, 3182–3190 (2010). doi:10.1200/JCO.2009.27.3359.
257. Pajtler, K. W. *et al.* Molecular Classification of Ependymal Tumors across All CNS Compartments, Histopathological Grades, and Age Groups. *Cancer Cell* **27**, 728–743 (2015). doi:10.1016/j.ccell.2015.04.002.
258. Ostrom, Q. T. *et al.* CBTRUS statistical Report: primary brain and central nervous system tumors diagnosed in the United States in 2008-2012. *Neuro. Oncol.* **17**, iv1–iv62 (2015). doi:10.1093/neuonc/nov189.
259. Schwartzentruber, J. *et al.* Driver mutations in histone H3.3 and chromatin remodelling genes in paediatric glioblastoma. *Nature* **482**, 226–231 (2012). doi:10.1038/nature10833.
260. Wu, G. *et al.* Somatic histone H3 alterations in pediatric diffuse intrinsic pontine gliomas and non-brainstem glioblastomas. *Nat. Genet.* **44**, 251–253 (2012). doi:10.1038/ng.1102.
261. Mackay, A. *et al.* Integrated Molecular Meta-Analysis of 1,000 Pediatric High-Grade and Diffuse Intrinsic Pontine Glioma. *Cancer Cell* **32**, 520-537.e5 (2017). doi:10.1016/j.ccell.2017.08.017.
262. Kansara, M., Teng, M. W., Smyth, M. J. & Thomas, D. M. Translational biology of

osteosarcoma. *Nat. Rev. Cancer* **14**, 722–735 (2014). doi:10.1038/nrc3838.
263. Kempf-Bielack, B. *et al.* Osteosarcoma relapse after combined modality therapy: An analysis of unselected patients in the Cooperative Osteosarcoma Study Group (COSS). *J. Clin. Oncol.* **23**, 559–568 (2005). doi:10.1200/JCO.2005.04.063.
264. Leiner, J. & Le Loarer, F. The current landscape of rhabdomyosarcomas: an update. *Virchows Arch.* **476**, 97–108 (2020). doi:10.1007/s00428-019-02676-9.
265. Li, Q. *et al.* CDK1 and CCNB1 as potential diagnostic markers of rhabdomyosarcoma: Validation following bioinformatics analysis. *BMC Med. Genomics* **12**, 1–13 (2019). doi:10.1186/s12920-019-0645-x.
266. Yogev, O. *et al.* In vivo modeling of chemoresistant neuroblastoma provides new insights into chemorefractory disease and metastasis. *Cancer Res.* **79**, 5382–5393 (2019). doi:10.1158/0008-5472.CAN-18-2759.
267. Hua, Y. *et al.* Slow down to stay alive: HER4 protects against cellular stress and confers chemoresistance in neuroblastoma. *Cancer* **118**, 5140–5154 (2012). doi:10.1002/cncr.27496.
268. Ho, R. *et al.* Proliferation of human neuroblastomas mediated by the epidermal growth factor receptor. *Cancer Res.* **65**, 9868–9875 (2005). doi:10.1158/0008-5472.CAN-04-2426.
269. Varlet, P. *et al.* Comprehensive analysis of the ErbB receptor family in pediatric nervous system tumors and rhabdomyosarcoma. *Pediatr. Blood Cancer* **69**, 1–11 (2022). doi:10.1002/pbc.29316.
270. Izycka-Swieszewska, E. *et al.* Expression and significance of HER family receptors in neuroblastic tumors. *Clin. Exp. Metastasis* **28**, 271–282 (2011). doi:10.1007/s10585-010-9369-1.
271. Redaelli, S. *et al.* Lorlatinib treatment elicits multiple on- and off-target mechanisms of resistance in ALK-driven cancer. *Cancer Res.* **78**, 6866–6880 (2018). doi:10.1158/0008-5472.CAN-18-1867.
272. Roskoski, R. Small molecule inhibitors targeting the EGFR/ErbB family of protein-tyrosine kinases in human cancers. *Pharmacol. Res.* **139**, 395–411 (2019). doi:10.1016/j.phrs.2018.11.014.
273. Wang, S. Q. *et al.* Afatinib reverses multidrug resistance in ovarian cancer via dually inhibiting ATP binding cassette subfamily B member 1. *Oncotarget* **6**, 26142–26160 (2015). doi:10.18632/oncotarget.4536.
274. Rusnak, D. W. *et al.* The effects of the novel, reversible epidermal growth factor receptor/ErbB-2 tyrosine kinase inhibitor, GW2016, on the growth of human normal and tumor-derived cell lines in vitro and in vivo. *Mol. Cancer Ther.* **1**, 85–94 (2001). doi:10.1158/1535-7163.MCT-11-0697.
275. Radic-Sarikas, B. *et al.* Lapatinib potentiates cytotoxicity of YM155 in neuroblastoma via inhibition of the ABCB1 efflux transporter. *Sci. Rep.* **7**, 1–8 (2017). doi:10.1038/s41598-017-03129-6.
276. Harrington, L. S., Findlay, G. M. & Lamb, R. F. Restraining PI3K: mTOR signalling goes back to the membrane. *Trends Biochem. Sci.* **30**, 35–42 (2005). doi:10.1016/j.tibs.2004.11.003.
277. Liu, Y. *et al.* Dual mTOR/PI3K inhibition limits PI3K-dependent pathways activated upon mTOR inhibition in autosomal dominant polycystic kidney disease. *Sci. Rep.* **8**, 1–8 (2018). doi:10.1038/s41598-018-22938-x.
278. Jin, T. *et al.* RAF inhibitors promote RAS-RAF interaction by allosterically disrupting RAF autoinhibition. *Nat. Commun.* **8**, (2017). doi:10.1038/s41467-017-01274-0.
279. Sturm, O. E. *et al.* The mammalian MAPK/ERK pathway exhibits properties of a negative feedback amplifier. *Sci. Signal.* **3**, 1–8 (2010). doi:10.1126/scisignal.2001212.
280. Zhang, J. guang *et al.* MicroRNA-21 (miR-21) represses tumor suppressor PTEN and promotes growth and invasion in non-small cell lung cancer (NSCLC). *Clin. Chim. Acta* **411**, 846–852 (2010). doi:10.1016/j.cca.2010.02.074.
281. Meng, F. *et al.* MicroRNA-21 Regulates Expression of the PTEN Tumor Suppressor Gene in Human Hepatocellular Cancer. *Gastroenterology* **133**, 647–658 (2007).

doi:10.1053/j.gastro.2007.05.022.
282. Ferrara, M. G. *et al.* PTEN Loss as a Predictor of Tumor Heterogeneity and Poor Prognosis in Patients With EGFR-mutant Advanced Non–small-cell Lung Cancer Receiving Tyrosine Kinase Inhibitors. *Clin. Lung Cancer* **22**, 351–360 (2021). doi:10.1016/j.cllc.2020.12.008.
283. Shao, C., Li, Z., Ahmad, N. & Liu, X. Regulation of PTEN degradation and NEDD4–1 E3 ligase activity by Numb. *Cell Cycle* **16**, 957–967 (2017). doi:10.1080/15384101.2017.1310351.
284. Hölzel, M. *et al.* NF1 Is a Tumor Suppressor in Neuroblastoma that Determines Retinoic Acid Response and Disease Outcome. *Cell* **142**, 218–229 (2010). doi:10.1016/j.cell.2010.06.004.
285. Dohse, M. *et al.* Comparison of ATP-binding cassette transporter interactions with the tyrosine kinase inhibitors imatinib, nilotinib, and dasatinib. *Drug Metab. Dispos.* **38**, 1371–1380 (2010). doi:10.1124/dmd.109.031302.
286. Hegedus, C. *et al.* Interaction of nilotinib, dasatinib and bosutinib with ABCB1 and ABCG2: Implications for altered anti-cancer effects and pharmacological properties. *Br. J. Pharmacol.* **158**, 1153–1164 (2009). doi:10.1111/j.1476-5381.2009.00383.x.
287. De Gooijer, M. C. *et al.* Buparlisib is a brain penetrable pan-PI3K inhibitor. *Sci. Rep.* **8**, 1–8 (2018). doi:10.1038/s41598-018-29062-w.
288. Ghayad, S. E. *et al.* Endocrine resistance associated with activated ErbB system in breast cancer cells is reversed by inhibiting MAPK or PI3K/Akt signaling pathways. *Int. J. Cancer* **126**, 545–562 (2010). doi:10.1002/ijc.24750.
289. Porro, A. *et al.* Direct and coordinate regulation of ATP-binding cassette transporter genes by Myc factors generates specific transcription signatures that significantly affect the chemoresistance phenotype of cancer cells. *J. Biol. Chem.* **285**, 19532–19543 (2010). doi:10.1074/jbc.M109.078584.
290. Bénard, J. *et al.* Prognostic value of MDR1 gene expression in neuroblastoma: results of a multivariate analysis. *Prog. Clin. Biol. Res.* **385**, 111–116 (1994).
291. Dhooge, C. R. M. *et al.* Expression of the MDR1 gene product P-glycoprotein in childhood neuroblastoma. *Cancer* **80**, 1250–1257 (1997). doi:10.1002/(SICI)1097-0142(19971001)80:7<1250::AID-CNCR8>3.0.CO;2-O.
292. Haber, M. *et al.* Association of high-level MRP1 expression with poor clinical outcome in a large prospective study of primary neuroblastoma. *J. Clin. Oncol.* **24**, 1546–1553 (2006). doi:10.1200/JCO.2005.01.6196.
293. Bourhis, J. *et al.* Correlation of MDR1 gene expression with chemotherapy in neuroblastoma. *J. Natl. Cancer Inst.* **81**, 1401–1405 (1989). doi:10.1093/jnci/81.18.1401.
294. Goldstein, B. L. J. *et al.* Expression of the Multidrug Resistance, MDR1, Gene in Neuroblastomas. *J. Clin. Oncol.* **8**, 128–136 (1990). doi:10.1200/JCO.1990.8.1.128.
295. Fu, D., Bebawy, M., Kable, E. P. W. & Roufogalis, B. D. Dynamic and intracellular trafficking of P-glycoprotein-EGFP fusion protein: Implications in multidrug resistance in cancer. *Int. J. Cancer* **109**, 174–181 (2004). doi:10.1002/ijc.11659.
296. Yamagishi, T. *et al.* P-glycoprotein mediates drug resistance via a novel mechanism involving lysosomal sequestration. *J. Biol. Chem.* **288**, 31761–31771 (2013). doi:10.1074/jbc.M113.514091.
297. Llaudõ, I. *et al.* Do drug transporter (ABCB1) SNPs and P-glycoprotein function influence cyclosporine and macrolides exposure in renal transplant patients? Results of the pharmacogenomic substudy within the symphony study. *Transpl. Int.* **26**, 177–186 (2013). doi:10.1111/tri.12018.
298. Gayet, L. *et al.* Control of P-glycoprotein activity by membrane cholesterol amounts and their relation to multidrug resistance in human CEM leukemia cells. *Biochemistry* **44**, 4499–4509 (2005). doi:10.1021/bi048669w.
299. Li-Blatter, X., Beck, A. & Seelig, A. P-glycoprotein-ATPase modulation: The molecular mechanisms. *Biophys. J.* **102**, 1383–1393 (2012). doi:10.1016/j.bpj.2012.02.018.
300. W. Robey, R., R. Massey, P., Amiri-Kordestani, L. & E. Bates, S. ABC Transporters: Unvalidated Therapeutic Targets in Cancer and the CNS. *Anticancer. Agents Med. Chem.* **10**, 625–633

(2010). doi:10.2174/187152010794473957.
301. Libby, E. & Hromas, R. Dismounting the MDR horse. *Blood* **116**, 4037–4038 (2010). doi:10.1182/blood-2010-09-304311.
302. Martin, C. *et al.* The molecular interaction of the high affinity reversal agent XR9576 with P-glycoprotein. *Br. J. Pharmacol.* **128**, 403–411 (1999). doi:10.1038/sj.bjp.0702807.
303. Weidner, L. D. *et al.* Tariquidar is an inhibitor and not a substrate of human and mouse P-glycoprotein. *Drug Metab. Dispos.* **44**, 275–282 (2016). doi:10.1124/dmd.115.067785.
304. Kannan, P. *et al.* The 'specific' P-glycoprotein inhibitor tariquidar is also a substrate and an inhibitor for Breast Cancer Resistance Protein (BCRP/ABCG2). *ACS Chem. Neurosci.* **2**, 82–89 (2011). doi:10.1021/cn100078a.
305. Fox, E. & Bates, S. E. Tariquidar (XR9576): A P-glycoprotein drug efflux pump inhibitor. *Expert Rev. Anticancer Ther.* **7**, 447–459 (2007). doi:10.1586/14737140.7.4.447.
306. Seyffer, F. & Tampé, R. ABC transporters in adaptive immunity. *Biochim. Biophys. Acta - Gen. Subj.* **1850**, 449–460 (2015). doi:10.1016/j.bbagen.2014.05.022.
307. Sicchieri, R. D. *et al.* ABCG2 is a potential marker of tumor-initiating cells in breast cancer. *Tumor Biol.* **36**, 9233–9243 (2015). doi:10.1007/s13277-015-3647-0.
308. Benderra, Z. *et al.* MRP3, BCRP, and P-glycoprotein activities are prognostic factors in adult acute myeloid leukemia. *Clin. Cancer Res.* **11**, 7764–7772 (2005). doi:10.1158/1078-0432.CCR-04-1895.
309. Damiani, D. *et al.* The prognostic value of P-glycoprotein (ABCB) and breast cancer resistance protein (ABCG2) in adults with de novo acute myeloid leukemia with normal karyotype. *Haematologica* **91**, 825–828 (2006).
310. Damiani, D. *et al.* ABCG2 overexpression in patients with acute myeloid leukemia: Impact on stem cell transplantation outcome. *Am. J. Hematol.* **90**, 784–789 (2015). doi:10.1002/ajh.24084.
311. Yuan, Y. *et al.* The clinical significance of FRAT1 and ABCG2 expression in pancreatic ductal adenocarcinoma. *Tumor Biol.* **36**, 9961–9968 (2015). doi:10.1007/s13277-015-3752-0.
312. Ota, S. *et al.* Immunohistochemical expression of BCRP and ERCC1 in biopsy specimen predicts survival in advanced non-small-cell lung cancer treated with cisplatin-based chemotherapy. *Lung Cancer* **64**, 98–104 (2009). doi:10.1016/j.lungcan.2008.07.014.
313. Wang, X. K. *et al.* Afatinib circumvents multidrug resistance via dually inhibiting ATP binding cassette subfamily G member 2 In vitro and in vivo. *Oncotarget* **5**, 11971–11985 (2014). doi:10.18632/oncotarget.2647.
314. Liang, S. C. *et al.* ABCG2 Localizes to the Nucleus and Modulates CDH1 Expression in Lung Cancer Cells. *Neoplasia (United States)* **17**, 265–278 (2015). doi:10.1016/j.neo.2015.01.004.
315. Filipits, M. *et al.* Clinical role of multidrug resistance protein 1 expression in chemotherapy resistance in early-stage breast cancer: The Austrian Breast and Colorectal Cancer Study Group. *J. Clin. Oncol.* **23**, 1161–1168 (2005). doi:10.1200/JCO.2005.03.033.
316. Li, J. *et al.* Association of expression of MRP1, BCRP, LRP and ERCC1 with outcome of patients with locally advanced non-small cell lung cancer who received neoadjuvant chemotherapy. *Lung Cancer* **69**, 116–122 (2010). doi:10.1016/j.lungcan.2009.09.013.
317. Schaich, M., Soucek, S., Thiede, C., Ehninger, G. & Illmer, T. MDR1 and MRP1 gene expression are independent predictors for treatment outcome in adult acute myeloid leukaemia. *Br. J. Haematol.* **128**, 324–332 (2005). doi:10.1111/j.1365-2141.2004.05319.x.
318. Plasschaert, S. L. A. *et al.* Expression of multidrug resistance-associated proteins predicts prognosis in childhood and adult acute lymphoblastic leukemia. *Clin. Cancer Res.* **11**, 8661–8668 (2005). doi:10.1158/1078-0432.CCR-05-1096.
319. Henderson, M. J. *et al.* ABCC multidrug transporters in childhood neuroblastoma: Clinical and biological effects independent of cytotoxic drug efflux. *J. Natl. Cancer Inst.* **103**, 1236–1251 (2011). doi:10.1093/jnci/djr256.
320. Norris, M. D. *et al.* Expression of the Gene for Multidrug-Resistance–Associated Protein and Outcome in Patients with Neuroblastoma. *N. Engl. J. Med.* **334**, 231–238 (1996).

doi:10.1056/nejm199601253340405.
321. Sampson, A., Peterson, B. G., Tan, K. W. & Iram, S. H. Doxorubicin as a fluorescent reporter identifies novel MRP1 (ABCC1) inhibitors missed by calcein-based high content screening of anticancer agents. *Biomed. Pharmacother.* **118**, 109289 (2019). doi:10.1016/j.biopha.2019.109289.
322. Burkhart, C. A. *et al.* Small-molecule multidrug resistance-associated protein 1 inhibitor reversan increases the therapeutic index of chemotherapyin mouse models of neuroblastoma. *Cancer Res.* **69**, 6573–6580 (2009). doi:10.1158/0008-5472.CAN-09-1075.
323. Kuss, B. J. *et al.* In vitro and in vivo downregulation of MRP1 by antisense oligonucleotides: A potential role in neuroblastoma therapy. *Int. J. Cancer* **98**, 128–133 (2002). doi:10.1002/ijc.10159.
324. Peaston, A. E. *et al.* MRP1 gene expression level regulates the death and differentiation response of neuroblastoma cells. *Br. J. Cancer* **85**, 1564–1571 (2001). doi:10.1054/bjoc.2001.2144.
325. Yu, D. M. T., Huynh, T., Truong, A. M., Haber, M. & Norris, M. D. ABC Transporters and Neuroblastoma. in *Advances in Cancer Research* vol. 125 139–170 (Elsevier Inc., 2015). doi:10.1016/bs.acr.2014.10.005.
326. Poręba, M., Strózyk, A., Salvesen, G. S. & Drąg, M. Caspase substrates and inhibitors. *Cold Spring Harb. Perspect. Biol.* **5**, 1–20 (2013). doi:10.1101/cshperspect.a008680.
327. Wang, Y., Luo, W. & Wang, Y. PARP-1 and its associated nucleases in DNA damage response. *DNA Repair (Amst).* **81**, 1–18 (2019). doi:10.1016/j.dnarep.2019.102651.
328. Billen, L. P., Shamas-Din, A. & Andrews, D. W. Bid: A Bax-like BH3 protein. *Oncogene* **27**, S93–S104 (2008). doi:10.1038/onc.2009.47.
329. Feng, H. *et al.* Transferrin Receptor Is a Specific Ferroptosis Marker. *Cell Rep.* **30**, 3411-3423.e7 (2020). doi:10.1016/j.celrep.2020.02.049.
330. Lu, Y. *et al.* MYCN mediates TFRC-dependent ferroptosis and reveals vulnerabilities in neuroblastoma. *Cell Death Dis.* **12**, (2021). doi:10.1038/s41419-021-03790-w.
331. Floros, K. V. *et al.* MYCN upregulates the transsulfuration pathway to suppress the ferroptotic vulnerability in MYCN-amplified neuroblastoma. *Cell Stress* **6**, 21–29 (2022). doi:10.15698/cst2022.02.264.
332. Alborzinia, H. *et al.* MYCN mediates cysteine addiction and sensitizes neuroblastoma to ferroptosis. *Nat. Cancer* **3**, 471–485 (2022). doi:10.1038/s43018-022-00355-4.
333. Müller, M. *et al.* Combining APR-246 and HDAC-inhibitors: A novel targeted treatment option for neuroblastoma. *Cancers (Basel).* **13**, 1–23 (2021). doi:10.3390/cancers13174476.
334. Torii, T. *et al.* In vivo knockdown of ErbB3 in mice inhibits Schwann cell precursor migration. *Biochem. Biophys. Res. Commun.* **452**, 782–788 (2014). doi:10.1016/j.bbrc.2014.08.156.